THE EFFECTS OF DIFFERENTIAL AND COMBINATORIAL INHIBITION OF MYOSTATIN AND ACTIVIN A IN THE *G610C* MURINE MODEL OF OSTEOGENESIS IMPERFECTA

A Dissertation

presented to

the Faculty of the Graduate School

at the University of Missouri-Columbia

In Partial Fulfillment

of the Requirements for the Degree

Doctor of Philosophy

---

by

CATHERINE LAARIPOUH OMOSULE

Dr. Charlotte L. Phillips, Dissertation Supervisor

MAY 2021

The undersigned, appointed by the dean of the Graduate School, have examined the dissertation entitled

THE EFFECTS OF DIFFERENTIAL AND COMBINATORIAL INHIBITION OF MYOSTATIN AND ACTIVIN A IN THE *G610C* MURINE MODEL OF OSTEOGENESIS IMPERFECTA

presented by Catherine L. Omosule

a candidate for the degree of Doctor of Philosophy of Biochemistry,

and hereby certify that, in their opinion, it is worthy of acceptance.

Dr. Charlotte Phillips

Dr. Michael Roberts

Dr. Laura Schulz

Dr. Michael Petris

Dr. Scott Peck

DEDICATION

All thanks to God for his benevolence and guidance during this Ph.D journey and throughout my life. I dedicate this, and my life's work to my daughter Zoey-Isabelle. I am amazed by your growth, and constantly blown away by your intelligence. You will grow up to have immense influence on the people around you. Use your strengths to better mankind, and love graciously! My husband Anthony Omosule- your enthusiasm and dedication to helping me achieve my potential as a mother, a career woman and wife, is the pillar on which I rest.

I would like to express my sincerest thanks and appreciation to all my family and friends, who have been pillars and supporters of my pursuits in no small manner. Besides my biological parents, Alice Abena Kugbie and Paul Seidu, I have acquired many other parents whose presence in my life have been blessings: Mary Opoku, Ninfa Matiase, and Agnes Adedipe. My siblings: Patrick Dontege Seidu, Augustine Seidu, Vivian Ama Asiraa and Isaac Seidu; you continuously shower me with love and have cared for me in unmentionable ways. To my community of friends: Fr. Dominic Obour, Jessica Boateng, the Oshokoya family, the Ojewola family, the Portell family, the Bempah family, the Shoyinka family; my friends and cheerleaders from my undergraduate studies: Dr. Flore N'Guessan-Miller, (Dr.) Andrea Redmond-Wilson, Dr. Andreana A. Awog-Badek, Elizabeth K. Faalong and many others whose presence in my life have enriched me for the better, thank you.

ACKNOWLEDGEMENTS

This Ph.D would not have been possible without you, Dr. Charlotte Phillips. You have always championed my pursuit for success during this training program and have been accepting of me, my family, my goals and dreams. You have mentored and encouraged me in the difficult times, and have celebrated with me in good times. Thank you for showing me how to be a mother, wife, Christian, accomplished scientist and leader!

I also sincerely thank my committee members: Dr. Laura Schulz, Dr. Scott Peck, Dr. Michael Petris and Dr. Michael Roberts. My interactions with you have enriched my academic and professional visions. Thank you for your help and guidance. Special thanks goes to Dr. Schulz who has exemplified scientific collaboration and has enthusiastically reviewed multiple manuscripts and helped flesh out multiple project plans.

I also thank other Phillips' lab members for their contributions towards my projects: Dr. Youngjae Jeong and Dr. Victoria Gremminger. Dominique (Nicki) Joseph, Brooke Weiler, Spencer Silvey, Ashley Aguillard, Koral Campbell, Alp Kahveci, Salah Daghlas, David Martin, Kristin Lenz- thank you for giving me the opportunity to teach and mentor you and for being exceptional undergraduate researchers. Collaborations have been vital to the successful completion of my research projects and so, I thank Dr. Sarah Dallas, Anita Yixia Xie, and all the members of the Dallas lab (UMKC), Michael Brodt (WashU) and Dr. Kevin Middleton for assisting me with projects.

My previous undergraduate experiences and the brilliant researchers who accommodated my early steps into scientific research influenced my desire to pursue a

research-based career. And so I thank Dr. Zezong Gu, Janice Cui and all members of the Gu lab, as well as Dr. George P. Smith and emeritus professor Dr. Dix Pettey, curators of the Mathematics in Life Sciences fellowship through whose encouragement I partook in my first scientific research experience. Further, I am grateful to the Kennedy-Lugar Youth Exchange and Service program (YES) who kick started my journey across several thousands of miles from Ghana to Missouri, USA.

Lastly, I thank the Biochemistry department and all its staff, faculty and students; and curators of the Wayne L. Ryan Fellowship Foundation and Foundation for Women's Wellness for their support.

TABLE OF CONTENTS

LIST OF TABLES

LIST OF FIGURES

THE EFFECTS OF DIFFERENTIAL AND COMBINATORIAL INHIBITION OF MYOSTATIN AND ACTIVIN A IN THE G610C MURINE MODEL OF OSTEOGENESIS IMPERFECTA

Catherine L. Omosule

Charlotte Phillips, Dissertation Research

Abstract

Bone fragility, increased susceptibility to fracture, and low bone mineral density (BMD) are hallmarks of osteogenesis imperfecta (OI), a rare skeletal disorder that arises primarily from defects in the generation, quantity and quality of type I collagen. OI is classically grouped into 4 types based on disease severity: I (mild), II (perinatal lethal), III (severe, progressively deforming) and IV (moderately severe). There is currently no cure for OI, and present day therapeutic management depends on bone-antiresorptive drugs and intramedullary rodding of long bones, both of which can have significant adverse effects and outcomes.

Myostatin and activin A are ligands in the TGF-β superfamily with known regulatory roles in the development and physiology of muscle and bone. In mice, myostatin is well known as a regulator of muscle mass. Its inhibition is associated with increased muscle mass and fiber number. Activin A is a known pro-osteoclastogenic molecule, increasing the differentiation of bone-resorbing osteoclasts. Its inhibition is associated with increased bone formation *in vivo*. Both myostatin and activin A effect canonical signaling cascades through the activin type IIB receptor (ActRIIB).

The following studies are divided into two segments. In the first segment, we explored the effects of genetic myostatin inhibition relative to postnatal pharmacological myostatin inhibition in the mild to moderate type I/IV *G610C* mouse model of OI.

Heterozygous *G610C* mice (*+/G610C*) carry a mutation in their *Col1a2* genes, reflecting the causative mutation in a human founder population exhibiting compromised skeletal health including decreased BMD and bone strength. We hypothesized that the inhibition of myostatin would improve muscular and skeletal properties in *+/G610C +/mstn* (genetic myostatin inhibition) and Regn647-treated wild-type (Wt) and *+/G610C* mice (postnatal pharmacological myostatin inhibition). Indeed, myostatin deficiency endowed *+/G610C* mice with larger hindlimb muscles but it was only through genetic inhibition of myostatin that the overall skeletal properties in the *G610C* mouse was improved.

In the second segment, we explored and compared inhibition of myostatin, activin A, or both ligands using monoclonal antibodies in Wt and *+/G610C* mice, hypothesizing that the combined inhibition of myostatin and activin A (Combo) will more potently improve musculoskeletal properties due to increased muscle mass and decreased bone resorption. Indeed, the combinatorial treatment with both myostatin and activin consistently increased muscle mass, and bone microarchitecture and strength in all mice regardless of genotype or sex. These findings demonstrate the potential of myostatin for increasing muscle mass in OI, but also suggest that combinatorial inhibition treatment strategy of myostatin and activin A provides greater post-natal skeletal improvements than myostatin or activin A inhibition alone.

CHAPTER I

INTRODUCTION AND LITERATURE REVIEW

Parts of this Chapter have been published: Omosule CL and Phillips CL. Deciphering myostatin's regulatory, metabolic, and developmental influence in skeletal diseases. Front. Genet. 2021; 12:662908 doi: 10.3389/fgene.2021.662908

INTRODUCTION

Bone is composed of cells within an extracellular matrix made of organic and inorganic phases. Inorganic hydroxyapatite crystals [$Ca_{10}(PO_4)_6(OH)_2$] make up 60% of the weight of bone while the organic component (mostly type I collagen) makes up 25%, and water, 5%[(1)]. Volumetrically, the inorganic and organic phases and water occupy 36%, 36% and 28% respectively[(1)]. About 10% total bone water is associated with collagen fibrils and hydroxyapatite crystals whereas the remaining 90% is in the lacunocanalicular system, bone marrow and bone vasculature (blood vessel system)[(2)]. Osteoblasts, osteoclasts, osteocytes and bone lining cells make up the cellular constituent.

In vertebrates, bones serve a multitude of functions: attachment sites for muscle and tendons, organ housing and protection, reservoir for a multitude of minerals including calcium, magnesium, and storage for biological molecules and ligands including collagen fibers and osteocalcin[(3)]. In concert with muscles and tendons, the skeletal system facilitates locomotion as well. Bones also serve as sites for hematopoiesis, lymphopoiesis and myelopoiesis, generating hematocytes, lymphoid and myeloid lineage cells, respectively which have roles in osteo-immunology[(4)]. Additionally, granulocyte colony stimulating factor (G-CSF), a hematopoietic cytokine is released by osteocytes[(4)].

Idiopathic, genetic, and aging related bone disorders like osteoporosis and rare bone disease like osteogenesis imperfecta (OI) constitute a huge economic burden and negatively impact quality of life. In OI, a rare genetic skeletal disorder, patients have weak bones that fracture with little trauma, physical disability, growth deficiency, muscle weakness and skeletal deformities[5]. OI primarily arises from mutations in the type I collagen genes COL1A1 and COL1A2. In bone, type I collagen constitutes 90% of all proteins, making defects to the structure and quantity of type I collagen protein detrimental to its strength, geometry, and microarchitecture[6]. A complete cure for OI will rely on genetic manipulations to the defective contributory genes, techniques that are yet to be mastered. Thus, current therapeutic OI management relies on bisphosphonates, a class of drugs that inhibit bone breakdown. Bisphosphonates increase bone mass but can be detrimental when used in pediatric OI patients[7–9]. The insertion of surgical rods into long bones of OI patients is also employed. Intramedullary rods sometimes fail to extend or when they do extend can migrate into soft tissues and joints and need to be replaced via additional surgery[10,11]. These adverse effects further the need to explore better therapeutics for managing OI.

Bone and muscle are intricately connected. Bones respond to loading forces from muscles by adjusting their geometry, mass, and strength[12–14]. Both bones and muscle secrete ligands that have reciprocal regulatory functions. Myostatin (growth differentiation factor 8, GDF8) is a muscle-secreted ligand which negatively regulates the number and size of muscle fibers during growth[15]. Activin A is a bone-secreted ligand which increases differentiation of bone-resorbing osteoclasts[16]. Both activin A and myostatin belong to the TGF-β superfamily of proteins and effect canonical signaling

changes through activin receptor type IIB (ActRIIB), which also interacts with multiple ligands including activins B,C,E, other GDFs and bone morphogenetic proteins (BMPs)[17,18]. Multiple versions of the soluble decoy ActRIIB receptor have improved muscle and bone properties in rodent and primate models, including OI mouse models[19–22]. In clinical trials however, promiscuity of these decoy receptors resulted in adverse effects that resulted in study termination [18,23].

In this review, I summarize our current understanding of bone development, the intricate and reciprocal relationship between muscle and bone, osteogenesis imperfecta and the TGF-β ligands myostatin and activin A. I also provide evidence for pursuing the inhibition of activin A, myostatin or both as promising therapeutic targets for OI.

I.1 BONE DEVELOPMENT AND PHYSIOLOGY

Bone Development

The skeleton is patterned early during embryogenesis. First, mesenchymal stem cells (MSCs) from the paraxial and lateral plate mesoderm create dense cellular outlines for making the bones of the axial and appendicular skeleton respectively[24]. These osteochondroprogenitor MSCs then differentiate either into chondrocytes during endochondral ossification by which the appendicular skeleton, axial skeleton and posterior ends of the skull are formed; or directly into osteoblasts for intramembranous bone formation, which generates the clavicle and craniofacial bones [24,25].

A cartilage template or anlagen is necessary for endochondral ossification, which begins when proliferating chondrocytes, stimulated by Indian hedgehog (Ihh), differentiate into hypertrophic chondrocytes (differentiated chondrocytes that are capable of producing extracellular matrix proteins and forming an ordered structure)[24,26]. This triggers recruitment of runt-related transcription factor 2 (Runx2)- and osterix (Osx)-expressing osteoblast progenitors, blood vessel endothelial cells and hematopoietic cells from the perichondrium into the newly established primary ossification center[24,26] (Figure 1). Here, hypertrophic cartilage is resorbed, osteoblast precursors differentiate into bone-forming osteoblasts, and hematopoietic and endothelial cells facilitate bone marrow formation, replacing the hyaline cartilage[24]. Secondary ossification centers then form at the ends of the developing bone, leaving between them and the primary ossification center, a cartilaginous growth plate (epiphyseal plate, Figure 1) to enable longitudinal bone growth during puberty[24,27]. After puberty, growth plates become thin and are replaced by bone[24].

Several ligands and hormonal factors regulate endochondral ossification. Parathyroid hormone-related peptide (PTHrP), fibroblast growth factor 18 (FGF18) and insulin-like growth factor (IGF-1) regulate chondrocyte proliferation[24]. In fact, reduced growth and dwarfism may occur with mutations in the PTHrP, Fgf18 and IGF-1 genes[24]. Bone morphogenic proteins (BMPs) also stimulate sex determining region Y (SRY)-box 9 (Sox9) expression. Sox9 is a key transcription factor in chondrogenesis and regulates expression of the chondrogenic genes Sox5 and Sox6 as well as the osteoblastic gene, Runx2[28,29].

In contrast to bones formed via the endochondral process, calvarial and facial bones and parts of the pectoral girdle arise via intramembranous bone formation and do not require a cartilage template[30]. Osteoblasts arise from osteochondrogenic cells and secrete bone matrix within membranous tissue which is later mineralized into bone tissue[30].

Bone patterning is an intricate process coordinated by a myriad of transcription factors. The homeobox proteins HOXD13 and HOXA13 appear to regulate the number and length of phalanges and the shape of toes and thumbs, respectively[24,31,32]. Likewise, paired box 3 (PAX3) regulates musculoskeletal patterning, with mutations resulting in finger and nasal bone defects and abnormalities in the upper limb[24,33]. Members of the transforming growth factor beta (TGF-β) superfamily of proteins including activins are also expressed during limb development and play strategic roles in skeletal patterning[29,34].

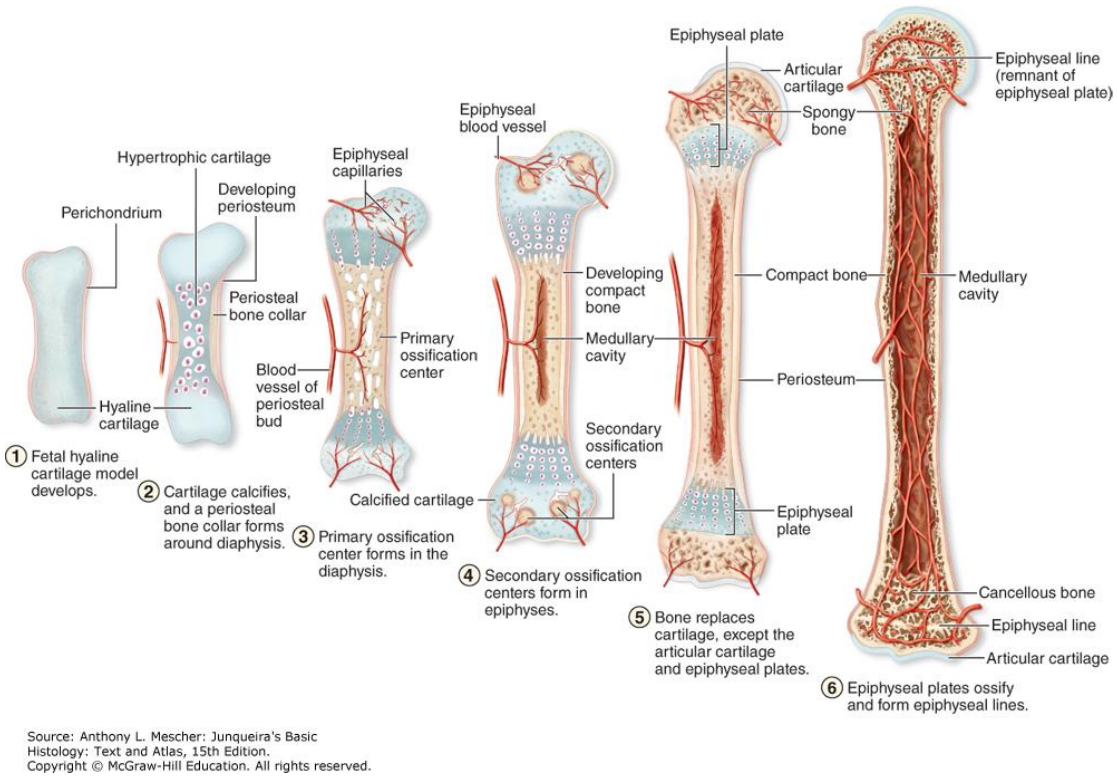

Figure I.1. Endochondral bone formation

In endochondral ossification, a hyaline cartilage forms the template from which bone develops. A primary ossification center is formed where cartilage is broken down, and osteoprogenitor cells differentiate into bone-forming osteoblasts. As the cartilage is transformed into the bone, the marrow cavity is created. Secondary ossification centers are also established at the ends of the long bones. Image from Mescher A.L., Junqueia's Basic Histology: Text and Atlas, 15th edition, https://accessmedicine.mhmedical.com/content.aspx?bookid=2430&sectionid=190278006 Copyright © The McGraw-Hill Companies, Inc.

Bone Cells

Osteoblasts are cuboidal cells that make up 4-6% of all bone cells, yet have indispensable roles in bone formation and maintenance[35]. Osteoblasts make osteoid, a non-mineralized bone matrix composed of type I collagen and non-collagenous proteins [osteocalcin (OCN), osteonectin, bone salioprotein II (BSP II), osteopontin (OPN)] and proteoglycans (decorin, biglycan)[35,36]. Osteoblasts also secrete matrix vesicles, 30 to 200nm in diameter, which contain phosphate and calcium bound together as hydroxyapatite crystals [$Ca_{10}(PO_4)_6(OH)_2$] for bone mineralization[35,36]. Further, osteoblasts regulate osteoclastogenesis by producing macrophage colony stimulating factor (M-CSF) and receptor activator of nuclear factor kappa beta ligand (RANKL), two key transcription factors in osteoclast generation[35]. Lastly, osteoblasts engulf and degrade apoptotic bodies during bone formation[37].

To become osteoblasts, osteochondrogenic MSCs must transition through multiple stages[35]. Committed osteoblast progenitor cells first express RUNX2, distal-less homeobox 5 (DLX5), OSX, COL1A1 and COL1A2, becoming pre-osteoblasts which are cuboidal in nature[35]. Pre-osteoblasts then actively secrete bone matrix proteins, exhibit high alkaline phosphatase (ALP) activity, and then transition into mature osteoblasts and express copious amounts of OCN, BSP I and II, and type I collagen[35].

Bone lining cells are quiescent osteoblasts which line bone surfaces to prevent unnecessary osteoclastic bone resorption, and are capable of becoming active osteogenic cells[35,36,38]. Bone lining cells can secrete RANKL and osteoprotegerin (OPG) to regulate osteoclast differentiation and also degrade collagen fibrils after bone resorption[36,39].

Osteocytes make up 90-95% of bone cells and can live for up to 50 years in humans[2,35,40]. There are far more osteocytes than osteoblasts (ten times) and osteoclasts (one thousand times)[2]. These spider-shaped cells have dendritic processes with which to interact with neighboring cells via gap junctions; have polarity and directionality; and are housed in lacunae, playing key roles in regulating osteoid mineralization, and responding to biomechanical signals[35,40]. Interstitial fluid flow within the lacunocanalicular system has been implicated in cell-to-cell communication during the osteocytic detection and response to mechanical signals. Osteocytes signal through the release of the secondary messengers nitric oxide, prostaglandins, ATP and Ca^{2+}[36].

The indispensable role of osteocytes in bone homeostasis is exemplified by their regulation of bone formation. Sclerostin (Sost) is an osteocyte-secreted glycoprotein that inhibits osteoblastogenesis by negatively regulating WNT and BMP signaling [41]. Osteocyte apoptosis is linked to increased expression of the pro-osteoclastogenic factors RANKL, TNF-α, IL-6 and IL-11, enhancing osteoclastogenesis and contributing to aging-related bone loss[2,35,42]. *In vitro,* osteocytes secrete more RANKL than osteoblasts implicating osteocytes as the major regulator of osteoclast differentiation[42,43]. Further, when RANKL expression is ablated in osteocytes, mice exhibit a severe osteopetrotic bone phenotype[43]. Osteocytes and osteoblasts also actively degrade bone, shown in their secretion of tartrate resistant acid phosphatase (TRAP)[44,45]. Lastly, osteocytes release extra-skeletal factors including fibroblast growth factor 23 (FGF23), a regulator of serum phosphate levels and renal phosphate excretion[35,40].

Osteoclasts are multinucleated cells that resorb bone. The pro-osteoclastogenic molecules M-CSF and RANKL stimulate differentiation of mononuclear cells in the

hematopoietic stem cell lineage into osteoclasts[36]. Like RANKL, osteoprotegerin (OPG) is a member of the tumor necrosis factor (TNF) superfamily and acts as an antagonist to osteoclastogenesis, competing with RANKL for binding to the RANK receptor on osteoclast precursors and protecting against excessive bone resorption[46].

To resorb bone, osteoclasts first seal off a region of interest using actin-rich podosomes under which they form their characteristic ruffled borders: finger-shaped projections of the osteoclast membranes which form a tight seal around the resorption pit into which proteinases like Cathepsin K and B, matrix metalloproteinases and TRAP are secreted, degrading the proteins in the bone ECM[2,46]. Hydrochloric acid generated by vacuolar H^+-ATPases acidify and degrade the bone mineral[2,46]. After degradation, osteoclasts endocytose the matrix proteins at the ruffled border and intracellularly traffic them to be released at the basolateral membrane[47].

Type I Collagen

In vertebrates, the collagen superfamily consists of 27 members which can be found within cartilage, bone, skin, tendons, basement membranes and extracellular matrices[48]. Type I collagen often occurs as a heterotrimer, however, homotrimeric type I collagen, which is more resistant to degradation by proteinases, has been found in cancer, osteoarthritis and osteoporosis as well as within embryonic tissues and adult human skin[49]. In bone, type I collagen consists of two α1(I) and one α2(I) polypeptide chains encoded by the *Col1a1* and *Col1a2* genes, respectively. These left handed helical polypeptides have repeating Gly-X-Y sequences with glycine in every 3rd position due to its small size and lack of side chains[48]. The X position is often occupied by proline whereas hydroxylysine and hydroxyproline occupy the Y position. Following

transcription and ribosomal translation, the pre-pro-polypeptide type I collagen chains are transported into the endoplasmic reticulum (ER) where posttranslational modifications including signal peptide removal from the N-terminal, proline and lysine hydroxylation, and hydroxylysine glycosylation, occur[48,50]. The heat shock protein 47 (HSP47, also Serpin H1) stabilizes the procollagen molecule and acts as a molecular chaperone in the ER[51,52]. The complex procollagen folding process is further assisted by the molecular chaperones: prolyl-4-hydroxylase, osteonectin, prolyl-3-hydroxylase 1(P3H1), cyclophilin B (CyPB), cartilage-associated protein (CRTAP), protein disulfide isomerase (PDI) and FK506-binding protein (FKBP65) [52,53]. Formation of the collagen triple helix begins at the C-terminal region when two α1(I) and one α2(I) polypeptides associate via diffusion and are stabilized by intra- and inter- molecular disulfide bones[5]. Once propagation towards the N-terminal is complete, procollagen molecules are moved through the golgi stacks where additional modifications and assembly into secretory vesicles take place, assisted by HSP47[5,48,50].

In the extracellular space, N proteinases in the A Disintegrin and Metalloproteinase with Thrombospondin motifs (ADAMTS) family cleave the N-propeptide ends and bone morphogenetic protein 1 (BMP-1) cleaves the C-propeptide end of the procollagen molecule to release the mature type I collagen molecule (tropocollagen) which is about 300 nm long and 1.5 nm thick[50,54–56]. Lysyl oxidases then facilitate covalent crosslink formation between tropocollagen molecules by oxidizing side chains of some lysine and hydroxylysine molecules into alpha-aminoadipic-delta-semialdehydes to form collagen fibrils[57] . Additional proteinases able to cleave and degrade type I collagen include the matrix metalloproteinases-1, -8, -14 (MMPs-1, -8, -14)[56,58] and MMPs-2 and -9[56,58].

Type I collagen plays a crucial role in skeletal physiology. The inherent material properties of type I collagen and its organization and structure influence bone toughness and dictates the biomechanical properties of bone[59]. Besides, the tightly regulated series of steps in the collagen synthesis pathway makes errors in the assembly process caused by genetic mutations or pharmacologic agents particularly problematic, altering bone biomechanical properties and increasing the propensity to fracture[59] as seen in bone disorders like osteogenesis imperfecta (OI).

Bone Minerals

Bone minerals dictate the stiffness and resistance of bone tissue and make up approximately 60% of the weight of bone and 40% of its volume [1,36,60]. Bone minerals are composed of hydroxyapatite crystals which have calcium phosphate particles $[Ca_{10}(PO_4)_6(OH)_2]$[61], and ion species like Cl^- and Mg^{2+} [61,62]. The hydroxyapatite minerals in bone are formed and matured in matrix vesicles secreted by osteoblasts[1,35]. These matrix vesicles contain phosphatases like ALPL, which degrade phosphate-containing compounds,, and ion transporters like type III Na/Pi co-transporters which facilitate the uptake of phosphate ions[1,35,63]. Calcium intake is regulated by calcium binding proteins, phospholipids (BSPII and annexin), and calcium channels [35,36]. Within the matrix vesicles, tri-calcium phosphate ($Ca_3(PO_4)_2$) crystals form and are hydroxylated to form bone mineral hydroxyapatite crystals which are then released into the extracellular space, binding collagen fibrils and the proteoglycan scaffold[35,36].

Postnatal Modeling and remodeling

The mechanical properties of bone are dependent on the inherent properties of the constituent type I collagen molecules, bone matrix proteins and minerals, bone mass, overall bone shape, geometry and microarchitecture, and the presence of micro-damage[14,36,59]. Type I collagen contributes to bone elasticity and resistance to tension, whereas minerals dictate bone stiffness and resistance to compression. Nevertheless, with age, the capacity of collagen and minerals to provide both strength and toughness is diminished[64].

In humans, cortical and trabecular bone make up 80% and 20% bone, respectively[65]. During growth, mechanical forces influence modeling, a process by which bones adapt to muscular and/or gravitational forces/stresses by changing their shape and geometry (Figure 2) [65]. In a separate process, bone remodeling facilitates the replacement of old micro-damaged bone with new bone to maintain homeostasis with the help of the bone basic multicellular unit (BMU) [65]. Remodeling involves coupling between osteoblasts and osteoclasts whereas modeling is uncoupled.

Peak bone mass is a critical determinant of one's bone health in later life [66]. Genetic factors as well as environmental influences such as adequate nutrition, body composition, physical activity and exercise early in life, and exposure to sex hormones at puberty impact peak bone mass attainment[67]. Between 11-14 years of age, girls have dramatic gains in BMD, followed by significant declines in skeletal mass growth at the femoral neck and lumbar spine regions[68]. On the other hand, boys continue to accumulate bone mass after puberty, between ages 15-18[68]. Nonetheless, by their mid-twenties, peak bone mass is generally achieved in both males and females[66]. Although minimal modeling persists in trabeculae in adulthood, adults generally accumulate new

bone only through remodeling, i.e. remodeling is a lifelong process[69]. Also, aging negatively influences osteocyte numbers, depletes the osteoprogenitor osteoblast pool and alters rates of modeling and remodeling[64].

Old bone accumulates micro-damages and is replaced with newly synthesized bone during bone remodeling, a tightly regulated process undertaken by the BMU which is comprised of osteoclasts which remove old bone and osteoblasts which replace degraded bone[70]. BMUs are responsible for bone turnover, at a rate of 10% each year in adult humans[2]. In a BMU, osteoclasts are the shortest lived-cells (approximately two week lifespan); active osteoblasts live for up to 3 months and the entire BMU lasts 6-9 months[2]. Approximately 50-70% of osteoblasts in the BMU die via programmed cell death[36,71]. Of the remaining osteoblasts, some are trapped within the osteoid matrix and transdifferentiate into osteocytes while the remaining cells become bone lining cells[36,71].

Bone remodeling involves 4 stages: 1) mononuclear monocyte-macrophage osteoclast precursors are recruited from circulation and activated to differentiate in the activation stage; 2) multinucleated osteoclasts form sealing zones into which they secrete TRAP, Cathepsin K, MMP-9 and gelatinase for organic matrix digestion; and hydrogen ions to decrease the pH in the resorbing compartment (~pH 4.5) and release bone minerals during the 2-4 week resorption stage; 3) bone formation is initiated with pre-osteoblast recruitment and activation in the reversal phase; and 4) osteoblasts produce collagenous matrices and mineralize them using matrix vesicles within the 4-6 month bone formation period[65].

A balance in bone resorption and formation is necessary for maintaining bone tissue homeostasis. Excessive bone resorption tips the balance towards osteopenia as seen

in some types of OI[72], whereas a significant reduction in bone resorption results in an osteopetrotic bone phenotype as seen in mice with loss of RANKL expression in osteocytes[43].

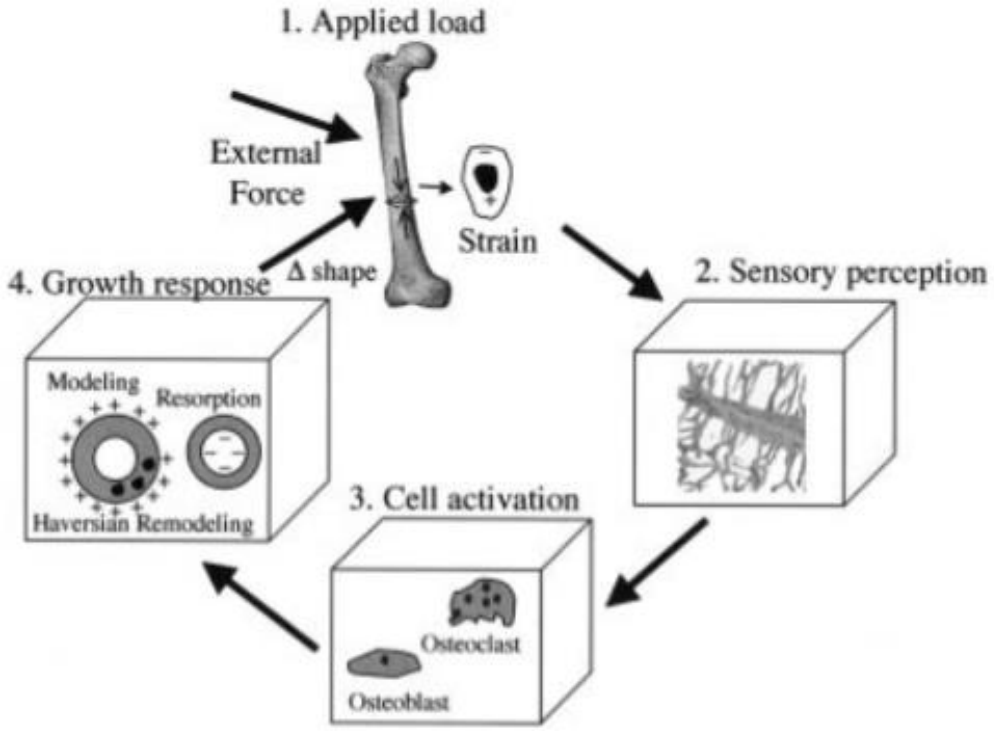

Figure I.2: Bone modeling**.** Movement elicits a bone response. Osteocytes within the lacunocalicular system perceive and transduce mechanical signals by secreting signaling molecules which direct bone formation (by osteoblast) or bone resorption (by osteoclast). A net positive bone formation increases bone mass and occurs primarily during childhood and puberty in a process known as modeling. Remodeling maintains bone homeostasis by coupling the actions of osteoclasts and osteoblasts, replacing old, worn-out bone with newly synthesized bone. Figure borrowed from Pearson and Liebemann, 2004 [(64)]**.**

I.2 MUTATIONS IN BONE STRUCTURE AND PROCESSING

Osteogenesis imperfecta

Defects in type I collagen structure, processing and/or quantity can cause osteogenesis imperfecta (OI), a heritable and generalized connective tissue disorder that affects 1 in 10-15000 live births[5,6,73]. Growth deficiencies, skeletal deformities, skeletal pain, bone fragility and an increased susceptibility to fracture are common manifestations[74,75]. Muscle weakness is also associated with OI[76–78]. In fact, 80% of type I OI patients have significant muscle weakness and decreased exercise tolerance relative to healthy peers [76]. OI patients are also often shorter than family members who do not have OI[79].

OI is generally referred to as a collagen-related disorder. Approximately, 85-90% of dominantly inherited OI is caused by mutations in the *COL1A1*/*COL1A2* genes whereas the remaining 10-15% is recessively inherited through defects in the collagen synthesis and mineralization pathway [74,80]. The 1979 OI characterization scheme proposed by Sillence et al. groups OI into 4 classes based on radiographical and physical presentations[81]. Type I patients present with osteoporosis, bone fracture, blue sclera and in adults, pre-senile deafness, and are considered mild OI. In type II, perinatal lethal OI, neonates die before or soon after birth and present with beaded ribs and broken femora. Type III is often referred to as the most severe survivable (most severe nonlethal) form of OI and is characterized by fractures at birth, progressive limb and spine deformity and short stature. Type IV patients experience moderately severe OI and present with osteoporosis, frequent fractures, and variable skeletal deformity but are ambulatory[81–83]. The advent of genetic and molecular techniques identified additional causative mutations

unassociated with type I collagen structure alone, resulting in 12 more types of OI[5,6] (Table 1) and over >1000-known distinct OI causative mutations[84]. The additional OI types are associated with deficient or abnormal collagen processing (post-translational modification, folding and cross-linking), bone mineralization, and osteoblast function[5,6]. These are also often inherited in an autosomal recessive manner (Table 1).

Quantitative defects in type I collagen generally lead to milder OI, whereas structural defects often result in more severe OI[48,74]. Mutations that affect collagen structure and disrupt the formation of the triple helical structure slows transport through the golgi apparatus resulting in over modification and retention of abnormal collagen chains in the endoplasmic reticulum (ER), leading to ER stress[5,85]. Mutations that substitute the critical glycine residue with a charged or bigger amino acid, or those that occur around the C-terminus often result in moderately severe disease phenotypes, whereas those occurring in the last 200 residues in the N-terminal result in less severe phenotypes[48,83]. Further, mutations that impact cleavage sites for the removal of the N and C propeptide ends also compromise collagen integrity[5]. Lastly, *COL1A1* mutations are more lethal OI relative to those in *COL1A2* due to collagen chain stoichiometry[48].

Table 1: Types of OI and causative mutations (Adapted from Marini et al., 2017)

Genetic Classification	Gene/Encoded protein	OI classification	Pattern of inheritance
Defects in Collagen structure	COL1A1/COL1A2	I, II, III, IV	AD
Anomalous bone mineralization	IFITM5 (Bone-restricted interferon induced transmembrane protein-like protein)	V	AD
	SERPINF1 (Pigment epithelium-derived factor)	VI	AR
Defects in collagen post translational modification	CRTAP (Cartilage-associated protein)	VII	AR
	P3H1 (Prolyl 3-hydroxylase 1)	VIII	AR
	PPIB (peptidyl-prolyl cis-trans isomerase B)	IX	AR
Altered collagen crosslinking	SERPINH1 (Heat shock protein 47)	X	AR
	FKBP10 (65kDa FK506-binding protein)	XI	AR
	BMP1	XII	AD/AR
Compromised osteoblast function	SP7 (Osterix)	XIII	AR
	TMEM38B (trimeric intracellular cation channel type B)	XIV	AR
	WNT1	XV	AR
	CREB3L1 (Old astrocyte specifically induced substance)	XVI	AD
	SPARC (osteonectin)	XVII	AR
	MBTPS2 (Membrane-bound transcription factor site-2 protease)	XVIII	AR

Current OI treatment strategies

Successfully managing OI requires a multidisciplinary team of behavioral, physical and occupational therapists, social workers, physicians, orthopedic surgeons, speech and language therapists, neurosurgeons, psychologists and clinical nurse specialists working together to improve the quality of life of patients[86]. Bisphosphonates, surgical rodding and physical therapy are the major managerial approaches for OI since a cure is currently elusive. While current management systems do not reverse the bone deformities or completely eliminate fracture rates, they reduce overall pain, decrease the frequency of fracture, increase mobility and improve the quality of life of OI patients[87].

Bisphosphonates (BPs) are pyrophosphate analogs (P-C-P) that bind strongly to calcium crystals in bone and suppress bone resorption by inactivating osteoclasts, which endocytose BPs when ingesting bone-resorption by-products[88]. Nitrogen-containing BPs are more potent and inhibit the farnesyl diphosphate synthase enzyme in the cholesterol biosynthesis pathway, leading to loss of prenylated proteins including prenylated GTPases, ultimately inhibiting vesicular trafficking, cytoskeletal dynamics and the formation of ruffled borders, leading to osteoclast apoptosis[88–91] (Figure 3). BPs without nitrogen functionality form non-hydrolyzable ATP analogs which accumulate within osteoclasts and become cytotoxic, impairing survival [88]. BPs have high affinity for calcium crystals and high resistance to degradation, and can accumulate to high concentrations in bone since they have an approximately 6-10 year half-life in the human skeleton[92].

In general, short term BP use increases bone mass and density, decreases bone turnover and fracture incidence and improves pain and wellbeing in children and adults with OI[75,90,93–95]. In adult osteoporotic patients, BP use has been associated with decreased fracture rates without rapid increases in bone resorption following BP cessation in postmenopausal women[92]. Nonetheless, there is concern that since BPs selectively targets bone remodeling, long term use will result in the accumulation of micro-damaged bone[93,96,97]. This is particularly concerning in growing children where BP discontinuation results in the formation of weaker less dense bone in contrast with the denser bone accrued during treatment, creating localized areas of increased bone fragility[8]. Also, BPs, like the nitrogen-containing palmidronate, which is widely used in OI children, is associated with delayed bone healing after intramedullary rodding osteotomies[9]. Further, caution has to be applied with BP use in females of child bearing age since BPs could cross the placenta, potentially affecting growing fetuses and causing hypocalcemia[96]. Although previous Cochrane Database Systematic Reviews have failed to find sufficient evidence for the standardization of BP use in children with OI (due to conflicting clinical outcomes on pain, fracture reduction and quality of life improvements), a recent 2016 review echoed a call for additional studies evaluating the optimal duration for safe BP therapy in children[90,98,99].

Intramedullary rods are surgically implanted in the bones of the upper and lower extremities and increase mobility, reduce the incidence of fracture and improve quality of life in people living with OI[100]. Even so, complications can arise when rods are incorrectly placed within long bones or when rods bend or migrate into bone metaphyses, joints or soft tissue[100]. These complications often necessitate additional surgical re-

roddings. Further, as children outgrow the implanted rods, replacement surgeries/osteotomies become necessary. Nevertheless, medical and surgical innovations in the last 2 decades have improved the types of intramedullary rods available with telescoping rods replacing non-elongating rods and lessening the frequency of re-operations while increasing safety and comfort in OI patients[11,100].

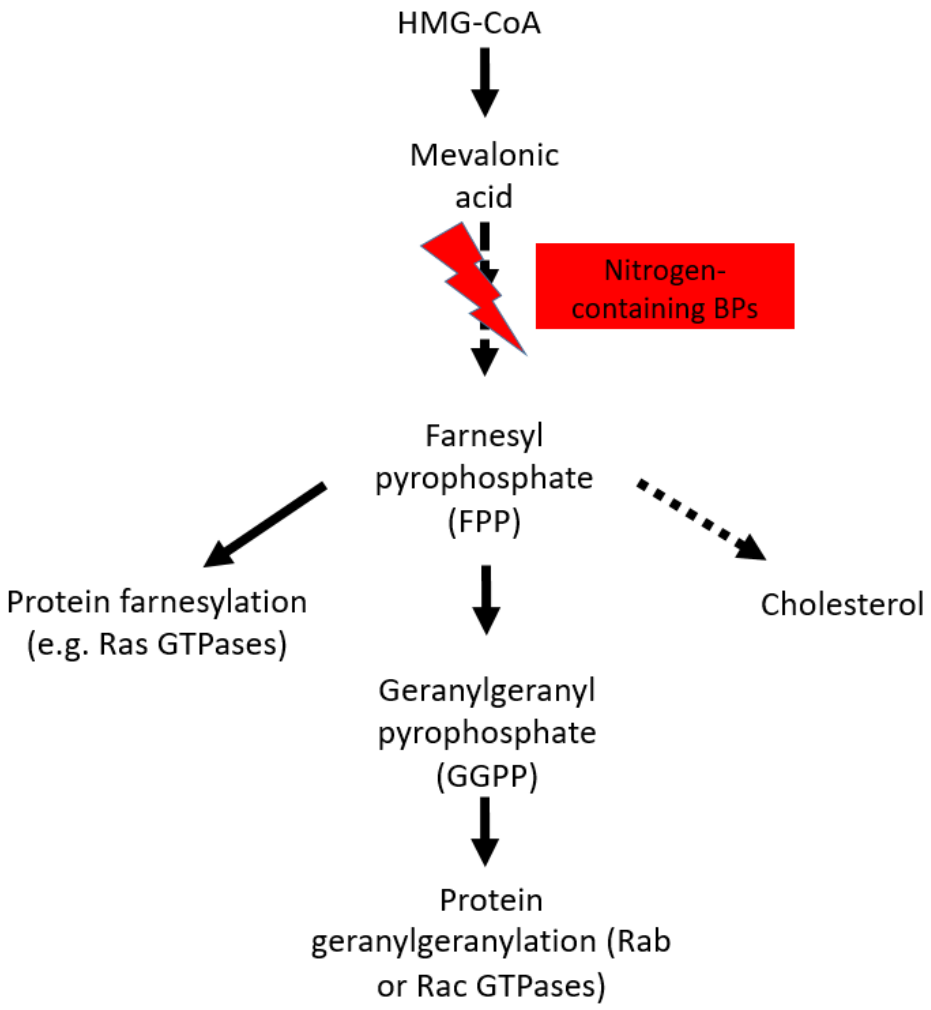

Figure I.3. Mechanism of action of nitrogen-containing bisphosphonates. Nitrogen-containing BPs selectively inhibit the synthesis of FPP from 3-hydroxy-3-methylglutaryl coenzyme A (HMG-CoA), inhibiting downstream cholesterol biosynthesis and protein farnesylation and geranylgeranylation.

Murine models of OI

The OI murine mouse (*Col1a2*^{oim}, *oim*) is a widely used model with a deleterious nucleotide mutation which shifts the reading frame and changes the identity of the last 48 amino acids at the C-terminal end of the α1(I) collagen propeptide[101]. Consequently, *oim* bones consist of homotrimeric α1(I) collagen chains that form a disorganized bone ECM with considerably reduced tensile strength[101,102]. Homozygous *oim/oim* mice experience multiple fractures and have osteopenia, cortical thinning, dorsal kyphosis and progressive skeletal deformity, modeling severe type III human OI[81,101]. Further, *oim/oim* mice have biomechanically weaker bones with inferior microarchitectural integrity. Femurs and tibiae in *oim/oim* mice are considerably shorter than wildtype (Wt) femurs and tibiae, never attaining Wt lengths with age although microarchitectural and biomechanical improvements occur[103]. The smaller sized bones in *oim/oim* mice have less collagen and more disorganized mineral matrix compared to Wt bones[103,104]. At 6.5 months of age, male *oim/oim* femurs have elevated mineral to matrix ratios and decreased carbonate to mineral ratio[105], resulting in more brittle bones.

Both homozygous and heterozygous (*oim/oim* and *+/oim*) mice have been employed in studies which have helped elucidate the pathogenesis of OI and the pathophysiological response of muscle and bone to therapeutics. Heterozygous *+/oim* mice possess intermediate femoral biomechanical strength and morphology relative to Wt and *oim/oim* mice and are useful for studying mild type I human OI[106,107]. *Oim/oim* bones model observations from human studies where a larger number of osteoclasts have higher resorptive capacity, as well as large numbers of immature osteoblast progenitors which further increase osteoclastogenesis, and contribute to the observed bone phenotype

[108,109]. Moreover, the discovery that an inherent muscle pathology is present in OI was first demonstrated in the *oim* model[110]. *Oim/oim* mice have functionally inferior, smaller hind limb muscles with less fibrillar collagen, mitochondrial dysfunction, and a reduced capacity for exercise[110,111]. Heterozygous *+/oim* mice have similar muscle weights as Wt mice, but exhibit a mild muscle pathology[110].

The *G610C* mouse model of OI features a glycine to cysteine substitution in the *Col1a2* gene, phenotypically and genetically modeling a group of 64 OI patients in the Old Order Amish community in Lancaster, Pennsylvania, USA. Heterozygote *G610C* (*+/G610C*) mice model mild to moderately severe human type I/IV OI[79]. Since about 80% of moderately severe to lethal OI arise from mutations in glycine residues within type I collagen chains[79], the *G610C* mouse is a good model for studying dominantly inherited OI. *+/G610C* mice have reduced body mass, biomechanically inferior femurs that are unable to withstand increasing loads, as well as hyper-mineralized bones with decreased BMD, bone volume, mass and total tissue mineral content[79]. Lastly, healed fractures in *+/G610C* are biomechanically weaker, which has been attributed to abnormal fracture healing and decreased callus sizes[112].

In 2016, Mirigian and colleagues demonstrated in the *G610C* mice that the abnormal collagen triple helix structure disrupted procollagen folding leading to over-modification of procollagen chains and increased retention time in the ER[85]. This resulted in intracellular accumulation, ER dilation, increased cell stress and disruption of overall osteoblast function and maturation[85]. Rescuing ER stress partially alleviated trabecular bone properties but did not affect cortical bone parameters or biomechanical strength[113]. Furthermore, primary *+/G610C* osteoblast cells deposit less relative collagen versus Wt

osteoblasts *in vitro* [85]. Intracellular TGF-β signaling is also increased in *+/G610C* mice, with TGF-β signaling inhibition with a neutralizing antibody correcting the compromised bone properties to Wt levels[114]. Lastly, long bones in *+/G610C* mice are shorter and possess hypertrophic chondrocytes at the growth plate with significant ER dysfunction which likely contributes to growth deficiencies[115].

Although the *oim* mouse model is widely used, it models a rare cause of human OI, whereas the *G610C* mouse is a more representative model for many OI patients[79,116]. Additional models like the *Col1a1*$^{Jrt/+}$ and *Crtap*$^{-/-}$ mice provide additional OI genotype and phenotypes for study[117,118]. The *Col1a1*$^{Jrt/+}$ OI mouse is also an autosomal dominant OI mouse model, but differs from the *G610C* and *oim* in that it arises from a splice site mutation which results in deletion of an 18 amino acid sequence near the N-terminal end of proα1(I) collagen[117]. *Col1a1*$^{Jrt/+}$ mice exhibit skeletal, skin and tendon fragility and other manifestations clinically akin to combined type III/IV OI (moderate to severe OI) and Ehlers-Danlos Syndrome, (a connective tissue disorder characterized by joint laxity) as seen in a subset of OI/EDS patients[117]. Cartilage associated protein (CRTAP) is part of the triplex prolyl 3-hydroxylase (P3H) complex which is associated with collagen post-translational modification[118,119]. Mutations in CRTAP result in severe type II and VII OI with a recessive inheritance pattern[118–120]. *Crtap*$^{-/-}$ mice exhibit a severe skeletal phenotype with brittle bones[118].

Both the *G610C* and *Crtap* mouse models have elevated TGF-β signaling[114], and treatment with TGF-β neutralizing antibody improved OI bone phenotype in both *+/G610C* and recessive OI *Crtap*$^{-/-}$ mice. The more severe *Col1a1*$^{Jrt/+}$ mouse however, which has high TGF-β signaling in bone tissue, failed to show improvements in bone

mass and strength in response to the same neutralizing antibody[121]. Further, both *+/G610C* and *Crtap*$^{-/-}$ mice show increases in bone mass and strength with sclerostin antibody treatment, an anabolic bone therapy, although treatment was ineffective in the *Col1a1*$^{Jrt/+}$ mice [118,122,123]. The distinct molecular and genetic causes of OI as well as differences in disease severity contributes to variances in response to treatment and further suggests that treatment efficacies will differ based on disease severity, phenotype and causative mutation.

MUSCLE - BONE INTERACTIONS

Muscle - bone crosstalk

Muscles and bones are physiologically linked at the genetic, biochemical and biomechanical (i.e. functional and anatomic levels) levels[124,125]. First, muscle and bone cells are derived from the same mesodermal MSC lineage[124]. Second, mechanical forces from muscle dictate bone strength and mass, with increasing muscle masses during growth stimulating bone modeling, concomitant with increases in bone strength, whereas disuse and bed rest lead to declines in muscle and bone function[12,126]. Thus, skeletal muscle, constituting roughly 40% of body mass[127,128] (relative to the 15% of body weight accounted for by the human skeleton)[3], is a master influencer of bone geometry, mass and strength and without whose influence bone strength declines[12,14]. This adaptive biomechanical property is dependent on the level of applied strain, with higher strains resulting in bone formation and lower strains linked to bone resorption[129] (Figure 2). Third, bone cells secrete ligands (osteokines) which impact muscle homeostasis whereas muscle cells secrete myokines which regulate bone growth and function[130–132]. Conditioned media from primary osteocytes and the osteocytic MLO-Y4 cell line

increased muscle contractile force *ex-vivo* and induced myoblast differentiation *in-vivo*; possibly via osteocyte-triggered Wnt signaling induced intracellular Ca^{2+} signaling in myoblasts[131]. This intricate connection makes the potential to improve neuromuscular and skeletal disorders dependent on understanding the physiological and pathological relationships between muscle and bone.

Muscle-Bone Crosstalk: Biomechanical

Whole body vibrations can stimulate bone formation, however, the majority of mechanical load capable of triggering bone formation comes from muscle contractions or loading[13,133]. During growth, voluntary mechanical loading dictates bone strength, so that childhood bone disorders like severe OI which limit the ability of children to exercise, adversely affects bone strength[12]. At around 30-40 years of age, muscle strength begins to decline[14]. Bone, which no longer experiences maximum loading from muscle contractions, initiates significant remodeling to re-adapt to the decreased muscle strength, and then begins to steadily decline around 35 years of age, with inactivity furthering the decline[14].

Within a few days of disuse or immobilization, muscle atrophy occurs[134–137]. Changes in the expression of the forkhead box O (FOXO) and peroxisome proliferation-activated receptor gamma coactivator 1 (PGC1) transcription factors and increased expression of ubiquitin ligases and autophagy markers quickly result in a 10% loss of muscle myofiber size after only 4 days of disuse or immobilization in mice[134]. The balance is shifted from protein synthesis to protein degradation. Within four days of immobilization, contractile strength decreases regardless of age in mice[134], with younger mice experiencing more significant losses in myofiber size (-19.9%) relative to aged

mice (-12.6%) by 14 days[135]. Further, in mice sent into space (a microgravity environment) for 4 weeks, gene-metabolite networks that maintain immune fitness and muscle homeostasis are suppressed, concomitant with decreases in mitochondrial content[137].

In humans, data suggest that a 4-6 week period of bed rest decreases muscle mass and accounts for a loss of up to 40% of muscle strength accompanied by significant losses in BMD[135] which is often not recovered after 6 months[135], underscoring the importance of normal weight bearing activity in the maintenance of musculoskeletal equilibrium. Thus, as an adaptive response to bed rest, spinal cord injury, spaceflights and prolonged period of immobilization, loss of mass and functional integrity of muscle and bone are incurred [126,138–140]. Studies of paraplegics provide further evidence of the association between muscle atrophy and bone loss[141]. Paralysis caused by spinal cord injuries which completely immobilizes and denervates lower extremities and atrophies muscle decreases femoral and tibial bone mass by at least 50% and 25% respectively, and likewise trabecular BMD [126,138].

Muscle-Bone Connection: Biochemical

Muscles secrete a myriad of autocrine and paracrine factors collectively known as myokines. These myokines affect tissue homeostasis and metabolism in bone, liver, muscle, fat and cardiac tissue[142,143]. During exercise, myocytes release irisin, which effects changes in muscle and fat tissue, inducing thermogenic browning of adipose cells, regulating glucose homeostasis and whole body energy expenditure, blunting diet-induced obesity, and promoting insulin resistance with the potential to improve metabolic diseases like diabetes[142]. Irisin also increases mitochondrial content in muscle[143] and

has been shown to influence bone as well, increasing bone mass, strength and microarchitectural properties while also protecting against bone loss and facilitating early recovery of bone mass after murine hind-limb suspension, a model of muscle and bone disuse[144,145].

Exercising muscles also secrete L-β-aminoisobutyric acid (L-BAIBA), which like irisin mediates insulin sensitivity, prevents diet-induced obesity and regulates thermogenic browning of white adipose tissue[143]. In the hindlimb unloading rodent model, L-BAIBA also protected mice from loss of muscle mass and muscle contractile function[146]. In bone, like irisin, L-BAIBA prevents bone loss during hindlimb unloading and ROS-induced osteocytic apoptosis by upholding mitochondrial integrity[146].

Lastly, muscles secrete **myostatin**, a member of the TGF-β superfamily of proteins with potent regulatory roles in muscle fiber number and size, which is further discussed in section I.4 below.

Bone-derived factors that influence organ homeostasis are collectively called osteokines. FGF23[147], osteocalcin[148], lipocalin[149], RANKL, OPG, platelet-derived growth factor BB (PDGF-BB), vascular endothelial growth factor A (VEGFA)[3] and activin A[150] are a few known osteokines. Osteocytes secrete FGF23, which helps maintain serum phosphate levels and cardiac and kidney homeostasis[147,151]. Also, osteoblasts secrete osteocalcin (OCN) which was suggested to be an endocrine hormone with extensive effects in the whole body energy and metabolism and adipose, bone, brain, muscle and liver tissue homeostasis although several studies have failed to show the robust influences of OCN in fertility, muscle mass or glucose metabolism as initially proposed[148]. Nonetheless, OCN appears to have vascular roles, stimulating the

P13K/Akt/eNOS endothelial nitric oxide synthase pathway for vasodilation and protecting against ER stress in vascular endothelial cells and smooth muscle cells[152]. Moreover, lipocalin-2, also secreted by osteoblasts, induces insulin secretion, promotes glucose tolerance and regulates satiation and food intake [149]. Furthermore, OPG is a soluble decoy receptor to the osteoclastogenic marker RANKL that is produced by osteoblasts, osteocytes, and discovered more recently, in muscle cells[153]. Recombinant OPG maintained muscle integrity in a murine model of Duchene muscular dystrophy (DMD) and increased extensor digitorum longus (EDL)-specific contractile force and endurance for physical activity[153]. The RANK/RANKL pathway also appears to have roles in immunity, brain, sex hormone regulation in females and mammary gland regulation[154,155]. Lastly, as previously indicated, bone releases a host of factors including RANKL, OPG, M-CSF, WNT, Sost, BMPs, etc. that regulate bone cell differentiation and activity.

I.4 TGF-β LIGANDS IN MUSCULOSKELETAL REGULATION

Current OI therapeutics have failed to fix the underlying genetic causes of the disease and have relied heavily on bone anti-resorption. The bone anabolic therapies parathyroid hormone (PTH) and anti-sclerostin monoclonal antibody have shown some promise in improving bone mass in mouse models of osteoporosis and OI[156,157]. In osteoporotic patients, teriparatide (human PTH) reduced fracture incidence and improved bone microarchitecture[158]. Randomized clinical trials with teriparatide show a bone anabolic response with sustained increases in BMD and estimated vertebral strength in patients with mild type 1 OI[158]. Sclerostin antibodies have also fared well in clinical trials with osteoporotic patients, and provide hope for OI patients[159]. Preliminary data from on-

going clinical trials for OI (reviewed in table 2) show some efficacy for improving skeletal integrity in mild type I OI but not moderate or severe OI. Besides, PTH and anti-sclerostin therapy are the only bone anabolic therapies currently in clinical trials.

MSC transplantation therapy has also been considered an attractive alternative to treating OI. With this therapy, donor MSCs are administered intravenously after *in-vitro* expansion[160]. While stem cell therapy can be administered prenatally or postnatally, and can potentially correct the genotype, it is currently an experimental therapy with low engraftment success rates, but arguably impressive outcomes if successful[160]. Thus, further research is required to identify additional therapeutics to improve skeletal health in all forms of OI.

There exist several ligands in the TGF-β superfamily of proteins that regulate muscle and bone growth and function. Among them, myostatin and activin A are being considered in this dissertation for their ability to elevate muscle and bone properties in OI, as previously observed in osteoporotic and DMD mouse models[161–165]. These observations and more are further discussed in the following sections.

Table I.2: Ongoing clinical trials for OI. Data retrieved from Clinicaltrials.gov (January 2021)

Drug	Type of treatment	Mechanism of Action	Clinical trial phase	Patient demographics	Preliminary Study Outcomes	ClinicalTrials.gov identifier
Forteo (Teriparatide)	Human parathyroid hormone	Anabolic	4	Adult; All OI types	Type I OI patients had robust improvements in BMD No significant treatment outcomes for type III/IV OI	NCT00131469
BSP804 (setrusumab)	Monoclonal anti-sclerostin antibody	Anabolic	2b	Adult; All OI types	Increased bone formation and decreased bone formation in moderate OI	NCT01417091
Fresolimumab	TGF-β neutralizing antibody		1	N/A	Study is actively recruiting participants	NCT03064074
Denosumab	Monoclonal anti-RANKL antibody	Anti-Catabolic	2	Children; Type VI OI; Mixed ages; Type I	Reduced bone resorption and enhanced longitudinal bone growth in children	NCT01799798
MSC Transplantation	Pre- and/or postnatal MSC transplantation		1/2	N/A	Studies are actively recruiting participants	NCT04623606/NCT02172885
Humatrope	Growth hormone therapy	Effects metabolic changes	3	Children; Type III/IV OI	study completed, ongoing data analyses	NCT00001305
Romosozumab	Anti-sclerostin antibody		1	Children and Adolescents; All OI types	Trial to begin in 2021	NCT04545554
Combined teriparatide and zoledronic acid			4	Adult OI patients, all OI types	Study is actively recruiting participants	NCT03735537

TGF-β Superfamily

The TGF-β superfamily consists of multiple growth factors and ligands (approximately 30 members) with muscle and bone-regulatory functions, directing the development and proliferation of cells [166]. Multiple subfamilies exist within this superfamily. These include the TGF-β, activin, GDF, BMP and Nodal subfamilies[17]. Isoforms of TGF-β have been detected in mouse embryo cartilage, chondrocytes and osteocytes, and in adult mice, bone marrow cells, chondrocytes and cartilage[167]. During both endochondral and intramembranous bone formation, several isoforms of TGF-β also persist in different cartilage zones and at mineralization sites[167]. The Nodal subfamily regulates stem cell pluripotency during embryogenesis[17]. Further, BMP subfamily members regulate skeletal development, influencing osteochondrogenic cell commitment to the osteoblast lineage[17].

Activin A belongs to the activin subfamily and is a paracrine hormone with roles in bone metabolism[17,162]. Structurally, activin A is a homodimeric molecule and consists of two β inhibin subunits (βA/βA) connected by a disulfide bone[168]. The inhibin subunits are first synthesized as large precursor prepropeptides with an N-terminal prodomain and a C-terminal mature domain[168]. Following dimerization, proteolytic cleavage by furin proteinases creates the biologically active dimeric activin A molecule[169]. Inhibins, follistatin and follistatin-like proteins are natural inhibitors of activin A activity[168].

Myostatin, also known as GDF8, is universally recognized as a negative regulator of muscle mass [15]. Conserved across species, myostatin shares 89% sequence homology with growth differentiation factor 11 (GDF11), another TGF-β ligand [15,170,171].

Myostatin is initially synthesized by myocytes as a pre-promyostatin molecule composed of an N-terminal signal sequence (for secretion), an N-prodomain region (essential for proper folding of myostatin and subsequently proteolytically processed), and the biologically active C-terminal domain. The precursor pre-promyostatin must undergo proteolytic cleavage to form the biologically active myostatin molecule, which exists as a disulfide-linked dimer of two C-terminal domains[172,173] (Figure 4A). The cleaved propeptide domain also plays a regulatory role through non-covalent binding to the active myostatin C-terminal domain to form an inactive latent myostatin complex[174]. Other natural inhibitors of myostatin include follistatin, follistatin-like 3 (FSTL-3), and GDF-associated serum protein 1 and 2 (GASP-1 and -2) [175].

Activin A and myostatin preferentially bind type II receptors for which they have high affinities and will also bind type I receptors to effect signaling cascades through SMAD proteins[176]. In its active form, myostatin binds and signals primarily through activin receptor type II B (ActRIIB), a serine/threonine kinase, which dimerizes with activin receptor-like kinase 4 (ALK4) while activin A favorably first binds ActRIIA and then recruits ALK4[162], effecting changes in the Smad signaling pathway (Figure 4B).

Several studies in rodent and primate models and a few in human have pursued inhibiting activin A and/or myostatin. A few relevant studies have been compiled in Table 3.

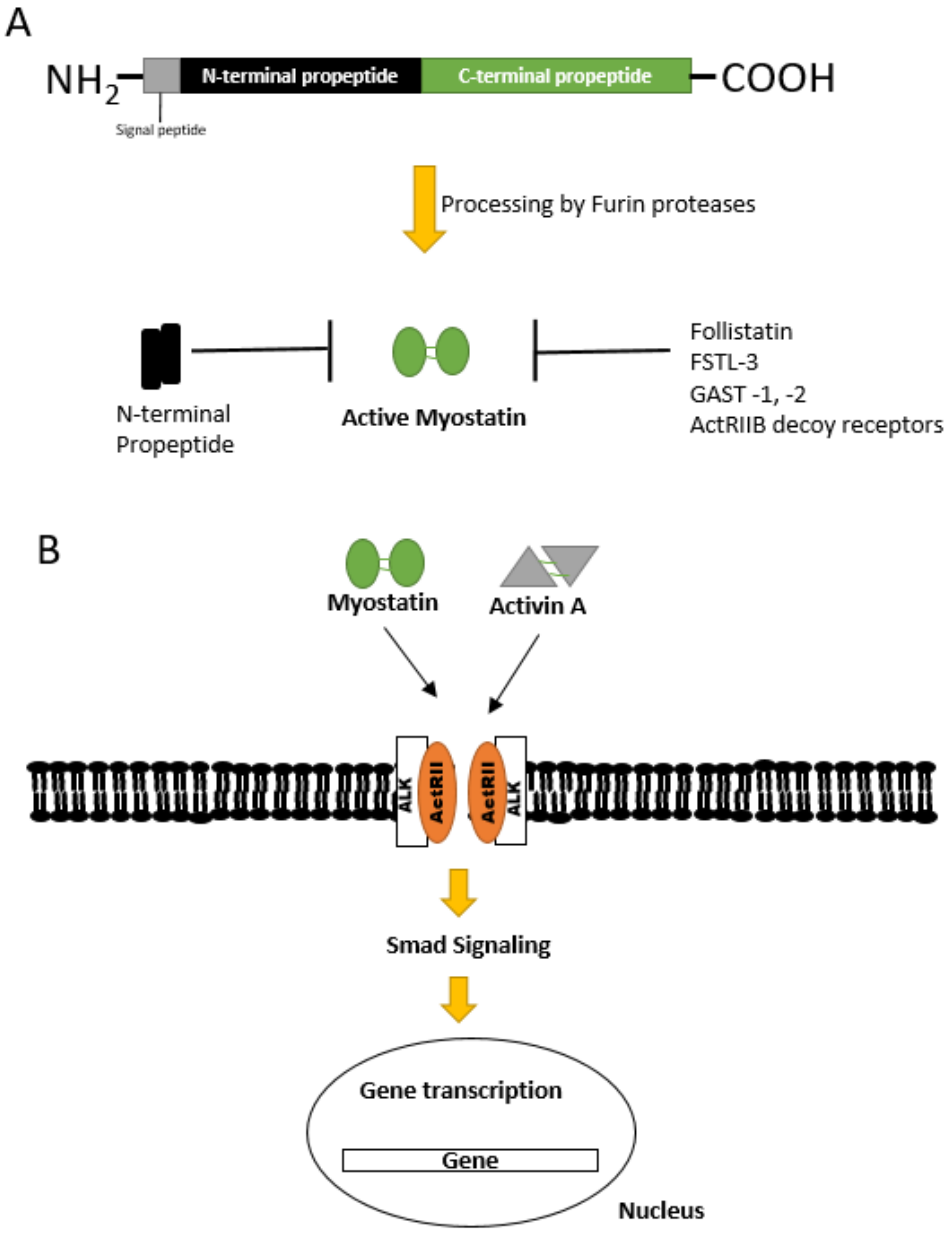

Figure I.4. A) Pre-promyostatin is synthesized as a 375 amino acid peptide with a signal peptide domain and N- and C-terminal domains. Cleavage by furin proteases generate an active myostatin C-terminal dimer which can then form non-covalent complexes with the N-terminal fragments, becoming latent. B) Myostatin and activin A effect cellular changes via the type I/II activin receptors and intracellular Smad signaling cascades.

Table I.3: Previous Research on myostatin and activin A inhibition in humans and rodent and primate models

Author	Species	Condition	Treatment	Muscle Properties	Bone properties
Pearsall et al., 2008	Mouse	Wt	ActRIIA; 10mg/kg; 2X/wk; for 12 weeks	N/A	↑Bone formation, mass and strength
		OVX mice			
Carlson et al., 2011	mouse	MDX; 30 days old	ActRIIB (RAP-031); 10mg/kg; 2X/wk; for 90 days	↑ Body and muscle mass	N/A
Pistilli et al., 2011	Mouse	MDX; 4 weeks old	sActRIIB-mFc (RAP-031) 10mg/kg for 12 weeks	↑ Mass and contractile strength	N/A
Arounlet et al., 2013	Mouse	C57BL6; adult (24months old)	Myostatin propeptide; 20mg/kg for 4 weeks	↑Mass and fiber size	No effect on bone
Chiu et al., 2013	Mouse	Osteoporotic model (10 or 18 months old)	ActRIIB-Fc; 2X/wk; for 30 days	↑ Mass and contractile function	↑ BMD and serum bone formation markers in 10 month old
Bialek et al., 2014	Mouse	$Mstn^{-/-}$; $BMP3^{-/-}$; Wt C57BL/6J; 8 weeks old	Soluble mstn decoy receptor; 10mg/kg; for 4 weeks	↑ Mass	↑ Femoral and vertebral BV/TV; and vertebral strength
			Neutralizing myostatin antibody; 60mg/kg; for 4 weeks	↑ Mass	No improvements
Toledo et al., 2015	Mouse	C57BL6 cancer cachexia model	Combination formoterol (muscle growth promoter) and ActRIIB	Reversed muscle wasting	N/A
Bechir et a.,l 2016	Mouse	MDX; 3 month old	sActRIIB-mFc; 10mg/kg; 2X/wk; for 8 weeks	↑ Body and muscle mass; ↑ muscle force production	N/A
Tinklenberg et al., 2016	mouse	Neb cKO; 14 days old	ActRIIB-mFc/RAP-031; 10mg/kg once	↑Body and muscle mass and myofiber size	N/A

Author	Species	Condition	Treatment	Muscle Properties	Bone properties
Puolakkainen et al., 2017	Mouse	MDX; 6-7 weeks old	ActRIIB-mFc; 5mg/kg/wk for 7 weeks	N/A	↑ femoral bone volume, Tb.N, vertebral bone mass; ↓ osteoclast number
Nielsen et al., 2017	Mouse	MDX; 6-7 weeks old	ActRIIB (RAP-031 and RAP-435)	↑myonuclei number and fiber cross section density	N/A
Morvan et al., 2017	Mouse	SCID; 12 week old	Anti- ActRIIA antibody	↑ Mass	N/A
			Anti-ActIIB antibody; 6 or 20mg/kg/wk		N/A
			Combined anti-ActIIA/B antibodies (Bimagrumab)	Maximal ↑ in body mass (16-22%); muscle mass (18-38%) and contractile function	N/A
Puolakkainen et al., 2017	Mouse	C57BL closed tibial fracture model; 12 weeks old	ActRIIB-mFc; 10mg/kg; 2X/wk; for 2 or 4 weeks	N/A	↑ Callus BV/TV, TB.N, BMD; strength and stiffness
Nagy et al., 2018	Mouse	Wt; 9 weeks old	ActRIIB-mFc/RAP-031; 10mg/kg; 2X/wk for 5 weeks	↑ Mass, myofiber size and body mass	N/A
Jeong et al., 2018	Mouse	C57BL/6 Wt; 8 weeks old	sActRIIB-mFc; 10mg/kg; 2X/wk; for 8 weeks	↑ Masses in all models; ↑contractile function in oim/oim only	N/A
		OI (*+/G610C*; 8 weeks old)		N/A	↑ BV/TV in all models; ↑ bone strength in *+/G610C* only
		OI (*oim/oim*); 8 weeks old		N/A	↑ BV/TV in all models; ↑ bone strength in *+/G610C* only

Author	Species	Condition	Treatment	Muscle Properties	Bone properties
Tauer et al., 2019	Mouse	OI (*Col1a1*$^{JRT/+}$); 8 weeks old	Soluble ActRIIB specific to only ActA and Mstn (ACE-2494); 10mg/kg 2X/wk for 4 weeks	↑ Mass	↑ Bone length, geometry only
		Wt; 8 weeks old			↑ Bone length, mass, strength
Tinklenberg et al., 2019	mouse	Neb cKO; 14 days old	ActRIIB-mFc/RAP-031; 10mg/kg once	No improvements	N/A
Catonguay et al., 2019	Mouse	C57BL/6NTac; 9 weeks old	Follistatin (FST288-Fc); 2X/wk for 4 weeks.	Localized muscle growth, where applied	N/A
Omosule et al., 2020	Mouse	OI *(+/G610C)*; 5 weeks old	Anti-mstn antibody (Regn647); 10mg/Kg; 2X/wk for 11 weeks	↑ Mass	No improvements
		Wt; 5 weeks old			↑ Bone volume and strength
Morse et al., 2015	Rat	Fracture Model; 8 weeks old	ActRIIA (ACE-011); 10mg/kg 2X/wk (varying trt duration)	N/A	↑BMD and serum biomarkers of bone formation
Lotinun et al., 2010	Cynomolgus monkeys		ActRIIA (ACE-011); 10mg/kg; 2X/wk; for 3 months	N/A	↑ Trabecular bone volume, bone formation rate and osteoblast surface
Guo et al., 2017	Macaque Monkey	HIV model; Juvenile	ActRIIB-mFc; 10mg/kg/wk for 12 weeks	N/A	↑ BMD and serum osteocalcin
Sherman et al., 2013	Human	Post-menopausal Women	ActRIIA (Sotatercept); 4 doses (various concentration)	N/A	↑Callus formation
Attie et al., 2013	Human	Postmenopausal women	ActRIIB (ACE-031); 1 dose of 0.02-3mg/kg	↑ Mean total body lean mass	N/A

Activin A in Skeletal Biology

Activin A is abundant in bone matrix[150]. Bone marrow stromal cells, macrophages, osteoblasts and osteoclasts express activin A[16], which regulates osteoblast and osteoclast differentiation [19]. Activin A is considered an essential cofactor for osteoclastogenesis, enhancing Rankl- and Mcsf-stimulated TRAP-positive osteoclast formation in both murine bone marrow cells and RAW264.7 osteoclastic cells[16,17,161]. In fact, soluble recombinant ActRIIA receptors ablate Rankl-induced osteoclast formation[16]. Activin A also has a role in craniofacial development in mice[177]. Activin A knockout mice are born with cleft palates, with no lower incisors or whiskers, and die within 24 hours of birth [177,178].

Several studies reveal the anabolic effects of activin A on fracture healing[179]. Topical activin A administration to fractures dose-dependently promotes increases in callus weight and volume at the fracture site in ovariectomized (OVX) rat fibulas, with callus specific-chondrocytes and osteoblasts strongly expressing activin[179]. In addition, activin A implants further enhance BMP-2 and -3-stimulated ectopic endochondral bone formation in rats, although implants containing activin A alone did not induce bone formation[150].

There are conflicting reports on the roles of activin A in bone formation. Low doses of activin A prevents age-related vertebral bone loss in rats by increasing vertebral biomechanical strength, bone mass, and BMD[161]. Conversely, patients with multiple myeloma (MM) have increased circulating activin A, concomitant with increased bone resorption, bone disease and osteolysis[180]. Treating human MM murine model (SCID-

hu) mice with a soluble decoy receptor to activin A (RAP-011) restored trabecular bone volume fraction (BV/TV), increased osteoblast number per bone surface and decreased osteoclast number per bone area [181]. Another soluble activin receptor type IIA fusion protein (ActRIIA.muFc) increased bone formation *in vivo* by stimulating osteoblastogenesis and decreasing osteoclastogenesis in the murine MM model (5T2MM)[182]. Further, ActRIIA-mFc improved bone mass and strength in normal C57BL/6N mice but reversed the osteopenic bone phenotype in OVX mice[162].

More controversy surrounds the effects of activin A on osteoblast function [162]. Activin A inhibits osteoblast-directed mineralization in an autocrine, dose-dependent manner and decreases *Alpl* expression[183]. Inhibiting activin A with follistatin reverses the inhibition, increasing matrix mineralization and *Alpl* activity[183]. Activin A is also able to inhibit BMSCs differentiation into osteoblasts[181]. In the latter study, Dlx5 and Smad2 expression were significantly diminished with activin A administration suggesting that activin A inhibits osteoblast differentiation via a Smad2-dependent Dlx5-inhibition pathway[181]. BMSCs from MM patients had increased differentiation potential when treated with an activin A-neutralizing antibody[181]. Further, in human osteoblast cells, activin A was shown to stimulate changes in miRNA and gene transcription, reducing matrix mineralization *in vitro*[184].Nonetheless, some studies show that activin A does not affect osteoblast activity or the expression of the osteoblast markers *Runx2*, type I collagen, osteocalcin and osteopontin[183].

Activin A also performs some non-skeletal roles. In male and female reproductive biology, activin A maintains healthy estrogenic follicles in females and regulates the growth and maturation of Sertoli cells and germ cells in male testes[185]. More recently,

data has emerged showing a correlation between increased serum activin A levels and muscle atrophy in chronic obstructive pulmonary disease (COPD), suggesting a contribution of activin A to muscle wasting[186]. Further, myotubes respond to activin A treatment by upregulating ubiquitin ligases and autophagosome formation, and activating muscle catabolism via a p38β-MAPK-dependent signaling[187].

Myostatin in Musculoskeletal Homeostasis

Myostatin has been an attractive target for treating musculoskeletal dysplasias like osteoporosis, OI and Duchene muscular dystrophy (DMD) which are associated with compromised muscle and bone integrity since myostatin regulates muscle metabolism and homeostasis and likely affects bone cell function [15,188]. Homozygous myostatin null mice (*mstn*$^{-/-}$) have global increases in skeletal muscle mass and are about 30% larger than their Wt littermates[15]. Inducing myostatin knock-out in the skeletal muscle of adult mice also increases muscle mass, suggesting that post-developmental changes in skeletal mass accrual can occur[189]. In 2004, a loss of function mutation in the myostatin gene was reported in an infant[190]. In addition to significant reductions in his subcutaneous fat pads (i.e. decreased adiposity), the cross-sectional area (CSA) of his quadriceps was 7.2 SD above the mean CSA of his age matched cohort. Superior muscle strength and mass was observed when he was about 4 years old, shown in his ability to horizontally suspend two 3 kg dumbbells[190].

Therapeutic myostatin inhibition may improve lean muscle masses in sarcopenic or muscle-loss related disorders by changing body composition, favoring lower fat masses and increased dietary fat utilization for skeletal muscle growth, glucose utilization,

insulin sensitivity, and lean muscle mass [191–196]. *Mstn*$^{-/-}$ mice also exhibit lower resting metabolic rates, normal body temperatures and normal food intake[195], although myostatin deficient mice (*mstn*$^{+/-}$) are hyper-metabolic even though they have relatively low activity levels, increased energy expenditure even with normal food intake, and are more sensitive to leptin (leptin is a regulator of metabolism)[197]. Changes in body composition with myostatin inhibition are not limited only to genetic origins. Pharmacologically-induced myostatin inhibition in aging mice increased lean muscle mass relative to control mice[198]. Also, postnatal pharmacological myostatin inhibition has been pursued in many murine and primate species and have resulted in increased muscle masses[20–22,199,200].

Newborn myostatin null mice (*mstn*$^{-/-}$) have larger vertebral bone volume fraction (bone volume/total volume; BV/TV), due to increased bone volume (BV), trabecular thickness (Tb. Th), BMD, and improved cortical bone feature [bone area (BA),tissue mineral density (TMD)] compared to newborn wild type (Wt) mice[201]. Ossification in the cranium and sternum is also significantly enhanced[201]. The superior bone microarchitectural properties observed at birth in *mstn*$^{-/-}$ mice were maintained at 10-weeks of age, as reflected by higher BV, BMD and bone mineral content (BMC) compared to aged-matched Wt mice. In addition, BV, cortical thickness and TMD in tibiae and vertebral BMD were elevated in the 10 week old *mstn* $^{-/-}$ mice[201]. Similarly, primary *mstn*$^{-/-}$ chondrocytes express significant amounts of *Col10a1* mRNA, a marker of hypertrophic chondrocytes [201] further supporting a role for myostatin in the regulation of bone development.

Studies by Hamrick and colleagues have revealed enhanced skeletal phenotypes in *mstn*$^{-/-}$ and *mstn* $^{-/+}$ mice[202,203]. These skeletal augmentations were observed at regions of muscle insertion and linked to bone's biomechanical interactions with the increased muscle masses (mechanosensation). For example, triceps and deltoid muscles at the deltoid crest (point of insertion) in *mstn*$^{-/-}$ mice were significantly larger than in Wt mice. At the points of insertion of these muscles onto the humerus, higher cortical BA, BMC and periosteal circumference were observed[202]. Thus, in mice, increased femoral BMD is associated with the absence of myostatin[204]. Lastly, myostatin directly regulates bone cell metabolism and differentiation[205].

The data regarding the relationship between serum myostatin and aging in humans is mixed[206,207]. In a survey of elderly Chinese men and women, plasma myostatin levels correlated with lean body mass (LBM), suggesting that the amount of circulating myostatin is dependent on the amount of lean muscle present[208]. The research subjects were then divided into a low BMD and high BMD group. The relative abundance of myostatin was lower in the high BMD group compared to the low BMD group, supporting a negative relationship between circulating serum myostatin levels and lean muscle mass[208]. Further, a study of 254 older men and women in Japan showed no significant differences in serum myostatin between males and females, although sclerostin and osteocalcin showed sex-specific differences[209]. In addition, myostatin did not correlate with age in either men or women, or were any correlations found with height, weight, body mass index (BMI), or grip strength[209]. However, the authors noted they were unable to distinguish between active and inactive myostatin in their study and cited this as a potential reason for the absence of correlations[209]. Moreover in anorexia

nervosa (AN), adolescents often have low BMD with low body weights[206]. Serum myostatin levels did not correlate with BMD levels in AN patients whereas it was the serum levels of GDF11 which negatively correlated with BMD in AN patients[207].

Pharmacologic agents are able alter myostatin serum levels and could potentially impact the homeostatic state of the body[210]. Denosumab and zoledronic acid are potent bone antiresorptive agents that increase BMD and decrease fracture risks in osteoporosis. Denosumab is a human monoclonal antibody against RANKL, and works by inhibiting RANKL-induced osteoclastogenesis[211]; zoledronic acid is a third generation bisphosphonate that inhibits the key osteoclast enzyme farnesyl pyrophosphate synthetase[212,213]; and teriparatide is an osteo-anabolic agent also used to improve skeletal integrity. In a study comparing the effect of denosumab on BMD after pre-treatment with either zoledronic acid or Teriparatide, Tsourdi et al., also looked at baseline serum myostatin levels and how they compared after 6 months and 12 months of denosumab administration[210]. Teriparatide treatment significantly lowered serum myostatin levels in postmenopausal women. This decrease was maintained 6-months and 12-months following Denosumab administration. The administration of denosumab alone in the treatment naïve group of postmenopausal women did not impact serum myostatin levels although lumbar spine BMD was significantly increased[210]. Additionally, pre-treatment with zoledronic acid did not impact serum myostatin levels at baseline, only in combination with denosumab after 12 months[210].

Myostatin in Bone Cell Biology

Newborn myostatin null mice (*mstn*$^{-/-}$) possess superior bone microarchitectural properties which are maintained even at 10 weeks of age[201]. Osteoblasts, fibroblasts, bone-marrow derived stromal cells, chondrocytes and bone-marrow derived mesenchymal stem cells (BMSCs) express the membrane receptor ActRIIB to which myostatin preferentially binds[203,214]. Primary murine calvarial osteoblasts exhibit a dose dependent response to myostatin as evidenced by decreasing differentiation and mineralization with increasing myostatin. Alkaline phosphatase activity and osteocalcin secretion were both decreased, as well the expression of the osteoblast transcription factors, runt related transcription factor 2 (*Runx2*) and osterix (*Osx*) [215].

In an elegant phenotypic characterization study, Suh and colleagues showed that primary *mstn*$^{-/-}$ osteoblasts exhibit enhanced differentiation as shown by the upregulated expression of the osteogenic markers; *Runx2*, transcription factor 7 (*Sp7*), alkaline phosphatase (*Alpl*), osteocalcin (*Bglap*), bone salioprotein 2 (*Ibsp*) and osteopontin precursor (*Spp1*) relative to Wt primary osteoblasts [201]. Also, bone morphogenetic protein 2 (*Bmp2*), *Smad-1* and -9 and insulin growth factor 1 (*IGF-1*) were elevated[201,214]. BMSCs from *mstn*$^{-/-}$ mice also had higher differentiation potential versus Wt BMSCs. While mechanical stimuli increased the expression of *Runx2*, *IGF-1*, *Bmp2* and periostin (Osf-2), addition of exogenous recombinant myostatin did not change the osteogenic potential of *mstn*$^{-/-}$ BMSCs in vitro[214]. Pre-treatment with recombinant myostatin however, diminished the expression of osteogenic markers in *mstn*$^{-/-}$ BMSCs when mechanically stimulated[214]. Further, exogenous myostatin inhibited proliferation in human fetal osteoblasts (hFOBs) in a dose dependent manner as reflected by decreased *Alpl*, *Bglap*, and *Runx2* mRNA levels[208]. Lastly, Wt C57BL6/J males and female mice

exhibited increased femoral osteoblast number when treated with a soluble activin receptor type IIB decoy molecule (sActRIIB-mFc) designed as a ligand trap for circulating myostatin [19]. Female Wt mice also exhibited increased periosteal mineralizing surface (MS/BS), mineral apposition rate (MAR) and bone formation rate[19].

Both precursor and mature osteoclasts, but not macrophages express myostatin[216]. In osteoclasts, myostatin simultaneously activates ERK-dependent osteoclastogenic target genes independent of ERK while stimulating *pSMAD*2-dependent nuclear translocation of nuclear factor of activated T-cells (NFATC1)[216]. This culminates in increased expression of the key osteoclastogenic genes for integrin αv, integrin β3, DC-STAMP and the calcitonin receptor[216].

Primary *mstn*$^{-/-}$ osteoclasts have decreased expression of the osteoclastogenic markers: *Nfatc1*, *Fos*, *Src*, tartrate-resistant acid phosphatase type 5 precursor (*Acp5*) and Cathepsin K (*Ctsk*)[201]. Treatment with recombinant myostatin increased TRAP-positive multi-nucleated osteoclasts, enhanced TRAP activity and increased *Nfatc1* expression in a dose dependent manner[215]. To further explore the potential of myostatin to directly regulate osteoclastogenesis, Dankbar et al. differentiated bone marrow macrophages (BMMs) into osteoclasts in the presence of myostatin using the receptor activator of nuclear factor κB ligand (RANKL) and macrophage colony stimulating factor (M-CSF), two critical ligands in osteoclast formation[217]. Resultant osteoclasts were larger with increased cytoplasmic compartments (x8) and more nuclei (x7) implying that myostatin considerably augments RANKL-induced osteoclastogenesis[216]. In addition, BMMs from *mstn*$^{-/-}$ mice were smaller, less proliferative (-44%), and had half the number of nuclei as

BMMs from Wt mice. Although *mstn*$^{-/-}$ osteoclasts generated a larger number of resorption pits in vitro, no differences in resorption area per pit were observed. Thus, myostatin stimulates osteoclastogenesis, but does not appear to impact osteoclast activity[216]. Further, to investigate the effect of *mstn*$^{-/-}$ osteoblastic ligands on osteoclastogenesis, *mstn*$^{-/-}$ osteoblasts were co-cultured with Wt BMMs[216]. This resulted in the formation of 90% less osteoclasts compared to a co-culture of Wt osteoblasts with Wt BMMs. Likewise, *mstn*$^{-/-}$ BMMs co-cultured with Wt osteoblasts resulted in 50% less osteoclasts. Osteoclastogenesis and likewise skeletal metabolism are likely regulated by myostatin[216]. Lastly, histological analyses of Wt C57BL6/J mice treated for 11 weeks with the soluble activin receptor type IIB decoy molecule (sActRIIB-mFc), also revealed decreased osteoclast activity in female mice only[19]. Additional histological characterization of *mstn*$^{-/-}$ tibias revealed a 34% decrease in osteoclast number[216].

Osteocytes, considered as both mechanosensors and mechanotransducers, constitute about 95% of bone cells. Osteocytes relay mechanical signals from normal loading or its absence by secreting factors that influence osteoblast and osteoclast function. Myostatin can directly modulate key transcriptional and osteogenic factors at both the transcriptional and translational levels[40]. Treatment of the osteocytic cell-line Ocy454 with recombinant myostatin upregulated the mRNA and protein levels of sclerostin (*Sost*), dickkopf-1 (*Dkk1*) and RANKL, inhibitors of the WNT/β-catenin signaling pathway[188]. MicroRNAs are small single-stranded noncoding RNAs with regulatory roles in biological pathways[188]. In bone cells, miRNAs have been shown to have regulatory impacts in cellular function and differentiation[188]. MicroRNA-218 (miR-218) regulates the WNT pathway and inactivates Sost and Dkk2 during osteoblast

differentiation[218]. Osteocytes treated with myostatin expressed less miR-218; and released osteocytic exosomes (30-100nm microvesicles) also had less miR-218, consistent with increased expression of Sost and Dkk2[188]. MC3T3 preosteoblastic cells administered the resulting myostatin-modified osteocytic exosomes were less likely to differentiate and had lower levels of the activated β-catenin protein[188]. In contrast, the myostatin-modified osteocytic exosomes did not impact osteoclast proliferation and differentiation[188]. Therefore, these studies suggest myostatin impacts bone metabolism by regulating osteocytic control over osteoblast differentiation.

Pre- and Post-natal Influences of Inhibiting Myostatin and Activin A in OI Bone

Functional muscle deficits have been identified in children with mild to moderate OI even when their relatively smaller muscle masses have been taken into account[219,220]. Thus, treatments that improve both muscle and bone properties in OI regardless of the underlying mutation or disease severity promise to be beneficial. Several mouse models representing different mutations and OI disease severities have been challenged with genetic or pharmacological inhibition of myostatin alone or in combination with other TGF-β ligands including activin A[19–21,84,200,221]. In a recent study by Oestreich and colleagues, Wt and *+/oim* offspring born to myostatin deficient dams exhibit improved skeletal phenotypes in adulthood compared to those born to Wt and *+/oim* dams [221]. To investigate whether intrinsic biological processes pre- or post-implantation were driving the changes, *+/oim* embryos were transferred to *+/mstn* dams and *+/oim* dams (control) at d3.5 gestational age. Offspring born to recipient *+/mstn* dams also had increased femoral strength in adulthood as compared to offspring born to recipient *+/oim* dams suggesting that reduced maternal myostatin levels could confer skeletal advantages to

offspring post-conception, but before birth[221]. In another study, congenic myostatin deficiency increased body and muscle weights and significantly improved femoral biomechanical strength in *+/oim* mice[84]. Changes in the physiochemical and microarchitectural properties of bone were also observed in *oim/oim* mice with post-natal pharmacological inhibition of myostatin and other TGF-β ligands with ActRIIB-ligand traps, although to a lesser extent[19,21]. Muscle mass and function were also augmented[19–21]. Postnatal treatment of *+/G610C* mice with sActRIIB-mFc also increased femoral bone volume and strength, and muscle masses[19,20].

Treatment of Wt and *Col1a1*$^{Jrt/+}$ mice and with the ACE-2492 ActRIIB ligand trap, designed to bind only myostatin and activin A, resulted in dose-dependent increases in mass of hindlimb muscle groups[200]. A dose dependent increase in femoral length was also observed with ACE-2492 treatment relative to control. Additionally, ACE-2492 treated *Col1a1*$^{Jrt/+}$ mice exhibited increased periosteal and endocortical femoral diameters; and polar moment of inertia, similar to that seen with ActRIIB-mFc treatment in *+/G610C* mice[19]. However, biomechanical strength was not improved, and no significant microarchitectural changes in vertebrae were observed in *Col1a1*$^{Jrt/+}$ mice[200].

The variable responses of these molecularly distinct OI mouse models to potential therapeutic agents was evident in other studies employing therapeutic ligands like TGF-β and sclerostin neutralizing antibodies, thus further necessitating a precision medicine approach to treating OI[118,121,222]. More importantly, the evidence from these studies further validate myostatin's potency in muscle regulation. It also suggests that postnatal administration of myostatin alone may be inadequate to elicit significant bone responses in OI. Acting in concert with other TGF-β ligands and perhaps the current anabolic and

bisphosphonate therapies for OI, myostatin may more significantly impact postnatal musculoskeletal properties. A recent 2017 study puts this into practice[156]. In this study, Little and colleagues tested the efficacy of the anabolic sclerostin antibody treatment (Scl-Ab), a bisphosphonate (zoledronic acid, ZA), or combination of both ZA and Scl-Ab in skeletal properties of *+/G610C* mice. The combined treatment improved bone strength in *+/G610C* to Wt levels; and increased cortical thickness and tissue mineral density. Scl-Ab alone failed to improve tibial BMD, but increased trabecular bone microarchitecture[156]. An on-going clinical trial of zoledronic acid and Teriparatide seeks to investigate if the combined treatment approach will improve skeletal properties in human OI (NCT03735537).

Nonetheless, the study by Oestreich et. al [221] suggests that decreasing circulating maternal myostatin levels alters the uterine environment and could potentially induce more skeletal gains in offspring skeletal phenotypes in OI. Thus, further work characterizing the impact of decreasing maternal myostatin levels on fetal musculoskeletal outcomes remains to be undertaken, even though promising prenatal therapy is still far in the future and current patients and those diagnosed postnatally need help. It is however important to note that given the wide genetic and phenotypic variability that characterizes OI, multiple treatment approaches may be necessary to adequately improve associated musculoskeletal deficits.

RESEARCH GOALS AND OBJECTIVES

Functionally and anatomically, muscle and bone are connected. Their shared endocrine functions and pathways are evident in the secretion of autocrine and paracrine ligands[223]. Further, mechanical forces from muscle dictate bone strength and mass[12,14]. Thus, during growth, increasing muscle masses stimulate bone modeling with resultant increases in bone strength whereas disuse and bed rest lead to muscle atrophy and negatively impact bone strength.

Osteogenesis Imperfecta (OI) is a heritable genetic connective disorder that arises from alterations in type I collagen structure or processing resulting in fragile bones that break with minimal trauma. Classical autosomal dominant OI is grouped into 4 types according to disease severity: I (mild OI); II (perinatally lethal OI); III (most severe survivable form of OI); and IV (moderately severe OI)[81]. Functional muscle deficits have been identified in children with mild to moderate OI even when their relatively smaller muscle masses have been taken into account[219,220]. Thus, treatments that improve both muscle and bone properties in OI regardless of the underlying mutation or disease severity promise to be beneficial. Several mouse models representing different mutations and OI disease severities have been challenged with genetic or pharmacological inhibition of myostatin alone or in combination with other TGF-β ligands including activin A[19–21,84,200,221]. The *Col1a2*^{oim} mouse arose from a spontaneous mutation in *Col1a2* resulting in a non-functional protein. Heterozygote *oim* (+/*oim*) mice model mild human OI whereas homozygote *oim* (*oim/oim*) model a severe phenotype.

The *G610C* OI mouse model features a glycine to cysteine substitution, also in the *Col1a2* gene and is phenotypically similar to type I/IV OI patients in an Old Order Amish community in Pennsylvania[79]. Congenic inhibition of myostatin in heterozygote *+/G610C* mice increased muscle masses beyond Wt levels and improved overall bone volume[224]. Postnatal treatment of *+/G610C* mice with sActRIIB-mFc also increased femoral bone volume and strength, and muscle masses[19,20].

The regulatory impact of myostatin in murine muscle mass and fiber number is clearly evidenced by the impact of its inhibition on muscle hypertrophy and regeneration in *mstn*$^{-/-}$, OI, Duchenne muscular dystrophy (DMD) and osteoporotic mouse models. Pharmacological myostatin inhibition, particularly using ActRIIB ligand traps which inhibit multiple ligands, activin A and myostatin included, more potently affects the musculoskeleton than myostatin inhibition alone, suggesting a more combinatorial approach of inhibiting specific ActRIIB ligands in addition to myostatin inhibition is warranted. Since post-natal myostatin primarily affects muscle fiber hypertrophy, the potency of ActRIIB ligand traps in improving bone microarchitecture and strength is likely a collective result of increased mechanosensing due to larger muscle loads and changes to bone metabolism including those stimulated by activin A and other TGF-β ligands.

The work presented in the subsequent chapters builds up on previous research showing that a soluble type IIB decoy receptor (sActRIIB-mFc) improves muscle mass and function plus bone volume in the *oim/oim* mouse while increasing muscle mass, bone volume and bone strength in *+/G610C* mice[19,20]. In the study by Jeong et al., 8 week old male and female Wt, *+/G610C* and *oim/oim* mice were administered sActRIIB twice

weekly for 8 weeks. sActRIIB is specific for multiple ligands including activin A and myostatin, making it impossible to determine which ActRIIB target ligand robustly controls postnatal bone homeostasis. This is particularly important as clinical trials using the humanized ActRIIB decoy receptors in boys with DMD and postmenopausal women were prematurely terminated due to adverse events related to bleeding[18,23]. The bleeding episodes were attributed to the promiscuity of sActRIIB for multiple ligands, including BMP9 and 10, which have angiogenic roles[225].

In chapters II and III, the efforts undertaken to further investigate two of the prominent sActRIIB target ligands with known musculoskeletal effects; myostatin and activin A, are presented. Chapter II explores pre- and post-natal myostatin inhibition and its effects on muscle mass, bone cortical and trabecular microarchitecture and bone strength in *+/G610C* mice. In our postnatal study, 5 week old male and female Wt and *+/G610C* mice were treated with a monoclonal antibody with high specificity for myostatin (Regn 647, Mstn-Ab) for 11 weeks. Our data showed that prenatal/congenic myostatin inhibition resulted in greater bone improvements that post-natal myostatin inhibition. This may reflect myostatin's control over MSC differentiation, effecting genetic changes early on relative to the postnatal study where treatment was initiated at 5 weeks of age. Since muscle masses in both the congenic and post-natal were increased, but bone strength not remarkably improved in either, this suggests that inhibiting myostatin alone may be insufficient in improving skeletal integrity in OI. Interestingly, Wt male mice had noteworthy improvements in both bone microarchitecture and strength, suggestive of the potential benefit of myostatin neutralizing therapy for

improving skeletal strength and microarchitecture in disorders like osteoporosis where peak bone mass influences one's risks of disease acquisition.

In chapter III, we pursue a combinatorial myostatin and activin A inhibition strategy in comparison with activin A inhibition alone or myostatin inhibition alone (chapter II) or control antibody. Activin A is a pro-osteoclastogenenic molecule which also inhibits osteoblast differentiation[16,185]. Five-week-old Wt and *+/G610C* mice are treated with a monoclonal anti-activin A antibody (ActA-ab) or a combinatorial treatment regimen inhibiting both activin A and myostatin (Combo) to further investigate the potential of driving beneficial musculoskeletal changes in OI with a combinatorial treatment regimen.

In appendix A, data on the muscular and whole body metabolic properties of male and female *oim/oim* mice treated with either Mstn-Ab, ActA-Ab or combo are presented. Appendix B highlights contributory work on the impact of sActRIIB treatment on gene expression in osteoblasts, osteoclasts and osteocytes in Wt, *+/G610C* and *oim/oim* mice.

CHAPTER II

IMPACT OF GENETIC AND PHARMACOLOGIC INHIBITION OF MYOSTATIN IN A MURINE MODEL OF OSTEOGENESIS IMPERFECTA

This chapter has been published in the Journal of Bone and Mineral Research

Omosule CL, Gremminger VL, Aguillard AM, Jeong Y, Harrelson EN, Miloscio L, Mastaitis J, Rafique A, Kleiner S, Pfeiffer FM, Zhang A, Schulz LC, Phillips CL. Impact of Genetic and Pharmacologic Inhibition of Myostatin in a Murine Model of Osteogenesis Imperfecta. J Bone Miner Res. 2020 Nov 29. doi: 10.1002/jbmr.4223. Epub ahead of print. PMID: 33249643.

Catherine L. Omosule[1], Victoria L. Gremminger[1], Ashley M. Aguillard[1], Youngjae Jeong[1], Emily N. Harrelson[1], Lawrence Miloscio[2], Jason Mastaitis[2], Ashique Rafique[2], Sandra Kleiner[2], Ferris M. Pfeiffer[3], Anqing Zhang[4], Laura C. Schulz[5], Charlotte L. Phillips[1,6*]

[1]Department of Biochemistry, University of Missouri, Columbia, Missouri, 65211; [2] Regeneron Pharmaceuticals, Tarrytown, New York, 10591; [3]Department of Biomedical, Biological and Chemical Engineering; [4]Department of Biostatistics and Research Design; [5]Department of Obstetrics, Gynecology and Women's Health; [6]Department of Child Health, University of Missouri, Columbia, Missouri, 65211

Abstract

Osteogenesis imperfecta (OI) is a genetic connective tissue disorder characterized by compromised skeletal integrity, altered microarchitecture and bone fragility. Current OI treatment strategies focus on bone anti-resorptives and surgical intervention with limited effectiveness, and thus identifying alternative therapeutic options remains critical.

Muscle is an important stimulus for bone formation. Myostatin, a TGF-β superfamily myokine, acts through ActRIIB to negatively regulate muscle growth. Recent studies demonstrated the potential benefit of myostatin inhibition with the soluble ActRIIB fusion protein on skeletal properties, although various OI mouse models exhibited variable skeletal responses. The genetic and clinical heterogeneity associated with OI, the lack of specificity of the ActRIIB decoy molecule for myostatin alone, and adverse events in human clinical trials further the need to clarify myostatin's therapeutic potential and role in skeletal integrity.

In this study, we determined musculoskeletal outcomes of genetic myostatin deficiency and postnatal pharmacological myostatin inhibition by a monoclonal anti-myostatin antibody (Regn647) in the *G610C* mouse, *a model of mild-moderate type I/IV human OI*. In the postnatal study, 5 week old wildtype and *+/G610C* male and female littermates were treated with Regn647 or a control antibody for 11 weeks or for 7 weeks followed by a 4 week treatment holiday. Inhibition of myostatin, whether genetically or pharmacologically, increased muscle mass regardless of OI genotype, although to varying degrees. Genetic myostatin deficiency increased hindlimb muscle weights by 6.9-34.4%, whereas pharmacological inhibition increased them by 13.5-29.6%. Female *+/mstn*

+/G610C (*Dbl.Het*) mice tended to have similar trabecular and cortical bone parameters as Wt showing reversal of *+/G610C* characteristics, but with minimal effect of *+/mstn* occurring in male mice. Pharmacologic myostatin inhibition failed to improve skeletal bone properties of male or female *+/G610C* mice, although skeletal microarchitectural and biomechanical improvements were observed in male wildtype mice. Four week treatment holiday did not alter skeletal outcomes.

Key Words:

Preclinical Studies, Osteogenesis Imperfecta (OI), TGF-β, Bone-muscle interactions, COL1A2.

Introduction

Osteogenesis imperfecta (OI), commonly known as brittle bone disease, is a rare connective tissue disorder which affects 1:15,000-20,000 live births[6]. The majority of the deleterious variants in autosomal dominant OI occur in type I collagen genes, leading to quantitative and/or qualitative defects in collagen. Variants responsible for the recessive forms of OI generally occur in genes responsible for regulating the post-translational modification and folding of collagen, osteoblast differentiation and skeletal ossification and mineralization[6,226]. Patients with OI experience multiple fractures, exhibit altered bone microarchitecture and have significantly lower bone mineral density (BMD) and mass[227,228]. Currently, surgical interventions and the use of anti-resorptive drugs, the standard of care for OI, have limited success[84,226]. The most commonly used anti-resorptive drug, bisphosphonates (BPs), increase trabecular number and bone mineralization and decrease bone turnover[229,230]. However, continued usage can prolong bone healing after osteotomies[9] and impair metaphyseal modeling in children[231]. Also, data on the efficacy of BPs in improving clinical outcomes including bone pain and fracture rates are incomplete[99]. Besides, surgical complications, immobilization during healing and instances of surgical rodding failures[10] make it vital to continue to pursue more effective treatment approaches.

The musculoskeletal system is a hive of cytokine production and metabolic activity[130]. Skeletal muscle produces myostatin[15], irisin[142], and insulin growth factor (IGF-1)[146,232] which regulate the osteogenic potential of bone; whereas bone-derived factors such as osteocalcin[233] and WNTs[131] have direct effects on muscular function[146]. The functionality of bone and muscle are biochemically and

biomechanically tied. The mechanostat theory postulates that the skeleton will continually adapt to increasing physiological loads, suggesting that increasing muscle mass is a stimulus for improving bone mass and strength[12] while decreasing loads results in bone loss[234]. Consequently, in the pursuit of alternative treatments for genetic and idiopathic disorders of the musculoskeletal system including sarcopenia, OI, and Duchenne muscular dystrophy (DMD), a major goal is to increase overall muscle mass to exploit the synergy between bone and muscle[18,19,84,147,235]. This has led to the exploration of the therapeutic potential of myostatin inhibition.

Myostatin is a TGF-β superfamily member and known regulator of muscle mass in humans[18], other primates[22], cattle[236] and rodents[15]. Myostatin null mice (*mstn*$^{-/-}$) exhibit skeletal muscle hyperplasia and hypertrophy[15]. Additionally, pharmacologic reduction of myostatin significantly increases muscle mass[20–22,237]. Myostatin deficiency also improves insulin sensitivity and glucose uptake in skeletal muscle[192]. As a result, therapeutics targeting the reduction of endogenous myostatin have been explored for their potential to improve muscle mass in murine models of aging[237] and diseases such as OI[20,21] and DMD[238]. The focus of many of these studies has primarily been on muscle, with much less emphasis on the direct and/or indirect effects of myostatin inhibition on bone[22,215,235]. Myostatin knockout mice have increased trabecular bone volume, trabecular number and trabecular thickness in distal femora[202]. In 2016, Oestreich et al. also reported that congenital deficiency of myostatin improves femoral bone strength in adulthood in both wildtype and heterozygote osteogenesis imperfecta murine model (*+/oim*) offspring[221].

Likewise, inhibitors and decoy receptors to myostatin, such as follistatin[239,240], the soluble activin type IIB decoy receptor (sActRIIB-mFc) and ACE-031 (ActRIIB-IgG1) have anabolic effects on bone following postnatal treatment in male and female C57BL/6J Wt mice, as well as in mstn$^{-/-}$[236,241], bone morphogenic protein 3 null (Bmp3$^{-/-}$)[241] and *+/G610C* mice[20,241]. However, when these striking enhancements to bone strength and muscle mass by the decoy receptors were explored in human clinical trials, particularly in studies of the ACE-031 receptor decoy in young boys with DMD[18] and postmenopausal women[23], adverse effects of telangiectasias and gingival bleeding, among others, were reported. These effects were attributed to the overlapping activin receptor type IIB (ActRIIB) usage by multiple TGF-β superfamily members[242] leading to cross-reactivity of the decoy receptor with activins, other growth differentiation factors, and ligands involved in angiogenesis such as bone morphogenic proteins 9 and 10[225]. To potentially avoid these negative adverse effects, we have pursued, in the following study, myostatin inhibition using a monoclonal humanized antibody (Regn647), which does not cross-react with other TGF-β ligands and is highly specific for myostatin. Specifically, we determine the effect of this pharmacologic myostatin inhibition to the effect of genetic myostatin deficiency on muscle and bone mass and function in the *G610C* mouse model of mild to moderate human OI.

The *G610C* murine OI model features a glycine to cysteine amino acid transition at position 610 of the triple helical domain of the α2(I) chain of type I collagen[79]. The *G610C* mouse is a knock-in mouse that replicates a COL1A2 gene variant in 64 OI individuals in an Old Order Amish kindred in Lancaster County, Pennsylvania[79]. Heterozygous *+/G610C* mice exhibit lower femoral bone mineral content (BMC), polar

moment of inertia (pMOI), trabecular bone volume fraction (BV/TV) and biomechanical strength; similar to the phenotypic features observed in the originating Amish kindred[79,243]. Furthermore, the *+/G610C* mouse exhibits near normal muscle function[243], whereas *+/G610C* osteoblasts exhibit endoplasmic reticulum (ER) stress and procollagen misfolding which contributes to defective matrix deposition and substandard bone[85].

OI is a clinically heterogeneous disorder[6]. Several preclinical studies in murine models of OI (*oim, G610C, JRT/*$^{+}$, and *Crtap*$^{-/-}$) reflect the genetic and phenotypic heterogeneity in OI and suggest gene variant- and severity-specific responses to treatments[19–21,118,118,121–123,156,200,244,245] (See Table 1). For example, sActRIIB-mFc treatment of *oim/oim* mice, which feature a frameshift mutation in the α2(I) chain of type I collagen and model severe type III human OI, resulted in improved muscle mass with increased contractile generating force and increased trabecular bone volume, without improving bone strength. In contrast, sActRIIB-mFc treatment of *+/G610C* mice failed to improve muscle contractility function, but significantly increased bone strength and trabecular bone volume[19,20]. Additionally, TGF-β neutralizing antibodies enhanced bone mass in *+/G610C*[114], but did not in the more severe malforming *Col1a1*$^{Jrt/+}$ mouse[121]; although *Col1a1*$^{Jrt/+}$ mice did show improved muscle mass and bone geometry with ActRIIB ligand trapping[200]. These differential responses warrant testing of the effectiveness of potential therapeutics in multiple OI models to delineate the impacts of disease severity and mutation variant on response to treatment.

We present the results of a tripartite study to investigate: 1) the influence of genetic myostatin deficiency on musculoskeletal properties in the *+/G610C* mouse; 2)

musculoskeletal outcomes in the *+/G610C* mouse after 11 weeks of postnatal myostatin inhibition using an anti-myostatin monoclonal antibody (Regn647); and 3) the effects of a 4-week treatment holiday following 7 weeks of Regn647 administration on muscle and bone properties.

Table II.1: Gene-variant and severity-specific responses to therapeutic agents in Osteogenesis imperfecta (OI) mouse models

Treatment	Mouse Model OI classification[a]	Muscle[b]			Bone[b]			References
		Mass	Cross-Sectional Area (mm^2)	Function[c]	BV/TV[d]	pMOI (mm^4)[e]	Ultimate Strength (N)	
ActRIIB ligand trapping	Col1a2$^{tm1.1Mcbr}$ (*+/G610C*) Type I/IV	↑	↑	No change	↑	↑	↑	(19,246)
	Col1a1$^{Jrt/+}$ (JRT) Type III	↑	↑		No change	↑	No change	(200)
	Col1a2^{oim} *(oim/oim)* Type III	↑	↑	↑	↑	No change	No change	(19,21,246)
Anti-TGF-β Antibody	Col1a2$^{tm1.1Mcbr}$ (*+/G610C*) Type I/IV				↑			(114)
	Col1a1$^{Jrt/+}$ (JRT) Type III				No change		No change	(121)
	Crtap$^{-/-}$ Type IV				↑	No change	↑	(114)
Anti-Sclerostin Antibody	Col1a2$^{tm1.1Mcbr}$ (*+/G610C*) Type I/IV				↑		↑ Femur, Vertebrae*	(122), *(156)
	Col1a1$^{Jrt/+}$ (JRT) Type III				↑		No change	(123)
	Col1a2^{oim} (*oim/oim*) Type III				↑		↑	(245)
	Crtap$^{-/-}$ Type IV				↑		↑	(118)

No data was found for blank spaces. [a]Sillence classification system[(81)] [b] ↑ indicates increased or improved parameter. [c]Based on Contractile generating force. [d]Bone Volume/Total Volume. [e]Polar Moment of Inertia.

Materials and Methods

Animals

The *G610C* (*Col1a2*$^{tm1.1Mcbr}$)[79] and *mstn* (*Mstn*$^{tm1Sjl/+}$)[15] mice used in this study were maintained on a C57BL/6J (Jackson Laboratory, Bar Harbor, Maine) background, housed in an AAALAC-accredited facility at the University of Missouri and had ad-libitum access to food and water. The protocols used in the study were approved by the University of Missouri ACUC and met the ARRIVE guidelines[247]. *G610C* mice were genotyped as previously described [41]. Genotypes of *mstn* mice were confirmed by PCR amplification of genomic DNA using the following primer sets for the *mstn*-KO and wildtype alleles [*mstn*-KO allele (forward: 5'ACCAGATGCGTACCTATCCATCCA3' and reverse: 5'ACTTCCATTTGTCACGTCCTGCAC3') and wildtype allele (forward: 5'AGTCAAGGTGACAGACACACCCAA3' and reverse: 5'TGGTGCACAAAGATGAGTATGCGGA3')], generating 500bp and 225bp amplicons respectively. For the postnatal myostatin inhibition study in Approach 2, wildtype (Wt) and heterozygous *G610C* (*+/G610C)* littermates were randomly assigned to treatment groups. All mice were humanely euthanized at 16 weeks of age; the age of peak bone mass attainment in mice[248].

Approach 1: Genetic myostatin inhibition

Breeding Strategy for genetic *+/G610C +/mstn*: Heterozygous myostatin deficient mice *(+/mstn*) and heterozygous *G610C (+/G610C*) mice were mated to generate Wt, *+/mstn*, *+/G610C*, and *+/mstn +/G610C (Dbl.Het)* offspring. Offspring were weaned at 3 weeks

of age and body weights measured weekly until sacrifice at 16 weeks of age. Offspring genotypes appeared to follow normal Mendelian distribution.

Confirmation of myostatin deficiency: Reduction of circulating myostatin levels in *+/mstn* and *+/mstn +/G610C (Dbl.Het)* mice was confirmed by measuring serum myostatin levels using a GDF8/myostatin Quantikine ELISA kit (R&D Systems, Minneapolis, Minnesota). In brief, blood collected during euthanasia was allowed to sit at room temperature and centrifuged to separate serum which was then collected and stored at -80ºC until analyses. Samples and standards were assayed in duplicate, read on a BioTek Synergy 2 MultiMode Reader (Winooski, VT, USA) and analyzed using the Gen5 Data Analysis Software, with an intra-assay coefficient of variation of 2.8% (n=36) (Winooski, VT, USA).

Approach 2: Postnatal inhibition of myostatin

Heterozygous *G610C* dams (*+/G610C*) were bred with Wt males to generate Wt and *+/G610C* offspring. Selection of dam genotype was due to colony availability. Parental genotypes were limited to a specific designated genotype to remove a potential variable. Mice were weaned at 3 weeks of age and randomly distributed into 3 groups. Beginning at 5 weeks of age, Wt and *+/G610C* mice were weighed and injected twice weekly with humanized monoclonal control or anti-myostatin antibody (10 mg/kg of body weight) for either 7 weeks (Mstn-Ab TRT Holiday) or 11 weeks (Mstn-Ab Wks 11-16). Both control (Regn1945; an hIgG4 isotype control) and anti-myostatin (Regn647; humanized monoclonal) antibodies were a generous gift from Regeneron Pharmaceuticals (Tarrytown, NY, USA). Regn647 has high binding affinity (K_D < 5 X

10^{-11} M) and specificity for myostatin but does bind its homolog, Growth Differentiation Factor 11 (GDF11), very weakly, such that the kinetics could not be measured under the experimental conditions (Table 2). The pharmacokinetic profile and dosage response of hindlimb muscles and body weights in mice following Regn647 treatment are in Figures 1 & 2. Regn647 treatment (10mg/Kg) for 3 weeks increased body (p-value = 0.068) and muscle weights in 8 week old mice (Figure 2).

At 16 weeks of age, the mice were euthanized and serum, hindlimb muscles (soleus, plantaris, gastrocnemius, tibialis anterior, and quadriceps), femurs, and tibias harvested.

Muscle Contractile Properties

Contractile properties of the left soleus (sol), gastrocnemius (gast), and tibialis anterior (TA) muscles in male and female WT and *+/G610C* mice treated with either control or anti-myostatin antibody were evaluated as previously described[110]. Briefly, mice were anesthetized and the left sol, gast, and TA muscle surgically exposed at their distal insertions. The distal tendon of each muscle was attached to the Grass force transducer and sequentially tested, sol→gast→TA. The distal tendon was adjusted in length so that the passive tension was zero grams. The sciatic nerve was isolated and placed on a stimulating electrode and a twitch was obtained as previously described[110]. At optimal length, a peak tetanic contraction (P_o) was elicited by pulses delivered at 150Hz, 300-ms duration, and an intensity of 6V for each type muscle[249]. All data were collected using PowerLab® (ADinstruments, Colorado Springs, CO).

Femoral Microarchitecture (μCT)

Excised right femora were cleaned of soft tissues, wrapped in gauze and stored in 1X PBS at -20˚C until analyses. Right femoral trabecular and cortical microarchitecture was investigated using the vivaCT 40 μCT scanner (SCANCO Medical AG, Bassersdorf, Switzerland) using these parameters: 70kVp, 114μA, 8W X-ray energy intensity and high-resolution CT-scan with 10 um isotropic voxel size (10 x 10 x 10 um)[250] and an integration time of 300ms. One hundred slices were contoured at the midshaft of each bone for cortical analyses and 630 slices contoured starting at the distal end for trabecular analyses. Scans were analyzed using the SCANCO Medical microCT software system (SCANCO Medical AG, Bassersdorf, Switzerland). 100 slices were each analyzed for trabecular and cortical parameters and thresholds set to 211 and 270 (lower) respectively and 1000 (upper). μCT Image analyses were performed and data reported according to recommendations by Bouxsein et al., 2010[251].

Femoral Biomechanical Testing

After μCT analyses, right femora were subjected to 3-point bending tests using the Stable Micro Systems TA-HDi Texture Analyzer (Texture Technologies Corp), software-version 07.14H. Bones were placed anterior-posteriorly on support stands that were 9 mm apart. Testing was performed using a load cell with maximum scale of 5 kg set on an automatic trigger force of 0.2N and a constant speed of 0.02mm/sec until bone failure. Ultimate load, yield load, stiffness, ductility (post-yield displacement) and work-to-fracture were determined from the load displacement curve using Microsoft Excel. Ultimate load was determined from the maximum load measured during the test, Stiffness was determined from the slope of a straight line fitted to the linear portion of the load displacement curve. Yield load was determined to be the load at which the load vs.

displacement curve deviated from linear. This was determined by appending a line perpendicular to the linear portion of the load displacement curve akin to the 0.2% offset rule[252,253]. Ductility was determined from the displacement following yield until ultimate fracture. Work-To-Fracture was determined by the area under the load vs. displacement curve.

Statistical analyses

Outliers were detected using the Grubbs1 method on GraphPad Prism (GraphPad Software, San Diego, CA, USA). Statistical analyses were performed using the SAS software (SAS Institute, Inc., Cary, NC, USA). Correlations, manova and anova analyses were performed. Log transformations and non-parametric rank transformation analyses were used when necessary to stabilize heterogeneous variations. Comparisons for weekly treatments in both the genetic and postnatal studies were performed using the first order autoregressive AR(1) model to account for the positively correlated repeated weekly measures. For approach 1, the congenital myostatin inhibition study, final body and muscle weights, bone microarchitectural and biomechanical data were analyzed independently as a 4 x 2 x 2 factorial [4 genotypes (Wt, *+/mstn*, *+/G610C*, *Dbl.Het*), 2 sexes (male, female), 2 dam genotypes *(+/mstn* or *+/G610C*)]. For approach 2, postnatal inhibition of myostatin, final body and muscle weights, bone microarchitectural and biomechanical data were also analyzed independently as a 2 x 2 x 3 [2 genotypes (Wt, *+/G610C*), 2 sexes, 3 treatments (Ctrl-Ab, Mstn-Ab TRT Holiday, and Mstn-Ab Wks 11-16)]. Differences were considered significant at $p \leq 0.1$. The congenital study was not powered to test differences as a consequence of dam genotype[221] and no significant differences were observed in bone parameters based on maternal genotype. Therefore,

offspring of the same genotype and sex were combined for analyses regardless of maternal genotype.

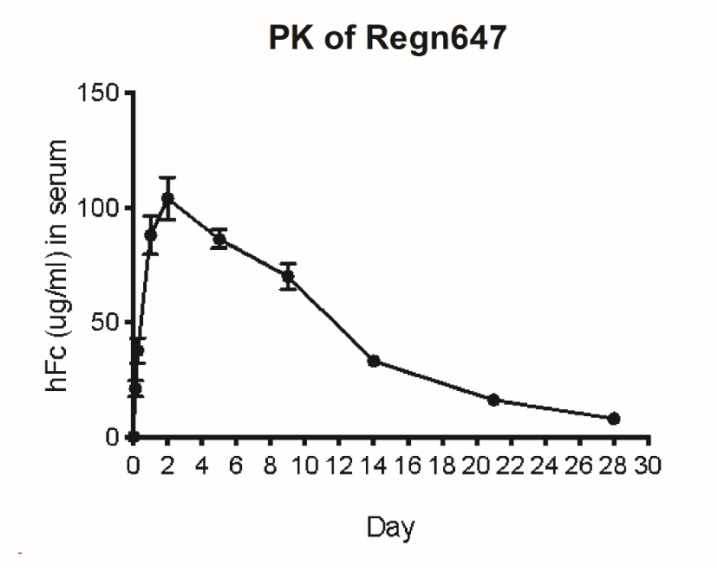

Figure II.1: The pharmacokinetic (PK) profile of the humanized anti-myostatin monoclonal antibody, Regn647 in mice. Quantitation of serum hFc levels over time after a single subcutaneous injection of 10 mg/kg Regn647 into 12-16 week-old mice (mixed background: 87.5% C57BL/6NTac 12.5% 129S6/SvEvTac; mice, n=4). Mice were baseline bled before the injection and then after 3, 6 hours, and 1, 2, 5, 9, 14, 21 and 28 days to collect serum. Antibody levels were measured using an hFc ELISA and plotted against time.

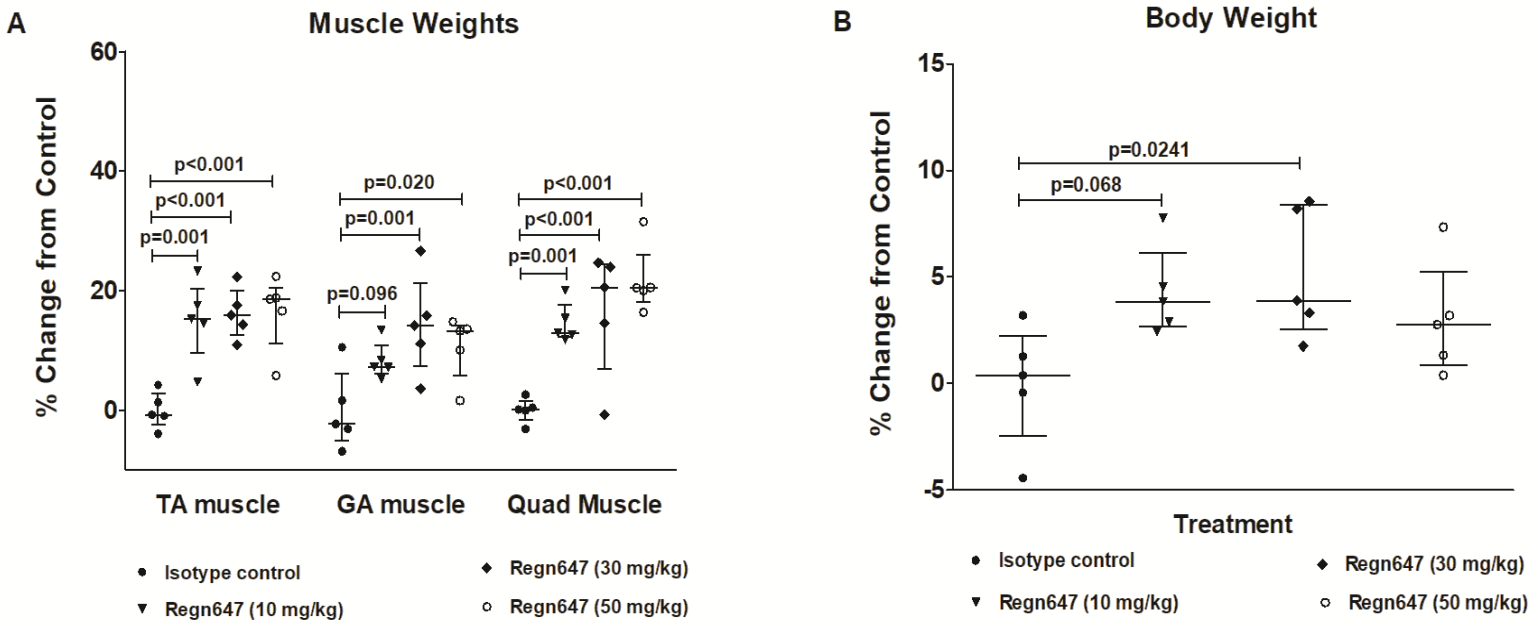

Figure II.2: Changes in hindlimb muscle (A) and body weights (B) following treatment with increasing doses of anti-myostatin Regn647 antibody in SCID mice. Eight week-old SCID mice (n=5) were injected intraperitoneally with either 10, 30, or 50 mg/kg of Regn647 or isotype control twice during the first week and once weekly for the following 3 weeks. After 4 weeks of treatment, tibialis anterior (TA), gastrocnemius (GA), and quadricep (Quad) muscles were dissected and weighed. Muscle and body weights are plotted as percent change to the values obtained from isotype control treated mice. The data were analyzed by one-way (body weight) or two-way anova (muscle weight). Values are median with interquartile range. p-values < 0.1 are indicated and considered significant.

Table II.2. Kinetic binding parameters of REGN647 (humanized monoclonal antibody to human myostatin (GDF8) and GDF11) determined by Surface plasmon resonance (SPR-Biacore) analysis

mAb tested	Antigen tested	k_a ($M^{-1}s^{-1}$)	k_d (s^{-1})	K_D (M)	$t_{1/2}$ (min)
REGN647	GDF8	6.39E+06	2.95E-04	4.62E-11	39
	GDF11	IC	IC	IC	IC
Isotype Control	GDF8	NB	NB	NB	NB
	GDF11	NB	NB	NB	NB

Where IC = Inconclusive data; slight binding, but insufficient to generate an equilibrium dissociation constant (K_D) NB= No binding.

Surface plasmon resonance (SPR) analysis of the binding of Regn647 to human GDF8 and GDF11 was conducted as previously described[254], using an amine coupling chemistry technique[255]. For analysis, all of the specific binding sensorgrams were double-reference subtracted as previously reported[256]. The kinetic parameters were obtained by globally fitting the double-reference subtracted data to a 1:1 binding model with mass transport limitation using Biacore T200 Evaluation software v 1.0 (GE Healthcare, Marlborough, MA). The dissociation rate constant (k_d) was determined by fitting the change in the binding response during the dissociation phase and the association rate constant (k_a) was determined by globally fitting analyte binding at different concentrations. The equilibrium dissociation constant (K_D) was calculated from the ratio of the k_d and k_a. The dissociative half-life ($t_{½}$) in minutes was calculated as $\ln 2/(k_d * 60)$.

Results

Approach 1: Genetic Myostatin Inhibition

Congenital myostatin inhibition increases muscle mass in mice

To assess the impact of inherent myostatin deficiency on musculoskeletal properties in the *G610C* mouse model of OI, heterozygous myostatin (*+/mstn*) and *+/G610C* mice were bred to produce offspring with the resulting genotypes: Wt, *+/mstn, +/G610C* and *+mstn +/G610C* (designated as *Dbl.Het*) (Fig.3A). Mice were weaned at 3 weeks of age and weighed weekly thereafter. Reduced circulating serum myostatin in *mstn* mutants was confirmed after euthanasia at 16 weeks of age. Male and female *+/mstn* offspring had 48.4% and 34% less circulating myostatin respectively when compared to their Wt littermates. *Dbl.Het* offspring also had decreases in circulating myostatin relative to Wt and *+/G610C* although the decrease was more substantial in male mice [male (42.9%, 36.5%) than the female (18.5%, 13%)] (Fig. 1B) mice, respectively.

Sixteen-week-old *+/G610C* mice have decreased body weights relative to age-matched *+/mstn* and *Dbl.Het* mice (Fig.4A). Female *+/G610C* mice also have lower body weights relative to Wt littermates (Fig.4A). Genetic myostatin deficiency in female *Dbl.Het* mice increased their body weights to female Wt and *+/mstn* littermate levels. Beginning at 5 weeks and 11 weeks of age in female and male mice respectively, *Dbl.Het* offspring exhibited increases in body weight relative to *+/G610C* littermates, which were maintained throughout the remaining course of the study (Fig.4B & 4C).

Wet muscle weights collected post-euthanasia reflected substantial increases in the gastrocnemius [Male 22.7%; Female 23.4%], quadriceps [Male 25.0%; Female 27.7%], tibialis anterior [Male 6.9%; Female 18.4%] and plantaris [Male 34.4%; Female 23.6%] muscles in congenital *Dbl.Het* mice relative to *+/G610C* littermates (Fig.5A-D). These increases in final body and muscle weights in the *+/G610C* mice as a result of congenital myostatin inhibition (*Dbl.Het*) rivaled those of Wt and *+/mstn* littermates.

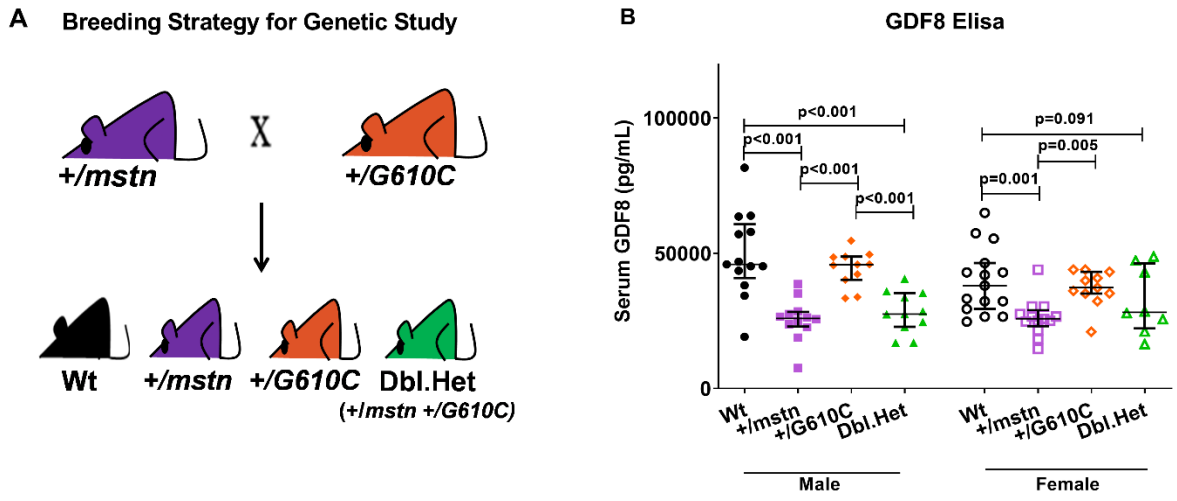

Figure II.3: Verification of myostatin deficiency in genetic model. A) Schematic of congenital *+/mstn* and *+/G610C* breeding strategy with the resultant offspring genotypes. B) Circulating serum myostatin (GDF8, pg/ml) levels in 16 week old male (solid data points) and female (open data points), Wildtype (Wt, black circle), heterozygote myostatin deficient (*+/mstn*, magenta square), heterozygote *G610C* (*+/G610C*, orange diamond) and double heterozygote *+/mstn* and *+/G610C* (Dbl.Het, green triangle) offspring (n= 8-15). Data were analyzed by MANOVA and AR(1) model. No genotype by sex or by dam genotype interactions were found. Offspring genotype main effect was evaluated. Values are median with interquartile range**.** p-values ≤ 0.1 are indicated and considered significant.

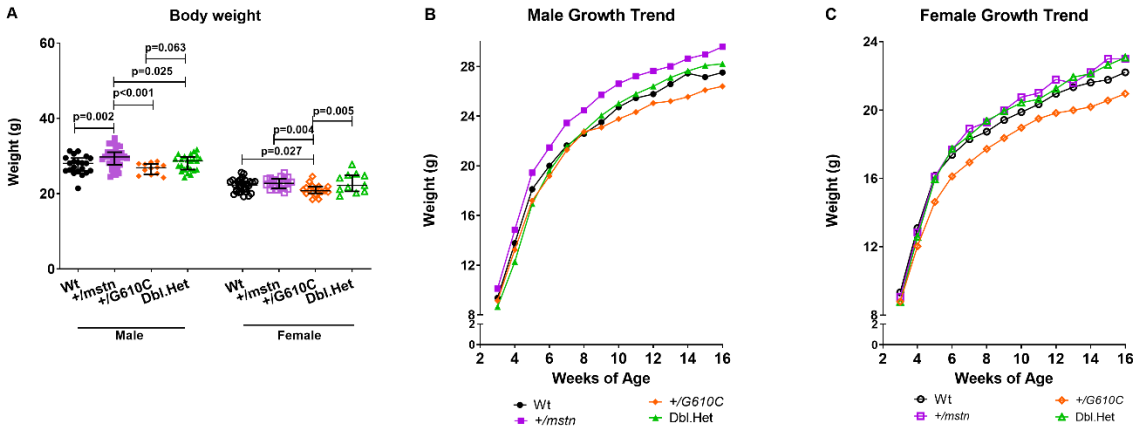

Significance values for weekly comparison of body weights of sex-matched *+/G610C* and *Dbl.Het* offspring from 3 weeks to 16 weeks of age

Sex	Comparison	Wk. 3	Wk. 4	Wk. 5	Wk. 6	Wk. 7	Wk. 8	Wk. 9	Wk. 10	Wk. 11	Wk. 12	Wk. 13	Wk. 14	Wk. 15	Wk. 16
Male	***+/G610C* vs *Dbl.Het***	ns	ns	ns	ns	ns	ns	ns	ns	0.089	0.115	0.027	0.016	0.024	0.037
Female	***+/G610C* vs *Dbl.Het***	ns	ns	0.056	0.0213	0.023	0.0196	0.021	0.03	0.094	0.035	0.002	0.004	0.003	0.003

Not significant (ns) at p<0.1. Data were analyzed by AR(1) model.

Figure II.4: Congenital myostatin deficiency increases body weight in the *+/G610C* mouse. A) Body weights (g) of male (solid data points) and female (open data points) Wildtype (Wt, black circle), heterozygote myostatin deficient (*+/mstn*, magenta square), heterozygote *G610C* (*+/G610C*, orange diamond) and double heterozygote *+/mstn* and *+/G610C* (Dbl.Het, green triangle) at 16 weeks of age (n= 12-34). B) Weekly weights of male Wt, *+/mstn*, *+/G610C* and *Dbl. Het* offspring starting from 3 weeks to 16 weeks of age (n=11-28). C). Weekly weights of female Wt, *+/mstn*, *+/G610C* and *Dbl. Het* offspring starting from 3 weeks to 16 weeks of age (n= 11-37). Data were analyzed by MANOVA and AR(1) model. No genotype by sex or by dam genotype interactions were found. Offspring genotype main effect was evaluated. Values are median with interquartile range**.** p-values ≤ 0.1 are indicated and considered significant for *+/G610C* vs. *Dbl.Het* comparisons (Table; bottom).

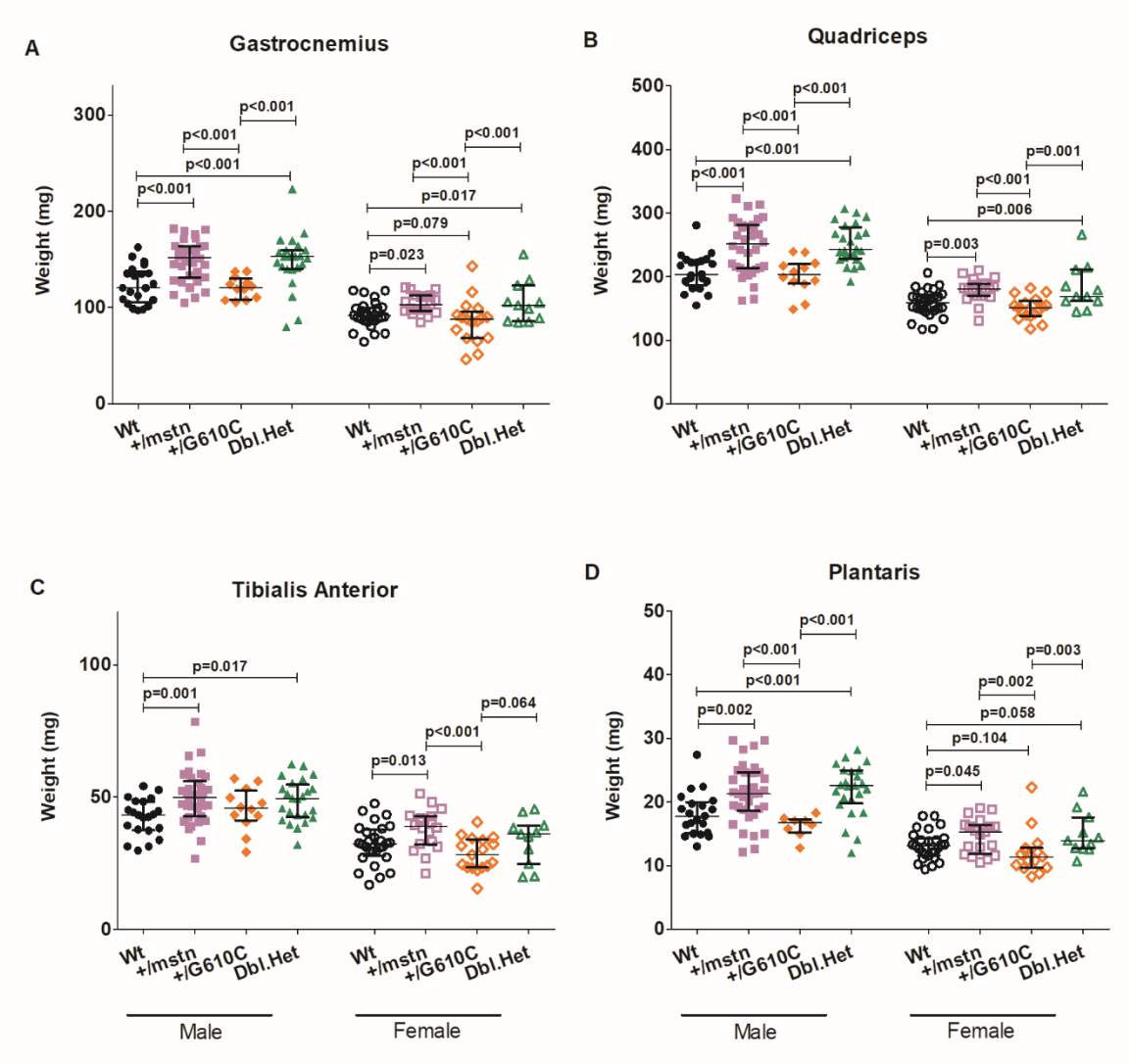

Figure II.5: Inherent myostatin deficiency increases wet muscle weights (mg) of the A) gastrocnemius, B) quadriceps, C) tibialis anterior, and D) plantaris at 16 weeks of age in Wildtype (Wt, black circle), heterozygote myostatin deficient (*+/mstn*, magenta square), heterozygote *G610C* (*+/G610C*, orange diamond) and double heterozygote *+/mstn* and *+/G610C* (Dbl.Het, green triangle) offspring (n=11-34). Data were analyzed by MANOVA. No genotype by sex or by dam genotype interactions were found. Offspring genotype main effect was evaluated. Values are median with interquartile range; p-values ≤ 0.1 are indicated and considered significant.

Congenital myostatin deficiency in +/G610C improves overall femoral microarchitecture in female mice.

Femoral microCT (μCT) analyses revealed that total volume (TV, Fig.6A), bone volume (BV, Fig. 6B) and trabecular spacing (Tb.Sp, Fig. 6C) were decreased in female *+/G610C* offspring, but restored to Wt levels in their myostatin deficient (*Dbl.Het*) counterparts. TV, BV and Tb.Sp were unchanged in male *+/G610C* mice relative to *Dbl.Het* littermates, and *+/G610C* mice had equivalent bone volume fraction (BV/TV, Fig.6D) as Wt and *Dbl.Het* littermates. Relative to *+/G610C*, *Dbl.Het* mice had equivalent trabecular number (Tb.N, Fig.6E), trabecular thickness (Tb.Th, Fig. 6F) and BMD (Fig.6G). Although male and female *+/G610C* mice had lower Tb.N and male *+/G610C* mice had lower Tb.Th relative to sex-matched Wt littermates, respectively, genetic myostatin deficiency restored them to Wt levels. Surprisingly, BMD (Fig.6G) was higher in female *+/G610C* and *Dbl.Het* offspring relative to Wt. BMD in male *+/G610C* was not different from Wt, although *Dbl.Het* males had higher BMD relative to Wt offspring.

In addition, mid-diaphyseal femoral cortical bone area (BA, Fig.7A) was unchanged regardless of genotype in male mice. However, female *+/G610C* mice had lower BA, which was restored in *Dbl.Het* offspring and was no longer different from Wt. Decreased cortical total area (TA, Fig.7B) in *+/G610C* and *Dbl.Het* offspring contributed to increased bone area fraction (BA/TA, Fig.7C) relative to Wt littermates. Polar moment of inertia (pMOI, Fig.7D), although decreased in *+/G610C* mice, was no longer different from Wt offspring in *Dbl.Het* offspring.

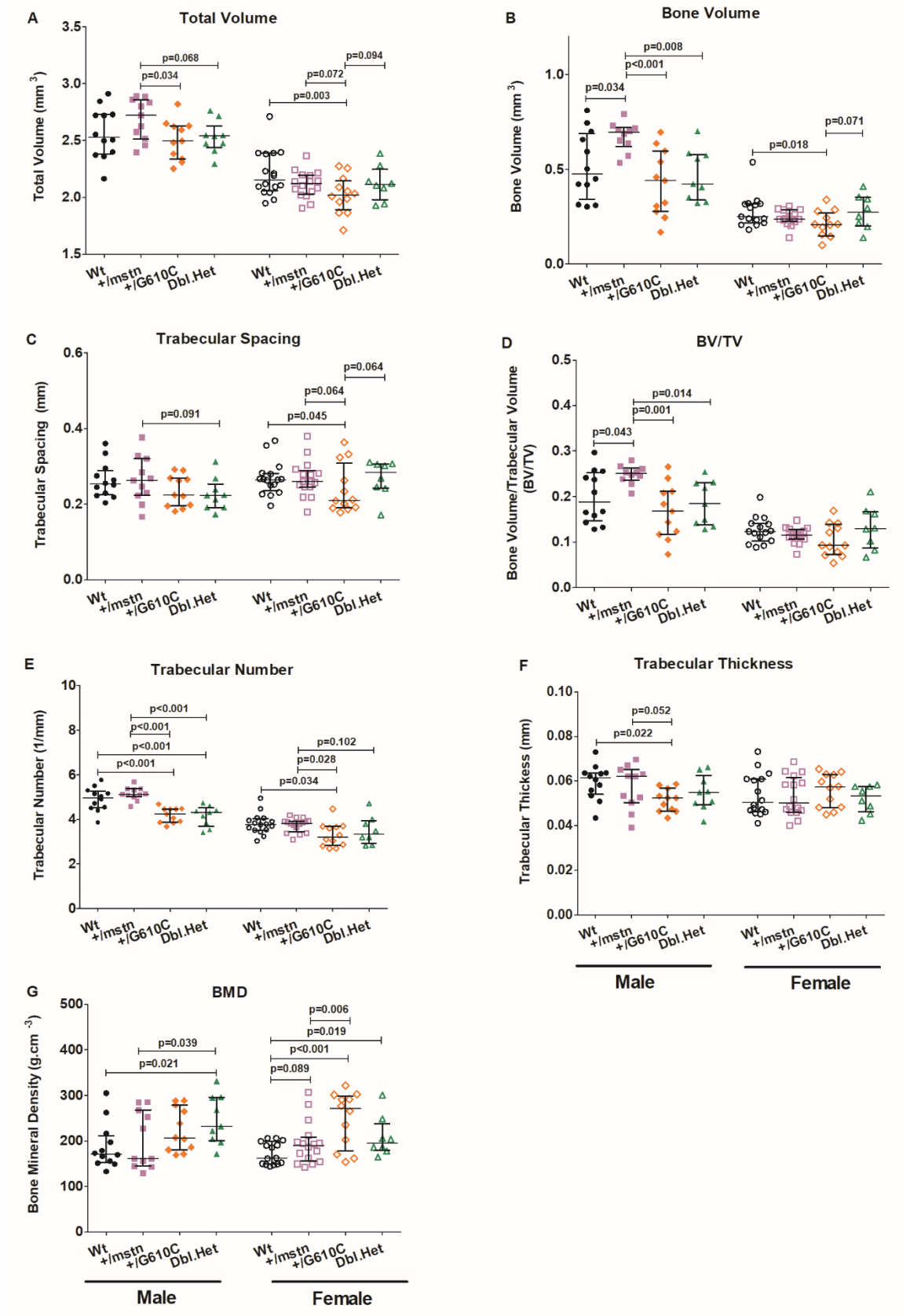
A
Total Volume
Total Volume (mm 3)
p=0.068
p=0.034
p=0.072
p=0.003
p=0.094
B
Bone Volume
Bone Volume (mm 3)
p=0.008
p<0.001
p=0.034
p=0.018
p=0.071
C
Trabecular Spacing
Trabecular Spacing (mm)
p=0.091
p=0.064
p=0.045
p=0.064
D
BV/TV
Bone Volume/Trabecular Volume (BV/TV)
p=0.014
p=0.001
p=0.043
E
Trabecular Number
Trabecular Number (1/mm)
p<0.001
p<0.001
p<0.001
p<0.001
p=0.102
p=0.028
p=0.034
F
Trabecular Thickness
Trabecular Thickess (mm)
p=0.052
p=0.022
G
BMD
Bone Mineral Density (g.cm -3)
p=0.039
p=0.021
p=0.006
p=0.019
p<0.001
p=0.089
Wt
+/mstn
+/G610C
Dbl.Het
Male
Female

Figure II.6: Inherent myostatin deficiency has minimal impact on femoral bone microarchitecture in *+/G610C* mice. µCT analyses of 16 week old male and female Wildtype (Wt, black circle), heterozygote myostatin deficient (*+/mstn*, magenta square), heterozygote *G610C* (*+/G610C*, orange diamond) and double heterozygote *+/mstn* and *+/G610C* (*Dbl.Het*, green triangle) offspring femora. Trabecular bone parameters: A) Total Volume (mm^3), B) Bone Volume (mm^3), C) Trabecular Spacing (mm), D) Trabecular Bone volume fraction (BV/TV), E) Trabecular Number (Tb. N; 1/mm), F) Trabecular Thickness (Tb. Th; mm), and G) Bone Mineral Density (BMD; g/cm^2). Data were analyzed by MANOVA. No genotype by sex or by dam genotype interactions were found. Offspring genotype main effect was evaluated. Values are median with interquartile range**.** p-values ≤ 0.1 are indicated and considered significant; n = 8-16.

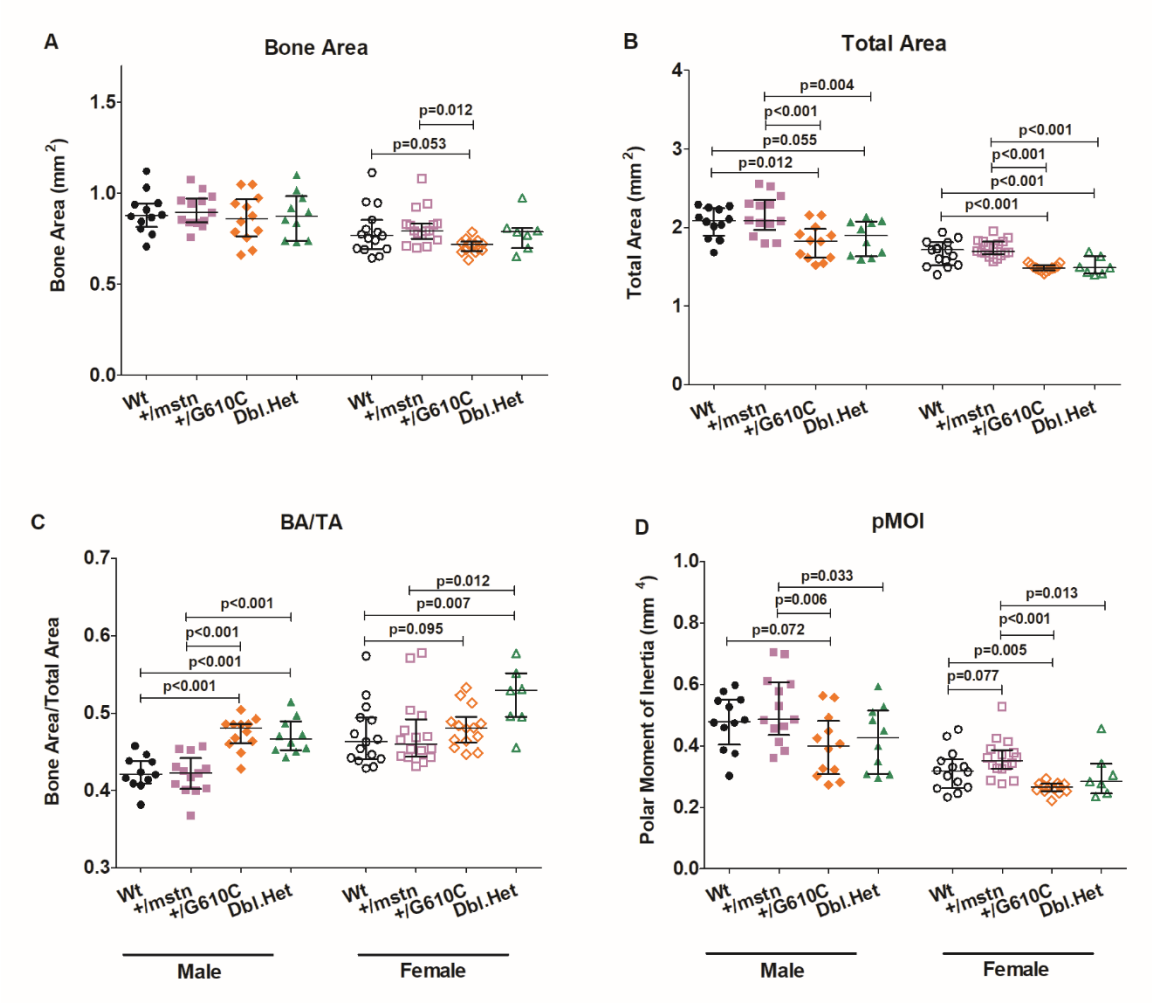

Figure II.7: Inherent myostatin deficiency failed to improve femoral cortical architecture in *+/G610C* mice. µCT analyses of 16 week old male and female Wildtype (Wt, black circle), heterozygote myostatin deficient (*+/mstn*, magenta square), heterozygote *G610C* (*+/G610C*, orange diamond) and double heterozygote *+/mstn* and *+/G610C* (Dbl.Het, green triangle) offspring mid-diaphyseal femoral cortical bone. Cortical bone parameters A) Bone Area (mm^2), B) Total Area (mm^2), C) Bone area fraction (Bone Area/Total Area; BV/TV), and D) Polar Moment of Inertia pMOI; (mm^4). Data were analyzed by MANOVA. No genotype by sex or by dam genotype interactions were found. Offspring genotype main effect was evaluated. Values are median with interquartile range**.** p-values ≤ 0.1 are indicated and considered significant; n = 7-17.

Congenital myostatin deficiency does not improve femoral bone strength

To evaluate bone biomechanical integrity, we assessed femoral biomechanical strength testing via 3-point bend analyses. In male mice, maximum load (Fig. 8B) was equivalent regardless of genotype. Female *+/G610C* and *Dbl.Het* mice, however, exhibited decreased maximum loads as compared to sex-matched Wt littermates. Yield load (Fig. 8C) remained unchanged in mice regardless of sex or genotype. Whereas female *+/G610C* offspring exhibit similar ductility (Fig. 8D), stiffness (Fig. 8E) and work-to-fracture (WTF, Fig. 8F) as Wt and *Dbl.Het* offspring, male *+/G610C* mice had reduced femoral stiffness and work to fracture relative to both Wt and *+/mstn.* Congenital myostatin deficiency restored stiffness to Wt levels but had no effect on WTF in male *Dbl.Het* mice.

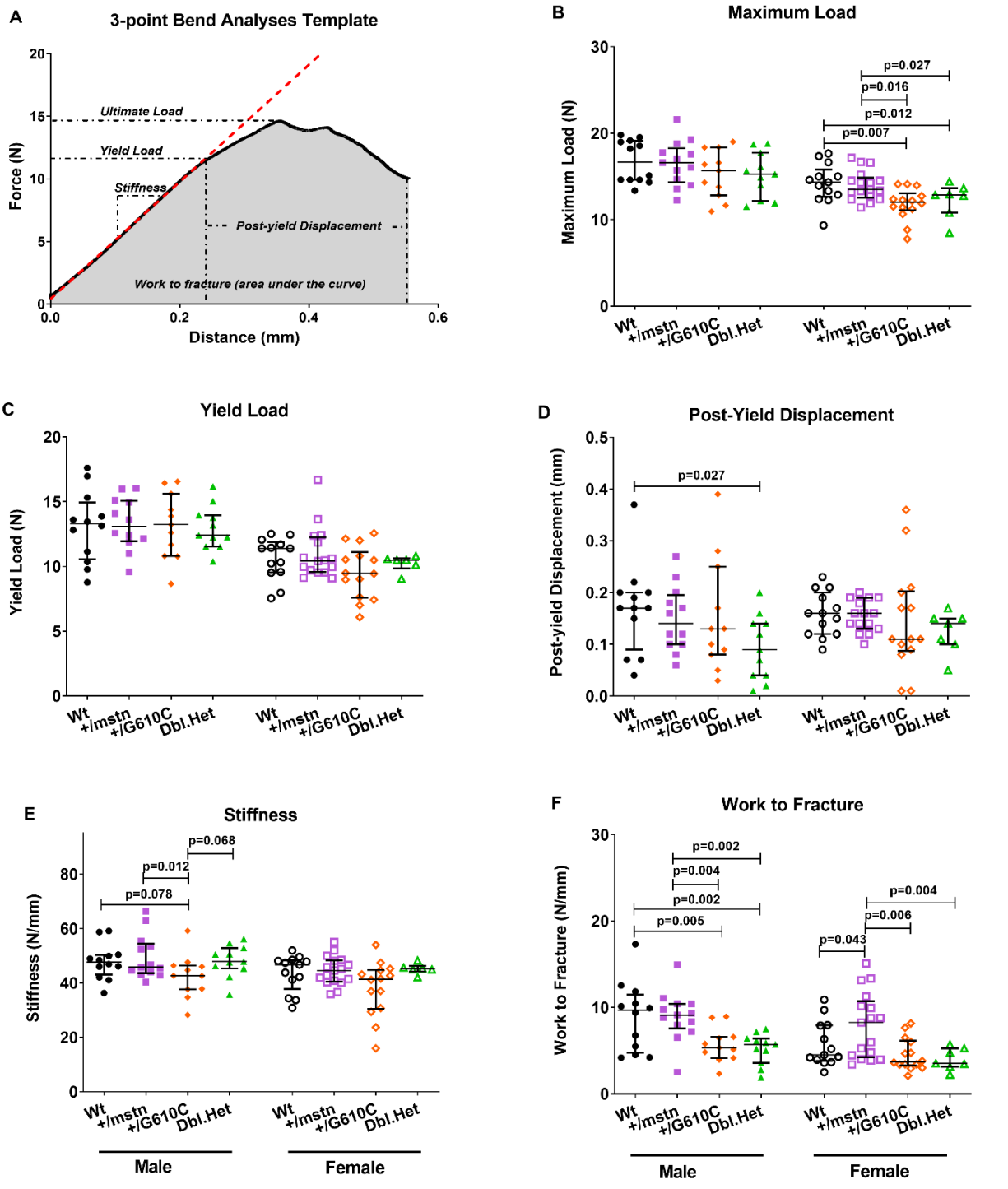

Figure II.8: Inherent myostatin deficiency does not improve femoral bone strength in *+/G610C* mice. Three-point bend biomechanical testing of 16 week old male and female (Wt, black circle), heterozygote myostatin deficient (*+/mstn*, magenta square), heterozygote *G610C* (*+/G610C*, orange diamond) and double heterozygote *+/mstn* and *+/G610C* (Dbl.Het, green triangle) offspring femurs. 3-point bend analysis was

performed as illustrated in (A). Biomechanical parameters: B) Maximum Load (N), C) Yield Load (N), D) Ductility (mm), E) Stiffness (N/mm) and F) Work to Fracture (Nmm). Data were analyzed by MANOVA. No genotype by sex or by dam genotype interactions were found. Offspring genotype main effect was evaluated. Values are median with interquartile range**.** P-values ≤ 0.1 are indicated and considered significant; n = 6-17.

Approach 2- Pharmacological Myostatin Inhibition

Pharmacologic myostatin inhibition improves muscle weights in the +/G610C mouse

We have previously reported the potent effects of sActRIIB-mFc on musculoskeletal properties in the *G610C* mouse[19,20]. However, sActRIIB-mFc binds multiple ligands in addition to myostatin. To determine whether myostatin inhibition was the primary effector of the valuable impact of sActRIIB-mFc on the bone phenotype, mice were administered intraperitoneal injections with Regn647 (humanized monoclonal antibody with high specificity to myostatin) twice a week for either 11 weeks or 7 weeks followed by a 4-week treatment hiatus (Fig.9A). At the end of the treatment period, control antibody (Regn1945) treated Wt and *+/G610C* mice had similar body weights as congenic Wt and *+/G610C* offspring from approach 1 [male Wt (28.32±0.82g; 27.54±0.52 g); female Wt (20.88±0.38 g; 22.11±0.33 g); male *+/G610C* (28.71±0.52 g; 26.69±0.43 g); female *+/G610C* (20.45±0.39 g; 20.96±0.35 g) respectively] (Fig.9B), demonstrating that non-specific control antibody treatment did not impact body weight.

Regn647 treatment resulted in increases in final body weights at 16 weeks of age in Wt animals regardless of sex [male +8.5%, female +11.0% (7-week treatment); male +9.1%, female +15.9% (11-week treatment)] relative to their control-treated counterparts (Fig.9B). Conversely, in both male and female *+/G610C* mice, we observed increases in final body weights in the 7-week treatment group only [male +5.7%, female +8.9%]; although the 11-week treatment *+/G610C* group exhibited similar increases but did not reach statistical significance [male +5.0% p=0.17, female +5.9% p=0.15]. These increases were observed to begin between 6 and 7 weeks of age in Wt mice and between

8 and 9 weeks of age in *+/G610C* mice with early responses in males. (Fig.9C-D; Table 3).

In Wt mice, postnatal myostatin inhibition also resulted in increased wet gastrocnemius, quadriceps, tibialis anterior and plantaris muscle weights regardless of sex and treatment duration (~ + 19.7-40%, + 21.9-38.6%, + 14.9-50.7% and + 11.4-30.4% respectively) (Fig.10). Interestingly, female Wt mice exhibited a more robust increase in wet muscle weights than their male littermates. The muscle weights of *+/G610C* male and female mice treated with Regn647 were also increased regardless of treatment duration [gastrocnemius (+13.5-26.2%), quadriceps (+16.3-28.5%), tibialis anterior (+24.6-29.6%) and plantaris (+16.0-23.0%)], although to a lesser extent than Wt (Fig.10). In-situ contractile generating force analyses revealed increases in relative peak tetanic forces in Wt female tibialis anterior muscle regardless of the Regn647 treatment duration and a decline in the relative peak tetanic force in gastrocnemius muscle in the 11 week Regn647 treatment (Fig.11). No significant treatment effect was found in male Wt and male and female *+/G610C* muscle functionality, respectively, possibly due to small sample sizes and high data variation.

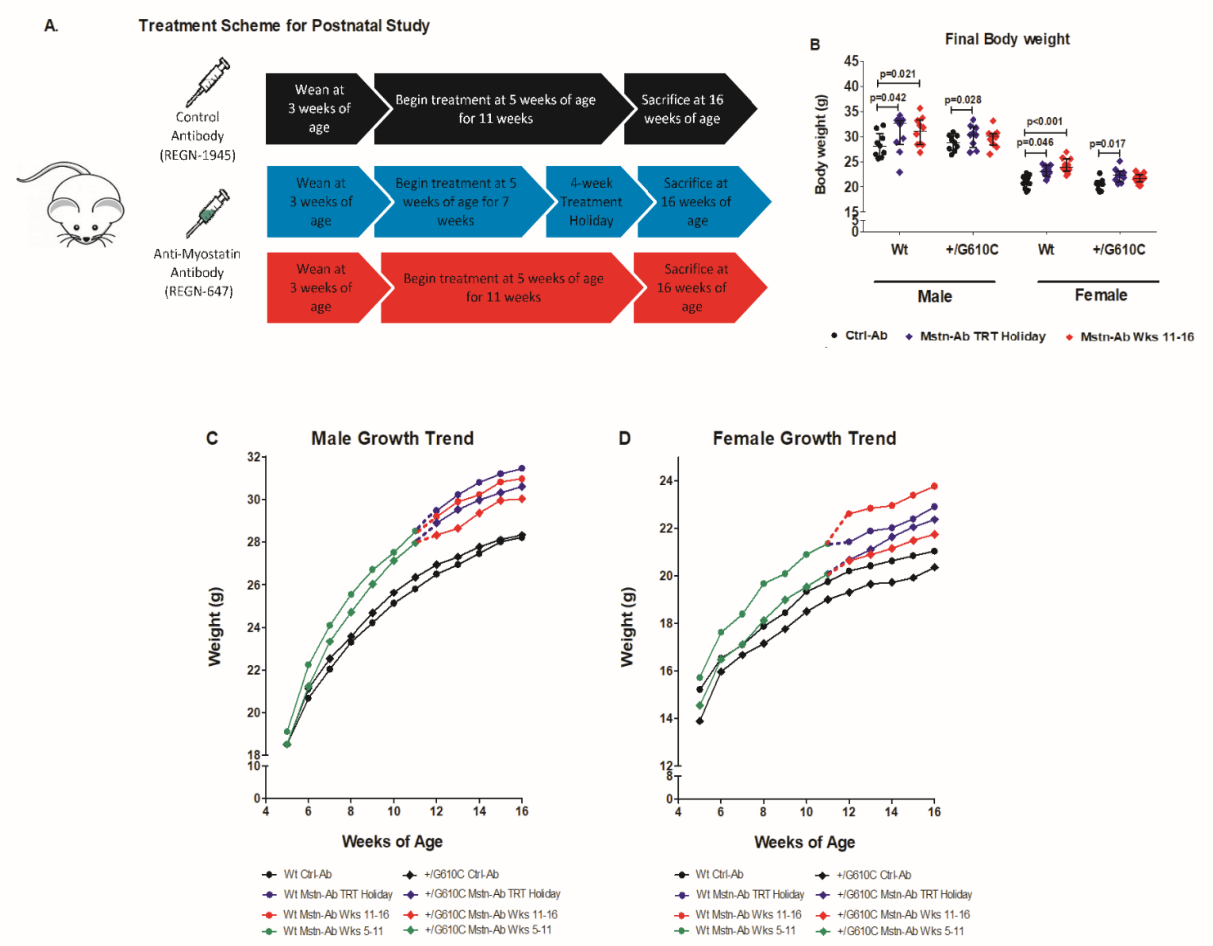

Figure II.9: Anti-myostatin antibody treatment increases body weights of Wt and *+/G610C* mice after only 1 week of treatment. A) Schematic of postnatal myostatin inhibition treatment regimen; Wt and *+/G610C* mice were treated twice weekly with either a monoclonal anti-myostatin antibody (Regn647) for 11 weeks (Mstn-Ab 11wk, *red*) or for 7 weeks followed by a 4-week treatment hiatus (Mstn-Ab 7wk, *blue*), or control antibody for 11 weeks (Regn1945, Ctrl-Ab, *black*). B) Body weights of male and female Wt and *+/G610C* mice at 16 weeks of age. C) and D) Weekly body weights of male and female mice starting at 5 weeks of age, respectively. Control treatment (black symbols) is administered from 5-16 weeks of age. Mstn-Ab treatment is administered from 5-11 weeks (green symbols) at which point the cohort is randomly divided into two groups: Mstn-Ab TRT Holiday [blue; no further Regn647 treatment ("treatment holiday") until sacrifice at 16 weeks of age] and Mstn-Ab Wks 11-16 (red; continuous Mstn-Ab treatment until sacrifice at 16 weeks of age). For significance values, see Table 2. Data were analyzed by MANOVA (in B) and AR(1) model (in C and D). No significant genotype by sex by treatment interaction was found. For (B), body weight values are median with interquartile range**.** p-values ≤ 0.1 are indicated and considered significant. For (C and D) values are means. n = 9-12.

Table II.3a: Significance values for weekly comparison of body weights of Mstn-Ab TRT Holiday and Mstn-Ab Wks 11-16 treated male *+/G610C* and Wt mice relative to their Ctrl-Ab treated counterparts (Fig. 7C).

Treatment	Wk. 5	Wk. 6	Wk. 7	Wk. 8	Wk. 9	Wk. 10	Wk. 11	Wk. 12	Wk. 13	Wk. 14	Wk. 15	Wk. 16
+/G610C Mstn-Ab TRT Holiday	ns	ns	ns	0.086	0.039	0.023	0.014	0.011	0.004	0.005	0.004	0.003
+/G610C Mstn-Ab Wks 11-16								0.065	0.078	0.036	0.014	0.024
Wt Mstn-Ab TRT Holiday	ns	0.044	0.008	0.004	0.001	0.002	0.001	0.001	0.000	0.000	0.001	0.000
Wt Mstn-Ab Wks 11-16								0.003	0.001	0.003	0.002	0.003

Not significant (ns) at p≤ 0.1. Data were analyzed by AR(1) model

Table II.3b: Significance values for weekly comparison of body weights of Mstn-Ab TRT Holiday and Mstn-Ab Wks 11-16 treated female *+/G610C* and Wt mice relative to their Ctrl-Ab treated counterparts (Fig. 7D).

Treatment	Wk. 5	Wk. 6	Wk. 7	Wk. 8	Wk. 9	Wk. 10	Wk. 11	Wk. 12	Wk. 13	Wk. 14	Wk. 15	Wk. 16
+/G610C Mstn-Ab TRT Holiday	ns	ns	ns	ns	0.062	0.101	0.105	0.084	0.070	0.016	0.007	0.011
+/G610C Mstn-Ab Wks 11-16								0.073	0.096	0.052	0.034	0.061
Wt Mstn-Ab TRT Holiday	ns	ns	0.071	0.013	0.022	0.029	0.026	ns	0.092	0.110	0.075	0.031
Wt Mstn-Ab Wks 11-16								0.005	0.005	0.006	0.003	0.001

Not significant (ns) at p≤ 0.1. Data were analyzed by AR(1) model

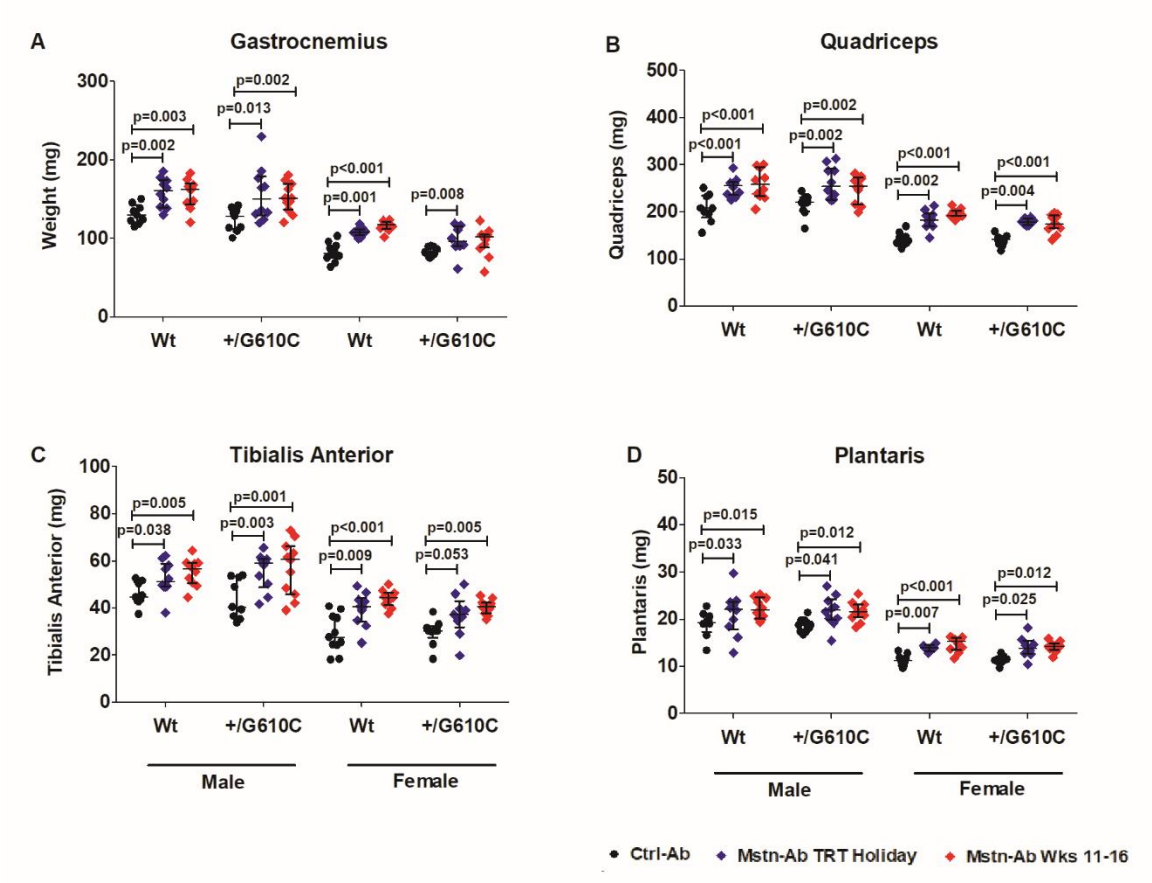

Figure II.10: Postnatal myostatin inhibition increases hindlimb muscle mass in Wt and *+/G610C* mice. Male and female Wt and *+/G610C* mice were treated twice weekly with either a monoclonal anti-myostatin antibody (Regn647) for 11 weeks (Mstn-Ab Wks 11-16, *red*) or for 7 weeks followed by a 4-week treatment hiatus (Mstn-Ab TRT Holiday, *blue*), or a control antibody for 11 weeks (Regn1945, Ctrl-Ab, *black*). Weights of A) Gastrocnemius B) Quadriceps C) Tibialis Anterior and D) Plantaris muscles at 16 weeks of age. Data were analyzed by MANOVA. Values are median with interquartile range. p-values ≤ 0.1 are indicated and considered significant. n = 9-12.

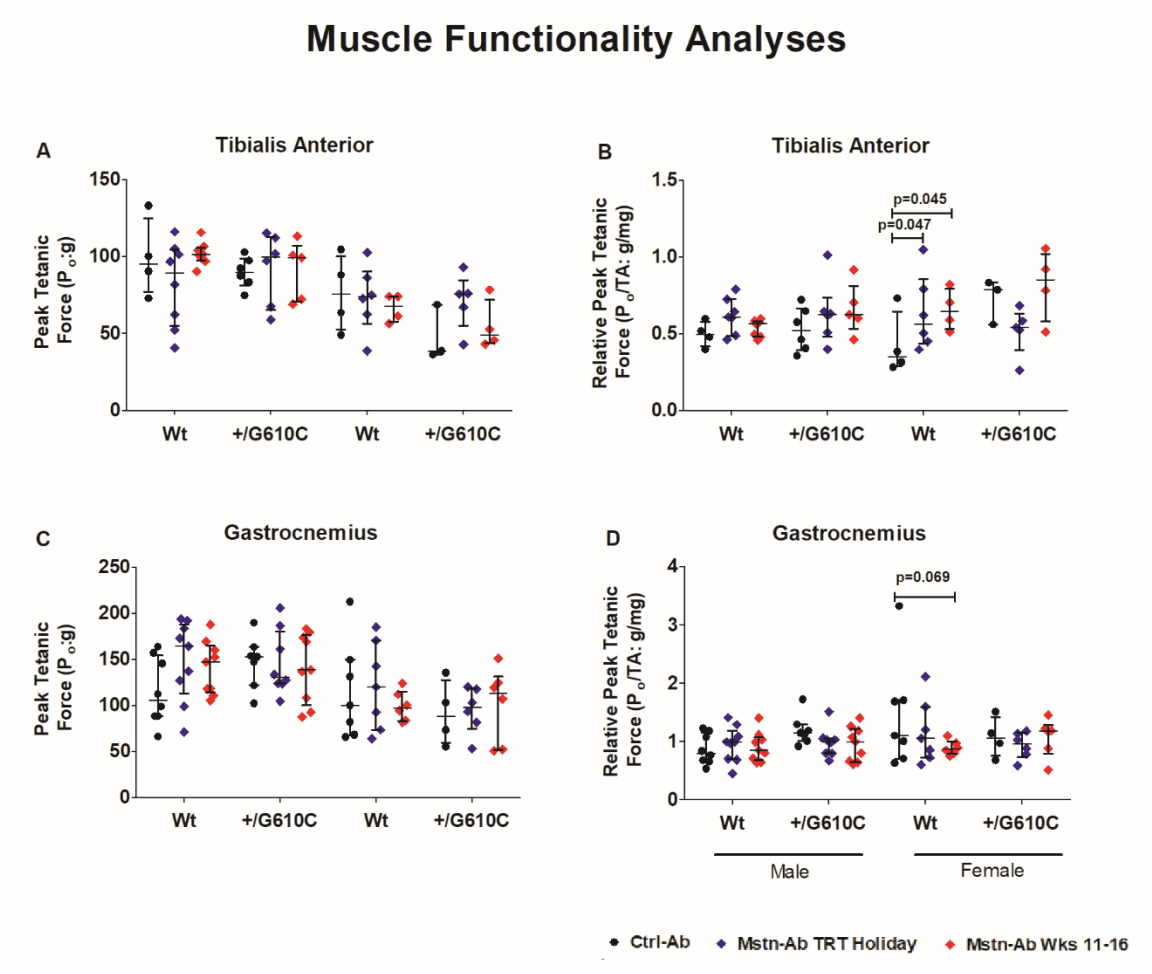

Figure II.11: Postnatal myostatin inhibition increases contractile force in Wt, but not *+/G610C* mice. Male and female Wt and *+/G610C* mice were treated twice weekly with either a monoclonal anti-myostatin antibody (Regn647) for 11 weeks (Mstn-Ab 11wk, *red*) or for 7 weeks followed by a 4-week treatment hiatus (Mstn-Ab TRT Holiday, *blue*), or a control antibody for 11weeks (Regn1945, Ctrl-Ab, *black*). Peak tetanic and relative peak tetanic forces of Tibialis Anterior (A and B) and Gastrocnemius (C and D) muscles at 16 weeks of age, respectively. Data were analyzed by MANOVA. Values are median with interquartile range. P-values ≤ 0.1 are indicated and considered significant. n = 3-9.

Pharmacologic myostatin inhibition improves bone microarchitecture in male Wt mice, but not female Wt or +/G610C male and female mice.

At 16 weeks of age, *+/G610C* mice had reduced trabecular bone microarchitectural parameters as compared to Wt littermates regardless of sex in accordance with known *+/G610C* bone properties[79]. µCT analyses also revealed that in *+/G610C* mice, TV (Fig.12A) was increased in males with the 11-week treatment but remained unchanged in female mice although there appeared to be a difference in TV in the 11 week treatment group relative to the 7 week treatment group. BV (Fig.12B), Tb.Sp (Fig.12C), BV/TV (Fig.12D), Tb.N (Fig.12E), Tb. Th (Fig.12F) and BMD (Fig.12G) appear essentially unaffected in either male or female *+/G610C* littermates by Regn647 treatment, although in male *+/G610C* the BV/TV in the 11 week Regn647 treatment group appeared to be increased. BV/TV was significantly increased in male Wt mice treated with Regn647 regardless of duration, but remained unchanged in female Wt mice. The increased BV/TV in male Wt mice reflects increases in BV, TV, Tb. N and Tb.Th. BMD is also increased in male Wt mice. In addition, female Wt mice experienced increased trabecular TV with Regn647 treatment with minimal impact on other trabecular bone parameters.

Evaluation of the mid-diaphyseal femoral cortical bone parameters demonstrated that neither male nor female *+/G610C* mice exhibited significant changes in cortical bone properties with Regn647 treatment [BA (Fig.13A), TA (Fig.13B), BA/TA (Fig.13C), pMOI (Fig.13D)]. The mid-diaphyseal femoral cortical bone TA (Fig.13B) was lower only in female *+/G610C* mice relative to Wt mice. While surprisingly, *+/G610C* male mice had increased BA/TA relative to Wt mice. BA, TA and pMOI were significantly

increased with Regn647 treatment in male Wt mice. However, these increases were not reflected in the bone area fraction BA/TA. Female Wt mice had increases in TA with Regn647 treatments, as well as increased pMOI with the 11-week Regn647 treatment.

Pharmacologic myostatin inhibition improves femoral bone strength in Wt male, but not Wt female or +/G610C mice.

Biomechanical testing by 3-point bend analyses revealed that *+/G610C* femurs are significantly compromised as compared to Wt with respect to maximum load (female only; Fig.14A), yield load (female only (Fig.14B) and ductility (both male and female; Fig.14C). Male *+/G610C* femurs had high yield loads compared to Wt. Myostatin inhibition increased femoral maximum load and yield load in male Wt mice, but had no significant impact in female Wt or *+/G610C* male and female mice. Increased femoral stiffness (Fig.14D) was observed in male Wt mice in the 11-week Regn647 treatment group with no significant increases in Wt female or *+/G610C* mice. The decreased ductility and work to fracture in *+/G610C* femurs relative to Wt remained unchanged with either treatment duration (Fig.14E). This appeared true for Wt femurs as well.

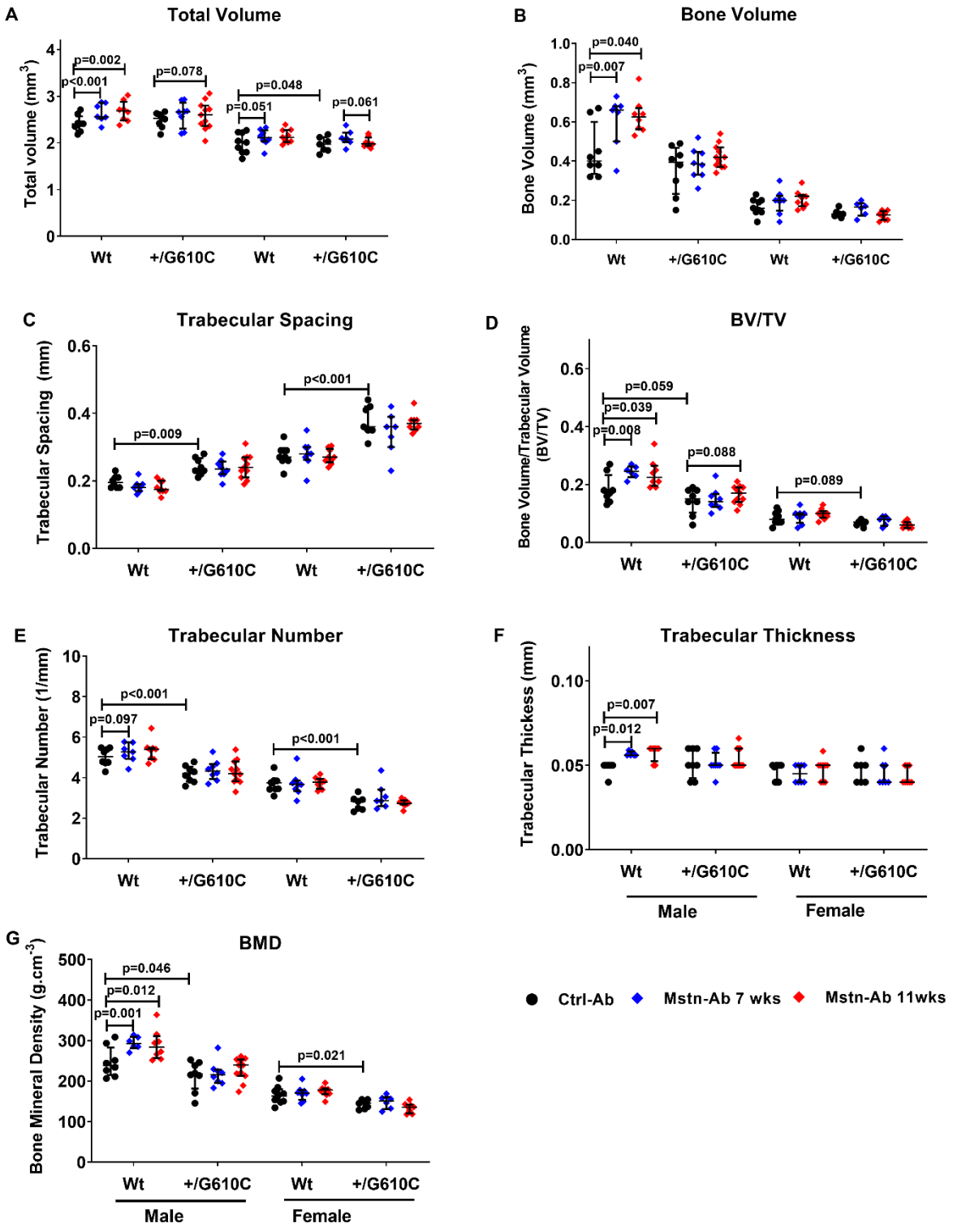

Figure II.12: Postnatal myostatin inhibition improves femoral trabecular bone parameters of Wt male mice. Femoral µCT analyses of 16 week old male and female Wt and *+/G610C* mice treated twice weekly with either a monoclonal anti-myostatin antibody (Regn647) for 11 weeks (Mstn-Ab Wks 11-16, *red*) or for 7 weeks followed by

a 4-week treatment hiatus (Mstn-Ab TRT Holiday, *blue*), or a control antibody for 11weeks (Regn1945, Ctrl-Ab, *black*). Trabecular bone parameters: A) Total Volume (mm^3), B) Bone Volume (mm^3), C) Trabecular Spacing (mm), D) Trabecular Bone volume fraction (BV/TV), E) Trabecular Number (Tb. N; 1/mm), F) Trabecular Thickness (Tb. Th; mm), and G) Bone Mineral Density (BMD; g/cm^2). Data were analyzed by MANOVA. Values are median with interquartile range. P-values ≤ 0.1 are indicated and considered significant. n = 6-11.

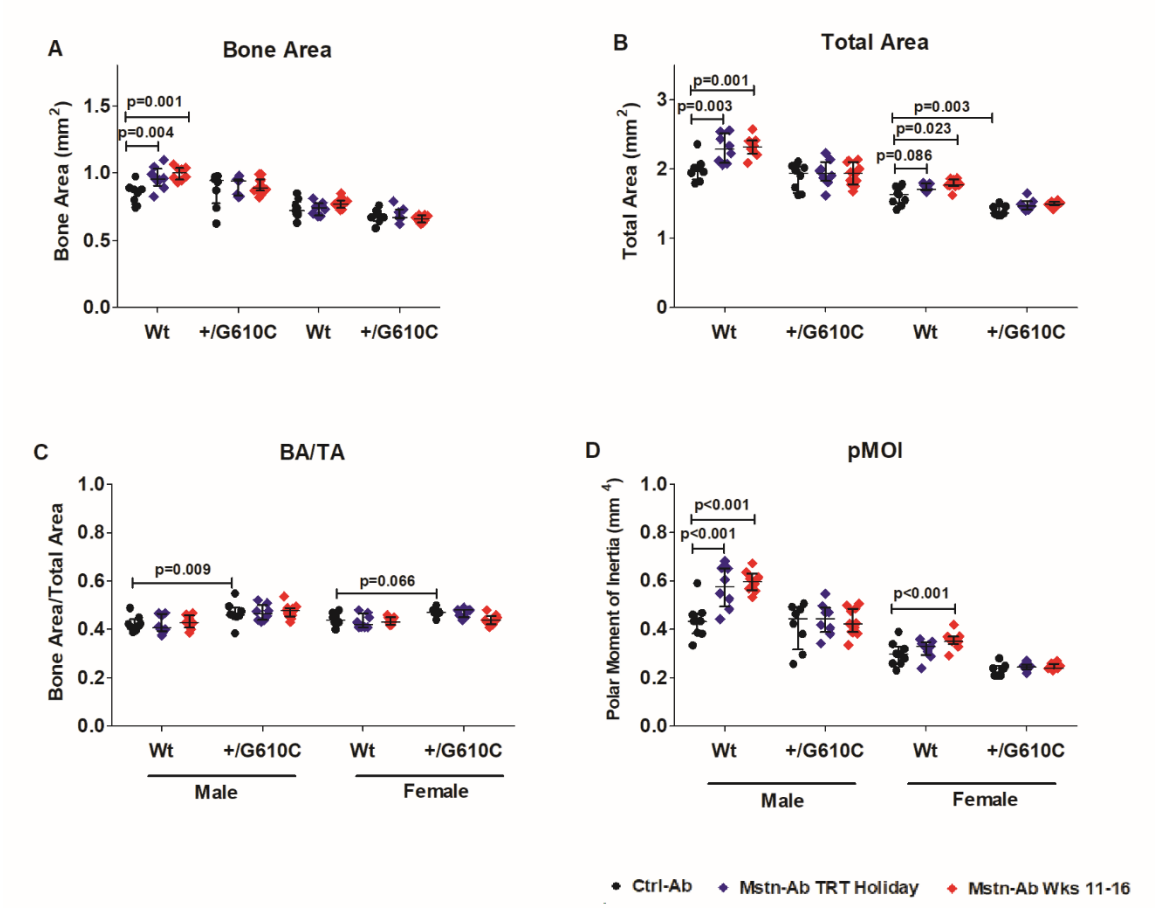

Figure II.13: Mid-diaphyseal femoral cortical bone parameters are improved in Wt males by post-natal myostatin inhibition. µCT analyses of mid-diaphyseal cortical bone of 16 week old male and female Wt and *+/G610C* mice treated twice weekly with either a monoclonal anti-myostatin antibody (Regn647) for 11 weeks (Mstn-Ab Wks 11-16, *red*) or for 7 weeks followed by a 4-week treatment hiatus (Mstn-Ab TRT Holiday, *blue*), or a control antibody for 11weeks (Regn1945, Ctrl-Ab, *black*). Cortical bone parameters: A) Bone Area (mm^2), B) Total Area (mm^2), C) Bone area fraction (BA/TA) and D) Polar Moment of Inertia (mm^4). Data were analyzed by MANOVA. Values are median with interquartile range. p-values ≤ 0.1 are indicated and considered significant. n = 6-11.

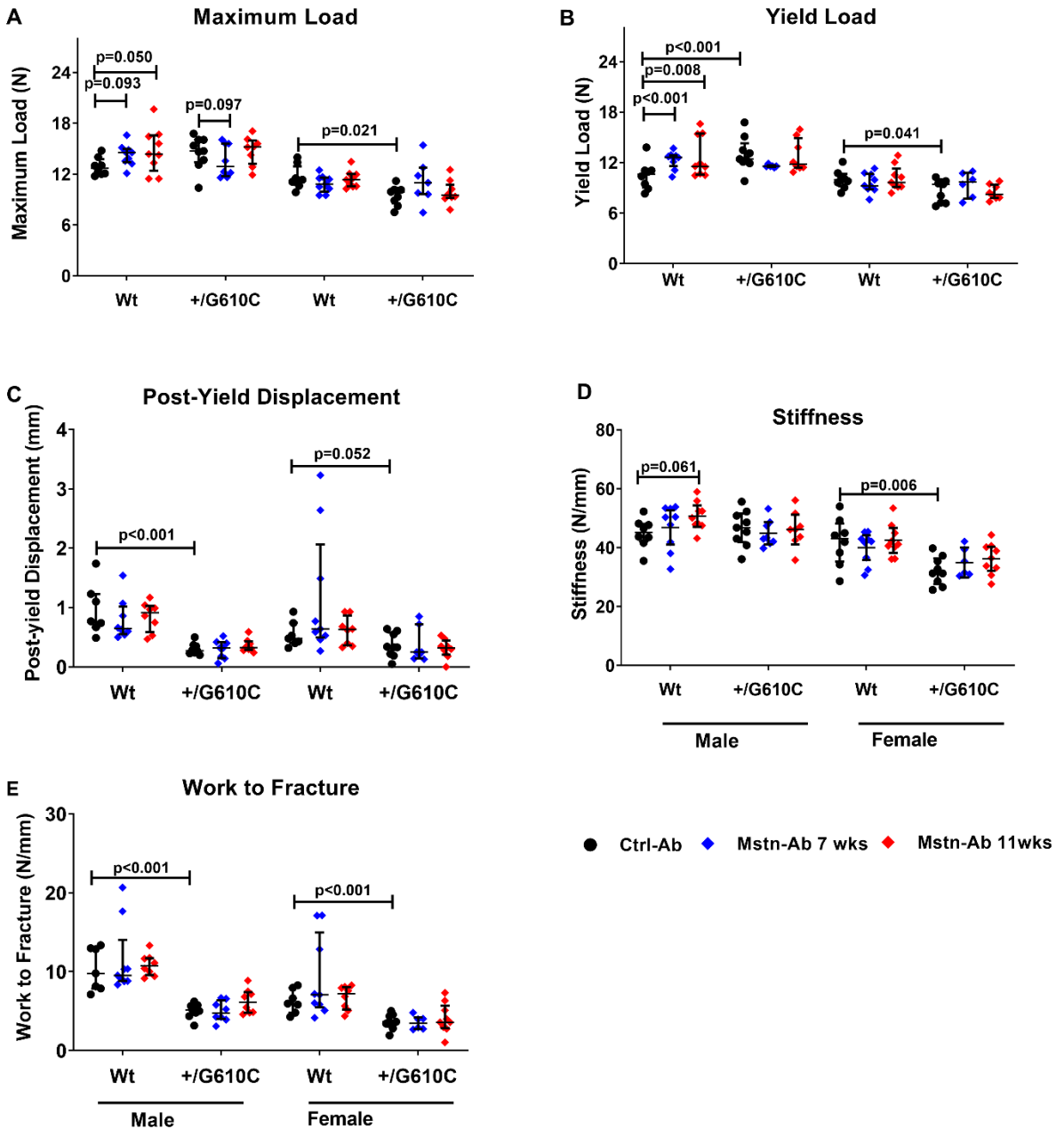

Figure II.14: Post-natal myostatin inhibition improves biomechanical properties of male Wt mouse femurs. Three-point bend biomechanical testing of femurs from 16 week old male and female Wt and *+/G610C* mice treated twice weekly with either a monoclonal anti-myostatin antibody (Regn647) for 11 weeks (Mstn-Ab Wks 11-16, *red*) or for 7 weeks followed by a 4-week treatment hiatus (Mstn-Ab TRT Holiday, *blue*), or a control antibody for 11weeks (Regn1945, Ctrl-Ab, *black*). Biomechanical parameters: A) Maximum Load (N), B) Yield Load (N), C) Ductility (mm), D) Stiffness (N/mm) and E) Work to Fracture (Nmm). Data were analyzed by MANOVA. Values are median with interquartile range. p-values ≤ 0.1 are indicated and considered significant. n = 6-11.

Discussion

This study demonstrated that inhibition of myostatin, whether genetic or pharmacological, increased individual hindlimb muscles in Wt mice and the *G610C* mouse model of OI. However, in bone, congenital myostatin deficiency had greater skeletal improvements, relative to the pharmacologic inhibition of myostatin. The *+/G610C* muscle response to genetic myostatin inhibition closely mirrored that of heterozygous *+/oim* mice with inherent myostatin deficiency (*+/oim +/mstn*) as previously reported[84,221]. However, in +/*oim* mice the response was more robust, with observed increases and restoration of the trabecular and bone biomechanical properties to Wt levels[221]. The divergent treatment outcomes echo several recent studies suggesting the influence of mutation and disease severity on treatment efficacy in OI[222]. In models of moderate (*+/G610C*) and severe (*Col1a1*$^{Jrt/+}$ and *Crtap*$^{-/-}$) OI, whether caused by dominant (*+/G610C* and *Col1a1*$^{Jrt/+}$) collagen or recessive (*Crtap*$^{-/-}$) mutations, pharmacologic inhibition of sclerostin, an inhibitory ligand to bone formation, improved bone mass and strength[118,122,123]. In contrast, *+/G610C* and *Crtap*$^{-/-}$ mice both respond to TGF-β inhibition, while the *Col1a1*$^{Jrt/+}$ mouse does not[114,118,121]. Furthermore, sActRIIB-mFc improved both *+/G610C* and *oim/oim* muscle mass, but increased muscle contractility only in *oim/oim* mice, while improving bone biomechanics only in *+/G610C*[19,20].

Using a genetic approach, we show that both *+/mstn* and *Dbl.Het* mice had reduced circulating serum myostatin levels relative to Wt and *+/G610C* littermates respectively, which did not reach 50% and exhibited sex differences consistent with potential gene dosage compensation and interactions affecting growth[257]. The observed

increases in *+/mstn* and *Dbl.Het* offspring body and muscle weights relative to their Wt and *+/G610C* littermates were consistent with previous studies[84,121]. *Dbl.Het* body and muscle weights were restored to Wt and *+/mstn* levels similar to the observed restoration of *+/oim +/mstn* body and muscle weights[84]. Although female *+/G610C* mice had improvements to trabecular bone properties and changes to cortical BA and pMOI with genetic myostatin deficiency, there was a lack of biomechanical improvement in the female *Dbl.Het* offspring bone suggesting the architectural improvements were insufficient to overcome the compromised morphologic and material properties[258] of the *+/G610C* bone. Although the µCT resolution used in this study discriminates trabecular microarchitecture in mice including sActRIIB-treated versus control-treated *+/G610C* mice[19] and *+/oim* relative to *+/oim +/mstn*[84], differences in specific microarchitectural parameters may have been blunted that could have been noted with a smaller voxel size[259]. Of additional interest was the observation that besides BV/TV and BV in males, and pMOI in females, *+/mstn* offspring have similar cortical and trabecular bone properties as Wt offspring and these similarities were present in the genetic *+/oim* x *+/mstn* cross as well[84].

Previous studies to reduce circulating endogenous myostatin using a soluble ActRIIB decoy molecule resulted in improved muscle and bone properties[19,20,22,200,241,260], yet proved problematic as ActRIIB binds multiple ligands, preventing the appreciation of specific mechanisms and responses as well as resulting in unwanted side-effects[18,23]. Consequently, to begin to decipher the role of the ActRIIB ligands, we explored myostatin inhibition in Wt and the *G610C* mouse using a specific monoclonal anti-myostatin antibody (Regn647) for 11 weeks. Regn647 treated Wt mice

responded swiftly to treatment with greater body weights after 1-2 weeks of treatment consistent with a previous study of sActRIIB-mFc administration[19]. In contrast, Regn647-treated *+/G610C* mice saw increases in body weights after 3-4 weeks of treatment.

Current management of OI relies on BPs, bone anti-resorptive agents, to stall bone resorption by inhibiting osteoclast activity[230]. Although intravenous BPs have been shown to reduce the risk of fractures, prolonged BP use is associated with an impairment of bone remodeling in children[97]. Thus, in the second treatment approach, we further investigated the effect of a 4-week treatment holiday after 7-week anti-myostatin antibody treatment. We did not observe changes in body weight or bone properties in the subsequent weeks after the anti-myostatin treatment was stopped (i.e. between 11 and 16 weeks of age) in either Wt or *+/G610C* mice, relative to the 11-week treatment group, suggesting that there was not a significant rebound effect from the absence of anti-myostatin antibodies on the musculoskeletal properties studied. Though we did not examine the skeletal properties at the 7- week time point in Wt and *+/G610C,* the lack of differences in skeletal properties at the end of the study, suggests the 4-week treatment hiatus was not detrimental.

Regn647 administration revealed sex- and disease-specific responses of bone. Muscle weights of all the mice were significantly increased with anti-myostatin treatment regardless of genotype or sex. However, significant improvements in trabecular and cortical bone properties as well as femoral biomechanical strength were only observed in male Wt mice. Previous reports suggest skeletal muscles of male C57 mice have less processed myostatin (- 40-60%)[261] and ACVR2B expression[262] as compared to female

mice, which may result in male and female mice requiring different anti-myostatin treatment dosages to elicit equivalent responses. The presence of sexual dimorphism in the myostatin signaling pathway, sex-hormone availability, and sex-specific bone response to treatment[105] further suggests different therapeutic agents may react differently and/or require different maximal treatment dosages or duration to achieve similar responses in male and female mice. Further, during puberty (3-8 weeks of age), male mice have more substantial increases in body weight and bone cross-sectional area relative to female mice[263]. Thus, the absence of a more pronounced skeletal impact with myostatin deficiency in male *Dbl.Het* mice also suggests that myostatin may have a less robust regulatory role in whole bone development.

Administration of sActRIIB-mFc improved bone volume and strength in a variety of mouse models including *G610C*[19,200]. Pearsall and colleagues previously showed that blockade of activin A with a soluble decoy receptor to activin A (ActRIIA-mFc) stimulated bone formation and improved skeletal integrity in C57BL/6N mice[162]. The lack of a robust response in bone parameters in *+/G610C* mice to Regn647 suggests that pharmacologic myostatin inhibition alone is insufficient to elicit the desired effects on bone[235,241]. This necessitates consideration of a combined treatment approach of inhibiting both myostatin and activin A, which may result in synergistic increases in musculoskeletal properties as was previously observed in muscle mass (+43.9% TA muscle, SCID mice[22]) relative to myostatin inhibition alone (+20.1%, TA muscle[22])[264]. Myostatin has been implicated in the inhibition of osteoblast differentiation and activity and the promotion of osteoclast differentiation by stimulating RANKL secretion[188,216]. Activin A is also a known pro-osteoclastogenic molecule[265],

further suggesting that simultaneous inhibition of both myostatin and activin A will more likely produce more pronounced skeletal responses similar to those observed with ActRIIB ligand trapping experiments[19,241]. However, gene mutation variance and disease severity may dictate treatment response as treatment with a myostatin and activin specific ActRII ligand trap did not improve skeletal features of the *Col1a1*$^{Jrt/+}$ mouse[200]. Musculoskeletal dysfunctions in the *G610C* mouse including, but not limited to defective mechanotransduction, compromised osteoblast differentiation, and malfunction as a result of endoplasmic reticulum stress[85], may blunt the *G610C* bone response to myostatin inhibition. A limitation of this study was the use of the maximal effective dose of anti-myostatin antibody based on Wt mice[22] as standard for treating *+/G610C* mice. Further studies are warranted to determine the maximal effective treatment dose for *+/G610C* mice, as well as potential synergism of anti-activin A to inhibit osteoclastogenesis.

In conclusion, both the genetic and pharmacologic inhibition of myostatin resulted in increased muscle mass in Wt and *+/G610C* mice, and improved bone mass and strength in Wt male mice. These data have implications for improving muscle mass as well as bone mass and strength in heritable and acquired bone fragility, including osteoporosis. Only genetic myostatin deficiency resulted in significant increases to bone volume and strength in the *+/G610C* mouse. In the pharmacologic study, circulating myostatin levels were reduced from 5 weeks of age until 16 weeks, whereas in the genetic study, the deficiency in circulating myostatin levels was present throughout development. Myostatin modulates muscle progenitor cell proliferation[203], and its loss of function results in muscle cell hyperplasia and hypertrophy[15], while postnatal myostatin inhibition leads to hypertrophy only, with no hyperplasia[20,22]. Consequently, the

synergistic impact of increased muscle mass and possible developmental reprogramming and epigenetic changes as a result of genetic myostatin deficiency in the *Dbl.Het* offspring underscores the importance of understanding the developmental changes in both muscle and bone, when compared with postnatal myostatin inhibition. Thus, benefits of congenital myostatin reduction are likely due to both developmental effects and ongoing myostatin deficiency. It is therefore possible that earlier administration of the anti-myostatin antibodies may be required to result in more robust increases in bone properties in OI.

CHAPTER III

COMBINATORIAL MYOSTATIN AND ACTIVIN A INHIBITION MORE POTENTLY IMPROVES MUSCLE AND BONE IN THE *G610C* MOUSE MODEL OF OSTEOGENESIS IMPERFECTA

Catherine L. Omosule[1], Dominique Joseph, Brooke Weiler[1], Victoria L. Gremminger[1], Spencer Silvey, Youngjae Jeong[1] Sandra Kleiner[2], Charlotte L. Phillips[1,3*]

[1]Department of Biochemistry, University of Missouri, Columbia, Missouri, 65211; [2] Regeneron Pharmaceuticals, Tarrytown, New York, 10591;[3]Department of Child Health, University of Missouri, Columbia, Missouri, 65211

Abstract

Introduction: Defects in the production, quantity and/or quality of type I collagen causes osteogenesis imperfecta (OI), a collagen-related bone disorder that is characterized by fragile osteopenic bone which easily fractures, and muscle weakness. We have previously shown that the soluble activin receptor type IIB decoy (sActRIIB) molecule which binds multiple TGF-β ligands including myostatin and activin A, increases muscle mass and improves bone strength in the mild to moderate *G610C* mouse model of OI. Here, we investigate the musculoskeletal effects of inhibiting activin A alone, myostatin alone, or both in wild type (Wt) and heterozygous *G610C* (*+/G610C*) mice using highly specific monoclonal antibodies.

Methods: Male and female Wt and *+/G610C* mice were treated twice weekly with intraperitoneal injections of monoclonal control antibody (Ctrl-Ab, Regn1995), activin A antibody (ActA-Ab, Regn2746), myostatin antibody (Mstn-Ab, Reg647) or both antibodies (Combo, Regn2746 and Regn647) from 5 to 16 weeks of age. Pre-euthanasia, whole body composition, metabolic and muscle force generation assessments were performed. Post euthanasia, hind limb muscles were evaluated for mass, and femurs evaluated for changes in microarchitecture and strength using microCT (μCT) and 3-point bend analyses.

Results: ActA-Ab had minimal effects on hindlimb muscles mass and force production, body weights and bone microarchitecture in *+/G610C* mice, although Wt male mice exhibited increases with ActA-Ab treatment. In fact, ActA-Ab treatment decreased bone strength in male *+/G610C* mice. Mstn-Ab, as previously reported, significantly improved

hindlimb muscle weights and overall body weights in Wt and male *+/G610C* mice, but had minimal skeletal impact in *+/G610C* mice. Conversely, Combo treatment outperformed ActA-Ab alone or Mstn-Ab alone, consistently increasing hindlimb muscle and body weights regardless of sex or genotype, and improving bone microarchitecture and strength in both male and female *+/G610C* and Wt mice.

Conclusion: Combinatorial inhibition of activin A and myostatin more potently increased muscle mass and bone microarchitecture and strength, recapturing most of the observed benefits of sActRIIB treatment in +/*G610C* mice.

Keywords: Osteogenesis imperfecta, myostatin, activin A, muscle, bone

Introduction

Osteogenesis imperfecta (OI) arises from defects in the structure, quantity and/or processing of type I collagen, which makes up about 90% of skeletal bone proteins[5,6]. OI affects 1 in 10-15000 live births[73,83]. Phenotypically, patients present with a range of features, key among which are bone fragility, decreased bone mineral density (BMD) and an increased propensity to fracture. Patients may also have skeletal deformities and growth retardation. OI is a connective tissue disorder, hence muscle weakness, joint hypermobility, dentinogenesis imperfecta, blue sclera, and hearing loss in adulthood are commonly associated extra-skeletal features[5,73]. Genetically, OI is variable, and has been associated with over 1500 causative mutations, about 85-90% of which affect the structure and quantity of type 1 collagen[74]. Classical autosomal dominant OI is grouped into four types according to disease severity: I (mild OI); II (perinatally lethal OI); III (most severe survivable form of OI); IV (moderately severe OI)[81]. A revised OI classification paradigm currently accounts for additional types of OI caused by defects in osteoblast development, bone mineralization, collagen folding and cross-linking, and collagen processing, resulting in 16 types of OI (I-XVI)[5,6]. To improve mobility with OI, orthopedic surgery, physical therapy and therapeutics, particularly bisphosphonate therapy, are employed[5,73]. Intramedullary rods stabilize and strengthen long bones[11], but can migrate into soft tissues and joints, necessitating replacement surgeries[10,266]. Children with OI have decreased trabecular bone thickness and number; decreased bone formation and increased bone remodeling relative to age-matched healthy children[109], so bisphosphonates, which are potent bone antiresorptive agents, are employed in an attempt to decrease bone-resorption [73]. However, bisphosphonate use in children delays healing

of osteotomies and impairs metaphyseal modeling[9,231]. Consequently, better treatment strategies need to be implemented.

The *G610C* mouse model of OI has defects in the α2(I) chain of type I collagen and models mild to moderate type I/IV human OI[79]. Heterozygous *G610C* mice (*+/G610C*) are phenotypically and genetically identical to an OI founder population with a glycine to cysteine transition in their collagen α2(I) chain[79]. Increased susceptibility to skeletal fracture, decreased bone strength and BMD characterize the *+/G610C* bone, which models patients' characteristics[79].

Transforming growth factor β (TGF-β) ligands, especially those in the bone morphogenetic proteins (BMPs), growth differentiation factors (GDFs) and activin subfamilies have long been known to influence bone development[34,267]. Myostatin, also known as GDF8, is secreted by myotubes and acts in an autocrine manner to negatively regulate muscle fiber size and number[15]. Bone-forming osteoblasts and bone-resorbing osteoclasts also secrete activin A, a pro-osteoclastogenic molecule that increases osteoclastogenesis and decreases the osteogenic potential and mineralization capabilities of osteoblasts *in vitro*[265,268]. Both myostatin and activin A signal through activin receptor type IIB (ActRIIB) which recruits type I tyrosine kinase receptors (Alk4,5,7) and elicits a canonical signaling cascade via Smad proteins. In addition to myostatin and activin A, ActRIIB binds multiple ligands including other activins (B,C,E), GDFs and BMPs[269].

Ligand traps inhibit the interactions of myostatin and activin A with their nascent receptors[18]. One such ligand trap, the soluble activin receptor type IIB decoy molecule

(sActRIIB-mFc, increased muscle mass, bone microarchitecture and strength in *+/G610C* mice[19,20]. ACE-031, another ligand trap which is a fusion protein of ActRIIB and IgG1-Fc, altered body composition by increasing lean body mass, BMD, and reducing overall fat mass in boys with Duchene muscular dystrophy (DMD)[18]. A trend towards functional improvements (6-minute walk test) was also observed although the trial was terminated due to adverse events likely caused by interactions of ACE-031 with other ActRIIB-specific targets[18].

More recently, we have reported on the ability of Regn647, a neutralizing monoclonal myostatin antibody (Regeneron Pharmaceutical Inc.), to increase muscle masses in Wt and *+/G610C* mice[224]. Bone responses were sex-dependent and OI inhibitory in response to Regn647 treatment. Male Wt mice had stronger bones and larger bone volumes whereas female Wt mice had no significant biomechanical improvements. Neither Regn647 treated *+/G610C* male nor female mice had improved bone strength[224]. This data, in contrast to the skeletal observations with sActRIIB treatment suggested that myostatin inhibition alone is unable to effect beneficial skeletal changes in OI, necessitating consideration of a combinatory treatment approach with other ActRIIB-target ligands. That said, Tauer and colleagues showed that ACE-2494, a myostatin and activin A-specific neutralizing antibody increased muscle and bone mass and biomechanical strength in wild type (Wt) mice, but failed to improve bone microarchitecture and strength in the *Col1a1*$^{JRT/+}$ mouse, another model of severe dominant OI[200], further suggesting that disease severity and mutation type may impact treatment response.

Nonetheless, the impact of myostatin inhibition on muscle mass is highly pronounced[20,21,199,200,224,270]. The mechanosensitive properties of bone suggest that increasing muscle mass may trigger changes in bone mass and strength[13,14]. Further, activin A inhibition has been shown to improve bone microarchitecture and strength in C57BL/6N mice, and the bone phenotype in the osteopenic ovariectomized (OVX) mouse model of osteoporosis[162]. OI is genetically and phenotypically variable, such that a treatment that fails to reflect desirable skeletal outcomes in one mouse model, provided it is not detrimental, could be beneficial in other mouse models. Thus, in an attempt to identify which ActRIIB target ligand more potently regulates postnatal skeletal muscle and bone properties in OI, we pursued investigation of inhibition of myostatin, activin A or both ligands with specific neutralizing monoclonal antibodies and report their effects on musculoskeletal properties of *+/G610C* mice in this study.

Methods

Study design, treatment and sample collection

Male and female wild type (Wt) and heterozygous *G610C* (*+/G610C*, *Col1a2*$^{tm1.1Mcbr}$)[79] mice on the C57BL/6 background were genotyped as previously described[19,20,224]. Mice had ad-libitum access to food and water in the University of Missouri AAALAC-accredited facility where they were housed. The University of Missouri ACUC approved study protocols which met the ARRIVE guidelines[247]. Mice were randomly assigned to control antibody (Regn1945) or treatment groups [Activin A antibody (ActA-Ab, Regn2476), Myostatin antibody (Mstn-Ab, Regn647), Combo (both ActA-Ab and Mstn-Ab)]. Treatment was performed as previously described[224]. In brief, mice were injected

twice each week for 11 weeks starting at 5-weeks of age, with 10mg/Kg of body weight of the indicated antibodies. When mice were humanely euthanized at 16 weeks of age, tissues were collected and stored for further analyses. Hindlimb muscles [soleus, extensor digitorum longus (EDL), plantaris, quadriceps, tibialis anterior (TA) and gastrocnemius], were collected and weighed. Femurs were also stored in 1X PBS at -20˚C until analyses.

Indirect Calorimetry and body composition analyses

Prior to sacrifice, between 14-16 weeks of age, indirect calorimetry was performed to evaluate substrate utilization rates, energy metabolism and activity levels using Promethion metabolic cages (Sable Systems, Las Vegas, USA). Mice were individually housed with free access to food and water, and acclimatized a day prior to data collection in the chamber. Metabolic data was acquired over the next two days, the average energy expenditure (EE), mean O_2 consumption (VO_2) and CO_2 production (VCO_2), food and water intake, activity (X, Y, Z-axes beam breaks) and respiratory quotient (RQ) from a full circadian cycle (one 7 pm – 7 am nocturnal phase; and one 7 am – 7 pm diurnal phase) were determined.

Body composition was then assessed using the Echo Magnetic Resonance Imaging (echoMRI) system. System tests were performed prior to each daily set of analyses. The system was also calibrated with a canola oil calibration system prior to use. For assessments, live mice were individually placed in the echoMRI body composition analyzer (E26-242-RMT, Echo Medical Systems, USA). Absolute and relative lean muscle mass, fat mass and total water were determined.

Muscle contractility

Prior to euthanasia, mice were anesthetized with an intraperitoneal injection of ketamine/xylazine/acepromazine. To maintain body temperature at 37˚C during the muscle contractility analyses, mice were placed on heating pads. The left hindlimb was immobilized and the sciatic nerve surgically exposed. The distal tendons of the muscle were attached to a Grass force transducer via silk 4.0, adjusted to the length of the muscle and stimulated to obtain peak twitch with the following parameters: 0.5ms, 0.3Hz, and 6V. Peak tetanic force was acquired using these parameters: 150Hz, 6V for 300ms for each muscle type[249]. All data were collected by using the Power Lab® version 8 software. The set up was performed for the left gastrocnemius, TA and soleus hindlimb muscles.

Femoral Microarchitecture

Excised right femora were cleaned of soft tissues, wrapped in gauze and stored in 1X PBS at -20˚C until analyses. MicroCT (µCT) analyses were conducted using the vivaCT 40 µCT scanner (SCANCO Medical AG, Bassersdorf, Switzerland) using these parameters: 70kVp, 114µA, 8W X-ray energy intensity and high-resolution CT-scan with 10 um isotropic voxel size (10 x 10 x 10 um)[250] and an integration time of 300ms as previously described[224].

Femoral Biomechanical Testing

Post- µCT, right femora were subjected to 3-point bend tests using the Instron 5942 Universal testing System (Instron, MA, USA) and the BlueHill 3 Software Version 3.53 (Illinois Tool Works Inc., IL, USA). Bones were placed anterior-posteriorly on support stands that were 9 mm apart. Testing was performed using a load cell with maximum

scale of 5 kg set on an automatic trigger force of 0.2N and a constant speed of 5mm/min until bone failure. Ultimate load, yield load, stiffness, post-yield displacement and work-to-fracture were determined from the load displacement curve using Microsoft Excel as previously described[224].

Statistics

GraphPad Prism (GraphPad Software, San Diego, CA, USA) was used to detect outliers and graph data. Correlations, manova and anova analyses were ran using SAS software (SAS Institute, Inc., Cary, NC, USA). Weekly body weights were analyzed, as previously described using the first order autoregressive AR(1) model[224]. Body and muscle weights at 16 weeks of age, bone microarchitectural and biomechanical data were analyzed independently as a 2 x 2 x 4 factorial [2 genotypes (Wt, *+/G610C*), 2 sexes (male and female), 4 treatments (Ctrl-Ab, Act-Ab, Mstn-Ab, Combo)]. For indirect calorimetry and body composition analyses, data was analyzed as a 2 x 2 x 2 factorial [2 genotypes (Wt, *+/G610C*), 2 sexes (male and female), 2 treatments (Ctrl-Ab, Combo)]. Differences were considered significant at $p \leq 0.1$. Mstn-Ab, ActA-Ab and some Ctrl-Ab data were collected at an earlier time, and a subset of the Ctrl-Ab and Mstn-Ab data previously reported[224].

Results

Growth Trends

Five-week-old male and female Wt and *+/G610C* mice were treated twice weekly with monoclonal antibodies to activin A (ActA-Ab, Regn2746) alone, myostatin (Mstn-Ab, Regn647) alone or both activin A and myostatin (Combo) and compared with control

antibody (Ctrl-Ab, Regn1945). During the 11-week study period, Ctrl-Ab-treated male and female Wt mice had similar body weights as Ctrl-Ab-treated male and female *+/G610C* mice (Figure 1, Table 1). Male and female Wt mice exhibited increases in body weight with ActA-Ab treatment within 1 and 3 weeks of treatment respectively, although ActA-Ab treatment failed to increase body weights in *+/G610C* mice during the study period. Mstn-Ab treatment increased body weights within 2 and 3 weeks of treatment in male and female Wt mice respectively; and within 2 weeks of treatment in male *+/G610C* mice (data previously published [PMID 33249643]), but failed to increase body weights in female *+/G610C* mice. Combinatorial inhibition of both activin A and myostatin (Combo treatment) rapidly increased body weights within the 1st week of treatment in female Wt and male & female *+/G610C* mice; and in the 2nd week of treatment in male Wt mice, respectively.

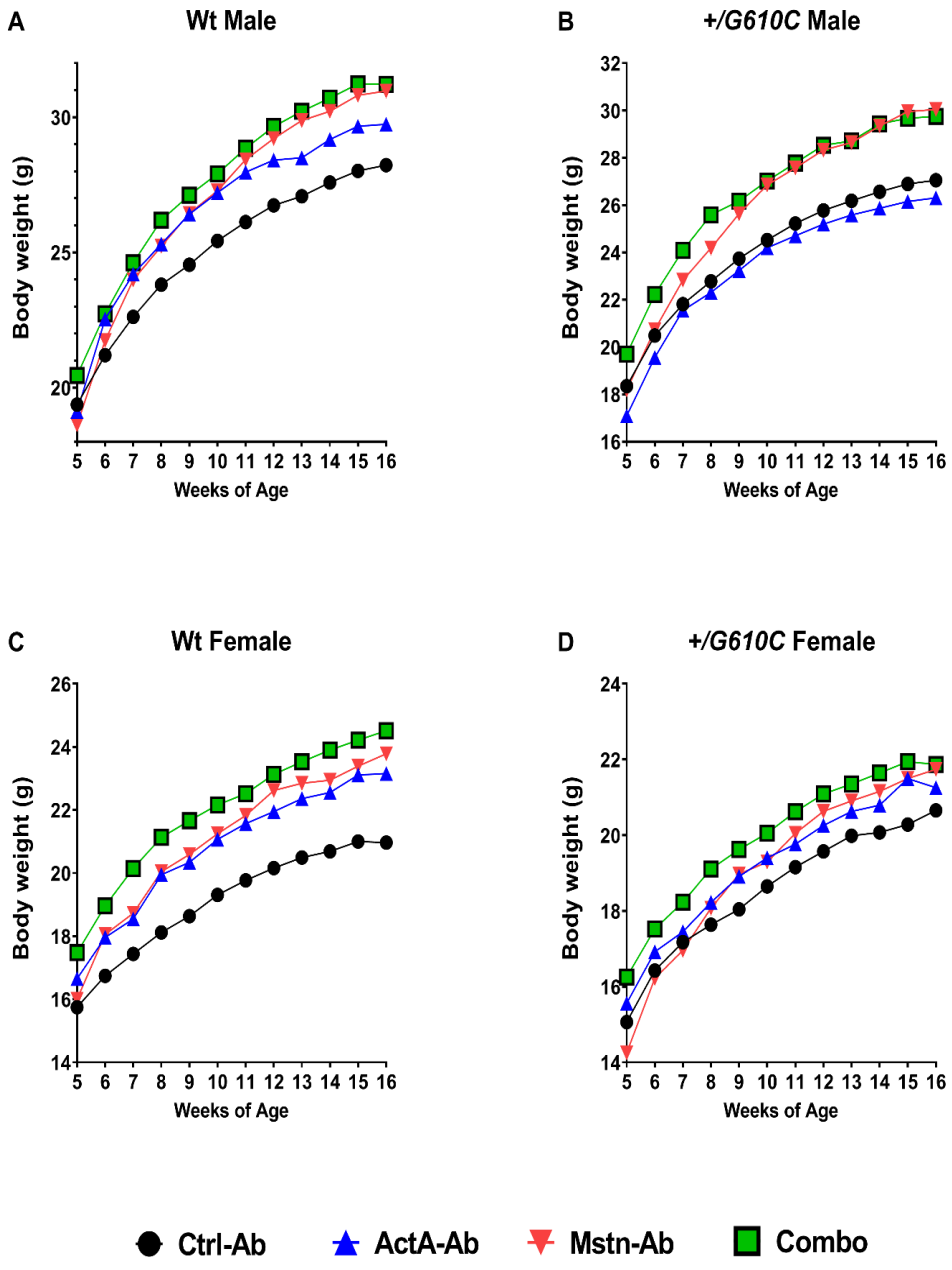

Figure III.1: Changes in body weight with Ctrl-Ab, ActA-Ab, Mstn-Ab and Combo treatment in Wt and *+/G610C* mice over 11-week period. Male Wt (A), Male *+/G610C* (B), Female Wt (C), and Female *+/G610C* (D), were treated with either control antibody (Ctrl-Ab, black circle); activin A antibody (ActA-Ab, blue triangle); myostatin antibody (Mstn-Ab, red triangle) or combination activin A and myostatin antibodies (Combo, green square). Mean values are plotted; n=8-17. $p<0.1$ is indicated (Table 1) and considered significant. Mstn-Ab data were used in an earlier publication[224] and have been included here for ease of comparing to ActA-Ab and Combo treatment data.

Table III.1: P-values for growth trends (Figure 1) in male and female Wt and *+/G610C* mice treated with ActA-Ab, Mstn-Ab or Combo versus Ctrl-Ab (Figure 1)

Genotype /Sex	Treatment	Wk5	Wk6	Wk7	Wk8	Wk9	Wk10	Wk11	Wk12	Wk13	Wk14	Wk15	Wk16
Male Wt vs *+/G610C*		n/s	n/s	n/s	n/s	n/s	n/s	n/s	n/s	n/s	n/s	0.096	n/s
Female Wt vs *+/G610C*		n/s	n/s	n/s	n/s	n/s	n/s	n/s	n/s	n/s	n/s	n/s	n/s
Male Wt	ActA-Ab	n/s	0.0749	0.0343	0.0448	0.0124	0.0176	0.0135	0.0254	0.0569	0.0784	0.064	0.0925
	Mstn-Ab	n/s	n/s	0.0827	0.0706	0.016	0.0187	0.0034	0.0017	0.0004	0.0008	0.0004	0.0005
	Combo	n/s	0.0403	0.0074	0.0014	0.0006	0.0009	0.0003	<0.0001	<0.0001	<0.0001	<0.0001	<0.0001
Male *+/G610C*	ActA-Ab	n/s	n/s	n/s	n/s	n/s	n/s	n/s	n/s	n/s	n/s	n/s	n/s
	Mstn-Ab	n/s	n/s	n/s	0.0632	0.012	0.0021	0.0018	0.0007	0.0011	0.0002	<0.0001	<0.0001
	Combo	0.048	0.011	0.0009	<0.0001	0.0004	0.0002	0.0002	<0.0001	0.0003	<0.0001	<0.0001	<0.0001
Female Wt	ActA-Ab	n/s	n/s	n/s	0.0159	0.0242	0.02	0.018	0.0181	0.0137	0.0137	0.0053	0.0065
	Mstn-Ab	n/s	0.074	0.079	0.0088	0.0079	0.0084	0.0052	0.0008	0.0009	0.0022	0.0012	0.0003
	Combo	0.0135	0.0015	0.0001	<0.0001	<0.0001	<0.0001	<0.0001	<0.0001	<0.0001	<0.0001	<0.0001	<0.0001
Female *+/G610C*	ActA-Ab	n/s	n/s	n/s	n/s	n/s	n/s	n/s	n/s	n/s	n/s	n/s	n/s
	Mstn-Ab	n/s	n/s	n/s	n/s	n/s	n/s	n/s	n/s	n/s	n/s	n/s	n/s
	Combo	0.093	0.122	0.137	0.038	0.0261	0.048	0.039	0.0325	0.0542	0.0269	0.019	0.0874

Overall body and hind limb muscle mass

At 16 weeks of age, Ctrl-Ab-treated Wt and *+/G610C* mice had equivalent body weights (Figure 2A). Increases in overall body weight with ActAA-Ab treatment were only observed in Wt mice [(female: +13.1%, p=0.001), (male: +5.3%, p=0.057)] (Figures 2A & 2B). In fact, male *+/G610C* mice exhibited a non-significant -4.1% average loss in body weight with ActA-Ab treatment. Mstn-Ab treatment increased overall body masses in male Wt (+9.3%), female Wt (+16.2%) and male *+/G610C* (+7.7%) mice although a +5.7% increase in female *+/G610C* mice did not reach statistical significance. Combo treatment consistently increased overall body mass regardless of genotype or sex [Male Wt: +10.7%, Male *+/G610C*: +7%, Female Wt: +14.8%, Female *+/G610C*: +7.5%].

Hindlimb muscle masses were also substantially increased with Mstn-Ab and Combo treatment regardless of genotype and sex, although Combo treatment consistently outperformed Mstn-Ab alone. ActA-Ab-treated Wt and male *+/G610C* mice showed trends towards increasing absolute weights of gastrocnemius (Figure 3A), quadriceps (Figure 3B), and TA muscles (Figure 3C), an effect that was lost when adjusted for overall body weight (Figures 4A, 4B and 4C). ActA-Ab failed to improve absolute or relative muscle mass in plantaris (Figure 3D), soleus (Figure 3E) or EDL (Figure 3F) muscles in all mice.

Gastrocnemius muscle weights were increased in male & female Wt and male *+/G610C* mice with Mstn-Ab whereas Combo consistently increased gastrocnemius muscle masses regardless of sex or genotype (Figures 3A & 4A). Both absolute and relative quadriceps muscles were also increased with Mstn-Ab and Combo treatment (Figures 3B & 4B).

Further, Mstn-Ab increased the absolute and relative TA weights in male *+/G610C* and female Wt mice (Figure 3C & 4C) although Combo treatment increased absolute and relative TA muscle masses in all mice. Absolute but not relative plantaris muscle masses were increased in male & female Wt and male *+/G610C* mice with Mstn-Ab treatment (Figure 3D & 4D) as did absolute and relative EDL masses in female Wt and male *+/G610C* mice (Figure 3F & 4F).

Combo treatment, however, increased both absolute and relative plantaris (Figure 3D & 4D) and EDL (Figure 3F & 4F) muscle masses in all mice, as well as the absolute and relative soleus (Figure 3E & 4E) muscle weights in all genotype groups except female *+/G610C* mice.

Muscle Contractility and Force Generation Assessment

Muscle contractiles are an important measure of *in-vivo* muscle function. We therefore assessed the effects of treatment on muscle force generation in hindlimb gastrocnemius, TA and soleus muscles (Figure 5). The absolute whole muscle contractile generation capacity (P_o) and relative contractile generating capacity (P_o/g) of hind limb gastrocnemius and TA muscles were equivalent in Wt and *+/G610C* mice, as previously reported[20], but relative tetanic force in soleus muscles was lower in female *+/G610C* relative to female Wt mice.

ActA-Ab treatment did not impact gastrocnemius muscle contractility in study mice (Figures 5A and 5B) but increased TA P_o in Wt female mice and soleus P_o/g in male Wt mice (Figures 5C, 5D).

Mstn-Ab had more widespread effects, increasing P_o of the gastrocnemius, soleus and TA hindlimb muscles in Wt male mice, soleus P_o in male *+/G610C;* and TA P_o in female Wt mice. TA P_o/g in male *+/G610C* was however decreased with Mstn-Ab treatment.

Surprisingly, Combo treatment decreased P_o in gastrocnemius and TA muscles in male *+/G610C* mice, and lowered gastrocnemius P_o/g in *+/G610C* gastrocnemius muscles and P_o/g in TA muscles in all mice regardless of sex or gender, a startling observation that was also previously made with sActRIIB treatment[20]. Unfortunately, this study was not powered to detect significant changes due to small animal numbers for the contractile assessments.

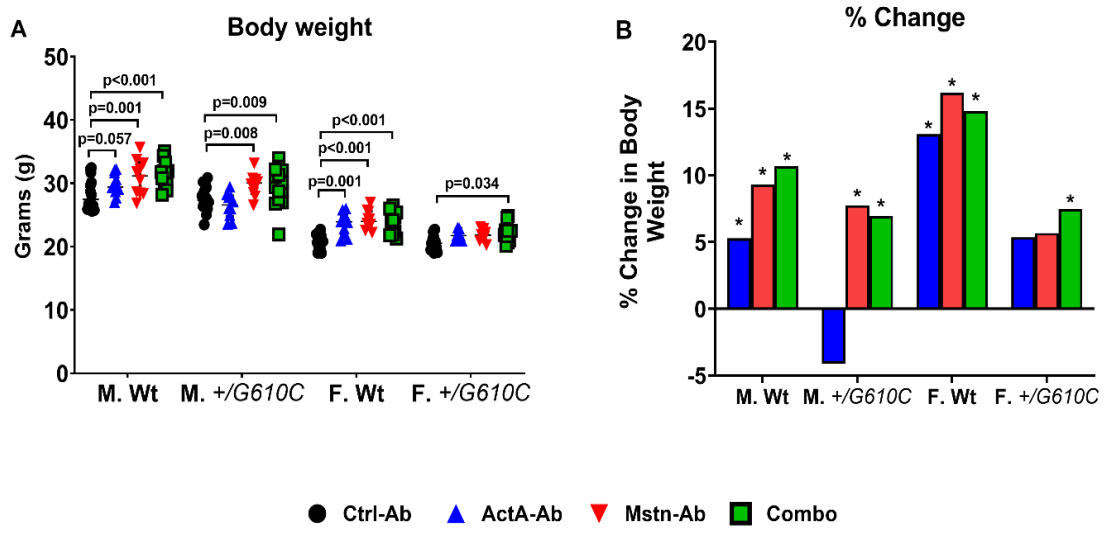

Figure III.2: Changes in body weight with control antibody and Combo treatment in Wt and *+/G610C* mice. A) Body weight, B) Percent change in body weight as a result of treatment with either control antibody (Ctrl-Ab, black circle); activin A antibody (ActA-Ab, blue triangle); myostatin antibody (Mstn-Ab, red triangle) or combination activin A and myostatin antibodies (Combo, green square). Values are median with interquartile range, n=8-15. P-values <0.1 are indicated and considered significant. Mstn-Ab data were used in an earlier publication[224] and have been included here for ease of comparing to ActA-Ab and Combo treatment data.

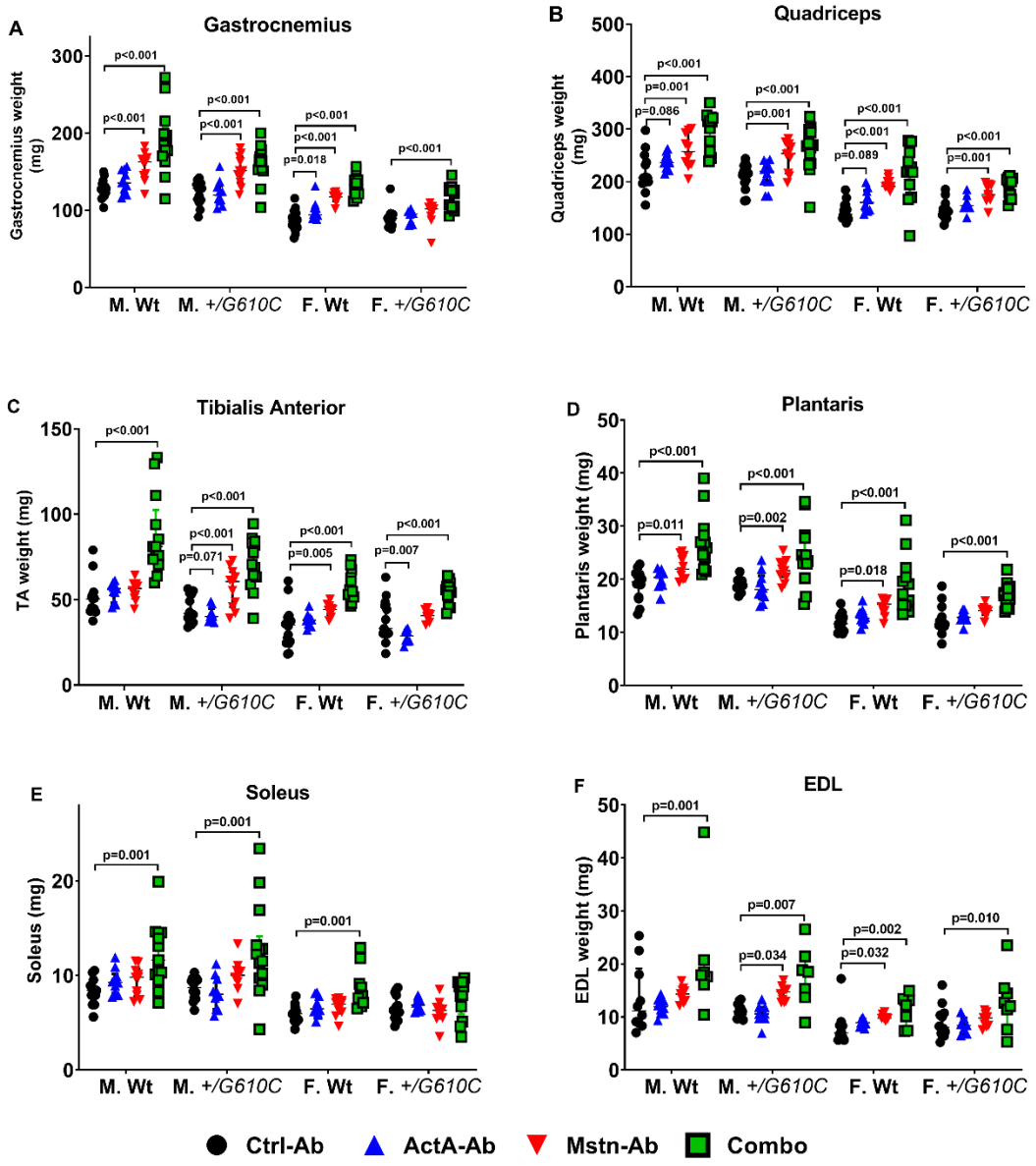

Figure III.3: Changes in whole hindlimb muscle masses (g) in Wt and *+/G610C* mice with treatment. A) Gastrocnemius, B) Quadriceps C) Tibialis Anterior D) Plantaris E) Soleus F) EDL muscle weights as a result of treatment with either control antibody (Ctrl-Ab, black circle); activin A antibody (ActA-Ab, blue triangle); myostatin antibody (Mstn-Ab, red triangle) or combination activin A and myostatin antibodies (Combo, green square). Values are median with interquartile range, n=8-15. P-values <0.1 are indicated and considered significant. Some of the Mstn-Ab data were used in an earlier publication[224] and have been included here for ease of comparing to ActA-Ab and Combo treatment data.

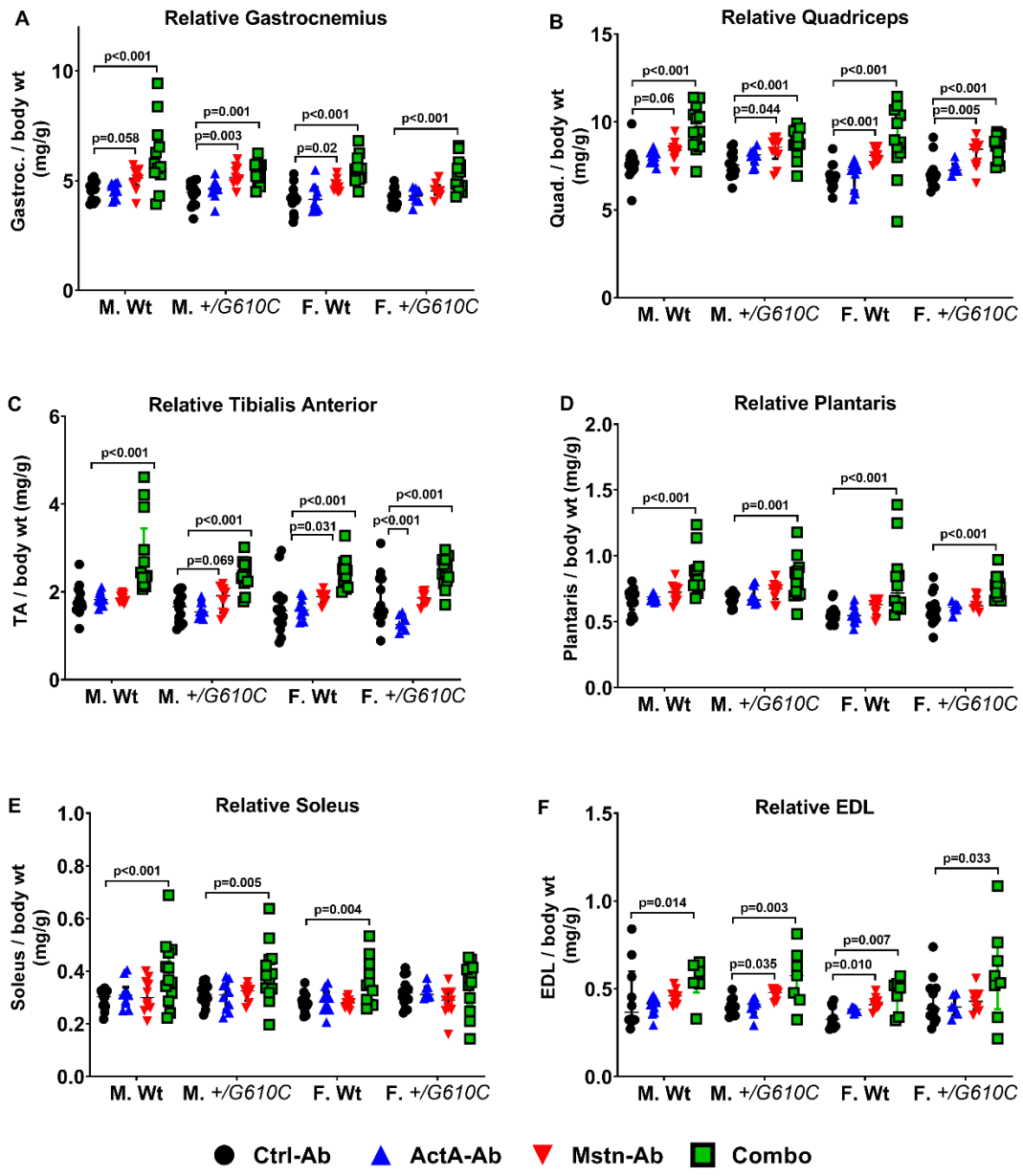

Figure III.4: Changes in relative hindlimb muscle masses in Wt and *+/G610C* mice with treatment. Relative A) Gastrocnemius, B) Quadriceps C) Tibialis Anterior D) Plantaris E) Soleus F) EDL muscle weights as a result of treatment with either control antibody (Ctrl-Ab, black circle); activin A antibody (ActA-Ab, blue triangle); myostatin antibody (Mstn-Ab, red triangle) or combination activin A and myostatin antibodies (Combo, green square). Values are median with interquartile range, n=8-15. P-values <0.1 are indicated and considered significant.

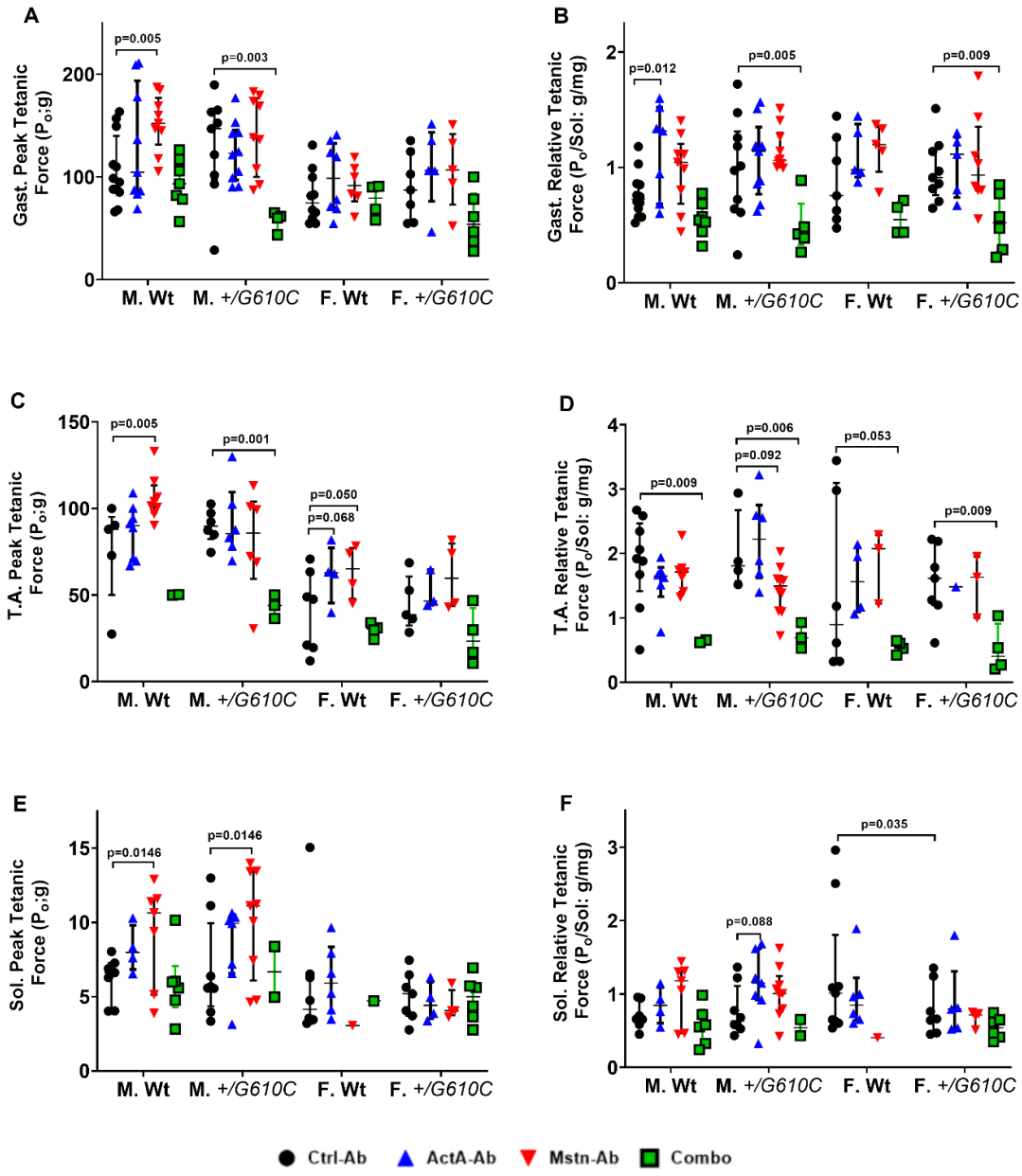

Figure III.5: Absolute and Relative hindlimb muscle contractile force generation of Ctrl-Ab, ActA-Ab, Mstn-Ab and Combo-treated Wt and *+/G610C* mice. A) Gastrocnemius peak tetanic force, B) Gastrocnemius relative tetanic force, C) TA peak tetanic force, D) TA relative tetanic force, E) Soleus Peak Tetanic Force F). Soleus Relative tetanic force. Mice were treated twice weekly with 10mg/kg of control antibody (Ctrl-Ab, black circle); activin A antibody (ActA-Ab, blue triangle); myostatin antibody (Mstn-Ab, red triangle) or combination activin A and myostatin antibodies (Combo, green square) for 11 weeks. Values are median with interquartile range, n=1-12. P-values <0.1 are indicated and considered significant. Mstn-Ab data were used in an earlier publication[224] and have been included here for ease of comparing to ActA-Ab and Combo treatment data.

Heart and Spleen Weights

In Ctrl-Ab-treated mice, absolute heart and spleen weights were comparable between male Wt and *+/G610C* mice, although female *+/G610C* mice had increased relative heart and spleen weights as compared to female Wt mice (Figure 6).

ActA-AB treatment did not impact heart weights, but increased absolute spleen weights in male and female Wt mice. Mstn-Ab decreased relative heart weights in male Wt and female *+/G610C* mice, and decreased relative spleen weights in male *+/G610C* mice. Combo treatment resulted in decreased relative heart and spleen weights in all mice regardless of sex and genotype. These decreases are likely a result of overall increases in body and muscle masses.

Absolute and relative fat mass

The absolute weights of inguinal fat, gonadal fat and brown adipose tissue (BAT) did not differ between Ctrl-Ab-treated Wt and *+/G610C* mice except for gonadal fat mass in male mice (Figure 7). Combo treatment stimulated an overall trend toward decreased fat mass in all mice, significantly decreasing relative inguinal fat and BAT mass in male Wt and female *+/G610C* mice respectively.

Body Composition

EchoMRI body composition analyses demonstrated that absolute lean muscle and total water masses in control *+/G610C* mice were lower than in control Wt mice. These decreases were no longer present when normalized to total body weight (Figures 8A, 8C). Also, main treatment effect was evident across all sex/genotype groups with significant changes in overall body composition with Combo treatment. Both absolute and relative

lean muscle mass were increased in mice regardless of genotype or sex with Combo treatment (Figure 8A). Overall fat masses and relative fat masses were prominently reduced with Combo administration in all treatment groups except absolute fat masses in male Wt mice (Figure 8B). Lastly, total body water was higher in all Combo-treated mice, concomitant with the observed increase in muscle mass (Figure 8C).

Energy expenditure and substrate utilization

Continuous indirect calorimetry measurements revealed that at baseline, Wt and *+/G610C*-Ctrl-Ab-treated mice displayed comparable average energy expenditure (EE, Figure 9A, 9B), VO_2 consumption (Figure 9C, 9D) and VCO_2 production (Figure 9E, 9F). The Combo treatment appeared to increase average EE in all mice except for male Wt mice, although the increase was only significant during the day in male *+/G610C* mice (Figure 9A, 9B). The Combo treatment also led to an increase in VO_2 consumption in male *+/G610C* mice during the day and increased VCO_2 production in female Wt mice at night. The mean respiratory quotient (RQ) remained unchanged regardless of sex, genotype or treatment (Figure 9G, 9H).

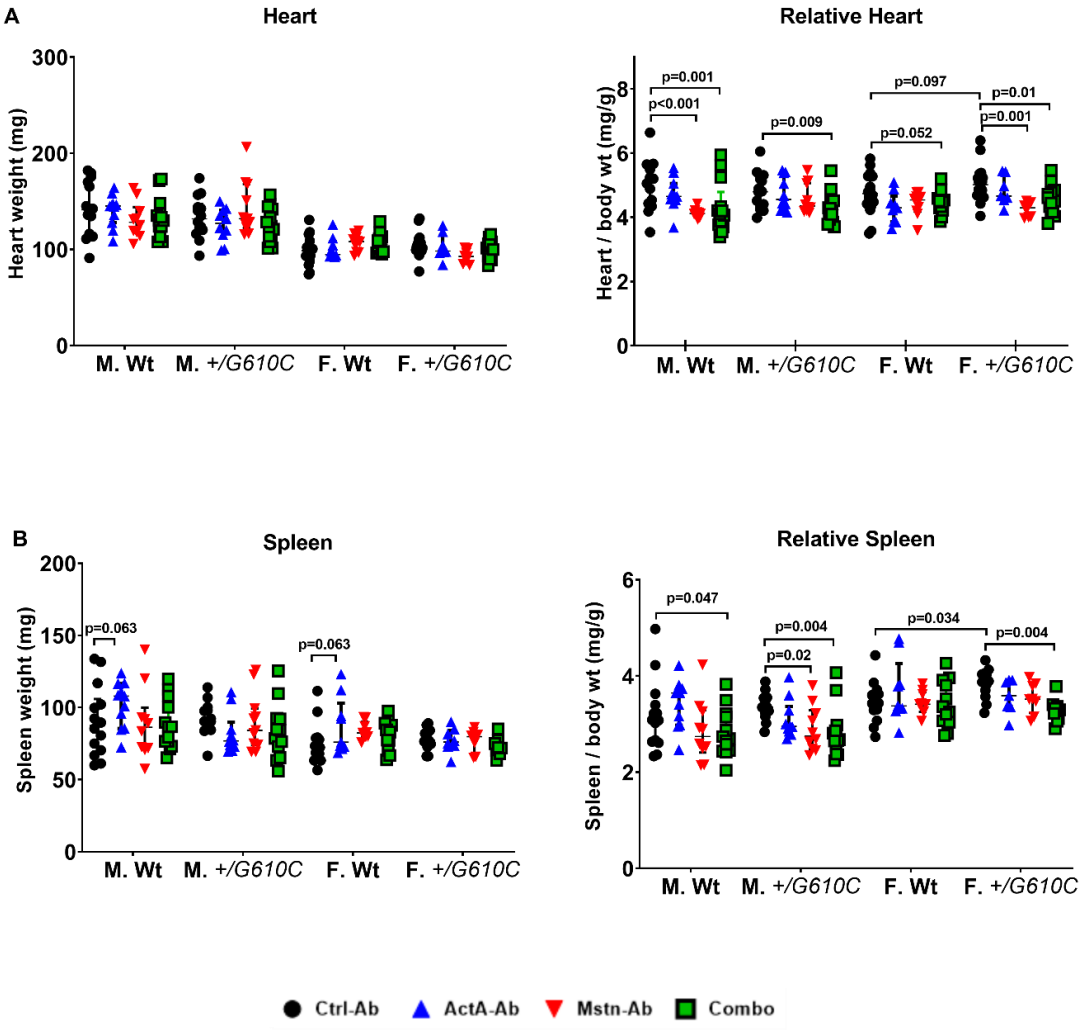

Figure III.6: Relative heart and spleen weights of Wt and *+/G610C* male and female mice treated with either control antibody (Ctrl-Ab, black circle); activin A antibody (ActA-Ab, blue triangle); myostatin antibody (Mstn-Ab, red triangle) or combination activin A and myostatin antibodies (Combo, green square). A) Absolute and relative heart weights, and B) Absolute and relative spleen weights at 16-weeks of age. Values are median with interquartile range, n=8-16. P-values <0.1 are indicated and considered significant.

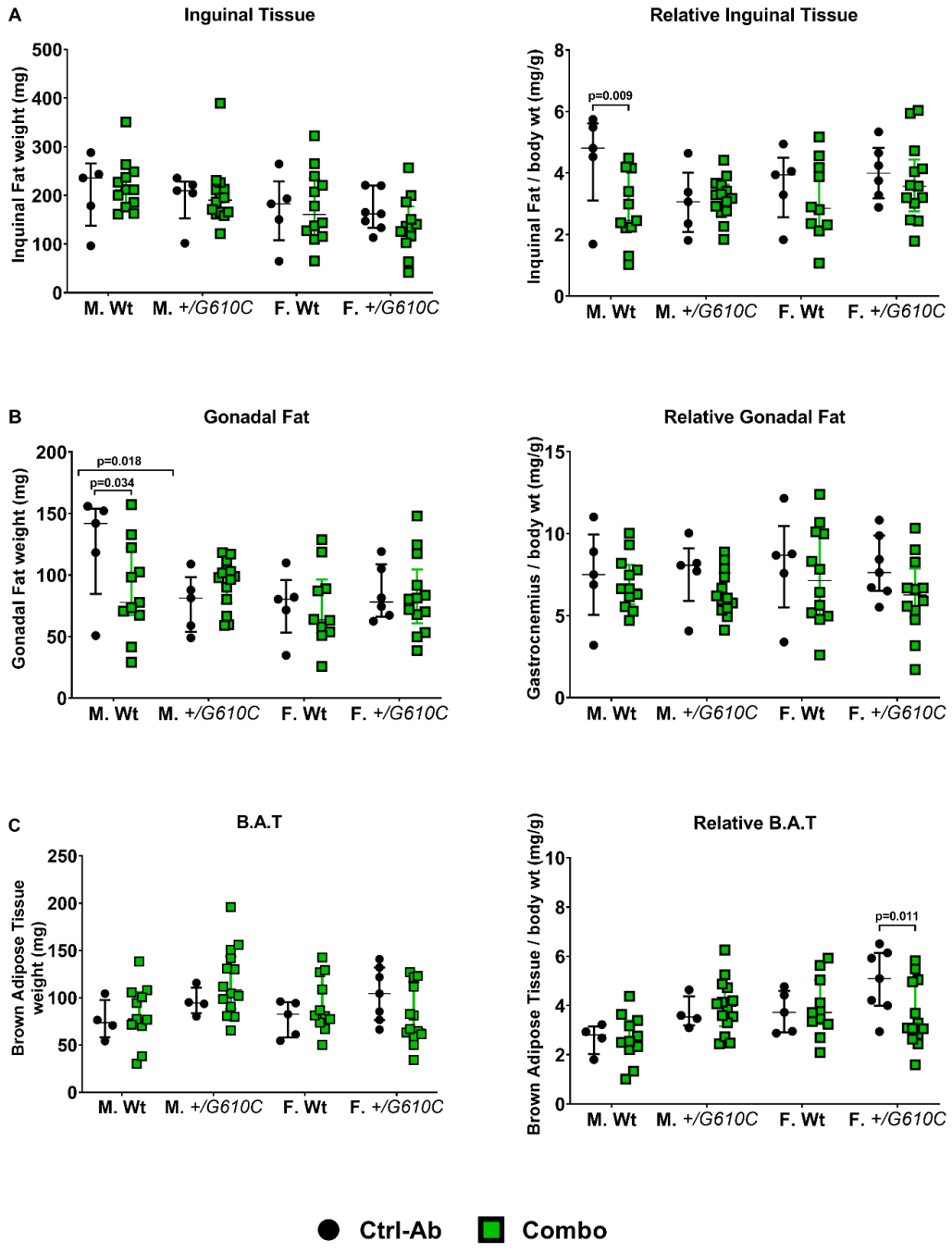

Figure III.7: Absolute and Relative fat masses in Wt and *+/G610C*-treated mice. A) Absolute and relative inguinal fat, B) Absolute and relative gonadal fat, and C) Absolute and relative brown adipose tissue (B.A.T) weights in Wt and *+/G610C* mice treated for 11-weeks with Control antibody (Ctrl-Ab, black circle) or combination activin A and myostatin antibodies (Combo, green square). Values are median with interquartile range, n=4-14. P-values <0.1 are indicated and considered significant.

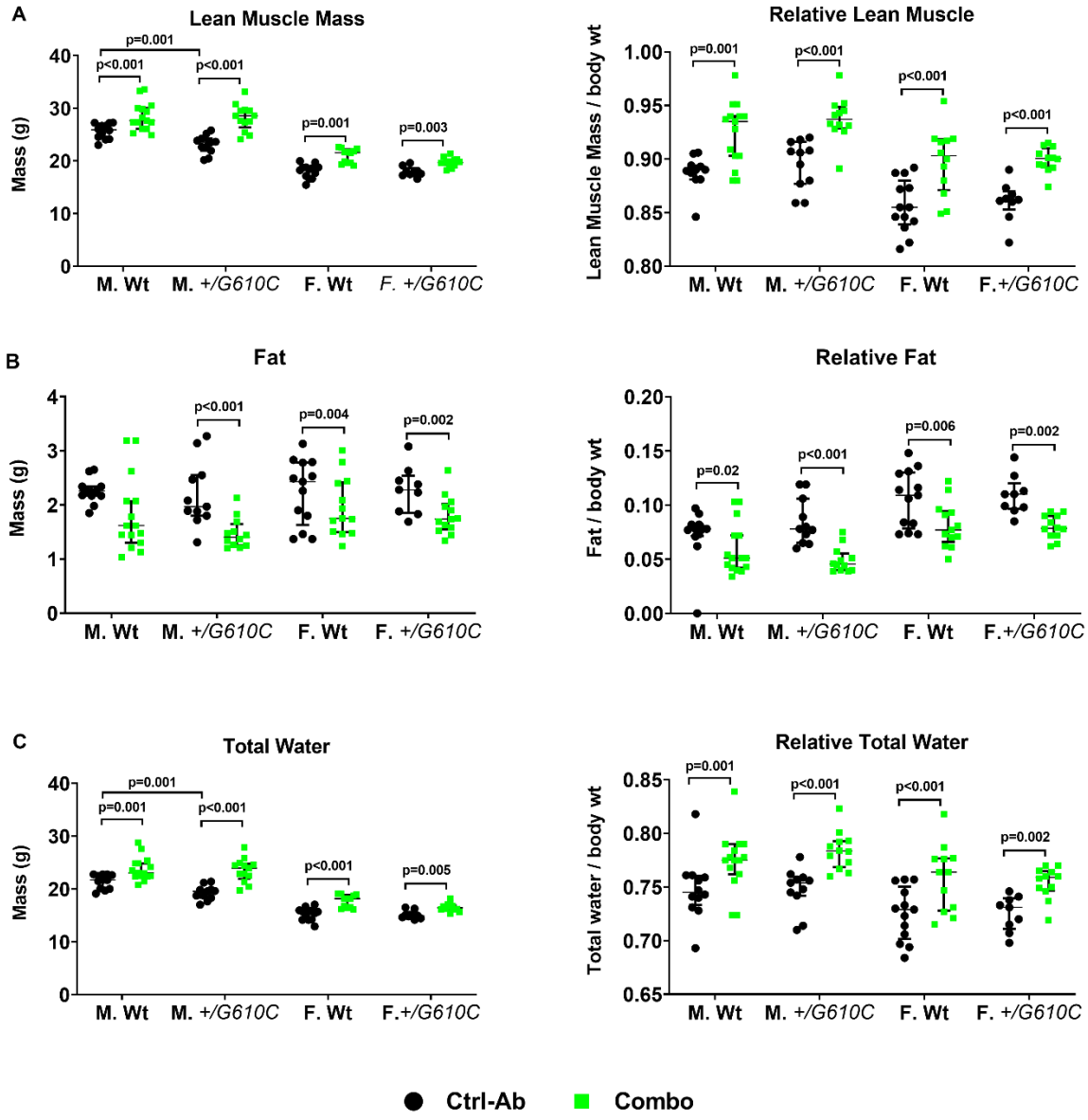

Figure III.8: Body Composition of Ctrl-Ab and Combo-treated Wt and *+/G610C* mice. A) Absolute and Relative Lean Muscle Mass, B) Absolute and Relative Fat mass, and C) Absolute and relative total water. Mice were treated twice weekly with 10mg/kg of control antibody (Ctrl-Ab, black circle); or combination activin A and myostatin antibodies (Combo, green square) for 11 weeks. Values are median with interquartile range, n=9-15. P-values <0.1 are indicated and considered significant.

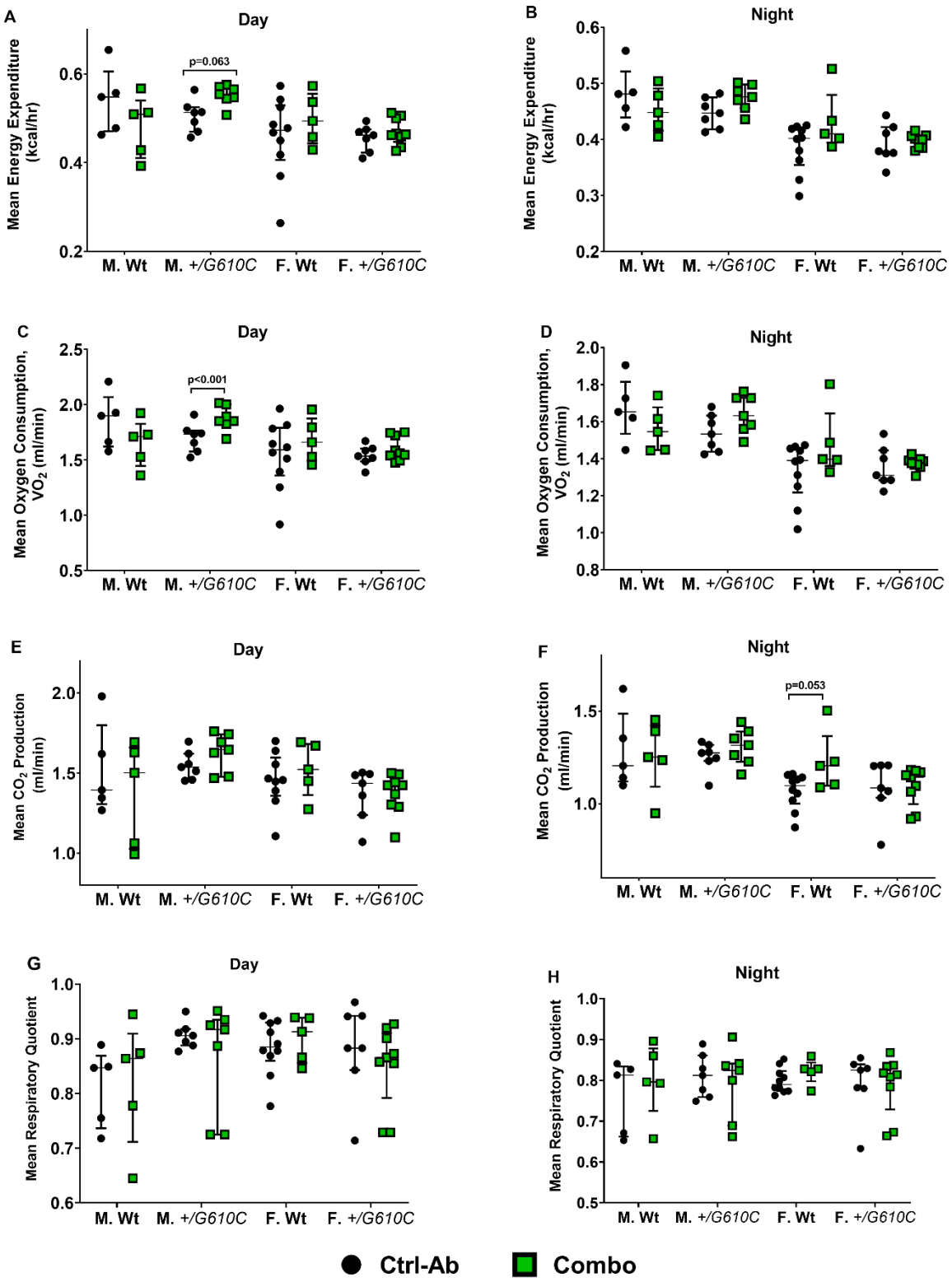

Figure III.9: Indirect calorimetry of Ctrl-Ab, and Combo-treated Wt and *+/G610C* mice. The treatment effects of inhibiting both activin A and myostatin (Combo) on A) Mean energy expenditure (day cycle), B) Mean energy expenditure (night cycle, C) Mean O_2

Consumption (Day cycle), D) Mean O_2 Consumption (Night cycle), E) Mean CO_2 Consumption (Day cycle), F) Mean CO_2 Consumption (Night cycle), G) Mean Respiratory Quotient (Day Cycle), H) Mean Respiratory Quotient (Night Cycle) are presented. Mice were treated twice weekly with 10mg/kg of control antibody (Ctrl-Ab, black circle); or combination activin A and myostatin antibodies (Combo, green square) for 11 weeks. Values are median with interquartile range, n=5-10. P-values <0.1 are indicated and considered significant.

Food and Water Intake

Sex-matched Wt control mice consumed similar amounts of food as *+/G610C* mice during both diurnal and nocturnal cycles (Figures 10A-D). Male Wt mice consumed less food and water with Combo treatment during the day (Figures 10A, 10C), whereas female Wt mice appeared to consume more food at night (Figure 10B). All other mice exhibited a trend towards lower food and water intake during both diurnal and nocturnal cycles with the Combo treatment.

Activity

Laser beams set across the X, Y, Z-axes recorded motion across the specific planes while mice were housed within the metabolic cages. Control Wt and *+/G610C* mice demonstrated similar activity levels across the X, Y and Z-axes during both day and night cycles (Figures 11A-11F). Thus, no main genotype effect on movement along parallel, perpendicular or vertical lanes were observed. During the night cycles, Combo treatment decreased movement along the X-axis in male Wt and along the Z-axis in female Wt and increased Y-axis beam breaks in female *+/G610C* mice. During both day and night cycles, Z-axis beam breaks or vertical rearing motions were decreased in male Wt mice with Combo treatment (Figures 11E, 11F). Overall, the Combo-treatment stimulated a trend towards decreased X- and Z-axes motion and increased Y-axes motion in female *+/G610C*. A trend towards increased X, Y, and Z-axes breaks during the day, and decreased Z-axis breaks during the night was observed in Combo-treated male *+/G610C* but did not reach significance. Female Wt mice also showed trends towards increased X-axis and decreased Y-and Z-axes motion that were not significant.

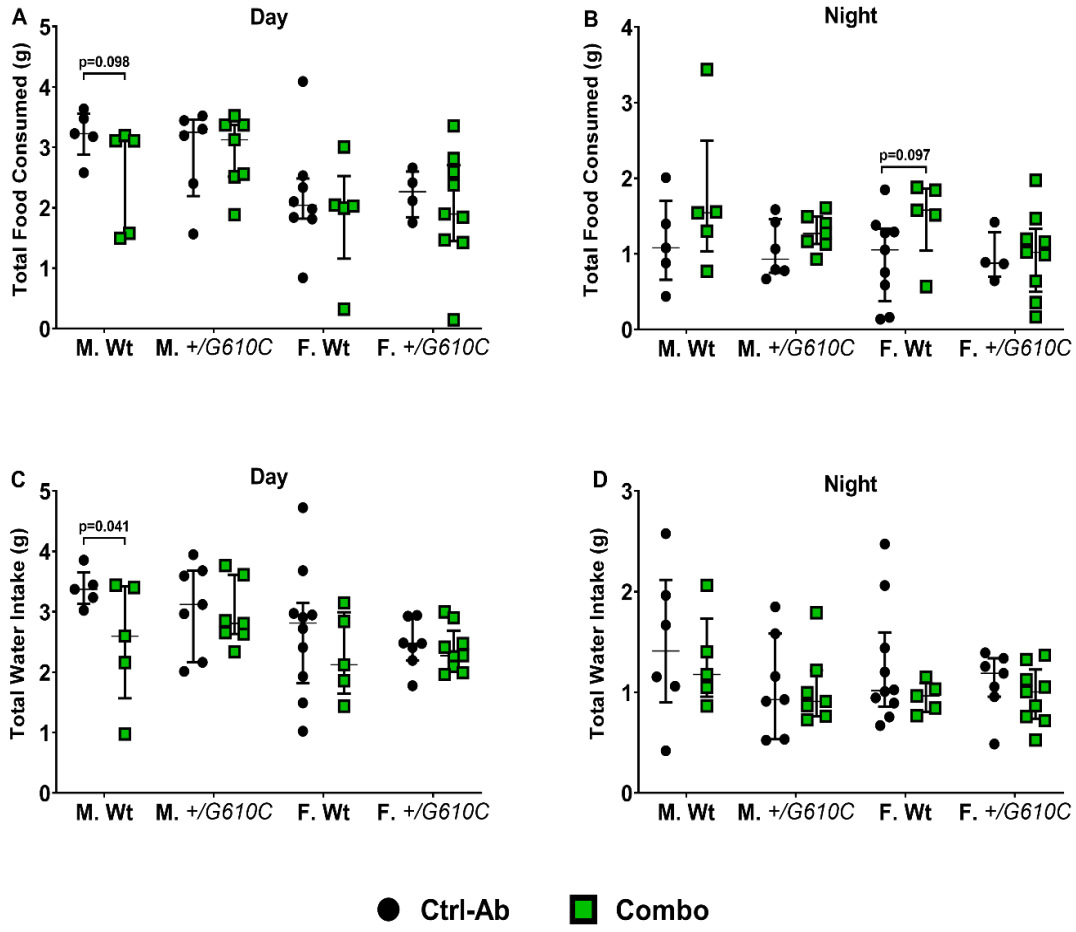

Figure III.10: Food and Water Intake of Ctrl-Ab and Combo-treated Wt and *+/G610C* mice A) Total Food Consumed (day cycle), B) Total Food Consumed (night cycle), C) Total Water Intake (Day cycle), D) Total Water Intake (Night cycle). Mice were treated twice weekly with 10mg/kg of control antibody (Ctrl-Ab, black circle); or combined activin A and myostatin antibodies (Combo, green square) for 11 weeks. Values are median with interquartile range, n=5-10. P-values <0.1 are indicated and considered significant.

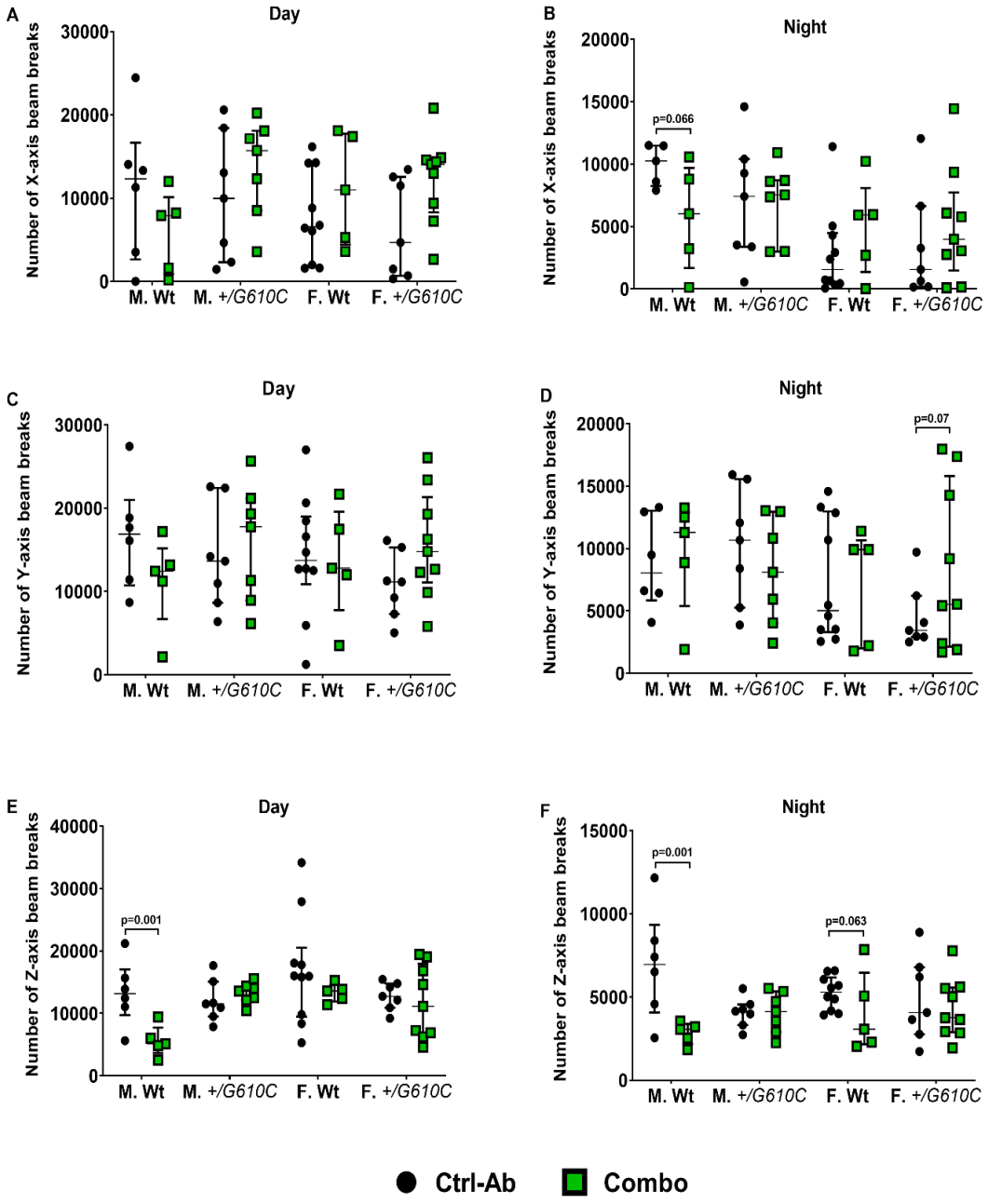

Figure III.11: Activity levels of Ctrl-Ab and Combo-treated Wt and *+/G610C* mice. A) Movement along the X-axis (day cycle), B) Movement along the X-axis (night cycle), C) Movement along the Y-axis (Day cycle), D) Movement along the Y-axis (Night cycle), E) Movement along the Z-axis (Day cycle), F) Movement along the Z-axis (Night cycle). Mice were treated twice weekly with 10mg/kg of control antibody (Ctrl-Ab, black circle); or combination activin A and myostatin antibodies (Combo, green square) for 11 weeks. Values are median with interquartile range, n=5-10. P-values <0.1 are indicated and considered significant.

Cortical Bone microarchitecture

Cortical microCT confirmed decreases in cortical bone parameters in mice with OI. Female *+/G610C* Ctrl-Ab-treated mice had decreased bone area (BA, Figure 12A), total area (Figure 12B), and polar moment of inertia (pMOI, Figure 12C) relative to female Wt mice at 16 weeks of age. Male *+/G610C* mice also had decreased total area (TA, Figure 12B) and pMOI (Figure 12C). The bone area fraction, BA/TA (Figure 12D) and tissue mineral density (TMD, Figure 12E) values in male and female *+/G610C* mice were higher than in their Wt counterparts. Finally, the lengths of Wt and *+/G610C* mouse femurs were equivalent (Figure 12F).

ActA-Ab treatment increased BA, TA and pMOI in male Wt mice but effected no changes in female Wt and male & female *+/G610C* mice. Mstn-Ab primarily increased BA, TA and pMOI in Wt mice, but decreased BA/TA in female *+/G610C* mice. The Combo-treatment improved BA, pMOI and TMD in all mice regardless of sex and gender. The Combo treatment also increased TA in male Wt and *+/G610C* mice, and BA/TA in male Wt, female Wt and male *+/G610C*. The Combo treatment did not impact femur length.

A summary of the treatment effects relative to Ctrl-Ab-treated Wt mice are shown in Table 2. ActA-Ab equalized BA in male and female *+/G610C* to Ctrl-Ab-treated Wt levels and further increased BA/TA levels. Mstn-Ab reversed BA and pMOI in male *+/G610C* to Ctrl-Ab Wt levels, whereas the Combo treatment restored BA and pMOI in all *+/G610C* to Wt levels.

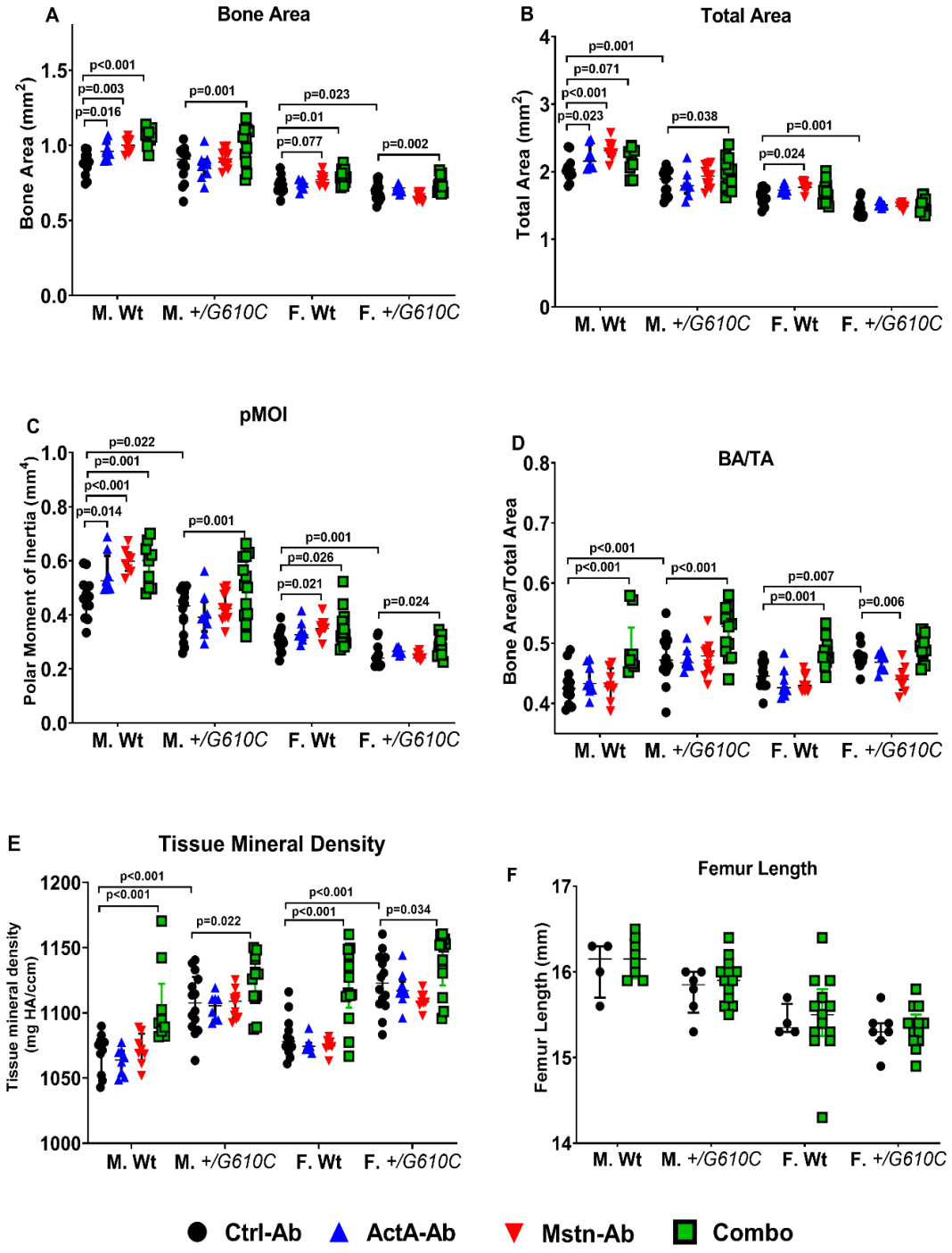

Figure III.12: Cortical bone microarchitecture of Ctrl-Ab, ActA-Ab, Mstn-Ab and Combo-treated Wt and *+/G610C* mice. A) Bone area (BA), B) Total Area (TA), C) Polar Moment of Inertia (pMOI), D) Bone Area fraction (BA/TA), E) Tissue Mineral Density, F) Femur Length. Mice were treated twice weekly with 10mg/kg of control antibody (Ctrl-Ab, black circle); activin A antibody (ActA-Ab, blue triangle); myostatin antibody

(Mstn-Ab, red triangle) or combination activin A and myostatin antibodies (Combo, green square) for 11 weeks. Values are median with interquartile range, n=4-13 for femur length; n=8-13 for cortical bone parameters. P-values <0.1 are indicated and considered significant. Mstn-Ab data were used in an earlier publication[224] and have been included here for ease of comparing to ActA-Ab and Combo treatment data.

Table III.2: Summary of ActA-Ab, Mstn-Ab or Combo treatment effects on cortical bone microarchitecture in *+/G610C* mice relative to sex-matched control Wt mice

	Bone Area		**Total Area**		**BA/TA**		**pMOI**	
Treatment/Sex	**Male**	**Female**	**Male**	**Female**	**Male**	**Female**	**Male**	**Female**
Ctrl-Ab	=	↓	↓	↓	↑	↑	↓	↓
ActA-Ab	=	=	↓	↓	↑	↑	↓	↓
Mstn-Ab	=	=	↓	↓	↑	=	=	↓
Combo	↑	=	↓	↓	↑	↑	=	=

Trabecular Bone Microarchitecture

Both male and female Ctrl-Ab-treated *+/G610C* mice have decreased trabecular bone volume (BV, Figure 13B), bone volume fraction (BV/TV, Figure 13C), trabecular number (Tb.N, Figure 13D) and bone mineral density (BMD, Figure 13G) relative to Ctrl-Ab-treated Wt mice. Trabecular spacing (Tb.Sp, Figure 13F) is also increased in both male and female Ctrl-Ab-treated *+/G610C* mice relative to Ctrl-Ab-treated Wt mice. No differences in trabecular thickness were observed between sex-matched Ctrl-Ab-treated Wt and *+/G610C* (Figure 13E). These data support previous reports of compromised trabecular bone microarchitecture in the *G610C* mouse model[19,79].

Combo treatment produced the most significant increases in trabecular bone properties in all mice relative to ActA-Ab alone or Mstn-Ab alone (Figure 13). ActA-Ab increased BV/TV, Tb.N and BMD in male Wt mice only and decreased Tb.Sp in both male Wt and *+/G610C* mice. Mstn-Ab treatment increased TV and BV/TV in female Wt mice, BV in Wt and male *+/G610C*, but decreased Tb.th and BMD in female *+/G610C* mice.

The Combo treated male and female Wt mice experienced significant gains in TV, BV, BV/TV, Tb.N, and BMD except for Tb.th where only male Wt mice had gains; and Tb.Sp which was decreased in male Wt mice. In both male and female *+/G610C* mice, the Combo treatment also increased BV, BV/TV, Tb.N, BMD; and decreased Tb.Sp.

Table 3 summarizes trabecular bone properties of ActA-Ab, Mstn-Ab, or Combo-treated *+/G610C* mice in comparison with sex-matched control Wt mice. ActA-Ab increased Tb.th in *+/G610C* female mice, reverting the bone phenotype to control Wt

levels. Mstn-Ab only reverted BV/TV in male and Tb.th in both male and female *+/G610C* mice to control Wt levels. Combo treatment consistently increased and reversed the trabecular bone microarchitecture properties BV/TV, Tb.N, Tb.th and BMD, to control Wt levels in both male and female mice.

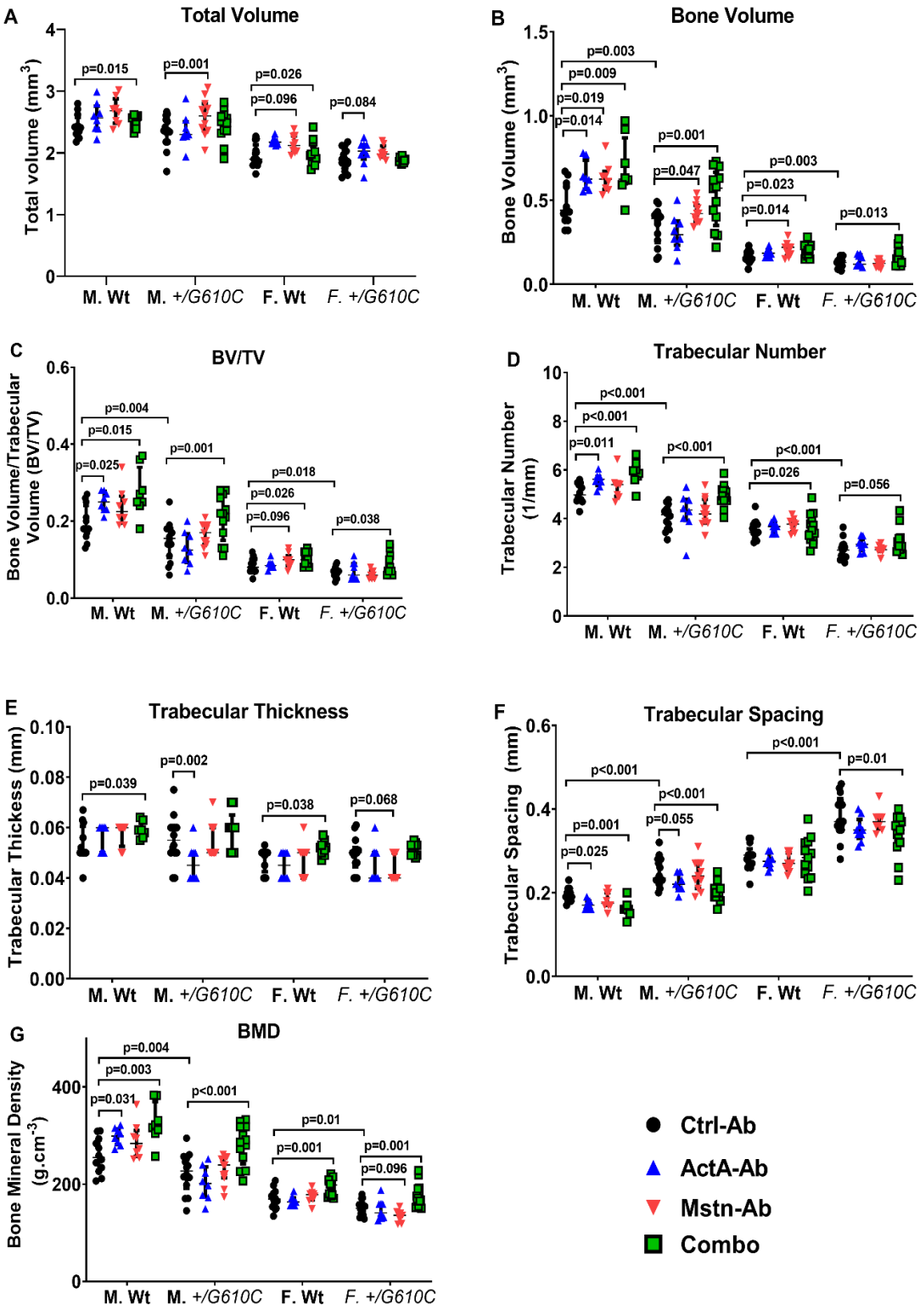

Figure III.13: Trabecular bone properties of Ctrl-Ab, ActA-Ab, Mstn-Ab and Combo-treated Wt and *+/G610C* mice. A) Total Volume (TV), B) Bone Volume (BV), C) Bone Volume fraction (BV/TV), D) Trabecular Number (Tb.N), E) Trabecular Thickness

(Tb.th), F) Trabecular Spacing (Tb.sp), F) Bone Mineral Density (BMD). Mice were treated twice weekly with 10mg/kg of control antibody (Ctrl-Ab, black circle); activin A antibody (ActA-Ab, blue triangle); myostatin antibody (Mstn-Ab, red triangle) or combination activin A and myostatin antibodies (Combo, green square) for 11 weeks. Values are median with interquartile range, n=8-14. P-values <0.1 are indicated and considered significant. Mstn-Ab data were used in an earlier publication[224] and have been included here for ease of comparing to ActA-Ab and Combo treatment data.

Table III.3: Summary of ActA-Ab, Mstn-Ab or Combo treatment effects on trabecular bone properties in *+/G610C* mice relative to sex-matched control Wt mice

	BV/TV		**Tb. N**		**Tb. th**		**BMD**	
Treatment/Sex	**Male**	**Female**	**Male**	**Female**	**Male**	**Female**	**Male**	**Female**
Ctrl-Ab	↓	↓	↓	↓	=	=	↓	↓
ActA-Ab	↓	↓	↓	↓	↓	=	↓	↓
Mstn-Ab	=	↓	↓	↓	=	=	↓	↓
Combo	=	=	=	↓	↑	↑	=	=

Femoral Biomechanical Properties

Among control mice, male *+/G610C* have higher maximum (Figure 14A) and yield loads (Figure 14B), similar stiffness (Figure 14C) and lower post-yield displacements (Figure 14D) and work-to-fracture (W.T.F., Figure 14E) as male Wt mice. Female *+/G610C* have lower maximum and yield loads, stiffness and W.T.F. relative to Wt female mice as previously reported[224].

The Combo-treatment consistently increased maximum load, yield loads and stiffness in all mice regardless of genotype and sex. It also enhanced W.T.F in male *+/G610C* mice and decreased post-yield displacement in male and female Wt mice. ActA-Ab treatment actually decreased biomechanical strength (maximum and yield loads and stiffness) in male *+/G610C* and female Wt mice; and W.T.F in female Wt mice, proving detrimental to bone biomechanical strength.

Mstn-Ab treatment resulted in higher post-yield displacement in female Wt and *+/G610C* mice; and W.T.F in female Wt mice; but decreased maximum load (Female Wt), yield load (Female Wt and *+/G610C*) and stiffness (Male *+/G610C*). A summary of these results in Table 4 show a consistently improved femoral biomechanical profile in male and female *+/G610C* mice with the Combo treatment.

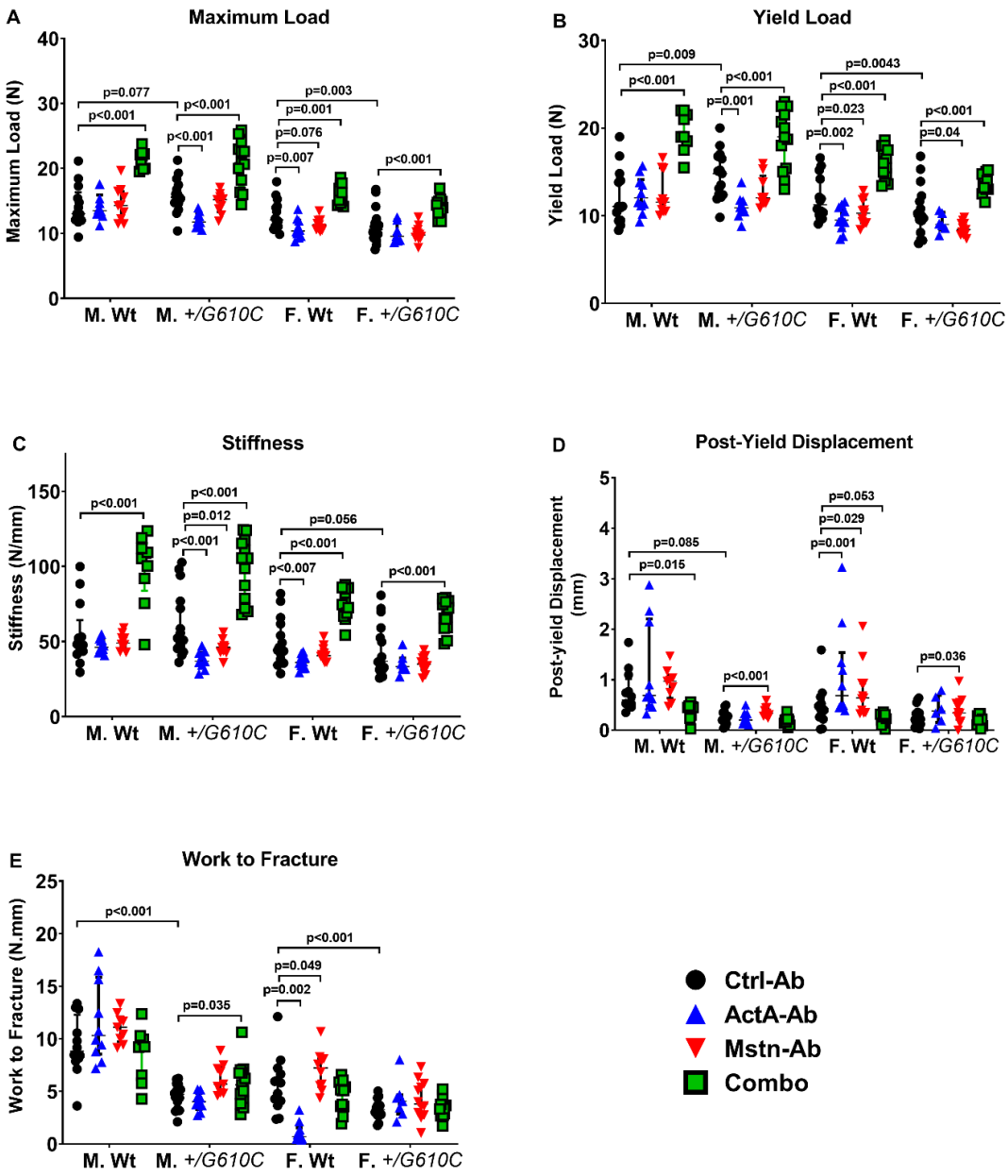

Figure III.14 Bone Biomechanical properties of Ctrl-Ab, ActA-Ab, Mstn-Ab and Combo-treated Wt and *+/G610C* mice. A) Maximum Load, B) Yield Load, C) Stiffness, D)Post-Yield Displacement, E) Work-to-fracture. Mice were treated twice weekly with 10mg/kg of control antibody (Ctrl-Ab, black circle); activin A antibody (ActA-Ab, blue triangle); myostatin antibody (Mstn-Ab, red triangle) or combination activin A and myostatin antibodies (Combo, green square) for 11 weeks. Values are median with interquartile range, n=7-16. P-values <0.1 are indicated and considered significant. Mstn-Ab data were used in an earlier publication[224] and have been included here for ease of comparing to ActA-Ab and Combo treatment data.

Table III.4: Summary of ActA-Ab, Mstn-Ab or Combo treatment effects on bone biomechanical properties in *+/G610C* mice relative to sex-matched control Wt mice

	Max Load		Yield Load		Stiffness		PYD		WTF	
Treatment/Sex	**Male**	**Female**	**Male**	**Female**	**Male**	**Female**	**Male**	**Female**	**Male**	**Female**
Ctrl-Ab	↑	↓	↑	↓	=	↓	↓	=	↓	↓
ActA-Ab	↓	↓	↓	↓	↓	↓	↓	=	↓	↓
Mstn-Ab	=	=	=	↓	=	↓	↓	=	↓	↓
Combo	↑	↑	↑	↑	↑	↑	↓	↓	↓	↓

Discussion

In the present study, we examined the inhibition of circulating activin A alone, myostatin alone, or in combination, through treatment with anti-activin A and anti-myostatin antibodies to improve bone and muscle properties in Wt and *+/G610C* mice. Our study revealed that combinatorial inhibition of both myostatin and activin A (Combo) significantly increased hindlimb muscles and overall body masses in mice regardless of sex or genotype to a greater degree compared to activin A or myostatin inhibition alone. The Combo treatment also improved bone microarchitecture and strength in both Wt and *+/G610C* mice. The results of myostatin inhibition alone has been previously published and did not significantly impact postnatal bone homeostasis in *+/G610C* mice[224] (Chapter II).

Bone is mechanosensitive, responding to forces, mostly from skeletal muscle by adjusting its mass and strength[14]. Accordingly, this intricate physiologic and anatomic connection points to both the necessity and opportunity of successful therapeutic approaches to musculoskeletal disorders to focus on both bone and muscle. Myostatin and activin A are ligands in the TGF-β superfamily which regulate musculoskeletal development and homeostasis[15,166,268,269]. Decreasing circulating myostatin levels dramatically increases skeletal muscle mass[15], while decreasing circulating levels of the pro-osteoclastogenic molecule, activin A, strengthens murine bone and improves bone geometry[162]. ActRIIB-ligand traps are known to reduce circulating levels of multiple ligands, including myostatin and activin A, whiles markedly increasing muscle and bone properties in Wt mice[20,200,224,241] and in multiple murine models of OI including the mild to moderate type I/IV *G610C* and the severe type III *OIM* (*oim/oim*) models[19,21]. The

significant enhancement of Wt and *G610C* muscle masses by the combinatorial inhibition of myostatin and activin A is comparable to results from a 2017 study by Latres and colleagues who observed that inhibiting myostatin in concert with activin A more potently increased skeletal muscle and overall lean body mass in SCID mice than inhibiting either ligand alone[22]. We found the increase was not limited to hindlimb muscle groups alone, since total lean muscle mass, as determined by EchoMRI analyses, was increased with Combo treatment, with paralleled decreases in overall body fat mass and increases in total body water. Interestingly, absolute heart and spleen weights were unchanged with Mstn-Ab and Combo treatments although relative weights were lower. This suggests that both treatments do not impact heart and spleen weights. The effect of Combo treatment on musculature provides further evidence that both activin A and myostatin regulate postnatal skeletal muscle homeostasis in mice. Activin A inhibition increased body weights and the weights of some hindlimb muscle groups in male and female Wt mice, with obvious improvements in bone microarchitecture in male Wt mice. However, inhibiting activin A decreased body weights in male *+/G610C* mice and hindlimb TA muscles of both male and female *+/G610C* mice.

Type I OI is considered the mildest type of OI. Yet, 80% of type I OI patients experience muscle weakness, generating less force per body weight relative to healthy controls[271] although in children, this inherent muscle pathology may not be solely due to inactivity. In a study of ambulatory type I OI children, Pouliot-Laforte et. al., found that OI children have equivalent activity levels as their age-matched healthy counterparts[271]. Further, even when their small muscle masses are accounted for, muscle frailty and deficient force production is still evident[219,271,272].This is particularly troubling since

upper and lower limb muscle strength influence ambulation levels in patients[273]. In addition, muscle weakness is hypothesized to contribute to the weak bone phenotype in OI since muscle influences bone mass, strength and geometry[14,274]. In this study, we observed that *+/G610C* mice have similar activity levels as Wt mice at 16 weeks of age, as previously reported[243,243]. Also, besides differences in force production in TA muscles, 16 week-old control *+/G610C* mice had similar absolute whole muscle contractile force as Wt mice, contrary to previous observations made in the more severe type III OI mouse (*oim/oim*) which has compromised muscle function[110,243]. In the study by Jeong et al., sActRIIB-mFc treatment reduced absolute peak tetanic forces in both Wt and *+/G610C* hindlimb muscles, similar to the observations in this study where the Combo treatment decreased muscle force production regardless of sex or genotype[20]. This is in contrast to the outcomes of myostatin inhibition alone (Figure 5) where Wt male gastrocnemius, TA and soleus muscles and *+/G610C* soleus muscles exhibited increased peak tetanic forces, although relative TA tetanic force in male *+/G610C* mice was reduced. The similar muscle force production profiles in both sActRIIB and Combo-treated mice suggests that myostatin and activin A are the primary regulators of the sActRIIB-muscle treatment response in previous studies[20] even though sActRIIB binds multiple targets. The startling observations can be attributed to the knowledge that myostatin affects AMPK signaling, modulates insulin sensitivity, glucose uptake, mitochondrial respiration, and maintenance of muscle durability and fatigue resistance[275]. Hence, deficiency results in loss of specific peak tetanic force [P_o/CSA(μm^2)] as seen in myostatin null (*mstn*$^{-/-}$) mouse muscle relative to Wt mice[276,277]. Also, muscles from *mstn*$^{-/-}$ mice have decreased capacity for exercise, and

are easily fatigued due to mitochondrial dysregulation and a higher preference for glycolysis[277,278], thus complete knock-out or removal of circulating myostatin will likely be detrimental to OI muscles. In fact, partial myostatin deficiency induced in severe homozygous *oim* (*oim/oim*) mice with sActRIIB treatment improved muscle force production[20]. Moreover, sActRIIB has been shown to alter gene expression profiles in mouse quadriceps muscles, reducing the expression of β-oxidation and oxidative metabolism genes, which decreases the rate of oxidative phosphorylation, and increases metabolic stress and muscle fatigability in Wt mice relative to control PBS-treated Wt mice[279,280]. Thus, the increases in muscle mass engineered by myostatin deficiency does not often mirror improvements in muscle force[276,280,281].

In contrast, Latres et al. demonstrated in 9-week-old SCID mice that inhibition of activin A and myostatin by monoclonal antibodies or with a decoy receptor for 21 days improved muscle force production [22]. It is noteworthy that in the latter study, mice were treated for 3 weeks compared to the 8 and 11 weeks of treatment undertaken by Jeong et al., or in this current study, respectively[20]. It is therefore possible that short term inhibition of both activin A and myostatin may result in more functional improvements in muscle mass and force relative to longer treatment strategies. An investigation using the *mdx* mouse model of Duchene muscular dystrophy mouse model did indeed show that long term myostatin inhibition was less effective at improving muscle force than short-term myostatin treatment[282]. Moreover, in separate studies investigating the impact of ActRIIB-mFc treatment in aging, a 30-day treatment of 18 month old mice with ActRIIB-mFc resulted in increased muscle force production while increases in muscle force were

observed after only 3 days of sActRIIB-mFc treatment in 10 to 12-month old orchidectomized C57BL6 mice [260].

Pre-pubertal OI patients have increased metabolic, heart and respiration rates along with higher than normal oral temperatures, and have been described as being in a hyper-metabolic state, which normalizes at the onset of puberty[283]. Also, type III OI patients are noted to be heat intolerant, and may become critically overheated during anesthesia[284]. This hyper-metabolic state is expected to deplete body fat stores, as observed in *mstn*$^{-/-}$ mice which have reduced overall body fat mass, less fat accumulation with age, and higher lean mass relative to Wt and *mstn*$^{-/+}$ mice [192,195,197,285]. Conversely, pediatric OI patients have similar subcutaneous forearm fat as healthy children and adolescents although muscle and bone CSA is lower especially in types I and III OI [286]. We observed in this study that Ctrl-Ab-treated Wt and *+/G610C* mice had equivalent fat masses, although adiposity was decreased in all mice with Combo treatment.

In 2017, a report on the presence of a metabolic phenotype in pre-pubertal *Col1a1*$^{Jrt/+}$ mice, similar to the pre-pubertal metabolic phenotype in OI patients was published[287]. Four-week-old *Col1a1*$^{Jrt/+}$ mice were shown to have higher energy expenditure (EE), average O_2 consumption and average CO_2 production, a phenotype that is mostly resolved by 8 weeks age (equivalent to a young human adult) [287]. *Col1a1*$^{Jrt/+}$ is a more severe model of OI caused the skipping of exon 9, which results in deletion of an 18 amino acid sequence in the triple helical domain the alpha I chain of type I collagen [287]. *Col1a1*$^{Jrt/+}$ mice ate similar amounts of food but consumed more water per lean body mass and moved much less than Wt mice at 4 weeks of age[287]. Our current study does not reveal genotypic influences on energy expenditure, food intake and activity, implying

that between 14 and 16 weeks of age, *+/G610C* mice do not exhibit a metabolic phenotype, although studies investigating the presence of a metabolic phenotype at an earlier age in *+/G610C* mice remain to be done.

In multiple studies, myostatin inhibition alone failed to improve post-natal bone microarchitecture in some murine models of disease, although myostatin enhances osteoclastogenesis and decreases osteoblast activity[19,188,199,200,216,224]. A soluble myostatin decoy receptor (ActRIIB-Fc) which inhibits activins-A, -B and –AB, BMP-11 and myostatin increased femoral trabecular bone mass, bone volume and vertebral bone strength in SCID mice whereas a neutralizing myostatin antibody did not, although both treatments substantially increased muscle mass [241,288]. Another study using an anti-myostatin antibody (YN41) failed to demonstrate increases bone microarchitecture in mice both on earth and in the microgravity space environment[199], although an ACVR2B decoy receptor did improve bone mass in mice both on earth and in the microgravity space[270]. Furthermore, myostatin KO mice administered ActRIIB-Fc exhibited increased bone volume, suggesting that ligands besides myostatin contribute to the regulation of postnatal bone homeostasis[241]. Lastly, the results in Chapter II demonstrated that myostatin inhibition alone is inadequate to effect beneficial changes in post-natal *+/G610C* bone[224].

Data on the impact of activin A in postnatal bone homeostasis is less clear. Activin A has been shown to improve fracture healing by promoting endochondral bone formation and improving bone mass and strength in aged rats[161,179]. Nonetheless, in more recent studies inhibiting activin A, typically using ActRIIA decoys, bone mass and strength in Wt and ovariectomized (OVX) C57BL6 mice are improved[162,179]. In this study, activin A

inhibition was detrimental to bone biomechanical strength in male *+/G610C* and female Wt mice, decreasing maximum and yield loads and work-to-fracture values. The combined inhibition of both activin A and myostatin, however synergistically increased bone microarchitectural and biomechanical properties in Wt and *+/G610C* mice, a likely result of the combined increase in lean muscle mass (since lean muscle mass positively correlates with BMD[289]) and direct effects of activin A and myostatin inhibition on bone homeostasis. This hypothesis failed to hold true when *Col1a1*$^{Jrt/+}$ mice were treated with ACE-2494, a soluble ActRIIB decoy receptor highly specific for myostatin and activin A alone[200]. Although substantial increases in musculature was observed with treatment, *Col1a1*$^{Jrt/+}$ mice did not exhibit improvements in bone mass and biomechanical properties[200]. Also, *oim/oim* mice treated with sActRIIB had increased muscle masses and trabecular bone volume but no increases in biomechanical strength, whereas sActRIIB-treated *+/G610C* mice had both larger hindlimb muscles and better femoral microarchitectural and biomechanical properties. These observations further reinforce the notion that the underlining mutation, the extent of OI severity and degree of bone and muscle tissue pathology indeed dictate therapeutic responses.

To summarize, in this study, we were able to elicit increases in postnatal *+/G610C* muscle mass, skeletal bone microarchitecture and strength with a treatment strategy inhibiting both activin A and myostatin using highly specific monoclonal antibodies. Decreases in muscle contractility function with the combination treatment warrants additional studies to determine the optimum treatment duration for myostatin inhibition therapy. Since current bisphosphonate treatments fail to increase muscle force production, exercise tolerance and exhaustion[290], and current OI clinical trials are not

muscle-focused, identifying a bone anabolic and muscle-strengthening therapy has the potential to be highlt beneficial in OI management. Even in the absence of increasing muscle strength, the preservation of muscle mass in conditions where deteriorating muscle mass is inevitable such as microgravity or bed rest[199,270] warrants further investigations of both myostatin and activin A inhibition as treatment strategies.

The bone responses to the combined inhibition of activin A and myostatin (Combo) revealed improvements that were greater than the additive effects of inhibiting myostatin or activin A alone, suggesting that our observations are a combined result of the synergistic responses to the absence of myostatin and activin A perhaps, in addition to increased mechanotransduction, necessitating additional studies to elucidate the mechanism by which the Combo treatment improved bone microarchitecture and strength. Since sActRIIB treatment increased osteoblast and osteoclast numbers and decreased osteoclast activity in Wt and *+/G610C*[19], it is likely that the Combo treatment may stimulate similar pathways.

Lastly, peak bone mass in C57BL6 mice is attained at 16 weeks of age, akin to young adulthood in humans[248,291]. This suggests that a treatment like the Combo may not have to be initiated in-utero or right after birth since initiating treatments in pre-pubertal mice still improved the OI bone phenotype in this study.

CHAPTER IV

SUMMARY AND FUTURE DIRECTIONS

The objectives of this dissertation research were to 1) investigate the effect of prenatal genetic myostatin deficiency in the mild to moderate *G610C* mouse model of osteogenesis imperfecta (OI), 2) investigate the effect of post-natal pharmacological myostatin inhibition in wildtype and *+/G610C* OI mice, 3) investigate the influence of post-natal activin A inhibition in wildtype and *+/G610C* OI mice, and 4) investigate the effects of combined myostatin and activin A inhibition on muscle and bone properties in wildtype and *+/G610C* OI mice. My investigations have demonstrated that 1) both genetic and pharmacological myostatin inhibition enhance muscle mass in male and female wildtype and *+/G610C* OI mice, 2) genetic myostatin inhibition demonstrates greater skeletal influences in *+/G610C* mice relative to post-natal pharmacological myostatin inhibition alone and, 3) although activin A inhibition exhibited some detrimental effects in bone and muscle in *+/G610C* mice, 4) the combined inhibition of activin A and myostatin demonstrated greater enhancement of muscle and bone properties in *+/G610C* mice relative to inhibiting each ligand individually.

In humans and monkeys, serum myostatin levels are approximately 5 and 9 times less than that found in mice respectively, whereas serum levels of activin A are greater in monkeys and humans [(22)]. To obtain maximal increases in muscle mass in primates, a combinatory myostatin and activin A antibody neutralization treatment was required even though no changes in femoral bone mineral density (BMD) or mineral content (BMC) were reported[(22)]. These observations, in addition to the observed musculoskeletal impacts of sActRIIB treatment influenced the pursuit of this dissertation research.

Postnatal bone homeostasis is highly dependent on regulation by the osteoblasts, osteoclasts and osteocytes. Osteoblasts and osteoclasts are differentially regulated by myostatin and activin A, so investigating the impact of how the combinatorial inhibition of myostatin and activin A synergistically affect bone cell activity and number are critical steps. Hence, below, I first describe proposed future experiments that would elucidate the mechanisms behind which increased bone microarchitecture and strength were observed with the Combo treatment in Chapter III (Objective 1). Further, OI is a physically and genetically heterogeneous diseases, and recent data suggests that disease severity and variant (mutation) type will likely impact therapeutic response. Thus, the second set of experiments are to explore the skeletal impact of anti-activin A antibody, anti-myostatin antibody or Combo treatment in homozygous *OIM* mice (*oim/oim*) which exhibit severe skeletal phenotypes, completing the research initiated in appendix A which investigate the impacts of ActA-Ab, Mstn-Ab and Combo treatment on muscle mass, muscle force production and body composition (Objective 2). Lastly, objective 3 outlines experiments to identify potentially dysregulated biological pathways in *+/G610C* and *oim/oim* mice that contribute to the skeletal pathology of OI. Specifically, investigations into mitochondrial functional capacities in primary osteoblasts are proposed since osteoblasts rely on energy for bong formation.

FUTURE DIRECTIONS

Objective 1: To elucidate mechanisms of action of combinatorial anti-myostatin and anti-activin A treatment on bone cell differentiation and function in Wt and *+/G610C* mice.

Rationale: In Chapter III, we observe significant improvements in cortical and trabecular bone microarchitecture and biomechanical properties in both *+/G610C* and Wt mice with the combined anti-myostatin and anti-activin A antibody treatment. Increases in bone formation or decreases in bone resorption as a result of changes in the activity and number of the bone forming osteoblasts and bone-resorbing osteoclasts may have contributed to the observed skeletal phenotype. sActRIIB-mFc increased the numbers of osteoblasts in both Wt and *+/G610C* mice regardless of sex[19], but only increased osteoclast number in Wt male mice[19]. Osteoclast activity (N.Oc/BPm) was substantially decreased in male and female *+/G610C* mice as well. Also, sActRIIB-mFc-treated *+/G610C* mice exhibited increased periosteal bone formation with males also exhibiting increases in periosteal mineralizing surface and mineral apposition rates, and females exhibiting increases in endocortical mineralizing surface/bone surface (MS/BS). Moreover, serum procollagen 1 intact N-terminal propeptide (P1NP) levels, a marker of bone formation, were increased in female *+/G610C* mice with sActRIIB-mFc treatment, culminating to increased overall bone formation[19]. Of the sActRIIB-mFc targets, activin A is a known pro-osteoclastogenic molecule which also inhibits osteoblast differentiation[16,265], thus its removal will likely decrease osteoclast numbers per bone surface, leading to bone accumulation. Recent data suggests myostatin also stimulates osteoclast differentiation and inhibits osteoblast activity, inhibiting bone formation *in vitro* and *in vivo*[188,215]. Therefore, it is possible that Combo treatment augmented cortical and trabecular bone properties in mechanisms similar to the above. Thus, elucidating the mechanism of Combo action will shed light on the applicability of this treatment to subsequent studies and clarify whether it acts via an anabolic or catabolic pathway.

Approach:

Mice: Wt and *+/G610C* male and female mice will be treated as described in Chapter III. In brief, 5 week old mice will be randomly distributed into 4 treatment groups: control antibody (Ctrl-Ab), anti-myostatin antibody (Mstn-Ab), anti-activin A antibody (ActA-Ab) or combinatory ActA-Ab and Mstn-Ab (Combo). Mice will be administered twice weekly intraperitoneal injections of 10mg/kg of body weight of the respective treatment for 11 weeks. Mice will be injected 10 and 3 days before euthanasia with alizarin red (20mg/kg; Acros Organics, Morris Plains, NJ, USA) and calcein (5 mg/Kg; MP Biomedical, Santa Ana, CA, USA) fluorescent dyes which bind to newly synthesized bone. At sacrifice, femurs will be cleaned of extraneous tissue, fixed in 10% neutral buffered saline for 2 days and transferred to 70% ethanol for long-term storage. Dynamic histological analyses of the left femur based on calcein and alizarin dye injections will be undertaken to determine endocortical and periosteal mineral apposition rates (MAR) and bone formation rates, providing insight into osteoblast activity. Static histological analyses on the right femur will quantify osteoblast and osteoclast number as well as the number of bone cells per bone surface as previously described[19,224].

Anticipated results: We hypothesize that the observed improvements in bone microarchitecture will be a cumulative result of increased osteoblast numbers and decreased osteoclast activity.

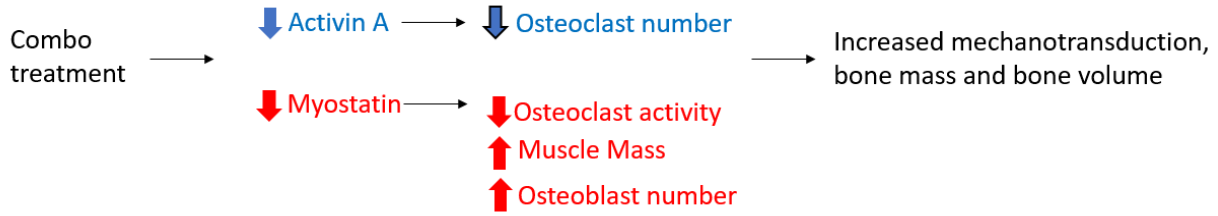

Figure Obj.1.1: Hypothesis for Objective 1.

Objective 2: To evaluate the impacts of inhibiting activin A, myostatin or both on skeletal properties in the severe type III OI mouse model

Rationale: In Appendix A, we present data on the muscle phenotype of homozygous *oim/oim* mice treated with Ctrl-Ab, ActA-Ab, Mstn-Ab or Combo. Homozygous *OIM* (*oim/oim*) mice, exhibit a more severe skeletal phenotype, mimicking severe type III OI. We observed consistent increases in muscle mass, and significant increases in overall lean muscle mass and concomitant decreases in overall body fat, suggesting effective changes in body composition with Mstn-Ab and Combo treatment. Myostatin influences differentiation of mesenchymal stem cells, a role that places it at a key regulator of postnatal muscle, bone and fat homeostasis[15]. In fact, myostatin null mice have substantially larger muscles due to hypertrophy and hyperplasia, less body fat and overall increase in bone density[202,204,292]. Also, mice administered recombinant myostatin have significant suppression of bone formation and higher bone resorption rates[215]. Not surprisingly, ActRIIB ligand traps had anabolic effects in *oim/oim* bone, increasing the trabecular bone properties BV/TV and Tb.N although bone strength was not

impacted[19,21], a deviation from the observation in *+/G610C*, where mice had improved bone microarchitecture and strength with treatment[19]. Conversely, inhibiting activin A and myostatin in the severe *Col1a1*$^{Jrt/+}$ OI mouse failed to correct the bone phenotype[200]. Disease severity and mutation type can influence response to disease, in yet undiscovered ways, so it is vital to determine if the severe *oim/oim* mouse bone will respond to Combo treatment in this present study. Further, the *in vivo* effects of activin A or myostatin inhibition have not been studied in *oim/oim* mice. As previously discussed, ligand traps to ActRIIB interact with multiple other ligands, so determining the roles of activin A and myostatin in postnatal *oim/oim* bone regulation will be novel information that will contribute to understanding the pathology of OI.

Approach: 5 week old Wt and *oim/oim* male and female mice will be treated as previously described in Chapter III. 10 days and 3 days prior to sacrifice, calcein and alizarin dyes will be administered for dynamic and static histomorphometry (Future Directions, Objective 1). Right femurs, stored in 1X PBS at -20C later harvest, will be subjected to μCT analyses (Chapter III; Method: MicroCT Analyses). Post-uCT analyses, right femurs will be subjected to 3 point bend tests for biomechanical testing (Chapter III; Method: 3-point bending).

Anticipated results: It is likely that the Combo treatment will result in improvements to bone microarchitecture and strength. However, *oim/oim* mice have more severe skeletal muscle and bone pathology, so it is uncertain whether increases in muscle and bone volume with Combo treatment will be insufficient to elicit changes in bone strength.

Lastly, post-natal Combo treatment will not change the quality of the defective type I collagen and mineral matrix, thus whether increased ECM and mineral deposition by osteoblasts and decreased osteoclastic bone resorption will be sufficient to overcome the bone quality defects is uncertain.

Objective 3: To determine if mitochondrial dysfunction contributes to the skeletal bone phenotype in *+/G610C* and *oim/oim* mice.

Rationale: Recently, mitochondria in the skeletal muscle of homozygous oim (*oim/oim*) mice were discovered to be severely functionally compromised, likely contributing to the observed inherent muscle pathology and weakness[111]. I performed preliminary analyses of mitochondria in de-marrowed 4-month old *oim/oim* bones and observed significantly decreased mitochondrial DNA copy number relative to nuclear copy number ($p = 0.0378$), suggesting decreased mitochondrial number in the *oim/oim* bone (Figure Obj.3_1). Further, *oim/oim* muscle show severe mitochondrial dysfunction and decreases in mitochondrial biogenesis, mitophagy and citrate synthase markers[111].

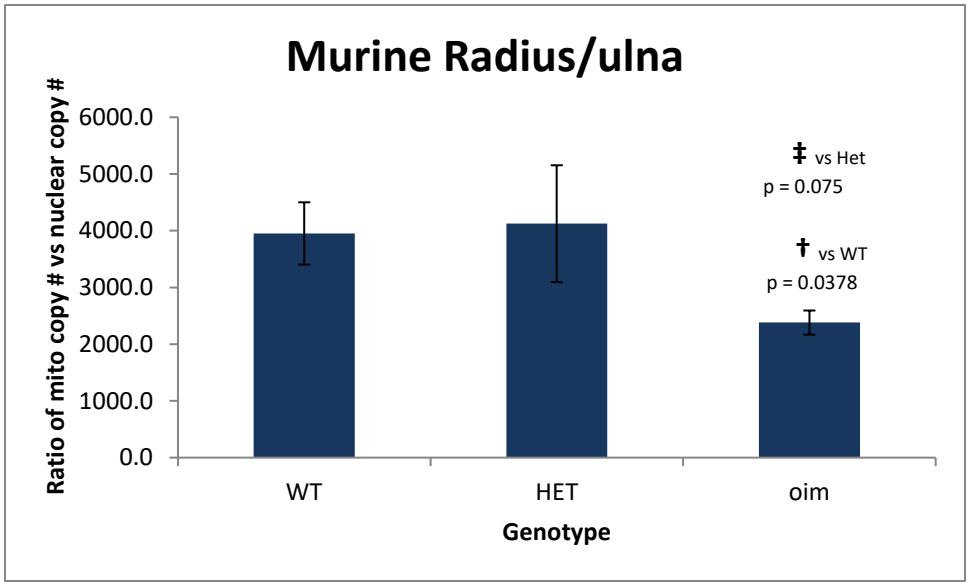

Figure Obj.3.1: Decreased mitochondrial DNA number versus nuclear DNA in murine ulna/radius number suggests lower mitochondrial content in *oim/oim* bones. n= 4-7, † p< 0.05 vs WT, ‡ p=0.075 vs +/oim (Het), by ttest.

The vital functions of the mitochondria have been widely examined in tissues with very high energy demands such as skeletal muscle and fat[293]. Though much less focus has been placed on the effect of mitochondrial dysfunction on the bone, several studies have suggested the importance of mitochondrial integrity in bone mineralization, growth, remodeling, and homeostasis[146,293]. Osteogenic induction of the osteoblastic cell line, MC3T3-E1, and primary osteoblasts are associated with mitochondrial biogenesis and robust oxygen consumption[294]. Moreover, primary mitochondrial diseases caused by missense mutations in the mitochondrial membrane protein Opa3 impairs bone growth and strength and decreases skeletal bone integrity[293]. Further, loss of the mitochondrial ATP-independent serine protease HtrA2/Omi, a protein quality control protease, resulted in age-related pathologies including osteoporosis in mice[295]. Also, osteocytes with impaired mitochondria have been shown to be more susceptible to apoptosis[146]. Lastly, both osteoblasts[296] and osteoclasts[297] have significant amounts of mitochondria, making insights into the status of mitochondria in bone cells relevant information, also osteoblasts suppress oxidative phosphorylation and show a preference for glycolysis during differentiation and mineralization[298].

Mitochondria produce energy, trigger cell death[299] and release reactive oxygen species (ROS) during normal function[299,300]. Mitochondrial dysfunction is a broad term that refers to abnormalities in ATP generation via the oxidative phosphorylation pathway or imbalances in the generation and detoxification of ROS and metabolite metabolism[301,302].

ROS, particularly H_2O_2, have important roles in intracellular signaling events that regulate proliferation, differentiation and inflammation [303,304]. However, oxidative stress,

which arises from an imbalance between excessive ROS generation and cellular antioxidant enzyme activity can damage cellular components[305]. High levels of H_2O_2 in MC3T3-E1 osteoblastic cells induces autophagy and apoptosis[306] and inhibit activities of the intracellular antioxidant enzymes manganese superoxide dismutase (SOD) and glutathione peroxidase, leading to the loss of bone integrity[307]. *In vivo* systems of disuse-induced bone loss, which exhibit increases in intracellular ROS production, were protected from bone loss following treatment with vitamin C, an antioxidant[308]. Thus, a negative correlation exists between increased oxidative stress and bone health[309] [310]. Inflammatory cytokines can stimulate ROS overproduction and contribute to oxidative stress[311]. Oxidative stress then induces preosteoclast differentiation, decreases osteoblast activity and stimulates osteoblast and osteocyte apoptosis[311]. This sequence of events uncouples the synergy between osteoblasts and osteoclasts during bone remodeling, favoring osteoclast activity and resulting in decreased bone mass. Thus, systemic inflammation and oxidative stress may underwrite the increased osteoclastogenesis observed in the *oim* mouse[312]. In addition, a growing body of evidence suggests that in osteoporosis, molecular damage due to ROS-induced oxidative stress are evident[313,314]. Nojiri and colleagues showed that mice completely deficient in superoxide dismutase 1 (SOD1), an antioxidant enzyme, had increased cellular ROS and decreased bone mass and quality resulting in a severe bone fragility phenotype[308].

Approach: To assess mitochondrial dysfunction, citrate synthase activity, the quantity of the electron transport chain (ETC) complexes (I, II, III, IV) and mitochondrial respiration

capacity will be determined. These can be used to infer the bioenergetic capacity of cells, predict mitochondrial content and are important indicators of oxidative capacity[315].

Primary osteoblasts will be obtained from calvaria of 7-10 day old pups of the correct genotypes (Wt, *+/G610C* and *oim/oim*) as previously described [316,317]. Mitochondrial respirometry will be evaluated in primary calvarial osteoblasts using the Seahorse XFe24 (Agilent) to determine oxygen consumption rates (OCR) and extracellular acidification rates (ECAR), first at basal respiration and then when induced during a mitochondrial stress test. The mitochondrial stress test (Agilent Systems) will enable us to assess maximal ADP production and maximal respiration through sequential additions of oligomycin, FCCP and a combination of Rotenone and antimycin A. Oligomycin inhibits mitochondrial ATP production, FCCP results in maximal cellular respiration since it uncouples the mitochondrial membrane and rotenone and antimycin A block complexes I and III in the electron transport chain.

Citrate synthase enzyme activity also will be determined in primary osteoblast lysates using a commercially available citrate synthase enzyme activity assay (CSE1, Detroit R&D), and normalized to protein concentration. ETC complex compoenents and other energy sensing and mitochondrial regulatory protein contents will be detected via western blots: for mitochondrial protein content- complexes I-IV of the OXPHOS pathway (Abcam, ab110413)[318]; energy sensing- AMPK (Cell Signaling #40H9) and SIRT1 (Cell Signaling #8469); mitogenesis- PGC1a (Abcam, ab54481) and mitochondrial transcription factor A (Tfam) (Abcam, ab131607); mitophagy- BCL2-interacting protein 3 (BNIP3) (Cell Signaling #44060), Parkin (Cell Signaling #4211) and Microtubule-Associated Protein 1 Light Chain 3 (LC3) (Cell Signaling #3868). Lastly oxidative stress

and inner mitochondrial membrane potentials will be measured to determine cell stress and the ability of primary osteoblasts to produce ATP.

Anticipated Results: Mitochondria from both *+/G610C* and *oim/oim* calvaria will exhibit mitochondrial dysfunction as evidenced by decreased respirometry, decreased citrate synthase activity, loss of membrane potential and decreased levels of mitochondrial proteins involved in the oxidative phosphorylation pathway, energy sensing, mitochondrial biogenesis, and mitophagy relative to Wt osteoblasts, although *oim/oim* mice will be expected to exhibit more significant mitochondrial dysfunction due to being more severely compromised. This aim will **provide novel insights into the status of mitochondria in the *oim/oim* bone** and determine whether oxidative stress and mitochondrial dysfunction contribute to the pathophysiology of bone in OI.

APPENDIX A

EFFECT OF ANTI-ACTIVIN A AND ANTI-MYOSTATIN ANTIBODY TREATMENT ON MUSCLE AND WHOLE BODY COMPOSITION IN THE *OIM* MOUSE, A MODEL SEVERE OF OSTEOGENESIS IMPERFECTA

Catherine L. Omosule[1], Dominique Joseph, Brooke Weiler[1], Victoria L. Gremminger[1], Spencer Silvey, Sandra Kleiner[2], Charlotte L. Phillips[1,3*]

[1]Department of Biochemistry, University of Missouri, Columbia, Missouri, 65211; [2] Regeneron Pharmaceuticals, Tarrytown, New York, 10591; [3]Department of Child Health, University of Missouri, Columbia, Missouri, 65211

Abstract

Approximately 85-90% of patients who have osteogenesis imperfecta (OI), a skeletal disorder affecting 1 in 10-15,000 live births, have mutations in one of the two genes that encode the proteins for type I collagen: COL1A1 and COL1A2. Type I collagen is the major protein constituent of bone, so alterations in its expression and primary structure can lead to compromised structural integrity, processing and quantity, which may result in skeletal deformity, fragility, and recurrent bone fractures, as experienced by patients with OI. Homozygous *oim/oim* mice model severe human type III OI, often characterized as progressively deforming OI.

In this study, we investigate the effects of inhibiting activin A and/or myostatin, ligands with regulatory roles in pre-and post-natal muscle and bone regulation, in the *oim/oim* mouse. We treated Wt and *oim/oim* mice for 11 weeks with 10mg/Kg of body weight of monoclonal antibodies to either anti-activin A antibody (ActA-Ab), anti-myostatin antibody (Mstn-Ab) or both anti-activin A and anti-myostatin antibodies (Combo) relative to a control antibody (Ctrl-Ab) regimen.

We demonstrate that in control antibody treated mice, *oim/oim* mice have reduced muscle masses while female *oim/oim* mice exhibit a metabolic phenotype relative to sex-matched control antibody treated Wt mice. In *oim/oim* mice, the ActA-Ab treatment had minimal impacts on muscle mass but induced a metabolic phenotype (increased energy expenditure and mean oxygen consumption). Mstn-Ab and the Combo treatment had more significant impacts on muscle mass and more consistently increased lean muscle mass and decreased fat mass in Wt and *oim/oim* mice.

Introduction

Skeletal tissue is important for the maintenance of balance, storage of minerals and ions, protection of internal organs from trauma and mobility. Bone is composed of type I collagen, a heterotrimeric molecule that makes up 90% of the bone proteins. Type I collagen is synthesized from COL1A1 and COL1A2 genes, with mutations that impact its structure and synthesis causing musculoskeletal disorders like *osteogenesis imperfecta* (OI). OI is a rare, heritable connective tissue defect associated with low bone mass, bone fragility and skeletal deformity. Type III OI is the most severe survivable form, with patients exhibiting progressive physical and skeletal deformity and scoliosis, blue sclera and often hearing in adulthood[81]. A complete cure for OI is likely dependent on gene therapy, a currently un-mastered technique, hence therapeutic options that aim to improve quality of life by reducing fracture rates, improving bone pain and increasing mobility are continually being sought after[6,319]. Current management techniques include surgical rodding and the use of bisphosphonate, bone anti-resorptive agents. These improve mobility and increase bone mass, but fail to be without adverse effects, prompting the need for better OI treatment strategies[75,97,100]. OI is also characterized by intrinsic muscle weakness, a phenomenon that likely contributes to the weak skeletal phenotype, since bone and muscle are intricately connected[12,77,78,110]. Thus, therapeutics that address both bone and muscle weakness will likely be beneficial.

Myostatin and activin A are members of the TGF-β superfamily of proteins produced by muscle and bone cells, respectively, which elicit canonical signaling cascades via the activin type II and I receptor kinases, ActRIIB and Alk4/5/7, stimulating downstream intracellular Smad signaling[17,166,269]. As a negative regulator of muscle

mass, the absence of myostatin results in a double-muscled phenotype with substantial increases in muscle[15,320]. Myostatin deficiency via pharmacological agents also results in muscle hypertrophy in multiple species[20–22,192]. Activin A increases the differentiation potential in osteoclasts (bone-resorbing cells), but limits the differentiation potential in bone-producing osteoblasts[16,265]. Inhibition of activin A has been associated with increased callus formation during fracture healing and increased bone formation[162,182]. Although deficiency in myostatin alone is sufficient to elicit muscle hypertrophy, additive activin A inhibition more potently induces muscle mass formation, especially in primates[22]. Thus, ligand traps to ActRIIB induce significant increases to murine muscle mass and triggers improvements in the skeletal phenotype[20,21,200,224]. Even so, ActRIIB ligand traps lower serum levels of multiple ligands besides activin A and myostatin, obscuring the roles of myostatin and activin A in this postnatal muscle mass increase[23].

Currently, no data exists on the impacts of specific inhibition of activin A alone, myostatin alone or both in the severe type III *OIM* mice. Thus, in the present study, we examined the effect of anti-activin A antibody, anti-myostatin antibody or combined anti-activin A and anti-myostatin antibody therapy on muscular and whole body metabolism in homozygote *oim/oim* mice. The *oim* mouse originally arose from spontaneous nucleotide deletion in the C-terminal end of the *Col1a2* gene, generating a mouse with severely compromised skeletal phenotype. Homozygote *oim/oim* mice are small, with significantly smaller hindlimb muscles which exhibit an inherent muscle pathology with impaired contractile force generation capacities[110]. *Oim/oim* mice also exhibit a progressively deforming skeletal phenotype, synonymous to type III human OI[101].

Materials and methods

Animals: All experiments were approved by the University of Missouri Animal Care and Use Committee (ACUC) and met ARRIVE guidelines. All study mice had access to food and water at all times and were housed in AAALAC facility with 12hr alternating light and dark cycles. *Col1a2*$^{oim/oim}$ (*oim/oim*) mice and their Wt littermates were generated from heterozygous *OIM* crosses (*+/oim* X *+/oim*) and maintained on the C57BL6 background[(103)].

***Study Design*:** Male and female Wt and *oim/oim* mice were randomly assigned to one of 4 treatment groups: control antibody (Ctrl-Ab, Regn 1945), anti-activin A antibody (ActA-Ab, Regn2746), anti-myostatin antibody (Mstn-Ab, Regn647) or combination ActA-Ab and Mstn-Ab (Combo). Treatment was administered intraperitoneally starting at 5 weeks of age at 10mg/kg of body weight twice weekly. Before each injection, body weights were recorded. Mice were humanely euthanized at 16 weeks of age, following 11 weeks of treatment.

***Body Composition and Whole Body Metabolism assessment*:** Between 14-16 weeks of age, mice were placed in Promethion metabolic cages to track their energy expenditure, respiratory quotient, water and food intake, and activity levels. Mice were individually housed for 3 days, with the first day considered an acclimatization period. Data on the aforementioned parameters were collected in diurnal (7 am – 7 pm) and nocturnal (7 pm to 7 am) cycles.

Following metabolic cage assessments, whole body composition in live mice was assessed using the EchoMRI, as previously described in Chapter III (Methods).

***Muscle Force Generation Assessment*:** Prior to euthanasia, mice were anesthetized and gastrocnemius, TA and soleus muscle contractile force assessed as described in Chapter III (Methods).

***Hindlimb Tissue Collection*:** Post-sacrifice, left hindlimb gastrocnemius, quadriceps, tibialis anterior (TA), plantaris, soleus and extensor digitorum longus (EDL) muscles were harvested and weighed. Calluses were recorded at the time of hindlimb muscle collection.

Results

Casualties and Calluses:

During the course of the study, 2 female Wt (1 Mstn-Ab; 1 ActA-Ab) and 11 *oim/oim* mice (male and female; 3 Mstn-Ab; 5 ActA-Ab and 3 Ctrl-ab) mice died. One mouse died of a compound fracture sustained 2 weeks into ActA-Ab treatment by unknown means. Of the remaining experimental mice, 40 *oim/oim* male and female mice sustained at least one callus in their femurs, tibias or forelimbs (Table 1). Majority of the calluses observed were on the right and left femurs (n=34). Male *oim/oim* mice were more likely to have calluses on their long bones verses female *oim/oim*, and treatment did not appear to influence callus occurrence. No Wt mice sustained calluses.

Table A.1: Number of *oim/oim* mice with at least 1 callus on long bones (Femurs or tibias)

	Ctrl-Ab	ActA-Ab	Mstn-Ab	Combo
Male *oim/oim*	6	9	5	5
Female *oim/oim*	3	3	3	6

Table A.2: Percentage of *oim/oim* mice with at least 1 callus on long bones (Femurs or tibias)

	Ctrl-Ab	ActA-Ab	Mstn-Ab	Combo
Male *oim/oim*	50%	47%	33.3%	41.7%
Female *oim/oim*	16.7%	23%	30%	46.2%

Growth trend and body weights

Between 5 and 16 weeks of age, control male and female *oim/oim* mice had noticeably smaller body weights relative to their age and sex-matched Wt controls (Figure 1, Table 3). ActA-Ab treatment failed to increase body weights in all mice. Mstn-Ab treatment increased body weights after 6 and 3 weeks of treatment in Wt male and female mice respectively. Among *oim/oim* mice, males responded early to Mstn-Ab treatment with increased body weights within 2 weeks of treatment whereas females showed a trend towards increasing body weights after 8 weeks of treatment. The Combo-treatment increased body weights in both male and female Wt mice after 4 weeks of treatment, whereas in *oim/oim*, larger body weights were observed after 2 and 5 weeks of treatment in males and females, respectively (Figure 1, Table 3).

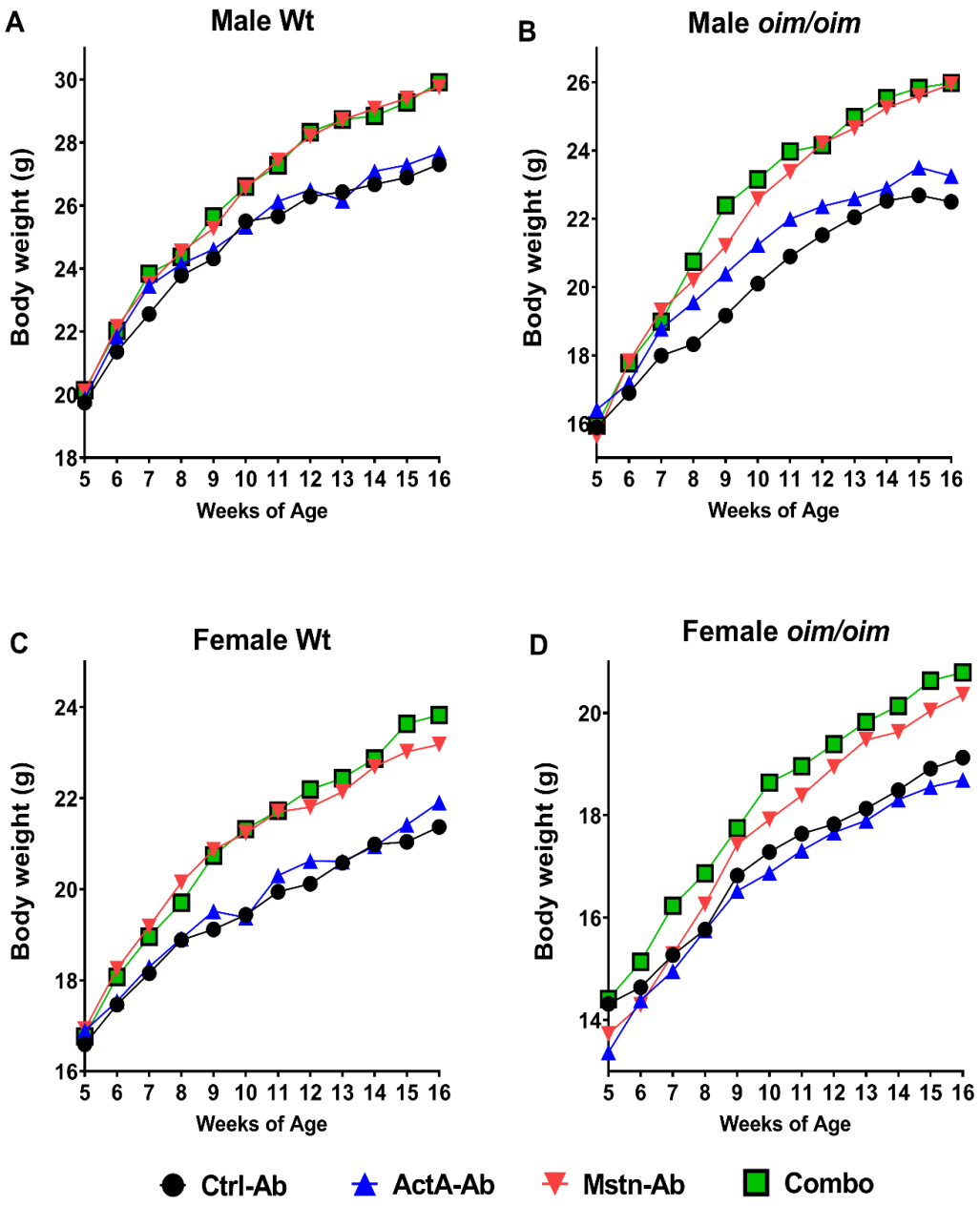

Figure A.1. Changes in body weight with control antibody, anti-myostatin antibody, anti-activin A antibody and combined anti-myostatin and anti-activin A antibodies (Combo) treatment in Wt and *oim/oim* mice over 11-week treatment period. Male Wt (A), Male *oim/oim* (B), Female Wt (C), and Female *oim/oim* (D), were treated with either control antibody (Ctrl-Ab, black circle); activin A antibody (ActA-Ab, blue triangle); myostatin antibody (Mstn-Ab, red triangle) or combination activin A and myostatin antibodies (Combo, green square). Mean values are plotted; n=8-17. $p<0.1$ is indicated and considered significant

Table A.3: P-values of changes in body weight in Wt and *oim/oim* mice treated with ActA-Ab, Mstn-Ab or Combo relative to Ctrl-Ab treated mice (Figure A.1).

Genotype/Sex	Treatment	Wk5	Wk6	Wk7	Wk8	Wk9	Wk10	Wk11	Wk12	Wk13	Wk14	Wk15	Wk16
Female Wt vs. *oim/oim*		<0.0001	<0.0001	<0.0001	<0.0001	<0.0001	<0.0001	<0.0001	<0.0001	<0.0001	<0.0001	<0.0001	<0.0001
Male Wt vs. *oim/oim*		0.0016	<0.0001	<0.0001	<0.0001	0.001	0.0019	0.0009	0.001	0.0004	0.0003	0.0022	0.0013
Male Wt	ActA-Ab	n/s	n/s	n/s	n/s	n/s	n/s	n/s	n/s	n/s	n/s	n/s	n/s
	Mstn-Ab	n/s	n/s	n/s	n/s	n/s	n/s	0.0203	0.0125	0.0033	0.002	0.0013	0.0018
	Combo	n/s	n/s	n/s	n/s	0.0733	n/s	0.0298	0.0061	0.0024	0.0044	0.0018	0.0007
Male *oim/oim*	ActA-Ab	n/s	n/s	n/s	n/s	n/s	n/s	n/s	n/s	n/s	n/s	n/s	n/s
	Mstn-Ab	n/s	n/s	0.0385	0.0083	0.0041	0.0005	0.0005	0.0004	0.0006	0.0003	0.0001	<0.0001
	Combo	n/s	n/s	0.0614	0.0012	<0.0001	<0.0001	<0.0001	0.0004	<0.0001	<0.0001	<0.0001	<0.0001
Female Wt	ActA-Ab	n/s	n/s	n/s	n/s	n/s	n/s	n/s	n/s	n/s	n/s	n/s	n/s
	Mstn-Ab	n/s	n/s	n/s	0.0644	0.0156	0.0131	0.0152	0.02	0.0316	0.0184	0.0063	0.0212
	Combo	n/s	n/s	n/s	n/s	0.0291	0.0115	0.0166	0.0054	0.0126	0.0113	0.0017	0.003
Female *oim/oim*	ActA-Ab	n/s	n/s	n/s	n/s	n/s	n/s	n/s	n/s	n/s	n/s	n/s	n/s
	Mstn-Ab	n/s	n/s	n/s	n/s	n/s	n/s	n/s	n/s	0.0529	n/s	n/s	0.0759
	Combo	n/s	n/s	n/s	n/s	n/s	0.045	0.0513	0.0208	0.0123	0.0151	0.0111	0.014

At the end of the study period at 16 weeks of age, both male and female control *oim/oim* mice were smaller in terms of body weight relative to their Wt counterparts [-17.5% and -8.6% respectively] (Figure 2A). ActA-Ab increased overall body weights in male *oim/oim* mice (+6.68%, p=0.0216) whereas female *oim/oim* body weights remained equivalent to control treated female Wt mice (Figures 2A, 2B). In Wt mice, Act-Ab did not affect overall body weight in mice. Mstn-Ab increased overall body weights in mice [(Male Wt: +10%, p=0.085), (Male *oim/oim*: +13.4%, p=0.001), (Female Wt: +7.1%, p=0.006), (Female *oim/oim*: +7.9%, p=0.039)] to a similar extent compared to the Combo treatment [(Male Wt: +8.9%, p=0.085), (Male *oim/oim*: +13.5%, p=0.001), (Female Wt: +8.2%, p=0.006), (Female *oim/oim*: +7.8%, p=0.039)].

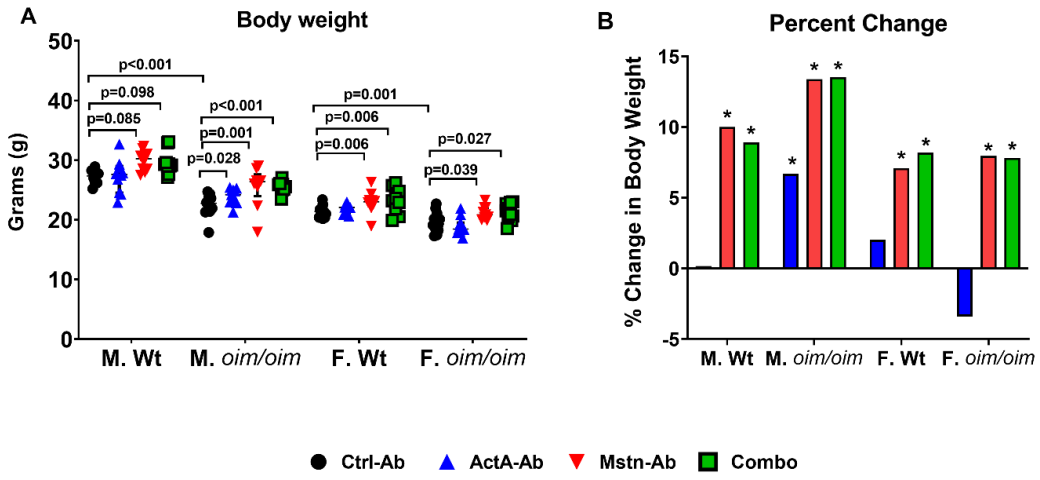

Figure A.2: Body weights of Ctrl-Ab, ActA-Ab, Mstn-Ab and Combo-treated Wt and *oim/oim* mice Wt and *+/G610C* mice. A) Body weight, B) Percent Change in body weight as a result of treatment with either control antibody (Ctrl-Ab, black circle); activin A antibody (ActA-Ab, blue triangle); myostatin antibody (Mstn-Ab, red triangle) or combination activin A and myostatin antibodies (Combo, green square). Values are median with interquartile range, n=8-13. P-values <0.1 are indicated and considered significant.

Absolute Hindlimb muscle weights at 16 weeks of age

At 16 weeks of age, absolute hindlimb muscle weights in control *oim/oim* male mice were considerably lower in the gastrocnemius (Figure 3A), quadriceps (Figure 3B) tibialis anterior (TA, Figure 3C), plantaris (Figure 3D) and soleus (Figure 3E) relative to Wt male mice. Female ctrl-Ab treated *oim/oim* mice also had smaller absolute quadriceps muscle masses relative to their Wt counterparts.

ActA-Ab treatment had minimal effects on absolute hindlimb muscles, only increasing hindlimb muscle weights in male Wt (gastrocnemius and plantaris), female Wt (TA) and decreasing plantaris weights in female *oim/oim* mice.

Mstn-Ab treatment had a more extensive muscle effect, but only in male mice, increasing muscle weights in male Wt (gastrocnemius, quadriceps, TA, plantaris and soleus) and male *oim/oim* (gastrocnemius, quadriceps, TA). Mstn-Ab alone was insufficient to elicit increases in female Wt or *oim/oim* hindlimb muscles.

The Combo treatment increased absolute weights in all hindlimb muscles evaluated in Wt male mice, including the EDL (Figure 3G), while their *oim/oim* counterparts had increased quadriceps, TA and soleus muscles. Female Wt mice also had increases in their gastrocnemius, quadriceps, and TA muscles with the Combo treatment, whereas female *oim/oim* saw increases in their quadriceps muscles only.

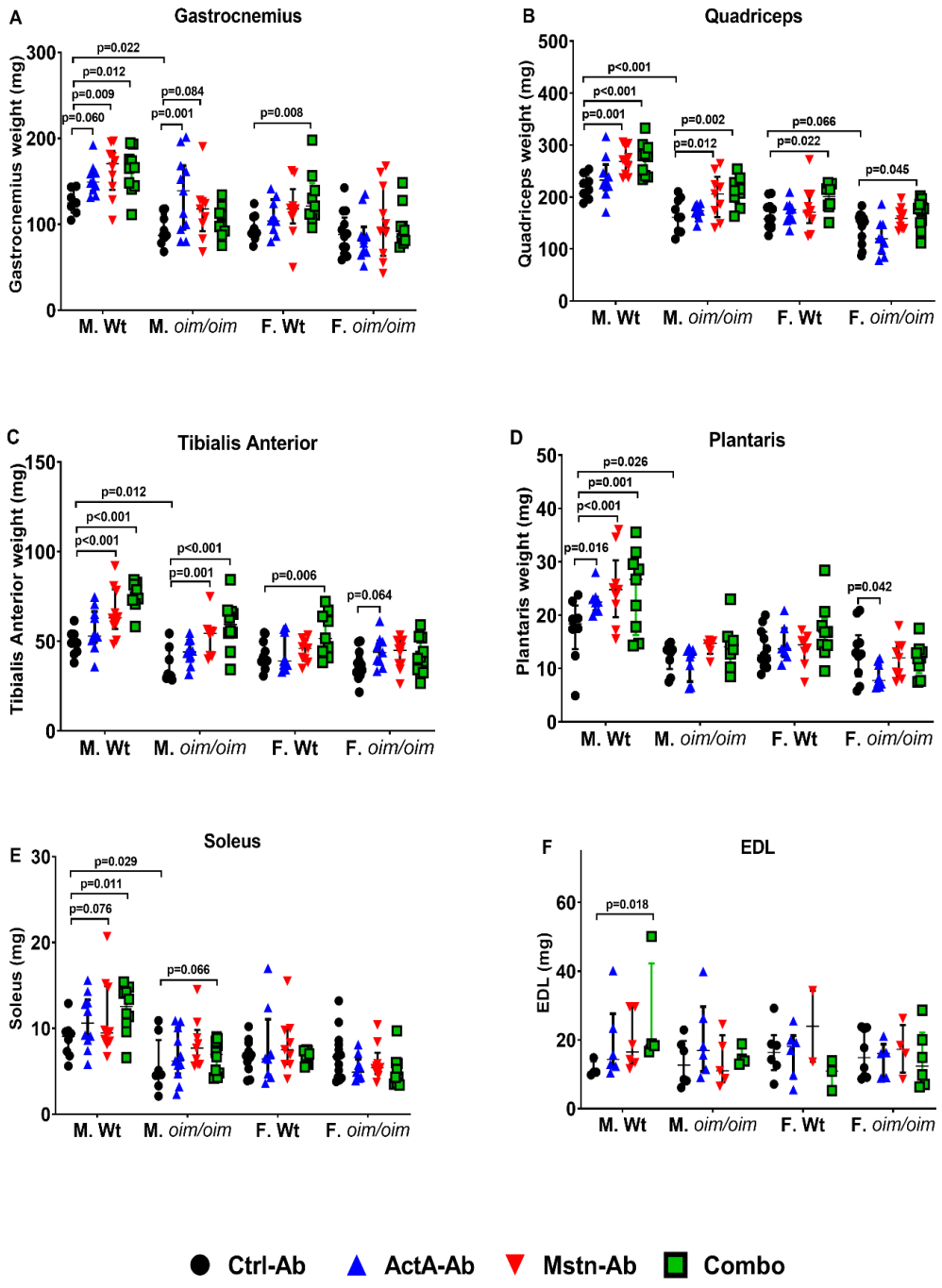

Figure A.3: Absolute hindlimb muscle weights of Ctrl-Ab, ActA-Ab, Mstn-Ab and Combo-treated Wt and *oim/oim* mice. A) Gastrocnemius, B) Quadriceps C) Tibialis Anterior (TA) D) Plantaris E) Soleus F) Extensor Digitorium Longus (EDL) weights as a result of treatment with either control antibody (Ctrl-Ab, black circle); activin A antibody (ActA-Ab, blue triangle); myostatin antibody (Mstn-Ab, red triangle) or combination activin A and myostatin antibodies (Combo, green square). Values are median with interquartile range, n=8-13. P-values <0.1 are indicated and considered significant.

Relative Hindlimb muscle weights at 16 weeks of age

Among control treated mice, Wt and *oim/oim* mice had equivalent relative hindlimb muscles masses except for the soleus muscles, where male *oim/oim* had lower relative soleus weights than male Wt. When total body weight is taken into account, the treatment effect on absolute muscle masses in the experimental mice appear proportional to their body weights. ActA-Ab increased relative weights in gastrocnemius [male *oim/oim*, (Figure 4A)] and plantaris muscles [male Wt, (Figure 4D)], but decreased relative plantaris weight in female *oim/oim* (Figure 4D). Mstn-Ab increased relative weights in TA and plantaris muscles [male Wt, (Figure 4C, and 4D)] and soleus muscles [male and female *oim/oim*, (Figure 4E)]. The Combo treatment increased relative quadriceps [male Wt, (Figure 4B)], TA [male and female Wt and male *oim/oim*, (Figure 4C)], plantaris [male Wt, (Figure 4D)] and soleus (female *oim/oim*, (Figure 4E)).

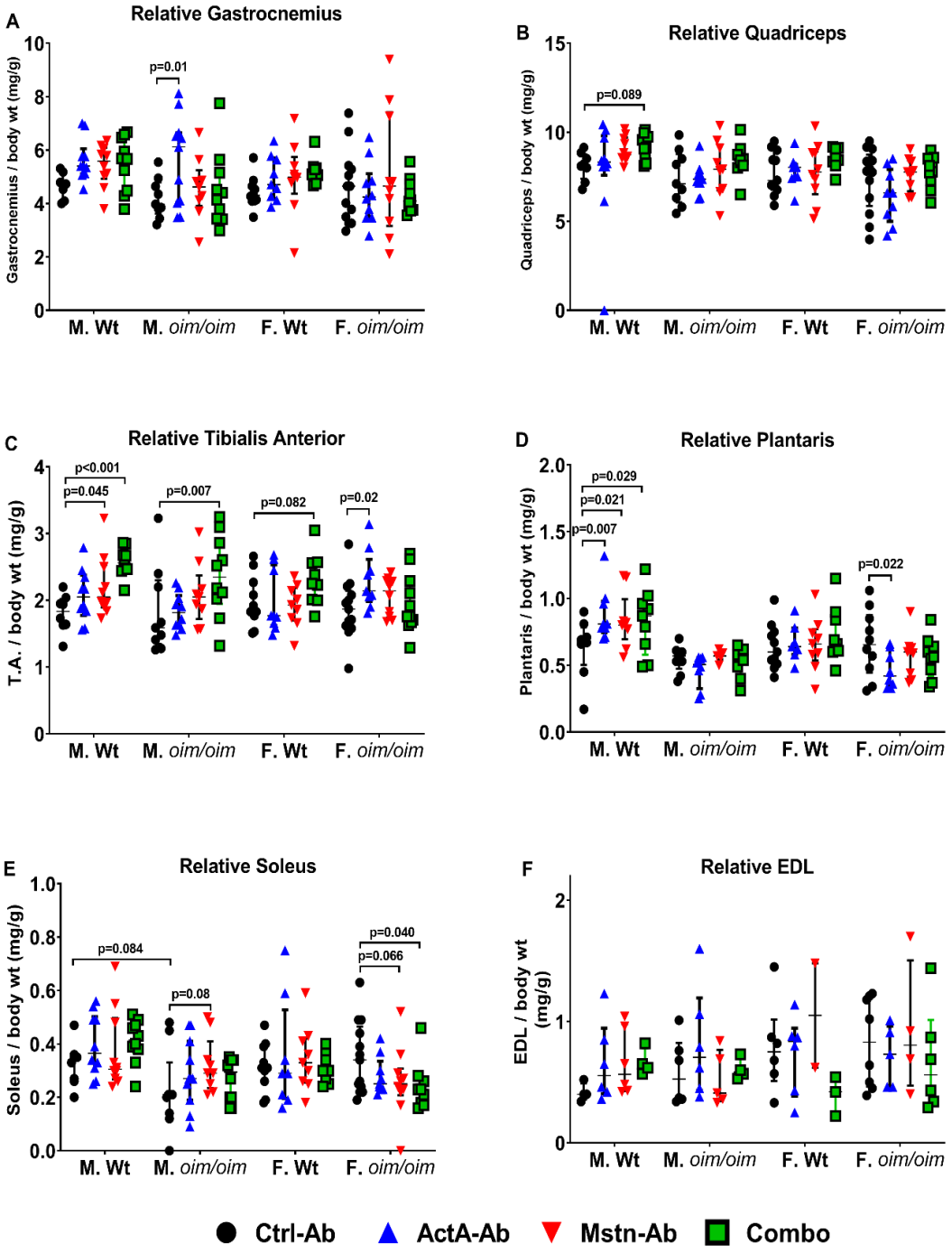

Figure A.4: Relative hindlimb muscle weights of Ctrl-Ab, ActA-Ab, Mstn-Ab and Combo-treated Wt and *oim/oim* mice. A) Relative Gastrocnemius , B) Relative Quadriceps C) Relative Tibialis Anterior (TA) D) Relative Plantaris E) Relative Soleus F) Relative Extensor Digitorum Longus (EDL) weights (mg/g) as a result of treatment with either control antibody (Ctrl-Ab, black circle); activin A antibody (ActA-Ab, blue triangle); myostatin antibody (Mstn-Ab, red triangle) or combination activin A and myostatin antibodies (Combo, green square). Values are median with interquartile range, n=8-13. P-values <0.1 are indicated and considered significant.

Muscle Force Generation Assessment

Control male and female *oim/oim* had equivalent peak tetanic and relative tetanic force generation capacities in their gastrocnemius muscles as Wt mice (Figures 5A, 5B).

Neither ActA-Ab nor Mstn-Ab treatment appears to increase peak or relative gastrocnemius muscle force production in either Wt or *oim/oim* mice although the study may be underpowered to detect changes. However, the Combo treatment increased the peak gastrocnemius force (P_o) in female Wt mice, but failed to cause significant changes in male Wt or male and female *oim/oim* mice.

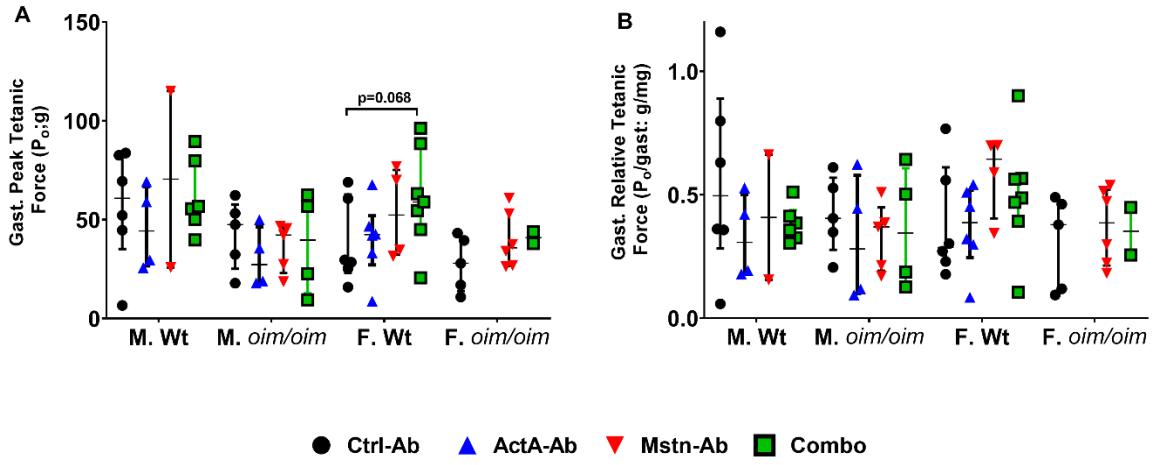

Figure A.5: Absolute and Relative hindlimb muscle contractile force generation of Ctrl-Ab, ActA-Ab, Mstn-Ab and Combo-treated Wt and *oim/oim* mice. A) Gastrocnemius peak tetanic force, B) Gastrocnemius relative tetanic force, Mice were treated twice weekly with 10mg/kg of control antibody (Ctrl-Ab, black circle); activin A antibody (ActA-Ab, blue triangle); myostatin antibody (Mstn-Ab, red triangle) or combination activin A and myostatin antibodies (Combo, green square) for 11 weeks. Values are median with interquartile range, n=1-12. Values are median with interquartile range, n=2-7. P-values <0.1 are indicated and considered significant.

Absolute and Relative Fat Mass

Wt and *oim/oim* mice had similar inguinal fat weights regardless of sex or treatment (Figure 6). Male Wt mice had larger absolute and relative gonadal fat masses compared to male *oim/oim* mice although gonadal fat weights were similar between female Wt and *oim/oim* mice (Figure 6C, 6D). Brown adipose tissue (BAT) masses were equivalent between genotypes (Figure 6E, 6F).

Mstn-Ab decreased relative BAT weights in female Wt mice. The Combo treatment had the greatest impact, with decreased absolute gonadal fat mass (Wt male), relative gonadal fat mass (male Wt, female *oim/oim*), and decreased BAT [absolute BAT (male *oim/oim*, female Wt); relative BAT (male and female *oim/oim*, female Wt)].

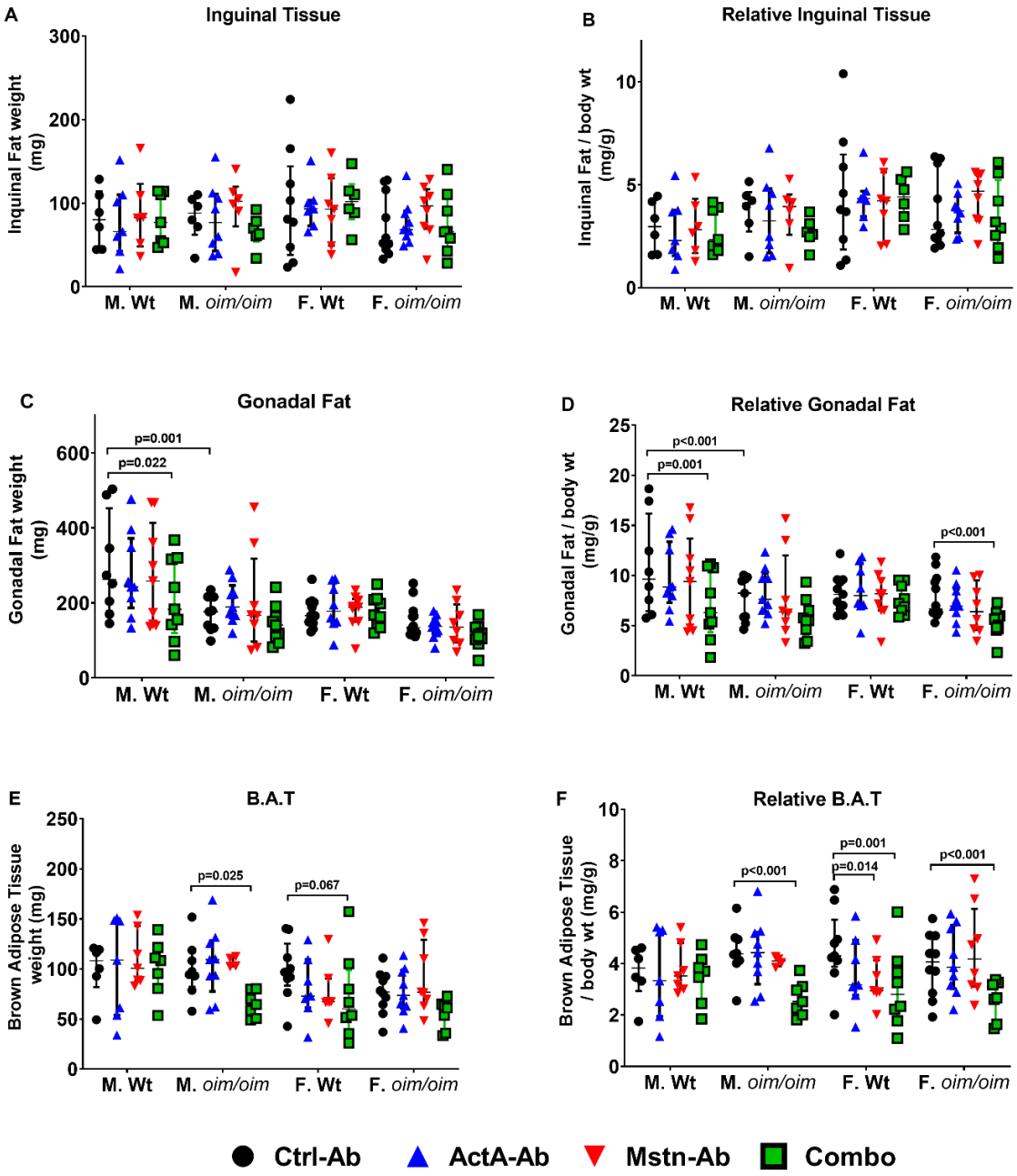

Figure A.6: Absolute and Relative fat mass of Ctrl-Ab, ActA-Ab, Mstn-Ab and Combo-treated Wt and *oim/oim* mice. A) Absolute Inguinal fat (g) , B) Relative Inguinal fat (mg/g) C) Absolute Gonadal Fat (g) D) Relative Gonadal Fat (mg/g) E) Absolute brown adipose tissue (BAT, g) F) Relative brown adipose tissue (BAT, mg/g) as a result of treatment with either control antibody (Ctrl-Ab, black circle); activin A antibody (ActA-Ab, blue triangle); myostatin antibody (Mstn-Ab, red triangle) or combination activin A and myostatin antibodies (Combo, green square). Values are median with interquartile range, n=4-10. P-values <0.1 are indicated and considered significant.

Body Composition

Body composition analyses, conducted with the EchoMRI, revealed lower absolute lean muscle masses in Ctrl-Ab-treated male and female *oim/oim* mice (Figure 7A) as compared to Wt mice, although relative lean muscle mass was increased in male *oim/oim* as compared to male Wt mice, with a similar trend for female *oim/oim* and Wt mice (Figure 7B). Male *oim/oim* mice also had decreased absolute and relative body fat mass as compared to Wt mice (Figures 7C, 7D). Both male and female Ctrl-Ab-treated *oim/oim* mice had lower total water masses, but higher relative total water masses compared to their Wt counterparts (Figure 7E, 7F).

ActA-Ab increased overall lean and total water masses in male *oim/oim* mice, increased relative fat in female Wt, but decreased both absolute and relative body fat in male Wt mice. Mstn-Ab increased overall lean muscle mass (male and female Wt, female *oim/oim*), relative lean mass (male Wt), total water (all genotype groups), relative total water (male and female Wt), and decreased overall and relative fat masses in male Wt mice. The Combo treatment consistently increased overall lean muscle mass (both absolute and relative) and total water mass (both absolute and relative) in all mice regardless of sex or genotype. The Combo treatment also decreased absolute and relative fat masses in male Wt and *oim/oim* mice and relative fat in female Wt mice.

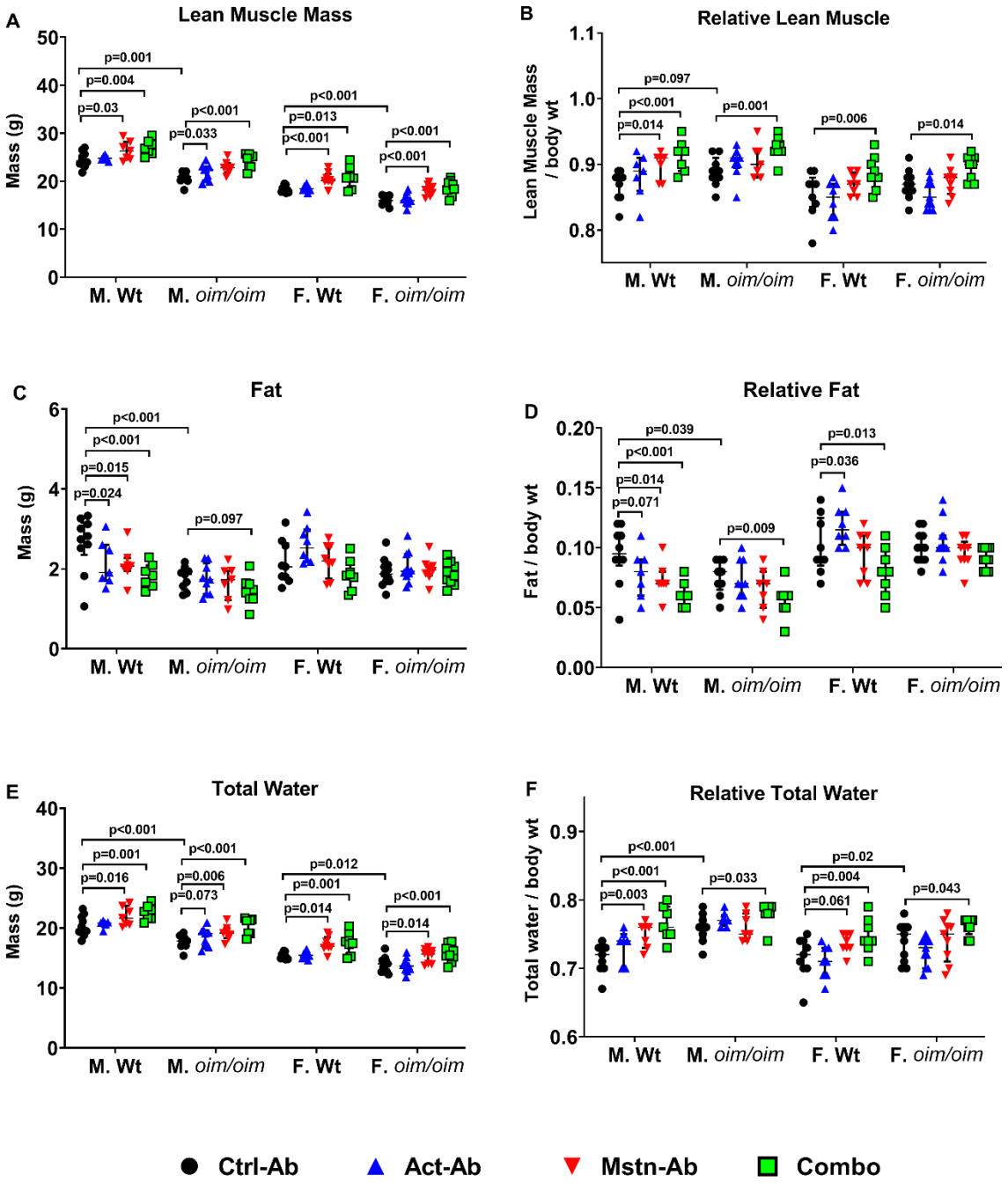

Figure A.7: Body Composition of Ctrl-Ab, ActA-Ab, Mstn-Ab and Combo-treated Wt and *oim/oim* mice. A) Absolute Lean Muscle Mass, B) Relative Lean Muscle Mass C) Absolute Fat mass, D) Relative Fat mass, E) Total water, F) Relative Total Water. Mice were treated twice weekly with 10mg/kg of either control antibody (Ctrl-Ab, black circle); activin A antibody (ActA-Ab, blue triangle); myostatin antibody (Mstn-Ab, red triangle) or combination activin A and myostatin antibodies (Combo, green square) for

11 weeks. Values are median with interquartile range, n=9-15. Pvalues <0.1 are indicated and considered significant

Absolute and Relative Heart and spleen weights

Male and female Wt mice had similar absolute heart and spleen weights as their *oim/oim* counterparts (Figures 8A-8D). However, relative heart and spleen weights were substantially larger in *oim/oim* mice (Figures 8B, 8D).

ActA-Ab treatment did not impact heart or spleen weights. Mstn-Ab treatment also did not impact heart weights but decreased relative spleen weights in *oim/oim* mice. The Combo treatment did not also impact heart weights but decreased absolute spleen weights in male *oim/oim* mice and relative spleen weights in both male and female *oim/oim* mice.

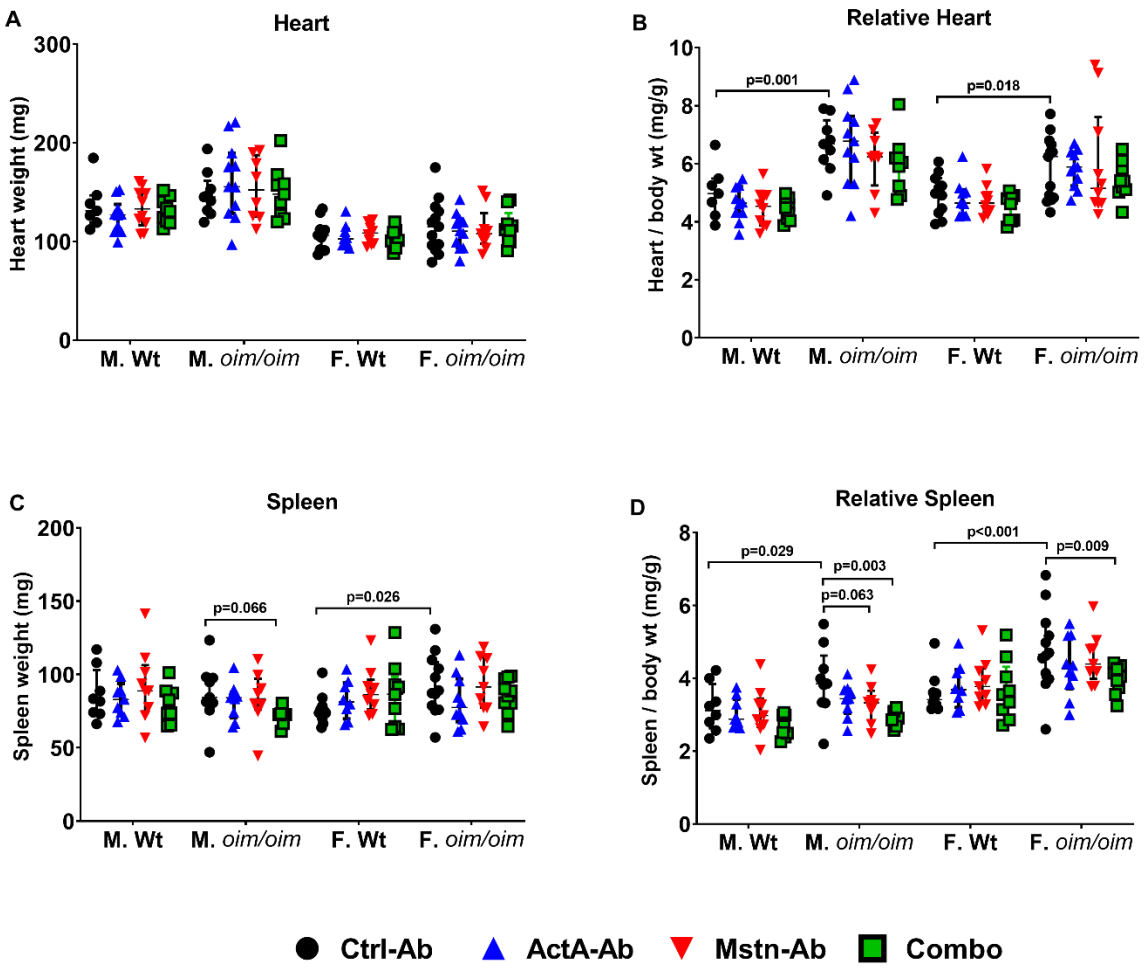

Figure A.8: Absolute and Relative heart and spleen weights of Ctrl-Ab, ActA-Ab, Mstn-Ab and Combo-treated Wt and *oim/oim* mice. A) Absolute Heart weight (mg), B) Relative Heart weight (mg/g) C) Absolute Spleen weight (g) D) Relative Spleen weight (mg/g) as a result of treatment with either control antibody (Ctrl-Ab, black circle); activin A antibody (ActA-Ab, blue triangle); myostatin antibody (Mstn-Ab, red triangle) or combination activin A and myostatin antibodies (Combo, green square). Values are median with interquartile range, n=8-13. Pvalues <0.1 are indicated and considered significant.

Metabolic status

Energy Status

Metabolic chamber analyses revealed that *oim/oim* female mice exhibit a metabolic phenotype around 14-16 weeks of age and were likely to respond to treatment with changes in energy status. In female *oim/oim* mice, energy expenditure (EE) (both mean and total) are decreased during both day (~ -10%) and night (~ -12.6%) (Figure 9A-D) whereas mean respiratory quotient (RQ) was increased during the day (+6.5%, Figure 9E). Male *oim/oim* mice exhibited a similar energy profile as Wt mice.

Interestingly, ActA-Ab treatment influenced energy status in mice, increasing EE in male *oim/oim* mice during the day and in *oim/oim* females at night, while increasing RQ in female Wt mice during the day cycle. Mstn-Ab did not alter EE or RQ in any of the study mice. Combo treatment increased mean EE (+15%, night cycle), total EE (+15%, night cycle), and decreased RQ (-6%, day cycle) in female *oim/oim* mice, also inducing a phenotype.

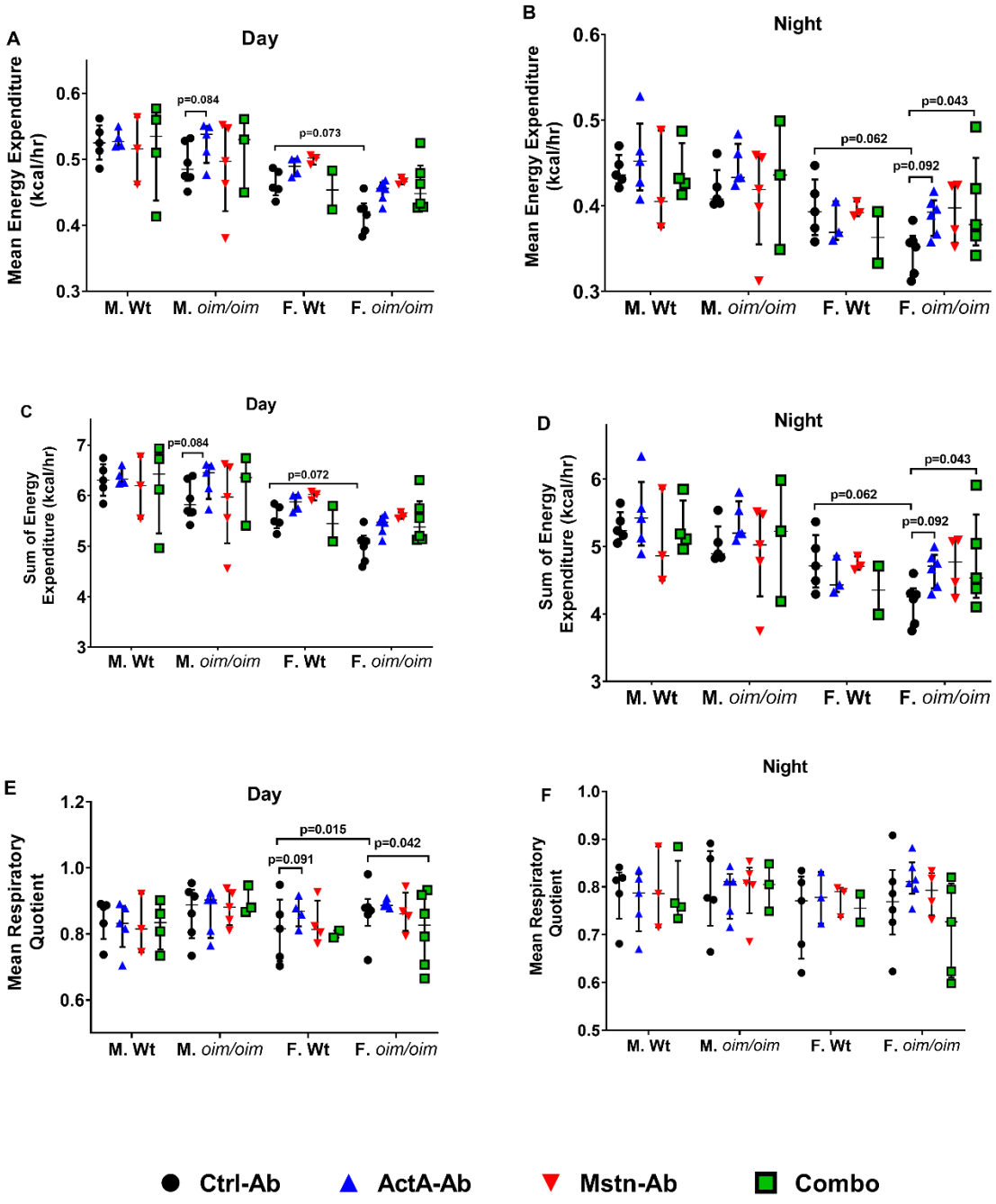

Figure A.9: Indirect calorimetry to assess energy status of Ctrl-Ab, ActA-Ab, Mstn-Ab and Combo-treated Wt and *oim/oim* mice. A) Mean energy expenditure (EE, day cycle), B) Mean energy expenditure (EE, night cycle), C) Sum of energy expenditure (EE, Day cycle), D) Sum of energy expenditure (Night cycle), E) Mean Respiratory Quotient (Day Cycle), F) Mean Respiratory Quotient (Night Cycle). Mice were treated twice weekly with 10mg/kg of control antibody (Ctrl-Ab, black circle); activin A antibody (ActA-Ab, blue triangle); myostatin antibody (Mstn-Ab, red triangle) or combination activin A and myostatin antibodies (Combo, green square) for 11 weeks. Values are median with interquartile range, n=2-6. P-values <0.1 are indicated and considered significant.

Substrate Utilization

Control female *oim/oim* had lower VO_2 consumption relative to Wt mice (Figure 10A-B) although VCO_2 production, food and water intake levels were equivalent in all control mice regardless of genotype (Figure 10C-H).

In female *oim/oim* mice, ActA-Ab increased VO_2 consumption and VCO_2 production during the night cycle (Figure 10A-10D). In male *oim/oim* mice, ActA-Ab increased VO_2 consumption during the day. ActA-Ab also increased VCO_2 production and water intake in female Wt mice while decreasing water intake in male Wt mice during the day cycle. Mstn-Ab only increased VCO_2 production and increased day time water intake in female Wt. The Combo treatment only increased VO_2 consumption in female *oim/oim* mice.

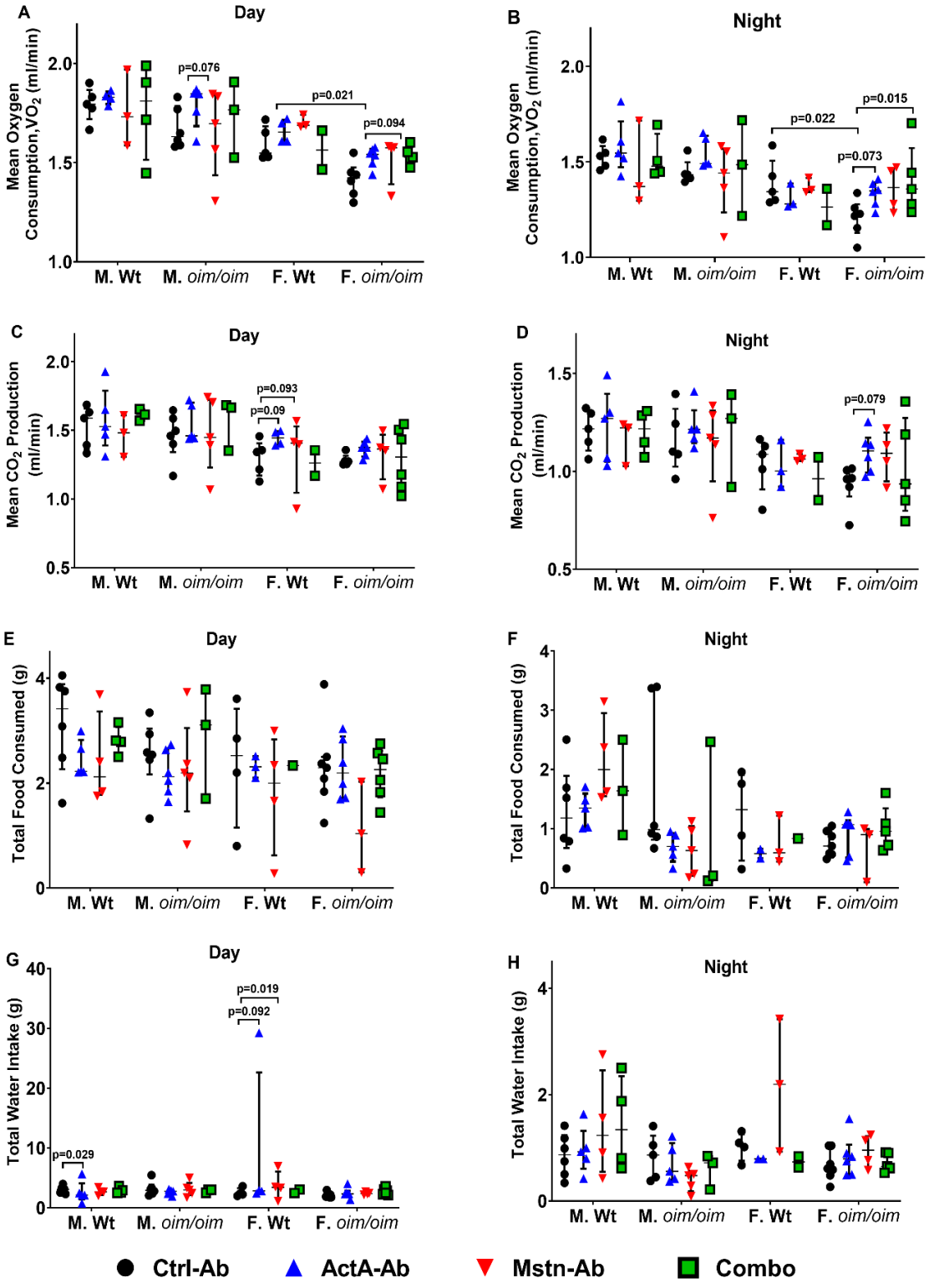

Figure A.10: Indirect calorimetry to assess substrate utilization in Wt and *oim/oim* mice treated with Ctrl-Ab, ActA-Ab, Mstn-Ab and Combo. A) Mean VO_2 Consumption (Day cycle), B) Mean O_2 Consumption (Night cycle), C) Mean CO_2 Consumption (Day cycle),

D) Mean CO_2 Consumption (Night cycle), E) Total Food Consumed (Day Cycle), F) Total Food Consumed (Night Cycle), G) Total Water Intake (Day Cycle), H) Total Water Intake (Night Cycle). Mice were treated twice weekly with 10mg/kg of control antibody (Ctrl-Ab, black circle); activin A antibody (ActA-Ab, blue triangle); myostatin antibody (Mstn-Ab, red triangle) or combination activin A and myostatin antibodies (Combo, green square) for 11 weeks.. Values are median with interquartile range, n=2-6. P-values <0.1 are indicated and considered significant.

Activity

Overall, control Wt mice had equivalent activity levels as *oim/oim* mice except for female Wt who exhibited more nighttime activity along the Z-axes than their *oim/oim* counterparts.

ActA-Ab treatment increased movement along the Y-axis in male Wt and female *oim/oim*; and along the Z-axis in male and female Wt mice; with similar activity trends in the X-axis for male and female Wt and female *oim/oim* mice during the day (Figures 11A-F). Mstn-Ab increased X-axis movements in female *oim/oim* during both day and night cycles, and increased Z-axis breaks during the day in female Wt mice. Lastly, the Combo treatment had no effect on movement along the X-and Y-axes, only increasing Z-axis movements in female *oim/oim* mice during the day and in male Wt mice at night.

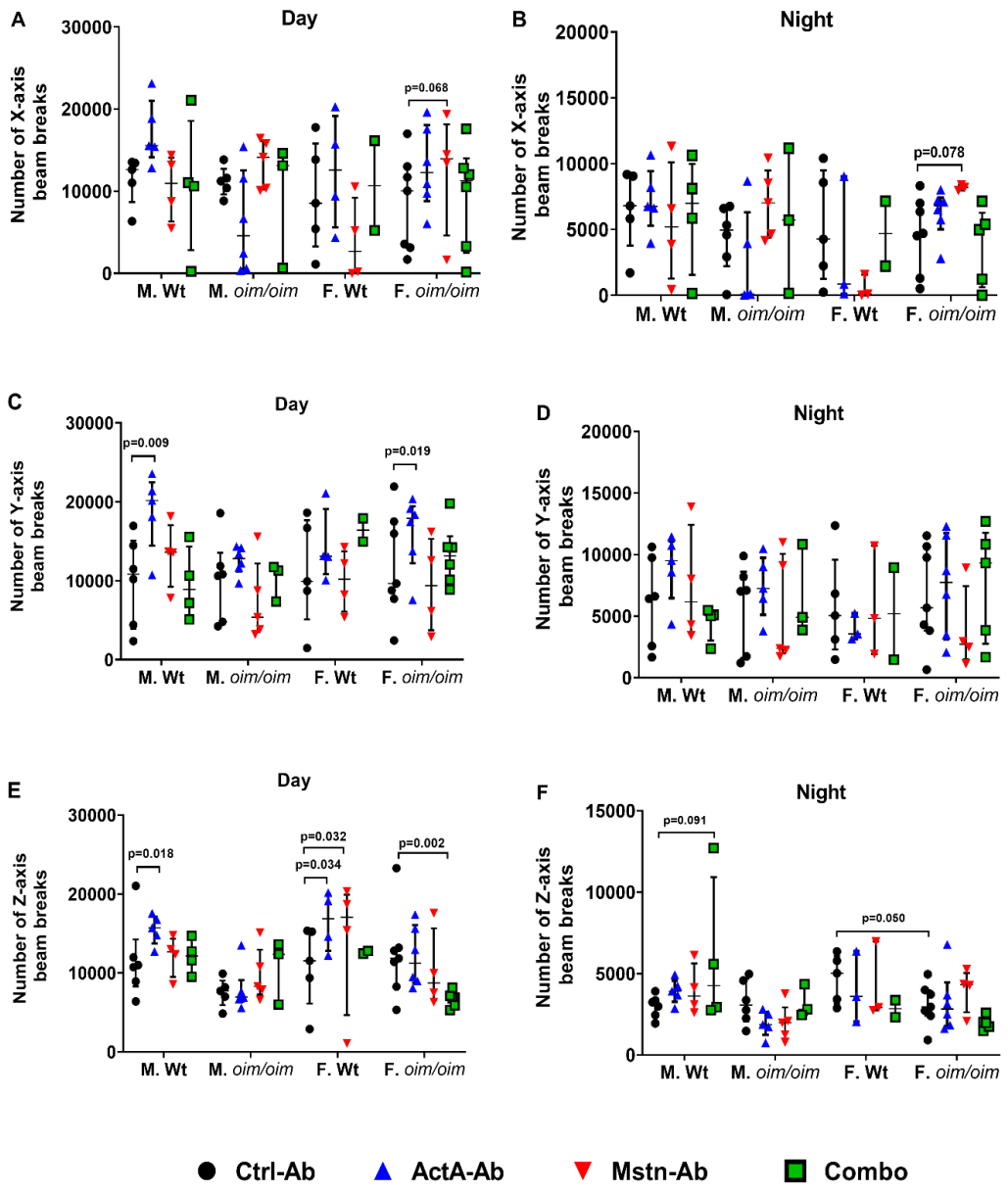

Figure A.11: Activity levels of Ctrl-Ab, ActA-Ab, Mstn-Ab and Combo-treated Wt and *oim/oim* mice. A) Movement along the X-axis (day cycle), B) Movement along the X-axis (night cycle), C) Movement along the Y-axis (Day cycle), D) Movement along the Y-axis (Night cycle), E) Movement along the Z-axis (Day cycle), F) Movement along the Z-axis (Night cycle). Mice were treated twice weekly with 10mg/kg of control antibody (Ctrl-Ab, black circle); activin A antibody (ActA-Ab, blue triangle); myostatin antibody (Mstn-Ab, red triangle) or combination activin A and myostatin antibodies (Combo, green square) for 11 weeks. Values are median with interquartile range, n=5-10. P-values <0.1 are indicated and considered significant.

Discussion

This study investigated the impact of anti-activin A antibody (ActA-Ab), and anti-myostatin antibody (Mstn-Ab) alone or in combination (Combo) on muscle properties and whole body metabolism in the severe type III *OIM* mouse (*oim/oim*). We determined that young adult female *oim/oim* mice exhibit features suggestive of a metabolic phenotype: low mean and total energy expenditure, decreased VO_2 consumption, and higher respiratory quotient as compared to female Wt mice. Both male and female *oim/oim* mice also had smaller hindlimb muscle mass and overall body weights, as previously reported[20,21,103,110]. Treatment with ActA-Ab failed to substantially increase hindlimb muscle and overall body weights in both Wt and *oim/oim* mice although male *oim/oim* exhibited a +6.68% increase in body weight at 16 weeks of age. Mstn-Ab and Combo-treated *oim/oim* mice had similar significant increases in overall body weight. However, the number of hindlimb muscle groups demonstrating significant increases in mass per genotype was much higher with the Combo treatment than with the Mstn-Ab treatment.

In a previous study, we demonstrated that regardless of genotype (Wt, *+/G610C*, *oim/oim*) male and female mice exhibit on average a +20% and +24% increase in body weight with sActRIIB treatment, respectively[20]. In this current study, we observed a +7%-14% overall increase in body weight with the Combo treatment, which is similar to Mstn-Ab treatment alone, whereas ActA-Ab alone only increased overall body weight in male *oim/oim* mice. sActRIIB-treated mice also exhibited increases in hindlimb muscle masses, although to varying degrees[20,21]. Latres and colleagues have also previously reported the ability of a combined anti-activin A and anti-myostatin antibody treatment

regimen to double TA muscle mass in SCID mice from +20.1% by anti-myostatin antibody alone to +43.9%, akin to the increases engineered by ActRIIB.hFc treatment (+48.8%)[22]. In the present study, Mstn-Ab significantly increased TA muscle weights in male Wt and *oim/oim* mice by +34.8% and +44.4%, respectively, while the Combo treatment resulted in +53.6% and +61.6% increases in male Wt and male *oim/oim* mice, respectively. We did not observe a doubling in TA muscle weight with the Combo treatment, although there is still an increase in muscle mass suggesting that activin A indeed regulates murine postnatal muscle size in concert with myostatin.

Interestingly, EchoMRI body composition analyses showed lower body lean muscle and total water mass, but higher relative lean muscle and total water mass, suggesting that for their size, *oim/oim* mice have greater lean muscle mass compared to Wt mice. The Combo treatment increased overall and relative lean muscle and total water masses regardless of sex or genotype. In Chapter III, we also observed increases in total lean body and water masses in the Combo-treated mice, suggestive of the ability of the Combo treatment to increases lean muscle in mice regardless of OI severity. *Col1a1*$^{Jrt/+}$ mice also administered a decoy receptor specific for myostatin and activin A alone also substantially increased muscle mass[200]. Previous observations of hypertrophy with sActRIIB-mFc treatment will suggest that the observed increases in muscle mass with the Combo treatment are due to larger muscle fibers (hypertrophy)[20].

OI patients are more likely to have heart disease and cardiac complications; extra-skeletal features related to the presence of abnormal or reduced type I collagen in heart tissue and valves[321]. *Oim/oim* mice have morphological changes in the structure of their heart stemming from less collagen content and resulting in higher passive inflation rates

and compliance, morphological alterations and functional adaptations [322]. Also, o*im/oim* mice have been shown to have lower absolute heart weights but normal relative heart weights compared to Wt mice[322], but have been reported to exhibit normal echocardiograms with similar heart rates as Wt mice[322]. Further, the Aga2 mouse model of OI caused by (dominant frameshift mutation in C-terminal region of *Col1a1*) exhibits heart dysfunction characterized by ventricular hypertrophy and defective myocardial matrix, consequently resulting in mortality[323]. While our study did not investigate heart morphology and function, we observed significantly larger heart weight to body weight ratios, confirming that *oim/oim* mice have relatively large hearts. Our antibody treatment strategies did not influence any changes in heart size, in line with the observation that myostatin-null mice do not exhibit a cardiac phenotype [324].

We also observed larger spleen weight to body weight ratios in homozygous *oim/oim* mice relative to Wt mice. Male o*im/oim* mice have been shown to have splenomegaly between 7-9 week-old [325], a phenotype associated with chronic inflammation. In our study, 16-week old female *oim/oim* mice had larger spleens compared to female Wt, but relative spleen weights were much bigger in both male and female *oim/oim* mice as compared to sex-matched Wt mice. It has also been previously reported that decreasing spleen weights using an anti-tumor necrosis factor α (TNFα) treatment failed to improve skeletal phenotype in female *oim/oim* mice[325]. The defective extracellular matrix in bone, combined with chronic inflammation can certainly compromise skeletal integrity with dysfunctional extracellular matrix being the driving force. In the present study, the Combo treatment significantly decreased absolute spleen weights in male *oim/oim,* and both absolute and relative spleen weights in both male and

female *oim/oim*. Whether the decrease in spleen weights reflects reduced inflammatory state and/or is associated with decreased fractures or improved bone strength will be important to determine.

The finding that female *oim/oim* mice exhibit a metabolic phenotype is particularly interesting. Although its clinical relevance is not understood, these findings challenge current researchers to determine the relationship of whole body energy metabolism to the pathogenesis of OI and its ability to respond to treatment. Young OI patients exhibit features reminiscent of a metabolic phenotype, and *Col1a1*$^{Jrt/+}$ mice have also been shown to exhibit a pre-pubertal metabolic phenotype. In this study, *oim/oim* mice were assessed between 14 and 16 weeks of age, when they are considered young adult mice. Additional characterizations of the age of onset of the metabolic phenotype as well as a characterization of glucose and insulin levels and in relation to the onset of the metabolic phenotype is certainly warranted. These observations vary from those made in Chapter III where both *+/G610C* male and female mice fail to exhibit a metabolic phenotype, instead exhibiting similar energy, metabolic and activity levels as their Wt counterparts. Both *Col1a1*$^{Jrt/+}$ and *oim/oim* mice are severe models of OI relative to the *G610C* model, which reflects mild to moderate OI severity. Hence, the stresses of repeated fractures, inflammation, skeletal deformity, functional impairment and perhaps cell stress[101,287,326], likely induces changes in energy and substrate utilization in these severe oim/oim and *Col1a1*$^{Jrt/+}$ murine OI models, resulting in metabolic phenotype.

Lastly, at sacrifice, 40 out of 110 *oim/oim* mice had at least one healed callus in their femurs or tibias, which were independent of the treatment, although Wt mice had no calluses. We were unable to determine whether the calluses occurred prior to treatment

initiation at 5 weeks of age or if they were acquired during the course of treatment. Nonetheless, in Chapter III, we observe increases to muscle mass and bone microarchitecture and strength with the Combo treatment. Although, the *+/G610C* mouse models is a relatively milder type of OI, we hypothesize that the Combo treatment will at least improve the *oim/oim* bone microarchitecture as seen with sActRIIB treatment[19]. Future studies to evaluate bone microarchitecture and biomechanics as a result of treatment with the anti-activin A antibody alone, anti-myostatin antibody alone, or both are described in Chapter IV (Objective 2).

APPENDIX B

OI MUTATION AND SEVERITY-SPECIFIC INFLUENCES ON GENE EXPRESSION IN BONE TREATED WITH THE SOLUBLE ACTIVIN TYPE IIB RECEPTOR DECOY IN THE OIM AND G610C MOUSE MODELS OF OSTEGENESIS IMPERFECTA

This appendix is a part of a publication in the Journal of Bone and Mineral research entitled "Skeletal Response to Soluble Activin Receptor Type IIB in Mouse Models of Osteogenesis Imperfecta" and was presented at the 2018 American Society for Biochemistry and Molecular Biology Annual Meeting, San Diego, CA.

Jeong Y, Daghlas SA, Xie Y, Hulbert MA, Pfeiffer FM, Dallas MR, Omosule CL, Pearsall RS, Dallas SL, Phillips CL. Skeletal Response to Soluble Activin Receptor Type IIB in Mouse Models of Osteogenesis Imperfecta. J Bone Miner Res. 2018 Oct;33(10):1760-1772. doi: 10.1002/jbmr.3473. Epub 2018 Jun 22. PMID: 29813187; PMCID: PMC6400483.

Catherine Omosule[1], Youngjae Jeong [1], and Charlotte Phillips[1, 2]

Department of Biochemistry[1], and Child Health[2], University of Missouri- Columbia

Abstract

Bone is a highly dynamic tissue which is continually remodeled by osteoblasts and osteoclasts, with regulation by osteocytes. In *Osteogenesis Imperfecta* (OI), a clinically heterogeneous disorder characterized by bone fragility, the functions of osteoblasts and osteoclasts are impaired. As a mechanosensitive tissue, bone responds to mechanical loads, some of the strongest of which are from skeletal muscles, by changing its mass and geometry.

The inhibition of myostatin, a negative regulator of muscle growth and a member of the TGF-β superfamily, induces muscle growth via hypertrophy. We investigated the effect of pharmacologically inhibiting myostatin through treatment with the soluble activin receptor Type IIB decoy molecule (sActRIIB-mFc), focusing on the gene expression patterns of bone cells derived from two molecularly distinct mouse models of OI (*osteogenesis imperfecta* murine [*OIM*] vs. *G610C*). Because the molecular defects that give rise to the *G610C* and *OIM* models differ and muscle function is differentially impacted, we hypothesized that the two models will respond differently to sActRIIB-mFc treatment. Homozygous mice (*oim/oim*) in the *OIM* model mimic severely deforming type III OI have a single nucleotide deletion in the *Col1a2* gene that leads to functional null proα2(I) collagen chains and the generation of homotrimeric type I collagen, whereas the *G610C* mouse, heterozygous for a missense mutation in the *Col1a2* gene, has a glycine to cysteine substitution at the 610 position of the triple helical domain and mimics mild to moderately severe type I/IV OI.

At two months of age, wildtype (Wt), *+/G610C*, and *oim/oim* male mice were treated bi-weekly either with vehicle (Tris-buffered saline) or sActRIIB-mFc for 8 weeks.

Quantitative RT-PCR analyses demonstrated that tibias from sActRIIB-mFc treated *oim/oim* mice exhibited increased gene expression levels of the markers of osteoblast, osteoclast, and osteocyte function and differentiation analyzed. This contrasts the significant improvements seen in the femoral cortical bone microarchitecture and biomechanical integrity of sActRIIB-mFc-treated Wt and *+/G610C* mice, which was not observed in the *oim/oim* mice.

In conclusion, our findings indicate that sActRIIB-mFc treatment has differential effects on the *G610C* and *OIM* mice, which may in part reflect differences in severity (severe in *oim/oim* vs. moderate in *+/G610C*), and/or their unique molecular defects.

Understanding the molecular impact of therapeutics is critical in order to develop more effective and targeted treatment for OI.

Introduction

Bone is a highly dynamic tissue composed of osteoblasts, osteoclasts and osteocytes. As a mechanosensitive organ, bone responds to mechanical load, some of the strongest of which come from skeletal muscle, by changing its shape. Thus, there exists a close relationship between muscle and bone mass[327]. Osteoblasts, osteoclasts and osteocytes make up the cellular constituents of bone. Osteoblasts make up 4-6% whereas osteocytes constitute up to 90% of bone cells[35,40,148]. Synergy between bone formation (osteoblasts), bone resorption (osteoclasts) and mechanosensation (osteocytes) is necessary for maintaining bone homeostasis.

Deficiency in myostatin (*mstn*), a member of the TGF-β superfamily and a negative regulator of muscle mass, has been shown to cause muscle hypertrophy and hyperplasia[15]. Inhibition of myostatin has also been shown to increase muscle mass and improve bone strength in several animal models of human disease affecting bone and muscle strength and quality[21,84].

Osteogenesis Imperfecta (OI), commonly known as brittle bone disease, is a genetic, clinically heterogeneous connective tissue disorder that affects 1 in 15,000 live births[83]. OI is characterized by skeletal deformities with bone fragility being a key feature. 90% of OI-causing mutations are due to autosomal dominant defects in type I collagen structure, a protein that provides tensile strength to bone[6]. Current therapies for OI have limited success with the use of antiresorptive drugs and surgical interventions[328]. Thus, it is imperative to develop new treatment approaches that

minimize fracture risks in OI. We hypothesize that myostatin deficiency in OI will improve bone strength and bone cell function due to increasing muscle mass.

The *G610C* mouse models an autosomal dominant mutation that affects a large group of individuals in the Old Order Amish community in Lancaster County, PA and is representative of mild to moderately severe human OI[79]. The patients and the *G610C* mouse have a missense mutation in the α2(I) gene that causes a glycine to cysteine substitution at position 610 of the triple helical domain. The defective collagen is then incorporated into heterotrimeric type I collagen of heterozygote *+/G610C* mice 50 percent of the time.

The osteogenesis imperfecta murine (*OIM)* model arose through a spontaneous mutation that caused a single nucleotide deletion in the *Col1a2* gene. This generates functional null proα2 (I) chains that cannot be incorporated into normal heterotrimeric type I collagen, leading to the production of homotrimeric type I collagen in homozygous *oim/oim* mice[101]. The heterozygote (*+/oim*) and homozygote (*oim/oim*) mice model the phenotype of human type I and type III OI, respectively[101].

In the following study, we have pharmacologically inhibited myostatin and other TGF-β family proteins including activin and GDF-11, via 8 weeks of biweekly administration of a soluble activin receptor type IIB decoy molecule (sActRIIB-mFc [10mg/kg]) or vehicle (Tris Buffered Saline) in the two molecularly distinct mouse models of OI *OIM* and *G610C* and have compared their tibial osteoblast, osteoclast, and osteocyte gene expression patterns.

Methods

Experimental design: Four (4)-month-old C57BL6/J wildtype (Wt), *+/G610C*, and *oim/oim* mice were treated either with vehicle (Tris-Buffered saline) or 10mg/kg of sActRIIB-mFc (RAP-031) via intraperitoneal injections for 8 weeks starting at 2 months of age[19,20]. Mice were euthanized at 4 months of age and tibiae snap frozen for analyses.

RNA isolation and analysis of gene expression by quantitative PCR: Snap frozen right tibiae (with marrow) were homogenized in TRIzol Reagent (Invitrogen, Carlsbad, CA) and total RNA was isolated using the RNeasy Kit (Qiagen, Germantown, MD) with in-column DNase treatment (Qiagen, Germantown, MD). Total RNA (2µg) was used to generate a cDNA library with a High Capacity Reverse Kit (Applied Biosystems, Foster City, CA). Gene expression levels for markers of differentiation and function of osteoblasts (Runx2, Sp7, Dlx5, Alpl, Bglap, and Serpinh1), osteoclasts (Tnfsf11, Csf1, Itgb3, and Ctsk), and osteocytes (Dmp1, Sost, Phex, and β-cat) were normalized to 18S, Pgk1, and Ubc as endogenous controls, using the $\Delta\Delta C_T$ method (Quantstudio 3 Real Time PCR System, Applied Biosystems, Foster City, CA) (Table 1). Results are plotted in bar graphs and the range of expression indicated by $2^{-(\Delta\Delta CT+SD)}$ and $2^{-(\Delta\Delta CT-SD)(329)}$.

Statistical Analyses: 2 X 2 X 2 factorials [2 genotypes (WT and *+/G610C* or WT and *oim/oim*), 2 sexes, and 2 treatments (vehicle and sActRIIB-mFc treated)] were set up and used to analyze experimental data using SAS software (SAS Institute Inc., Cary, NC)[19,20].

Table B.1. Gene expression assays and primer sequences

Gene	Primer Sequence
Runx2	Forward: ACAAGGACAGAGTCAGATTAC
	Reverse: CAGTGTCATCATCTGAAATACG
Sp7	Forward: TGCTTGAGGAAGAAGCTC
	Reverse: CTTCTTTGTGCCTCCTTTC
Dlx5	Forward: AGAGAAGGTTTCAGAAGACTC
	Reverse: AGATTTTCACCTGTGTTTGC
Alpl	Forward: GGATCTCATCAGTATTTGGAAG
	Reverse: AAAGAGACCTAAGAGGTAGTC
Bglap	Forward: ACCATGAGGACCATCTTTC
	Reverse: GGACATGAAGGCTTTGTC
Serpinh1	Forward: ATGTTCTTTAAGCCACACTG
	Reverse: TCGTCATAGTAGTTGTACAGG
Tnfsf11	Forward: TCTGTTCCTGTACTTTCGAG
	Reverse: TTCATGGAGTCTCAGGATTC
Csf1	Forward: CTCAGACATTGGATTCTTCTG
	Reverse: ATGTTCCCATATGTCTCCTTC
Itgb3	Forward: AACTTGATCTTTGCAGTGAC
	Reverse: TACTTCCAGCTCCACTTTAG
Dmp1	Forward: GAACAGTGAGTCATCAGAAG
	Reverse: AAAGGTATCATCTCCACTGRTC
Sost	Forward: TCAGGAATGATGCCACAG
	Reverse: GTACTCGGACACATCTTTG
Phex	Forward: TTTAGGATATTAGGTGCCGAG
	Reverse: TTACCCTTGAGAATTCTAGCC
Pgk1	Forward: CTATCATAGGTGGTGGAGAC
	Reverse: ACACTAGGTTGACTTAGGAG
Ubc	Forward: GAGACGATGCAGATCTTTG
	Reverse: ATGTTGTAGTCTGACAGGG

Results

Oerall, sActRIIB-mFc treatment increased cortical, trabecular and biomechanical properties in Wt and *+/G610C* mice. Homozygous *oim/oim* mice treated with sActRIIB-mFc had increased trabecular microarchitectural properties, but no improvements in cortical bone and bone strength were observed[19]. Interestingly, a previous publication discovered significant increases in muscle contractile strength in *oim/oim* mice only and not in Wt and *+/G610C* mice sActRIIB-mFc treatment [20].

Gene expression analyses revealed significant increases in the expression of alkaline phosphatase (*Alpl*, osteoblasts), β-catenin (*β-cat*, osteocytes) and cathepsin K (*Ctsk*, osteocytes) compared to WT littermates in control *oim/oim* male mice (Figure 1). A trend towards higher gene expression was observed in all genes analyzed in male control *oim/oim* mice relative to control WT mice. Male *+/G610C* tibiae had lower levels of the osteoclast expressed genes: colony stimulating factor 1 (*Csf1*), integrin β (*Itgb3*) and *Ctsk*. Female *oim/oim* mice appeared to have a downregulated trend in gene expression patterns in osteoclast and osteocyte genes and significantly downregulated sclerostin (*Sost*, osteocyte) expression (Figure 2). Control *oim/oim* mice also had similar gene expression of the pro-osteoclastogenic markers *Rankl* and *Csf1*, as well as *Itgb3*, an osteoclast marker. Female *+/G610C* mice exhibited nearly equivalent levels of gene expression as Wt for all the genes tested.

In male mice, sActRIIB-mFc treatment influenced tibial gene expression in *+/G610C* osteoclast and *oim/oim* osteoblasts and osteocytes (Figure 3). No significant changes in osteoblast, osteoclast or osteocyte markers were discovered with sActRIIB-

mFc treatment in Wt mice. Male *+/G610C* tibias demonstrated significant increases in transcript levels of *Alpl* (Osteoblast), dentin matrix protein 1 (*Dmp1*, Osteocyte) and Phosphate Regulating Endopeptidase Homolog, X-Linked (*Phex*, osteocyte) relative to vehicle treated counterparts. In female mice, sActRIIB-mFc treated mice exhibited a trend towards decreasing gene expression in all cell types and significantly downregulated expression of *Ctsk* (Osteoclast) and *Sost* (osteocyte), Figure 4. Conversely, female *+/G610C* mice exhibited a trend towards increased gene expression with increases in osterix (*Osx*, osteoblast), heat shock protein 47 (*Serpinh1*, osteoblast) and *Csf1* (osteoclast). Female *oim/oim* mice did not exhibit significant changes in their tibial gene expression profile with sActRIIB-mFc treatment.

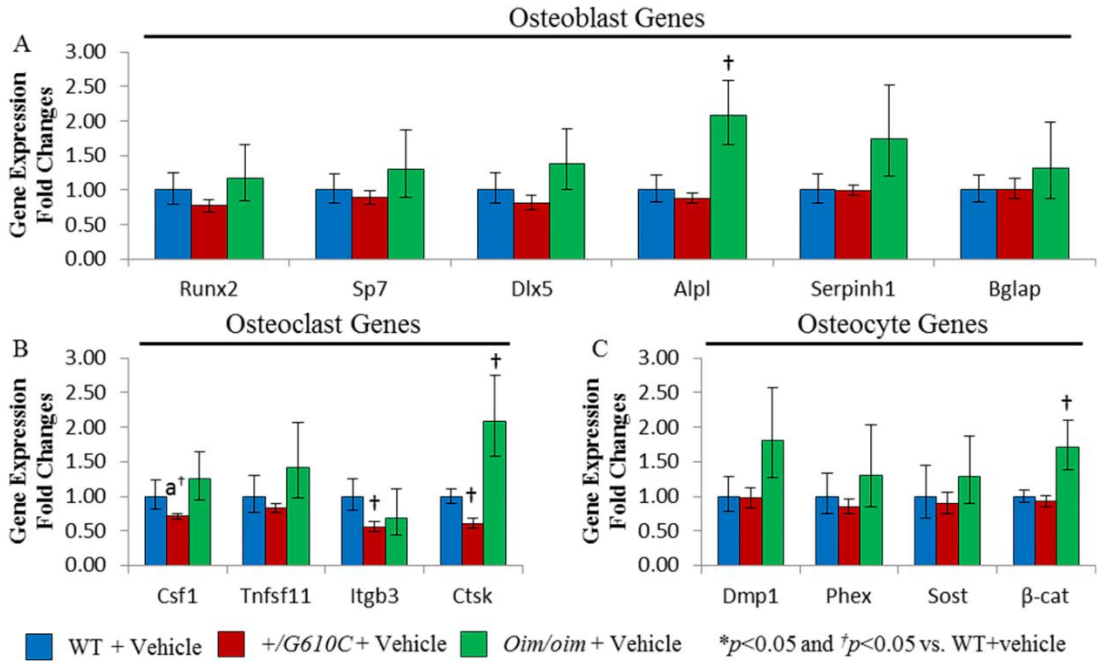

Figure B.1: Male *oim/oim* mice exhibited upregulation of osteoblast, osteoclast, and osteocyte marker genes as compared to WT counterparts. A) Relative fold changes of vehicle treated *+/G610C* and *oim/oim Runx2*, *Sp7* (Osterix), *Dlx5*, *Alpl* (Alkaline phosphatase), Serpinh1 (Hsp47), and *Bglap* (osteocalcin), B) *Csf1* (*M-CSF*), *Tnfsf11* (*Rankl*), *Itgb3* (Integrinβ−3), and *Ctsk* (Cathepsin K), and C) *Dmp1*, *Phex*, *Sost* (sclerostin), and *β-cat* (β catenin) mRNA levels with respect to vehicle treated WT mice. (n=10 WT+vehicle [blue], n=8 *+/G610C*+vehicle [red], and n=11 *oim/oim*+vehicle [green]) (Alpl gene expression levels of WT and *oim/oim* sample size were 7 and 8, respectively). Values are MEAN±SD. **p*<0.05; †*p*<0.05 vs. WT+vehicle treated mice; *[a]*p*=0.0676.

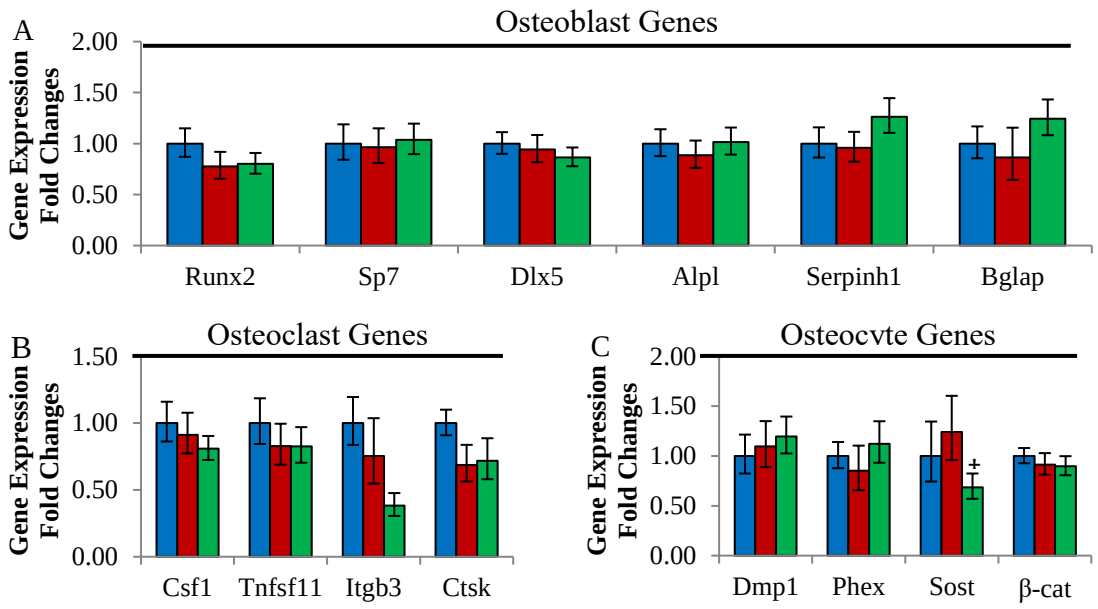

Figure B.2: Expression levels of vehicle-treated female mouse tibiae osteoblast, osteoclast, and osteocyte genes. A) Relative fold changes of vehicle-treated *+/G610C* and *oim/oim* mouse tibial osteoblast [*Runx2*, *Sp7* (Osterix), *Dlx5*, *Alpl* (Alkaline phosphatase), *Serpinh1* (Hsp47), and *Bglap* (osteocalcin)], B) osteoclast [*Csf1* (M-CSF), *Tnfsf11* (*Rankl*), *Itgb3* (Integrinβ-3), and *Ctsk* (Cathepsin K)], and C) osteocyte [*Dmp1*, *Phex*, *Sost* (sclerostin), and *β-cat* (β catenin)] mRNA levels with respect to vehicle-treated WT mice. (10 WT+vehicle [blue], 8 *+/G610C*+vehicle [red], and 11 *oim/oim*+vehicle [green]. Values are MEAN±SD. $^{*}p<0.05$; $^{\dagger}p<0.05$ vs. WT+vehicle treated mice.

WT + Vehicle *+/G610C* + Vehicle *Oim/oim* + Vehicle

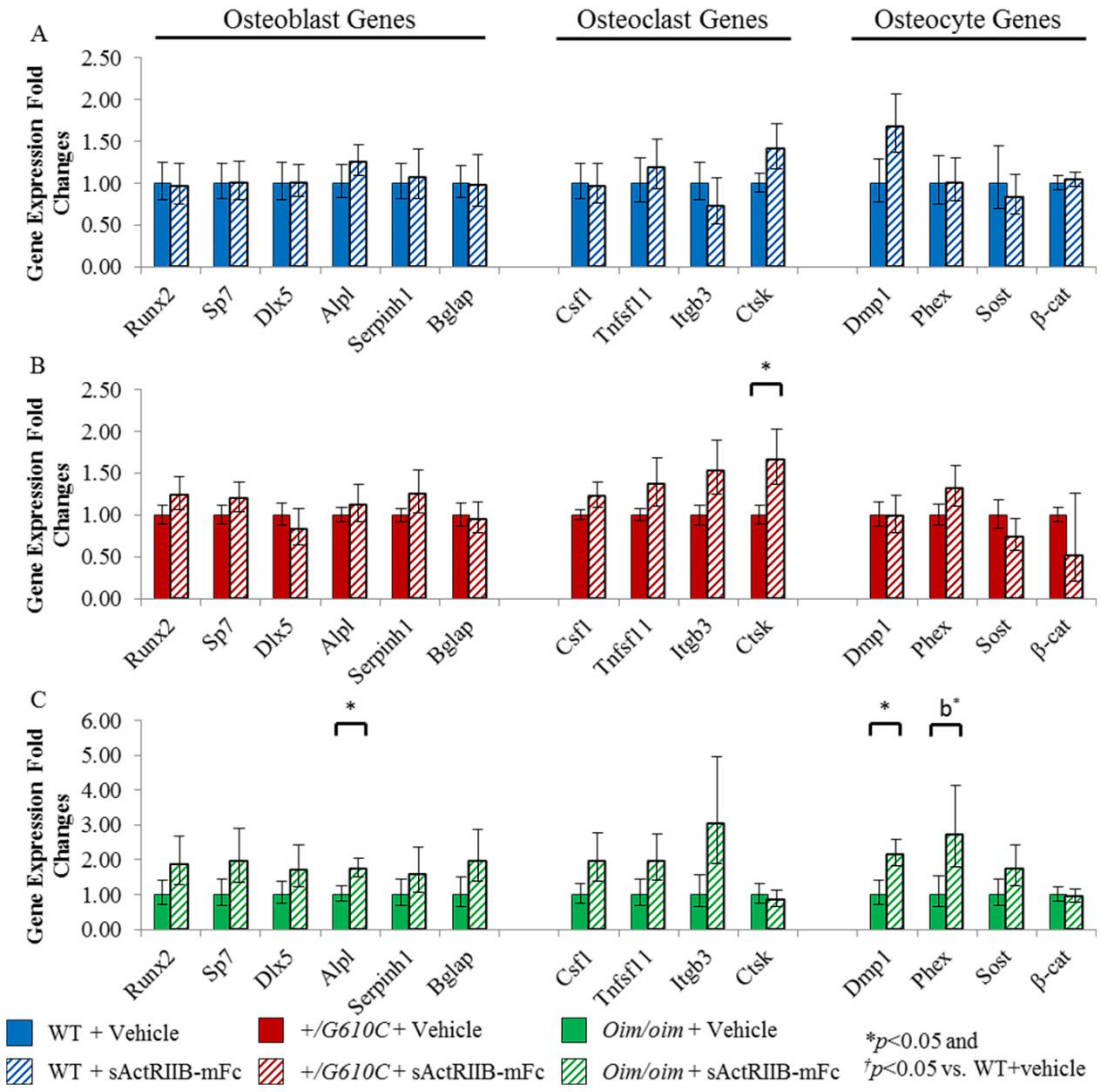

Figure B.3: sActRIIB-mFc treated male *oim/oim* mice demonstrated upregulation of osteoblast and osteocyte marker genes as compared to vehicle treated counterparts. A) Relative fold changes of sActRIIB-mFc treated WT osteoblast (*Runx2*, *Sp7*, *Dlx5*, *Alpl*, *Serpinh1*, and *Bglap*), osteoclast (*Csf1*, *Tnfsf11*, *Itgb3*, and *Ctsk*), and osteocyte (*Dmp1*, *Phex*, *Sost*, and *β-cat*) mRNA levels with respect to vehicle treated WT mice, B) Relative fold changes of sActRIIB-mFc treated *+/G610C* osteoblast, osteoclast, and osteocyte mRNA levels with respect to vehicle treated *+/G610C* mice, and C) Relative fold changes of sActRIIB-mFc treated *oim/oim* osteoblast, osteoclast, and osteocyte mRNA levels with respect to vehicle treated *oim/oim* mice. (n=10 WT+vehicle [blue], n=10 WT+sActRIIB-mFc [blue diagonal], n=8 *+/G610C*+vehicle [red], n=8 *+/G610C*+sActRIIB-mFc [red diagonal], n=11 *oim/oim*+vehicle [green], and n=11 *oim/oim*+sActRIIB-mFc [green diagonal] [Alpl gene expression level of WT and *oim/oim* sample size were 7 and 8, respectively]). Values are MEAN±SD. *$p<0.05$; †$p<0.05$ vs. WT+vehicle treated mice; *b$p=0.0545$.

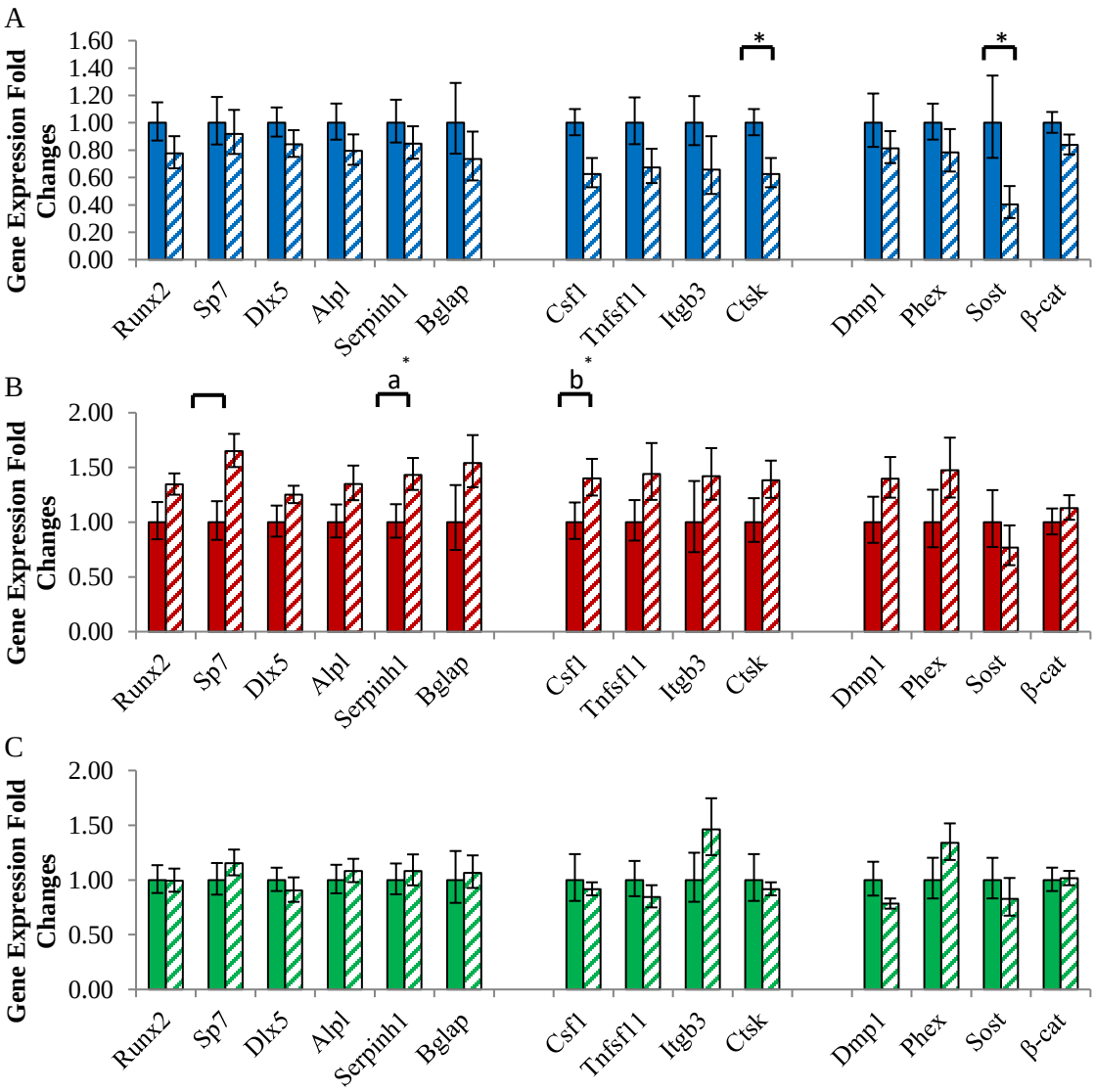

Figure B.4. Expression levels of vehicle- and sActRIIB-mFc-treated female mouse tibial osteoblast, osteoclast, and osteocyte genes. A) Relative fold changes of sActRIIB-mFc treated WT mouse tibial osteoblast (*Runx2, Sp7, Dlx5, Alpl, Serpinh1*, and *Bglap*), osteoclast (*Csf1, Tnfsf11, Itgb3*, and *Ctsk*), and osteocyte (*Dmp1, Phex, Sost*, and *β-cat*) mRNA levels with respect to vehicle-treated WT mouse tibiae, B) Relative fold changes of sActRIIB-mFc treated *+/G610C* mouse tibial osteoblast, osteoclast, and osteocyte mRNA levels with respect to vehicle-treated *+/G610C* mouse tibiae. C) Relative fold changes of sActRIIB-mFc treated *oim/oim* mouse tibial osteoblast, osteoclast, and osteocyte mRNA levels with respect to vehicle-treated *oim/oim* mouse tibiae. (10 WT+vehicle [blue], 10 WT+sActRIIB-mFc [blue diagonal], 8 *+/G610C*+vehicle [red], 8 *+/G610C*+sActRIIB-mFc [red diagonal], 11 *oim/oim*+vehicle [green], and 11 *oim/oim*+sActRIIB-mFc [green diagonal] [Alpl gene expression level of WT and *oim/oim* sample size were 7 and 8, respectively]). Values are MEAN±SD. $^{*}p<0.05$; $^{\dagger}p<0.05$ vs. WT+vehicle treated mice; $^{a*}p=0.0587$; $^{b*}p=0.0559$.

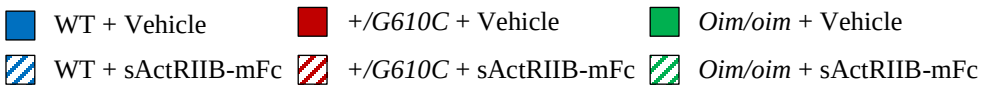
WT + Vehicle
+/G610C + Vehicle
Oim/oim + Vehicle
WT + sActRIIB-mFc
+/G610C + sActRIIB-mFc
Oim/oim + sActRIIB-mFc

Discussion

In this study, we observed that sActRIIB-mFc treatment results in substantial increases in femoral trabecular bone volume in Wt, *+/G610C* and *oim/oim* mice regardless of sex, as well as improvements in the cortical microarchitecture and femoral biomechanical strength in only Wt and *+/G610C* mice[19]. Gene expression analyses revealed a trend towards increased expression of osteoblastic genes in male *oim/oim* mice, a feature likely associated with the observation that *oim/oim* mice possess a large number of osteoblasts that are continuously stimulated, but fail to differentiate successfully into mature osteoblasts[72]. Male *+/G610C* mice also appeared to have decreases in the expression of osteoclastic genes.

Treatment with sActRIIB-mFc significantly decreased cathepsin K (osteoclast marker) and sclerostin (osteocyte marker) in female Wt mice but did not change gene expression in male Wt mice. Female *+/G610C* also exhibit increased expression of osterix and serpinh1 (osteoblast markers), colony stimulating factor 1 (*Csf1*, osteoclast marker); and increased cathepsin K (osteoclast marker) expression in male *+/G610C* mice. Lastly, although no changes in bone cell gene expression were observed in female *oim/oim* mice, the expression of alkaline phosphatase (*Alpl*, osteoblast marker); dentin matrix protein 1 (*Dmp1*, osteocyte marker) and phosphate regulating endopeptidase homolog X-linked (*Phex*, osteocyte marker) in male *oim/oim* mice wee increased. In sActRIIB-mFc-treated mice, histological analyses of femurs revealed increases in osteoblast numbers in all mice, but no impact on the number of active osteoblast (N.Ob/Bpm(mm^{-1})) was observed[19]. Although some of the genes assayed were upregulated with treatment, the absence of a consistent expression pattern in cell-specific

genes, likely suggests that at 4 months of age, mice, a steady state in bone modeling had already been achieved.

In conclusion, our findings indicate that sActRIIB-mFc treatment has differential effects on *G610C* and *OIM* mice, which may in part reflect differences in disease severity (severe in *oim/oim* vs. moderately severe in *+/G610C*), the presence of muscle pathology in *oim/oim* mice and/or their unique molecular defects. Study limitations include the use of intact tibiae, which contain bone marrow. Bone marrow is composed of multiple cells which may influence gene expression outcomes, likely diluting the specific gene expression profiles of bone cells.

BIBLIOGRAPHY

1. Mohamed AM. An Overview of Bone Cells and their Regulating Factors of Differentiation. Malays. J. Med. Sci. MJMS. 2008 Jan;15(1):4–12.

2. Manolagas SC, Parfitt AM. WHAT OLD MEANS TO BONE. Trends Endocrinol. Metab. TEM. 2010 Jun;21(6):369–74.

3. Han Y, You X, Xing W, Zhang Z, Zou W. Paracrine and endocrine actions of bone—the functions of secretory proteins from osteoblasts, osteocytes, and osteoclasts. Bone Res. [Internet]. 2018 May 24 [cited 2021 Jan 6];6. Available from: https://www.ncbi.nlm.nih.gov/pmc/articles/PMC5967329/

4. Walsh MC, Takegahara N, Kim H, Choi Y. Updating osteoimmunology: regulation of bone cells by innate and adaptive immunity. Nat. Rev. Rheumatol. 2018 Mar;14(3):146–56.

5. Marini JC, Forlino A, Bächinger HP, Bishop NJ, Byers PH, Paepe AD, Fassier F, Fratzl-Zelman N, Kozloff KM, Krakow D, Montpetit K, Semler O. Osteogenesis imperfecta. Nat. Rev. Dis. Primer. 2017 Aug 18;3:17052.

6. Forlino A, Marini JC. Osteogenesis imperfecta. The Lancet. 2016 Apr 16;387(10028):1657–71.

7. Hoyer-Kuhn H, Semler O, Schoenau E. Effect of Denosumab on the Growing Skeleton in Osteogenesis Imperfecta. J. Clin. Endocrinol. Metab. 2014 Nov 1;99(11):3954–5.

8. Rauch F, Cornibert S, Cheung M, Glorieux FH. Long-bone changes after pamidronate discontinuation in children and adolescents with osteogenesis imperfecta. Bone. 2007 Apr;40(4):821–7.

9. Munns CF, Rauch F, Zeitlin L, Fassier F, Glorieux FH. Delayed Osteotomy but Not Fracture Healing in Pediatric Osteogenesis Imperfecta Patients Receiving Pamidronate. J. Bone Miner. Res. 2004;19(11):1779–86.

10. Rosemberg DL, Goiano EO, Akkari M, Santili C. Effects of a telescopic intramedullary rod for treating patients with osteogenesis imperfecta of the femur. J. Child. Orthop. 2018 Feb 1;12(1):97–103.

11. Wilkinson JM, Scott BW, Clarke AM, Bell MJ. Surgical stabilisation of the lower limb in osteogenesis imperfecta using the Sheffield Telescopic Intramedullary Rod System. J. Bone Joint Surg. Br. 1998 Nov;80(6):999–1004.

12. Frost HM. Bone's mechanostat: A 2003 update. Anat. Rec. A. Discov. Mol. Cell. Evol. Biol. 2003 Dec 1;275A(2):1081–101.

13. Frost HM. Bone "mass" and the "mechanostat": a proposal. Anat. Rec. 1987 Sep;219(1):1–9.

14. Frost HM. On our age-related bone loss: insights from a new paradigm. J. Bone Miner. Res. Off. J. Am. Soc. Bone Miner. Res. 1997 Oct;12(10):1539–46.

15. McPherron AC, Lawler AM, Lee SJ. Regulation of skeletal muscle mass in mice by a new TGF-beta superfamily member. Nature. 1997 May 1;387(6628):83–90.

16. Fuller K, Bayley KE, Chambers TJ. Activin A Is an Essential Cofactor for Osteoclast Induction. Biochem. Biophys. Res. Commun. 2000 Feb 5;268(1):2–7.

17. Jann J, Gascon S, Roux S, Faucheux N. Influence of the TGF-β Superfamily on Osteoclasts/Osteoblasts Balance in Physiological and Pathological Bone Conditions. Int. J. Mol. Sci. 2020 Oct 14;21(20).

18. Campbell C, McMillan HJ, Mah JK, Tarnopolsky M, Selby K, McClure T, Wilson DM, Sherman ML, Escolar D, Attie KM. Myostatin inhibitor ACE-031 treatment of ambulatory boys with Duchenne muscular dystrophy: Results of a randomized, placebo-controlled clinical trial. Muscle Nerve. 2017 Apr 1;55(4):458–64.

19. Jeong Y, Daghlas SA, Xie Y, Hulbert MA, Pfeiffer FM, Dallas MR, Omosule CL, Pearsall RS, Dallas SL, Phillips CL. Skeletal Response to Soluble Activin Receptor Type IIB in Mouse Models of Osteogenesis Imperfecta. J. Bone Miner. Res. 2018 Oct;33(10):1760–72.

20. Jeong Y, Daghlas SA, Kahveci AS, Salamango D, Gentry BA, Brown M, Rector RS, Pearsall RS, Phillips CL. Soluble activin receptor type IIB decoy receptor differentially impacts murine osteogenesis imperfecta muscle function. Muscle Nerve. 2018 Feb;57(2):294–304.

21. DiGirolamo DJ, Singhal V, Chang X, Lee S-J, Germain-Lee EL. Administration of soluble activin receptor 2B increases bone and muscle mass in a mouse model of osteogenesis imperfecta. Bone Res. 2015 Feb 10;3:14042.

22. Latres E, Mastaitis J, Fury W, Miloscio L, Trejos J, Pangilinan J, Okamoto H, Cavino K, Na E, Papatheodorou A, Willer T, Bai Y, Hae Kim J, Rafique A, Jaspers S, Stitt T, Murphy AJ, Yancopoulos GD, Gromada J. Activin A more prominently regulates muscle mass in primates than does GDF8. Nat. Commun. 2017 Apr;8(1):15153.

23. Attie KM, Borgstein NG, Yang Y, Condon CH, Wilson DM, Pearsall AE, Kumar R, Willins DA, Seehra JS, Sherman ML. A single ascending-dose study of muscle regulator ACE-031 in healthy volunteers. Muscle Nerve. 2013 Mar;47(3):416–23.

24. Berendsen AD, Olsen BR. Bone development. Bone. 2015 Nov;80:14–8.

25. Yang J, Andre P, Ye L, Yang Y-Z. The Hedgehog signalling pathway in bone formation. Int. J. Oral Sci. 2015 Jun;7(2):73–9.

26. Maes C, Kobayashi T, Selig MK, Torrekens S, Roth SI, Mackem S, Carmeliet G, Kronenberg HM. Osteoblast Precursors, but Not Mature Osteoblasts, Move into Developing and Fractured Bones along with Invading Blood Vessels. Dev. Cell. 2010 Aug 17;19(2):329–44.

27. Mackie EJ, Tatarczuch L, Mirams M. The skeleton: a multi-functional complex organ. The growth plate chondrocyte and endochondral ossification. J. Endocrinol. 2011 Nov 1;211(2):109–21.

28. Akiyama H, Chaboissier M-C, Martin JF, Schedl A, de Crombrugghe B. The transcription factor Sox9 has essential roles in successive steps of the chondrocyte

differentiation pathway and is required for expression of Sox5 and Sox6. Genes Dev. 2002 Nov 1;16(21):2813–28.

29. Kawakami Y, Rodriguez-León J, Belmonte JCI. The role of TGFβs and Sox9 during limb chondrogenesis. Curr. Opin. Cell Biol. 2006 Dec 1;18(6):723–9.

30. Franz-Odendaal TA. Induction and patterning of intramembranous bone. Front. Biosci. Landmark Ed. 2011 Jun 1;16:2734–46.

31. Mortlock DP, Innis JW. Mutation of HOXA13 in hand-foot-genital syndrome. Nat. Genet. 1997 Feb;15(2):179–80.

32. Mariani FV, Martin GR. Deciphering skeletal patterning: clues from the limb. Nature. 2003 May;423(6937):319–25.

33. Tassabehji M, Read AP, Newton VE, Harris R, Balling R, Gruss P, Strachan T. Waardenburg's syndrome patients have mutations in the human homologue of the Pax-3 paired box gene. Nature. 1992 Feb 13;355(6361):635–6.

34. Kingsley DM. What do BMPs do in mammals? Clues from the mouse short-ear mutation. Trends Genet. 1994 Jan 1;10(1):16–21.

35. Capulli M, Paone R, Rucci N. Osteoblast and osteocyte: Games without frontiers. Arch. Biochem. Biophys. 2014 Nov 1;561:3–12.

36. Florencio-Silva R, Sasso GR da S, Sasso-Cerri E, Simões MJ, Cerri PS. Biology of Bone Tissue: Structure, Function, and Factors That Influence Bone Cells. BioMed

Res. Int. [Internet]. 2015 [cited 2018 Oct 4];2015. Available from: https://www.ncbi.nlm.nih.gov/pmc/articles/PMC4515490/

37. Cerri PS. Osteoblasts engulf apoptotic bodies during alveolar bone formation in the rat maxilla. Anat. Rec. A. Discov. Mol. Cell. Evol. Biol. 2005 Sep;286(1):833–40.

38. Miller SC, de Saint-Georges L, Bowman BM, Jee WS. Bone lining cells: structure and function. Scanning Microsc. 1989 Sep;3(3):953–60; discussion 960-961.

39. Everts V, Delaissé JM, Korper W, Jansen DC, Tigchelaar-Gutter W, Saftig P, Beertsen W. The Bone Lining Cell: Its Role in Cleaning Howship's Lacunae and Initiating Bone Formation. J. Bone Miner. Res. 2002;17(1):77–90.

40. Bonewald LF. The Amazing Osteocyte. J. Bone Miner. Res. 2011 Feb;26(2):229–38.

41. Bellido T, Ali AA, Gubrij I, Plotkin LI, Fu Q, O'Brien CA, Manolagas SC, Jilka RL. Chronic Elevation of Parathyroid Hormone in Mice Reduces Expression of Sclerostin by Osteocytes: A Novel Mechanism for Hormonal Control of Osteoblastogenesis. Endocrinology. 2005 Nov 1;146(11):4577–83.

42. Shandala T, Ng YS, Hopwood B, Yip Y-C, Foster BK, Xian CJ. The role of osteocyte apoptosis in cancer chemotherapy-induced bone loss. J. Cell. Physiol. 2012;227(7):2889–97.

43. Nakashima T, Hayashi M, Fukunaga T, Kurata K, Oh-hora M, Feng JQ, Bonewald LF, Kodama T, Wutz A, Wagner EF, Penninger JM, Takayanagi H. Evidence for

osteocyte regulation of bone homeostasis through RANKL expression. Nat. Med. 2011 Oct;17(10):1231–4.

44. Bianco P, Ballanti P, Bonucci E. Tartrate-resistant acid phosphatase activity in rat osteoblasts and osteocytes. Calcif. Tissue Int. 1988 Sep;43(3):167–71.

45. Solberg LB, Brorson S-H, Stordalen GA, Bækkevold ES, Andersson G, Reinholt FP. Increased Tartrate-Resistant Acid Phosphatase Expression in Osteoblasts and Osteocytes in Experimental Osteoporosis in Rats. Calcif. Tissue Int. 2014;94(5):510–21.

46. Boyce BF, Xing L. Functions of RANKL/RANK/OPG in bone modeling and remodeling. Arch. Biochem. Biophys. 2008 May 15;473(2):139–46.

47. Nesbitt SA, Horton MA. Trafficking of matrix collagens through bone-resorbing osteoclasts. Science. 1997 Apr 11;276(5310):266–9.

48. Myllyharju J, Kivirikko KI. Collagens, modifying enzymes and their mutations in humans, flies and worms. Trends Genet. 2004 Jan 1;20(1):33–43.

49. Sharma U, Carrique L, Vadon-Le Goff S, Mariano N, Georges R-N, Delolme F, Koivunen P, Myllyharju J, Moali C, Aghajari N, Hulmes DJS. Structural basis of homo- and heterotrimerization of collagen I. Nat. Commun. 2017 Mar 10;8(1):14671.

50. Wu M, Cronin K, Crane JS. Biochemistry, Collagen Synthesis. StatPearls [Internet]. Treasure Island (FL): StatPearls Publishing; 2020 [cited 2020 Nov 28]. Available from: http://www.ncbi.nlm.nih.gov/books/NBK507709/

51. Sauk JJ, Nikitakis N, Siavash H. Hsp47 a novel collagen binding serpin chaperone, autoantigen and therapeutic target. Front. Biosci. J. Virtual Libr. 2005 Jan 1;10:107–18.

52. Makareeva E, Leikin S. Procollagen triple helix assembly: an unconventional chaperone-assisted folding paradigm. PloS One. 2007 Oct 10;2(10):e1029.

53. Fratzl-Zelman N, Barnes AM, Weis M, Carter E, Hefferan TE, Perino G, Chang W, Smith PA, Roschger P, Klaushofer K, Glorieux FH, Eyre DR, Raggio C, Rauch F, Marini JC. Non-Lethal Type VIII Osteogenesis Imperfecta Has Elevated Bone Matrix Mineralization. J. Clin. Endocrinol. Metab. 2016 Sep 1;101(9):3516–25.

54. Deshmukh SN, Dive AM, Moharil R, Munde P. Enigmatic insight into collagen. J. Oral Maxillofac. Pathol. JOMFP. 2016;20(2):276–83.

55. Hopkins DR, Keles S, Greenspan DS. The bone morphogenetic protein 1/Tolloid-like metalloproteinases. Matrix Biol. J. Int. Soc. Matrix Biol. 2007 Sep;26(7):508–23.

56. Ricard-Blum S. The Collagen Family. Cold Spring Harb. Perspect. Biol. [Internet]. 2011 Jan [cited 2020 Nov 28];3(1). Available from: https://www.ncbi.nlm.nih.gov/pmc/articles/PMC3003457/

57. Mäki JM. Lysyl oxidases in mammalian development and certain pathological conditions. Histol. Histopathol. 2009;24(5):651–60.

58. Klein T, Bischoff R. Physiology and pathophysiology of matrix metalloproteases. Amino Acids. 2011 Jul;41(2):271–90.

59. Viguet-Carrin S, Garnero P, Delmas PD. The role of collagen in bone strength. Osteoporos. Int. 2006 Mar 1;17(3):319–36.

60. Feng X. Chemical and Biochemical Basis of Cell-Bone Matrix Interaction in Health and Disease. Curr. Chem. Biol. 2009 May 1;3(2):189–96.

61. Von Euw S, Wang Y, Laurent G, Drouet C, Babonneau F, Nassif N, Azaïs T. Bone mineral: new insights into its chemical composition. Sci. Rep. 2019 Jun 11;9(1):8456.

62. Neuman WF, Neuman MW. The Nature of the Mineral Phase of Bone. Chem. Rev. 1953 Aug 1;53(1):1–45.

63. Yoshiko Y, Candeliere GA, Maeda N, Aubin JE. Osteoblast Autonomous Pi Regulation via Pit1 Plays a Role in Bone Mineralization. Mol. Cell. Biol. 2007 Jun;27(12):4465–74.

64. Pearson OM, Lieberman DE. The aging of Wolff's "law": Ontogeny and responses to mechanical loading in cortical bone. Am. J. Phys. Anthropol. 2004;125(S39):63–99.

65. Clarke B. Normal Bone Anatomy and Physiology. Clin. J. Am. Soc. Nephrol. CJASN. 2008 Nov;3(Suppl 3):S131–9.

66. Huuskonen J, Väisänen SB, Kröger H, Jurvelin JS, Alhava E, Rauramaa R. Regular Physical Exercise and Bone Mineral Density: A Four-Year Controlled Randomized Trial in Middle-aged Men. The DNASCO Study. Osteoporos. Int. 2001 May 1;12(5):349–55.

67. NIH Consensus Development Panel on Osteoporosis Prevention, Diagnosis, and Therapy. Osteoporosis prevention, diagnosis, and therapy. JAMA. 2001 Feb 14;285(6):785–95.

68. Bonjour JP, Theintz G, Buchs B, Slosman D, Rizzoli R. Critical years and stages of puberty for spinal and femoral bone mass accumulation during adolescence. J. Clin. Endocrinol. Metab. 1991 Sep;73(3):555–63.

69. Kobayashi S, Takahashi HE, Ito A, Saito N, Nawata M, Horiuchi H, Ohta H, Ito A, Iorio R, Yamamoto N, Takaoka K. Trabecular minimodeling in human iliac bone☆☆Sources of funding for the article: This study was supported in part by a Health Sciences Research Grant for Comprehensive Research on Aging and Health from the Ministry of Health, Welfare, and Labor of Japan. Bone. 2003 Feb 1;32(2):163–9.

70. Parfitt AM. Osteonal and hemi-osteonal remodeling: The spatial and temporal framework for signal traffic in adult human bone. J. Cell. Biochem. 1994;55(3):273–86.

71. Jilka RL, Weinstein RS, Bellido T, Parfitt AM, Manolagas SC. Osteoblast programmed cell death (apoptosis): modulation by growth factors and cytokines. J. Bone Miner. Res. Off. J. Am. Soc. Bone Miner. Res. 1998 May;13(5):793–802.

72. Li H, Jiang X, Delaney J, Franceschetti T, Bilic-Curcic I, Kalinovsky J, Lorenzo JA, Grcevic D, Rowe DW, Kalajzic I. Immature Osteoblast Lineage Cells Increase Osteoclastogenesis in Osteogenesis Imperfecta Murine. Am. J. Pathol. 2010 May;176(5):2405–13.

73. Glorieux FH. Osteogenesis imperfecta. Best Pract. Res. Clin. Rheumatol. 2008 Mar 1;22(1):85–100.

74. Marini JC, Forlino A, Cabral WA, Barnes AM, San Antonio JD, Milgrom S, Hyland JC, Körkkö J, Prockop DJ, De Paepe A, Coucke P, Symoens S, Glorieux FH, Roughley PJ, Lund AM, Kuurila-Svahn K, Hartikka H, Cohn DH, Krakow D, Mottes M, Schwarze U, Chen D, Yang K, Kuslich C, Troendle J, Dalgleish R, Byers PH. Consortium for osteogenesis imperfecta mutations in the helical domain of type I collagen: regions rich in lethal mutations align with collagen binding sites for integrins and proteoglycans. Hum. Mutat. 2007 Mar;28(3):209–21.

75. Aström E, Söderhäll S. Beneficial effect of long term intravenous bisphosphonate treatment of osteogenesis imperfecta. Arch. Dis. Child. 2002 May;86(5):356–64.

76. Takken T, Terlingen HC, Helders PJM, Pruijs H, Van der Ent CK, Engelbert RHH. Cardiopulmonary fitness and muscle strength in patients with osteogenesis imperfecta type I. J. Pediatr. 2004 Dec;145(6):813–8.

77. Engelbert RH, van der Graaf Y, van Empelen R, Beemer FA, Helders PJ. Osteogenesis imperfecta in childhood: impairment and disability. Pediatrics. 1997 Feb;99(2):E3.

78. Boot AM, de Coo RFM, Pals G, de Muinck Keizer-Schrama SMPF. Muscle weakness as presenting symptom of osteogenesis imperfecta. Eur. J. Pediatr. 2006 Jun;165(6):392–4.

79. Daley E, Streeten EA, Sorkin JD, Kuznetsova N, Shapses SA, Carleton SM, Shuldiner AR, Marini JC, Phillips CL, Goldstein SA, Leikin S, McBride DJ. Variable Bone Fragility Associated With an Amish COL1A2 Variant and a Knock-in Mouse Model. J. Bone Miner. Res. 2010 Feb;25(2):247–61.

80. Marini JC, Blissett AR. New Genes in Bone Development: What's New in Osteogenesis Imperfecta. J. Clin. Endocrinol. Metab. 2013 Aug;98(8):3095–103.

81. Sillence DO, Senn A, Danks DM. Genetic heterogeneity in osteogenesis imperfecta. J. Med. Genet. 1979 Apr;16(2):101–16.

82. Obafemi AA, Bulas DI, Troendle J, Marini JC. Popcorn calcification in osteogenesis imperfecta: incidence, progression, and molecular correlation. Am. J. Med. Genet. A. 2008 Nov 1;146A(21):2725–32.

83. Forlino A, Cabral WA, Barnes AM, Marini JC. New perspectives on osteogenesis imperfecta. Nat. Rev. Endocrinol. 2011 Jun 14;7(9):540–57.

84. Oestreich AK, Carleton SM, Yao X, Gentry BA, Raw CE, Brown M, Pfeiffer FM, Wang Y, Phillips CL. Myostatin deficiency partially rescues the bone phenotype of osteogenesis imperfecta model mice. Osteoporos. Int. 2016 Jan;27(1):161–70.

85. Mirigian LS, Makareeva E, Mertz EL, Omari S, Roberts-Pilgrim AM, Oestreich AK, Phillips CL, Leikin S. Osteoblast malfunction caused by cell stress response to procollagen misfolding in α2(I)-G610C mouse model of osteogenesis imperfecta. J. Bone Miner. Res. 2016 Aug;31(8):1608–16.

86. Marr C, Seasman A, Bishop N. Managing the patient with osteogenesis imperfecta: a multidisciplinary approach [Internet]. J. Multidiscip. Healthc. 2017 [cited 2020 Dec 10]. Available from: https://www.dovepress.com/managing-the-patient-with--osteogenesis-imperfecta-a-multidisciplinary-peer-reviewed-fulltext-article-JMDH

87. Esposito P, Plotkin H. Surgical treatment of osteogenesis imperfecta: current concepts. Curr. Opin. Pediatr. 2008 Feb;20(1):52–57.

88. Rogers MJ. From Molds and Macrophages to Mevalonate: A Decade of Progress in Understanding the Molecular Mode of Action of Bisphosphonates. Calcif. Tissue Int. 2004 Dec 1;75(6):451–61.

89. Fisher JE, Rogers MJ, Halasy JM, Luckman SP, Hughes DE, Masarachia PJ, Wesolowski G, Russell RGG, Rodan GA, Reszka AA. Alendronate mechanism of action: geranylgeraniol, an intermediate in the mevalonate pathway, prevents inhibition of osteoclast formation, bone resorption, and kinase activation in vitro. Proc Natl Acad Sci USA. 1999;6.

90. Dwan K, Phillipi CA, Steiner RD, Basel D. Bisphosphonate therapy for osteogenesis imperfecta. Cochrane Database Syst. Rev. 2014 Jul 23;(7):CD005088.

91. Rogers MJ. New insights into the molecular mechanisms of action of bisphosphonates. Curr. Pharm. Des. 2003;9(32):2643–58.

92. Papapoulos SE. Bisphosphonates: how do they work? Best Pract. Res. Clin. Endocrinol. Metab. 2008 Oct 1;22(5):831–47.

93. Rauch F, Travers R, Plotkin H, Glorieux FH. The effects of intravenous pamidronate on the bone tissue of children and adolescents with osteogenesis imperfecta. J. Clin. Invest. 2002 Nov;110(9):1293–9.

94. Glorieux FH, Bishop NJ, Plotkin H, Chabot G, Lanoue G, Travers R. Cyclic administration of pamidronate in children with severe osteogenesis imperfecta. N. Engl. J. Med. 1998 Oct 1;339(14):947–52.

95. Plotkin H, Rauch F, Bishop NJ, Montpetit K, Ruck-Gibis J, Travers R, Glorieux FH. Pamidronate treatment of severe osteogenesis imperfecta in children under 3 years of age. J. Clin. Endocrinol. Metab. 2000 May;85(5):1846–50.

96. Eghbali-Fatourechi G. Bisphosphonate therapy in pediatric patients. J. Diabetes Metab. Disord. [Internet]. 2014 Dec 17 [cited 2020 Jan 7];13. Available from: https://www.ncbi.nlm.nih.gov/pmc/articles/PMC4279811/

97. Brunetti G, Papadia F, Tummolo A, Fischetto R, Nicastro F, Piacente L, Ventura A, Mori G, Oranger A, Gigante I, Colucci S, Ciccarelli M, Grano M, Cavallo L,

Delvecchio M, Faienza MF. Impaired bone remodeling in children with osteogenesis imperfecta treated and untreated with bisphosphonates: the role of DKK1, RANKL, and TNF-α. Osteoporos. Int. 2016;27(7):2355–65.

98. Ward L, Tricco A, Phuong P-N, Cranney A, Barrowman N, Gaboury I, Rauch F, Tugwell P, Moher D. Bisphosphonate therapy for children and adolescents with secondary osteoporosis. Cochrane Database Syst. Rev. [Internet]. 2007 [cited 2020 Nov 30];(4). Available from: https://www.cochranelibrary.com/cdsr/doi/10.1002/14651858.CD005324.pub2/full

99. Dwan K, Phillipi CA, Steiner RD, Basel D. Bisphosphonate therapy for osteogenesis imperfecta. Cochrane Database Syst. Rev. [Internet]. 2016 [cited 2020 Nov 30];(10). Available from: https://www.cochranelibrary.com/cdsr/doi/10.1002/14651858.CD005088.pub4/full

100. Mulpuri K, Joseph B. Intramedullary rodding in osteogenesis imperfecta. J. Pediatr. Orthop. 2000 Apr;20(2):267–73.

101. Chipman SD, Sweet HO, McBride DJ, Davisson MT, Marks SC, Shuldiner AR, Wenstrup RJ, Rowe DW, Shapiro JR. Defective pro alpha 2(I) collagen synthesis in a recessive mutation in mice: a model of human osteogenesis imperfecta. Proc. Natl. Acad. Sci. U. S. A. 1993 Mar 1;90(5):1701–5.

102. Misof K, Landis WJ, Klaushofer K, Fratzl P. Collagen from the osteogenesis imperfecta mouse model (oim) shows reduced resistance against tensile stress. J. Clin. Invest. 1997 Jul 1;100(1):40–5.

103. Carleton SM, McBride DJ, Carson WL, Huntington CE, Twenter KL, Rolwes KM, Winkelmann CT, Morris JS, Taylor JF, Phillips CL. Role of genetic background in determining phenotypic severity throughout postnatal development and at peak bone mass in Col1a2 deficient mice (oim). Bone. 2008 Apr;42(4):681–94.

104. Grabner B, Landis WJ, Roschger P, Rinnerthaler S, Peterlik H, Klaushofer K, Fratzl P. Age- and genotype-dependence of bone material properties in the osteogenesis imperfecta murine model (oim). Bone. 2001 Nov;29(5):453–7.

105. Boskey AL, Marino J, Spevak L, Pleshko N, Doty S, Carter EM, Raggio CL. Are Changes in Composition in Response to Treatment of a Mouse Model of Osteogenesis Imperfecta Sex-dependent? Clin. Orthop. 2015 Aug;473(8):2587–98.

106. Saban J, Zussman MA, Havey R, Patwardhan AG, Schneider GB, King D. Heterozygous oim mice exhibit a mild form of osteogenesis imperfecta. Bone. 1996 Dec;19(6):575–9.

107. McBride Jr DJ, Shapiro JR, Dunn MG. Bone Geometry and Strength Measurements in Aging Mice with the oim Mutation. Calcif. Tissue Int. 1998 Feb 1;62(2):172–6.

108. Zhang H, Doty SB, Hughes C, Dempster D, Camacho NP. Increased resorptive activity and accompanying morphological alterations in osteoclasts derived from the oim/oim mouse model of osteogenesis imperfecta. J. Cell. Biochem. 2007 Nov 1;102(4):1011–20.

109. Rauch F, Travers R, Parfitt AM, Glorieux FH. Static and dynamic bone histomorphometry in children with osteogenesis imperfecta. Bone. 2000 Jun;26(6):581–9.

110. Gentry BA, Ferreira JA, McCambridge AJ, Brown M, Phillips CL. Skeletal muscle weakness in osteogeneis imperfecta mice. Matrix Biol. J. Int. Soc. Matrix Biol. 2010 Sep;29(7):638–44.

111. Gremminger VL, Jeong Y, Cunningham RP, Meers GM, Rector RS, Phillips CL. Compromised Exercise Capacity and Mitochondrial Dysfunction in the Osteogenesis Imperfecta Murine (oim) Mouse Model. J. Bone Miner. Res. Off. J. Am. Soc. Bone Miner. Res. 2019 Sep;34(9):1646–59.

112. Zieba J, Munivez E, Castellon A, Jiang M-M, Dawson B, Ambrose CG, Lee B. Fracture Healing in Collagen-Related Preclinical Models of Osteogenesis Imperfecta. J. Bone Miner. Res. Off. J. Am. Soc. Bone Miner. Res. 2020 Jun;35(6):1132–48.

113. Bateman JF, Sampurno L, Maurizi A, Lamandé SR, Sims NA, Cheng TL, Schindeler A, Little DG. Effect of rapamycin on bone mass and strength in the α2(I)-G610C mouse model of osteogenesis imperfecta. J. Cell. Mol. Med. 2019 Mar;23(3):1735–45.

114. Grafe I, Yang T, Alexander S, Homan EP, Lietman C, Jiang MM, Bertin T, Munivez E, Chen Y, Dawson B, Ishikawa Y, Weis MA, Sampath TK, Ambrose C,

Eyre D, Bächinger HP, Lee B. Excessive transforming growth factor-β signaling is a common mechanism in osteogenesis imperfecta. Nat. Med. 2014 Jun;20(6):670–5.

115. Scheiber AL, Guess AJ, Kaito T, Abzug JM, Enomoto-Iwamoto M, Leikin S, Iwamoto M, Otsuru S. Endoplasmic reticulum stress is induced in growth plate hypertrophic chondrocytes in G610C mouse model of osteogenesis imperfecta. Biochem. Biophys. Res. Commun. 2019 29;509(1):235–40.

116. Pihlajaniemi T, Dickson LA, Pope FM, Korhonen VR, Nicholls A, Prockop DJ, Myers JC. Osteogenesis imperfecta: cloning of a pro-alpha 2(I) collagen gene with a frameshift mutation. J. Biol. Chem. 1984 Nov 10;259(21):12941–4.

117. Chen F, Guo R, Itoh S, Moreno L, Rosenthal E, Zappitelli T, Zirngibl RA, Flenniken A, Cole W, Grynpas M, Osborne LR, Vogel W, Adamson L, Rossant J, Aubin JE. First Mouse Model for Combined Osteogenesis Imperfecta and Ehlers-Danlos Syndrome. J. Bone Miner. Res. 2014;29(6):1412–23.

118. Grafe I, Alexander S, Yang T, Lietman C, Homan EP, Munivez E, Chen Y, Jiang MM, Bertin T, Dawson B, Asuncion F, Ke HZ, Ominsky MS, Lee B. Sclerostin antibody treatment improves the bone phenotype of Crtap−/− mice, a model of recessive Osteogenesis Imperfecta. J. Bone Miner. Res. 2016 May;31(5):1030–40.

119. Morello R, Bertin TK, Chen Y, Hicks J, Tonachini L, Monticone M, Castagnola P, Rauch F, Glorieux FH, Vranka J, Bächinger HP, Pace JM, Schwarze U, Byers PH, Weis M, Fernandes RJ, Eyre DR, Yao Z, Boyce BF, Lee B. CRTAP is required for

prolyl 3- hydroxylation and mutations cause recessive osteogenesis imperfecta. Cell. 2006 Oct 20;127(2):291–304.

120. Barnes AM, Chang W, Morello R, Cabral WA, Weis M, Eyre DR, Leikin S, Makareeva E, Kuznetsova N, Uveges TE, Ashok A, Flor AW, Mulvihill JJ, Wilson PL, Sundaram UT, Lee B, Marini JC. Deficiency of cartilage-associated protein in recessive lethal osteogenesis imperfecta. N. Engl. J. Med. 2006 Dec 28;355(26):2757–64.

121. Tauer JT, Abdullah S, Rauch F. Effect of Anti-TGF-β Treatment in a Mouse Model of Severe Osteogenesis Imperfecta. J. Bone Miner. Res. 2019;34(2):207–14.

122. Jacobsen CM, Barber LA, Ayturk UM, Roberts HJ, Deal LE, Schwartz MA, Weis M, Eyre D, Zurakowski D, Robling AG, Warman ML. Targeting the LRP5 pathway improves bone properties in a mouse model of Osteogenesis Imperfecta. J. Bone Miner. Res. 2014 Oct;29(10):2297–306.

123. Roschger A, Roschger P, Keplingter P, Klaushofer K, Abdullah S, Kneissel M, Rauch F. Effect of sclerostin antibody treatment in a mouse model of severe osteogenesis imperfecta. Bone. 2014 Sep;66:182–8.

124. Avin KG, Bloomfield SA, Gross TS, Warden SJ. Biomechanical Aspects of the Muscle-Bone Interaction. Curr. Osteoporos. Rep. 2015 Feb;13(1):1–8.

125. Kaji H. Linkage between muscle and bone: common catabolic signals resulting in osteoporosis and sarcopenia. Curr. Opin. Clin. Nutr. Metab. Care. 2013 May;16(3):272–7.

126. Rittweger J, Frost HM, Schiessl H, Ohshima H, Alkner B, Tesch P, Felsenberg D. Muscle atrophy and bone loss after 90 days' bed rest and the effects of flywheel resistive exercise and pamidronate: results from the LTBR study. Bone. 2005 Jun;36(6):1019–29.

127. Bentzinger CF, Wang YX, Rudnicki MA. Building Muscle: Molecular Regulation of Myogenesis. Cold Spring Harb. Perspect. Biol. 2012 Feb 1;4(2):a008342.

128. Yang W, Hu P. Skeletal muscle regeneration is modulated by inflammation. J. Orthop. Transl. 2018 Feb 7;13:25–32.

129. Sugiyama T, Meakin LB, Browne WJ, Galea GL, Price JS, Lanyon LE. Bones' adaptive response to mechanical loading is essentially linear between the low strains associated with disuse and the high strains associated with the lamellar/woven bone transition. J. Bone Miner. Res. Off. J. Am. Soc. Bone Miner. Res. 2012 Aug;27(8):1784–93.

130. Brotto M, Bonewald L. Bone and muscle: Interactions beyond mechanical. Bone. 2015 Nov;80:109–14.

131. Huang J, Romero-Suarez S, Lara N, Mo C, Kaja S, Brotto L, Dallas SL, Johnson ML, Jähn K, Bonewald LF, Brotto M. Crosstalk between MLO-Y4 osteocytes and C2C12 muscle cells is mediated by the Wnt/β-catenin pathway. JBMR Plus. 2017 Oct;1(2):86–100.

132. Hamrick MW. A role for myokines in muscle-bone interactions. Exerc. Sport Sci. Rev. 2011 Jan;39(1):43–7.

133. Judex S, Rubin CT. Is bone formation induced by high-frequency mechanical signals modulated by muscle activity? J. Musculoskelet. Neuronal Interact. 2010 Mar;10(1):3–11.

134. Suetta C, Frandsen U, Jensen L, Jensen MM, Jespersen JG, Hvid LG, Bayer M, Petersson SJ, Schrøder HD, Andersen JL, Heinemeier KM, Aagaard P, Schjerling P, Kjaer M. Aging Affects the Transcriptional Regulation of Human Skeletal Muscle Disuse Atrophy. PLOS ONE. 2012 Dec 19;7(12):e51238.

135. Bloomfield SA. Changes in musculoskeletal structure and function with prolonged bed rest. Med. Sci. Sports Exerc. 1997 Feb;29(2):197–206.

136. Akima H, Kuno S, Suzuki Y, Gunji A, Fukunaga T. Effects of 20 days of bed rest on physiological cross-sectional area of human thigh and leg muscles evaluated by magnetic resonance imaging. J. Gravitational Physiol. J. Int. Soc. Gravitational Physiol. 1997 Jan;4(1):S15-21.

137. Chakraborty N, Waning DL, Gautam A, Hoke A, Sowe B, Youssef D, Butler S, Savaglio M, Childress PJ, Kumar R, Moyler C, Dimitrov G, Kacena MA, Hammamieh R. Gene-Metabolite Network Linked to Inhibited Bioenergetics in Association With Spaceflight-Induced Loss of Male Mouse Quadriceps Muscle. J. Bone Miner. Res. 2020;35(10):2049–57.

138. Eser P, Frotzler A, Zehnder Y, Wick L, Knecht H, Denoth J, Schiessl H. Relationship between the duration of paralysis and bone structure: a pQCT study of spinal cord injured individuals. Bone. 2004 May;34(5):869–80.

139. Smith SM, Heer MA, Shackelford LC, Sibonga JD, Ploutz-Snyder L, Zwart SR. Benefits for bone from resistance exercise and nutrition in long-duration spaceflight: Evidence from biochemistry and densitometry. J. Bone Miner. Res. 2012;27(9):1896–906.

140. Hather BM, Adams GR, Tesch PA, Dudley GA. Skeletal muscle responses to lower limb suspension in humans. J. Appl. Physiol. Bethesda Md 1985. 1992 Apr;72(4):1493–8.

141. Russo CR. The effects of exercise on bone. Basic concepts and implications for the prevention of fractures. Clin. Cases Miner. Bone Metab. 2009;6(3):223–8.

142. Boström P, Wu J, Jedrychowski MP, Korde A, Ye L, Lo JC, Rasbach KA, Boström EA, Choi JH, Long JZ, Kajimura S, Zingaretti MC, Vind BF, Tu H, Cinti S, Højlund K, Gygi SP, Spiegelman BM. A PGC1-α-dependent myokine that drives brown-fat-like development of white fat and thermogenesis. Nature. 2012 Jan 11;481(7382):463–8.

143. Colaianni G, Storlino G, Sanesi L, Colucci S, Grano M. Myokines and Osteokines in the Pathogenesis of Muscle and Bone Diseases. Curr. Osteoporos. Rep. 2020 Aug 1;18(4):401–7.

144. Colaianni G, Cuscito C, Mongelli T, Pignataro P, Buccoliero C, Liu P, Lu P, Sartini L, Di Comite M, Mori G, Di Benedetto A, Brunetti G, Yuen T, Sun L, Reseland JE, Colucci S, New MI, Zaidi M, Cinti S, Grano M. The myokine irisin increases cortical bone mass. Proc. Natl. Acad. Sci. U. S. A. 2015 Sep 29;112(39):12157–62.

145. Colaianni G, Mongelli T, Cuscito C, Pignataro P, Lippo L, Spiro G, Notarnicola A, Severi I, Passeri G, Mori G, Brunetti G, Moretti B, Tarantino U, Colucci SC, Reseland JE, Vettor R, Cinti S, Grano M. Irisin prevents and restores bone loss and muscle atrophy in hind-limb suspended mice. Sci. Rep. 2017 Jun 6;7(1):2811.

146. Kitase Y, Vallejo JA, Gutheil W, Vemula H, Jähn K, Yi J, Zhou J, Brotto M, Bonewald LF. β-aminoisobutyric Acid, l-BAIBA, Is a Muscle-Derived Osteocyte Survival Factor. Cell Rep. 2018 Feb 6;22(6):1531–44.

147. Dallas SL, Prideaux M, Bonewald LF. The Osteocyte: An Endocrine Cell … and More. Endocr. Rev. 2013 Oct;34(5):658–90.

148. Manolagas SC. Osteocalcin promotes bone mineralization but is not a hormone. PLOS Genet. 2020 Jun 2;16(6):e1008714.

149. Mosialou I, Shikhel S, Liu J-M, Maurizi A, Luo N, He Z, Huang Y, Zong H, Friedman RA, Barasch J, Lanzano P, Deng L, Leibel RL, Rubin M, Nickolas T, Chung W, Zeltser LM, Williams KW, Pessin JE, Kousteni S. MC4R-dependent suppression of appetite by bone-derived lipocalin 2. Nature. 2017 Mar 16;543(7645):385–90.

150. Ogawa Y, Schmidt DK, Nathan RM, Armstrong RM, Miller KL, Sawamura SJ, Ziman JM, Erickson KL, Leon ER de, Rosen DM. Bovine bone activin enhances bone morphogenetic protein-induced ectopic bone formation. J. Biol. Chem. 1992 Jul 15;267(20):14233–7.

151. Gattineni J, Bates C, Twombley K, Dwarakanath V, Robinson ML, Goetz R, Mohammadi M, Baum M. FGF23 decreases renal NaPi-2a and NaPi-2c expression and induces hypophosphatemia in vivo predominantly via FGF receptor 1. Am. J. Physiol. Renal Physiol. 2009 Aug;297(2):F282-291.

152. Millar SA, Anderson SI, O'Sullivan SE. Osteokines and the vasculature: a review of the in vitro effects of osteocalcin, fibroblast growth factor-23 and lipocalin-2. PeerJ [Internet]. 2019 Jul 24 [cited 2021 Jan 6];7. Available from: https://www.ncbi.nlm.nih.gov/pmc/articles/PMC6660824/

153. Dufresne SS, Dumont NA, Bouchard P, Lavergne É, Penninger JM, Frenette J. Osteoprotegerin protects against muscular dystrophy. Am. J. Pathol. 2015 Apr;185(4):920–6.

154. Nagy V, Penninger JM. The RANKL-RANK Story. Gerontology. 2015;61(6):534–42.

155. Sigl V, Penninger JM. RANKL/RANK - from bone physiology to breast cancer. Cytokine Growth Factor Rev. 2014 Apr;25(2):205–14.

156. Little DG, Peacock L, Mikulec K, Kneissel M, Kramer I, Cheng TL, Schindeler A, Munns C. Combination sclerostin antibody and zoledronic acid treatment outperforms either treatment alone in a mouse model of osteogenesis imperfecta. Bone. 2017 Aug;101:96–103.

157. Li X, Ominsky MS, Warmington KS, Morony S, Gong J, Cao J, Gao Y, Shalhoub V, Tipton B, Haldankar R, Chen Q, Winters A, Boone T, Geng Z, Niu Q-T, Ke HZ,

Kostenuik PJ, Simonet WS, Lacey DL, Paszty C. Sclerostin antibody treatment increases bone formation, bone mass, and bone strength in a rat model of postmenopausal osteoporosis. J. Bone Miner. Res. Off. J. Am. Soc. Bone Miner. Res. 2009 Apr;24(4):578–88.

158. Orwoll ES, Shapiro J, Veith S, Wang Y, Lapidus J, Vanek C, Reeder JL, Keaveny TM, Lee DC, Mullins MA, Nagamani SCS, Lee B. Evaluation of teriparatide treatment in adults with osteogenesis imperfecta. J. Clin. Invest. 2014 Feb;124(2):491–8.

159. McClung MR. Sclerostin antibodies in osteoporosis: latest evidence and therapeutic potential. Ther. Adv. Musculoskelet. Dis. 2017 Oct;9(10):263–70.

160. Götherström C, Walther-Jallow L. Stem Cell Therapy as a Treatment for Osteogenesis Imperfecta. Curr. Osteoporos. Rep. 2020 Aug 1;18(4):337–43.

161. Sakai R, Fujita S, Horie T, Ohyama T, Miwa K, Maki T, Okimoto N, Nakamura T, Eto Y. Activin increases bone mass and mechanical strength of lumbar vertebrae in aged ovariectomized rats. Bone. 2000 Jul 1;27(1):91–6.

162. Pearsall RS, Canalis E, Cornwall-Brady M, Underwood KW, Haigis B, Ucran J, Kumar R, Pobre E, Grinberg A, Werner ED, Glatt V, Stadmeyer L, Smith D, Seehra J, Bouxsein ML. A soluble activin Type IIA receptor induces bone formation and improves skeletal integrity. Proc. Natl. Acad. Sci. 2008 May 13;105(19):7082–7.

163. Tang L, Yang X, Gao X, Du H, Han Y, Zhang D, Wang Z, Sun L. Inhibiting myostatin signaling prevents femoral trabecular bone loss and microarchitecture

deterioration in diet-induced obese rats. Exp. Biol. Med. Maywood NJ. 2016 Feb;241(3):308–16.

164. Tang L, Kang Y, Sun S, Zhao T, Cao W, Fan X, Guo J, Sun L, Ta D. Inhibition of MSTN signal pathway may participate in LIPUS preventing bone loss in ovariectomized rats. J. Bone Miner. Metab. 2020 Jan 1;38(1):14–26.

165. St. Andre M, Johnson M, Bansal PN, Wellen J, Robertson A, Opsahl A, Burch PM, Bialek P, Morris C, Owens J. A mouse anti-myostatin antibody increases muscle mass and improves muscle strength and contractility in the mdx mouse model of Duchenne muscular dystrophy and its humanized equivalent, domagrozumab (PF-06252616), increases muscle volume in cynomolgus monkeys. Skelet. Muscle [Internet]. 2017 Nov 9 [cited 2020 Oct 21];7. Available from: https://www.ncbi.nlm.nih.gov/pmc/articles/PMC5679155/

166. Wu M, Chen G, Li Y-P. TGF-β and BMP signaling in osteoblast, skeletal development, and bone formation, homeostasis and disease. Bone Res. 2016 Apr 26;4(1):1–21.

167. Janssens K, ten Dijke P, Janssens S, Van Hul W. Transforming Growth Factor-β1 to the Bone. Endocr. Rev. 2005 Oct 1;26(6):743–74.

168. Walton KL, Makanji Y, Harrison CA. New insights into the mechanisms of activin action and inhibition. Mol. Cell. Endocrinol. 2012 Aug 15;359(1):2–12.

169. Wang X, Fischer G, Hyvönen M. Structure and activation of pro-activin A. Nat. Commun. 2016 Jul 4;7(1):12052.

170. Poggioli T, Vujic A, Yang P, Macias-Trevino C, Uygur A, Loffredo FS, Pancoast JR, Cho M, Goldstein J, Tandias RM, Gonzalez E, Walker RG, Thompson TB, Wagers AJ, Fong YW, Lee RT. Circulating Growth Differentiation Factor 11/8 Levels Decline With Age. Circ. Res. 2016 Jan 8;118(1):29–37.

171. Gad JM, Tam PPL. Axis development: The mouse becomes a dachshund. Curr. Biol. 1999 Oct 21;9(20):R783–6.

172. Lee S-J, McPherron AC. Regulation of myostatin activity and muscle growth. Proc. Natl. Acad. Sci. 2001 Jul 31;98(16):9306–11.

173. Favia M, Fitak R, Guerra L, Pierri CL, Faye B, Oulmouden A, Burger PA, Ciani E. Beyond the Big Five: Investigating Myostatin Structure, Polymorphism and Expression in Camelus dromedarius. Front. Genet. [Internet]. 2019 [cited 2020 Dec 9];10. Available from: https://www.frontiersin.org/articles/10.3389/fgene.2019.00502/full

174. Bogdanovich S, Perkins KJ, Krag TOB, Whittemore L-A, Khurana TS. Myostatin propeptide-mediated amelioration of dystrophic pathophysiology. FASEB J. 2005;19(6):543–9.

175. Laurent MR, Dubois V, Claessens F, Verschueren SMP, Vanderschueren D, Gielen E, Jardí F. Muscle-bone interactions: From experimental models to the clinic? A critical update. Mol. Cell. Endocrinol. 2016 Sep 5;432:14–36.

176. Aykul S, Martinez-Hackert E. Transforming Growth Factor-β Family Ligands Can Function as Antagonists by Competing for Type II Receptor Binding. J. Biol. Chem. 2016 May 13;291(20):10792–804.

177. Matzuk MM, Kumar TR, Vassalli A, Bickenbach JR, Roop DR, Jaenisch R, Bradley A. Functional analysis of activins during mammalian development. Nature. 1995 Mar 23;374(6520):354–6.

178. Jhaveri S, Erzurumlu RS, Chiaia N, Kumar TR, Matzuk MM. Defective whisker follicles and altered brainstem patterns in activin and follistatin knockout mice. Mol. Cell. Neurosci. 1998 Nov;12(4–5):206–19.

179. Sakai R, Miwa K, Eto Y. Local administration of activin promotes fracture healing in the rat fibula fracture model. Bone. 1999 Aug 1;25(2):191–6.

180. Terpos E, Kastritis E, Christoulas D, Gkotzamanidou M, Eleutherakis-Papaiakovou E, Kanellias N, Papatheodorou A, Dimopoulos MA. Circulating activin-A is elevated in patients with advanced multiple myeloma and correlates with extensive bone involvement and inferior survival; no alterations post-lenalidomide and dexamethasone therapy. Ann. Oncol. 2012 Oct 1;23(10):2681–6.

181. Vallet S, Mukherjee S, Vaghela N, Hideshima T, Fulciniti M, Pozzi S, Santo L, Cirstea D, Patel K, Sohani AR, Guimaraes A, Xie W, Chauhan D, Schoonmaker JA, Attar E, Churchill M, Weller E, Munshi N, Seehra JS, Weissleder R, Anderson KC, Scadden DT, Raje N. Activin A promotes multiple myeloma-induced osteolysis and

is a promising target for myeloma bone disease. Proc. Natl. Acad. Sci. U. S. A. 2010 Mar 16;107(11):5124–9.

182. Chantry AD, Heath D, Mulivor AW, Pearsall S, Baud'huin M, Coulton L, Evans H, Abdul N, Werner ED, Bouxsein ML, Key ML, Seehra J, Arnett TR, Vanderkerken K, Croucher P. Inhibiting activin-A signaling stimulates bone formation and prevents cancer-induced bone destruction in vivo. J. Bone Miner. Res. Off. J. Am. Soc. Bone Miner. Res. 2010 Dec;25(12):2633–46.

183. Eijken M, Swagemakers S, Koedam M, Steenbergen C, Derkx P, Uitterlinden AG, Spek PJ van der, Visser JA, Jong FH de, Pols HAP, Leeuwen JPTM van. The activin A-follistatin system: potent regulator of human extracellular matrix mineralization. FASEB J. 2007;21(11):2949–60.

184. Baroncelli M, Drabek K, Eijken M, van der Eerden BCJ, van de Peppel J, van Leeuwen JPTM. Two-day-treatment of Activin-A leads to transient change in SV-HFO osteoblast gene expression and reduction in matrix mineralization. J. Cell. Physiol. 2020 May;235(5):4865–77.

185. Nicks KM, Perrien DS, Akel NS, Suva LJ, Gaddy D. Regulation of osteoblastogenesis and osteoclastogenesis by the other reproductive hormones, Activin and Inhibin. Mol. Cell. Endocrinol. 2009 Oct 30;310(1–2):11–20.

186. Zhou G, Gui X, Chen R, Fu X, Ji X, Ding H. Elevated serum Activin A in chronic obstructive pulmonary disease with skeletal muscle wasting. Clin. Sao Paulo Braz. 2019;74:e981.

187. Ding H, Zhang G, Sin KWT, Liu Z, Lin R-K, Li M, Li Y-P. Activin A induces skeletal muscle catabolism via p38β mitogen-activated protein kinase. J. Cachexia Sarcopenia Muscle. 2017 Apr;8(2):202–12.

188. Qin Y, Peng Y, Zhao W, Pan J, Ksiezak-Reding H, Cardozo C, Wu Y, Divieti Pajevic P, Bonewald LF, Bauman WA, Qin W. Myostatin inhibits osteoblastic differentiation by suppressing osteocyte-derived exosomal microRNA-218: A novel mechanism in muscle-bone communication. J. Biol. Chem. 2017 Jun 30;292(26):11021–33.

189. Welle S, Bhatt K, Pinkert CA, Tawil R, Thornton CA. Muscle growth after postdevelopmental myostatin gene knockout. Am. J. Physiol. Endocrinol. Metab. 2007 Apr;292(4):E985-991.

190. Schuelke M, Wagner KR, Stolz LE, Hübner C, Riebel T, Kömen W, Braun T, Tobin JF, Lee S-J. Myostatin Mutation Associated with Gross Muscle Hypertrophy in a Child [Internet]. http://dx.doi.org/10.1056/NEJMoa040933. 2009 [cited 2019 Oct 10]. Available from: https://www.nejm.org/doi/10.1056/NEJMoa040933?url_ver=Z39.88-2003&rfr_id=ori%3Arid%3Acrossref.org&rfr_dat=cr_pub%3Dwww.ncbi.nlm.nih.gov

191. Dong J, Dong Y, Dong Y, Chen F, Mitch WE, Zhang L. Inhibition of myostatin in mice improves insulin sensitivity via irisin-mediated cross talk between muscle and adipose tissues. Int. J. Obes. 2005. 2016 Mar;40(3):434–42.

192. Guo T, Jou W, Chanturiya T, Portas J, Gavrilova O, McPherron AC. Myostatin Inhibition in Muscle, but Not Adipose Tissue, Decreases Fat Mass and Improves Insulin Sensitivity. Calbet JAL, editor. PLoS ONE. 2009 Mar 19;4(3):e4937.

193. Wilkes JJ, Lloyd DJ, Gekakis N. Loss-of-function mutation in myostatin reduces tumor necrosis factor alpha production and protects liver against obesity-induced insulin resistance. Diabetes. 2009 May;58(5):1133–43.

194. Zhao B, Wall RJ, Yang J. Transgenic expression of myostatin propeptide prevents diet-induced obesity and insulin resistance. Biochem. Biophys. Res. Commun. 2005 Nov 11;337(1):248–55.

195. McPherron AC, Lee S-J. Suppression of body fat accumulation in myostatin-deficient mice. J. Clin. Invest. 2002 Mar;109(5):595–601.

196. Gu H, Cao Y, Qiu B, Zhou Z, Deng R, Chen Z, Li R, Li X, Wei Q, Xia X, Yong W. Establishment and phenotypic analysis of an Mstn knockout rat. Biochem. Biophys. Res. Commun. 2016 Aug 12;477(1):115–22.

197. Choi SJ, Yablonka-Reuveni Z, Kaiyala KJ, Ogimoto K, Schwartz MW, Wisse BE. Increased energy expenditure and leptin sensitivity account for low fat mass in myostatin-deficient mice. Am. J. Physiol. - Endocrinol. Metab. 2011 Jun;300(6):E1031–7.

198. Tavoian D, Arnold WD, Mort SC, Lacalle S de. Sex differences in body composition but not neuromuscular function following long-term, doxycycline-

induced reduction in circulating levels of myostatin in mice. PLOS ONE. 2019 Nov 21;14(11):e0225283.

199. Smith RC, Cramer MS, Mitchell PJ, Lucchesi J, Ortega AM, Livingston EW, Ballard D, Zhang L, Hanson J, Barton K, Berens S, Credille KM, Bateman TA, Ferguson VL, Ma YL, Stodieck LS. Inhibition of myostatin prevents microgravity-induced loss of skeletal muscle mass and strength. PLoS ONE [Internet]. 2020 Apr 21 [cited 2021 Feb 19];15(4). Available from: https://www.ncbi.nlm.nih.gov/pmc/articles/PMC7173869/

200. Tauer JT, Rauch F. Novel ActRIIB ligand trap increases muscle mass and improves bone geometry in a mouse model of severe osteogenesis imperfecta. Bone. 2019 Nov 1;128:115036.

201. Suh J, Kim N-K, Lee S-H, Eom J-H, Lee Y, Park J-C, Woo KM, Baek J-H, Kim J-E, Ryoo H-M, Lee S-J, Lee Y-S. GDF11 promotes osteogenesis as opposed to MSTN, and follistatin, a MSTN/GDF11 inhibitor, increases muscle mass but weakens bone. Proc. Natl. Acad. Sci. U. S. A. 2020 Mar 3;117(9):4910–20.

202. Elkasrawy MN, Hamrick MW. Myostatin (GDF-8) as a Key Factor Linking Muscle Mass and Skeletal Form. J. Musculoskelet. Neuronal Interact. 2010 Mar;10(1):56–63.

203. Elkasrawy M, Immel D, Wen X, Liu X, Liang L-F, Hamrick MW. Immunolocalization of Myostatin (GDF-8) Following Musculoskeletal Injury and

the Effects of Exogenous Myostatin on Muscle and Bone Healing. J. Histochem. Cytochem. 2012 Jan;60(1):22–30.

204. Hamrick MW. Increased bone mineral density in the femora of GDF8 knockout mice. Anat. Rec. A. Discov. Mol. Cell. Evol. Biol. 2003 May;272(1):388–91.

205. Kellum E, Starr H, Arounleut P, Immel D, Fulzele S, Wenger K, Hamrick MW. Myostatin (GDF-8) Deficiency Increases Fracture Callus Size, Sox-5 Expression, and Callus Bone Volume. Bone. 2009 Jan;44(1):17–23.

206. Pehlivantürk Kızılkan M, Akgül S, Derman O, Kanbur N. Bone mineral density comparison of adolescents with constitutional thinness and anorexia nervosa. J. Pediatr. Endocrinol. Metab. JPEM. 2018 Apr 25;31(5):545–50.

207. Wu Y, Qu J, Li H, Yuan H, Guo Q, Ouyang Z, Lu Q. Relationship between serum level of growth differentiation factors 8, 11 and bone mineral density in girls with anorexia nervosa. Clin. Endocrinol. (Oxf.). 2019;90(1):88–93.

208. Wu L, Zhu D, Wang B, Lu Y, He P, Zhang Y, Gao H, Zhu X, Xia W, Zhu H, Mo X, Lu X, Zhang L, Zhang Y, Deng F, Lei S. Relative abundance of mature myostatin rather than total myostatin is negatively associated with bone mineral density in Chinese. J. Cell. Mol. Med. 2018 Feb;22(2):1329–36.

209. Moriwaki K, Matsumoto H, Tanishima S, Tanimura C, Osaki M, Nagashima H, Hagino H. Association of serum bone- and muscle-derived factors with age, sex, body composition, and physical function in community-dwelling middle-aged and elderly adults: a cross-sectional study. BMC Musculoskelet. Disord. [Internet]. 2019

Jun 5 [cited 2020 May 7];20. Available from: https://www.ncbi.nlm.nih.gov/pmc/articles/PMC6549364/

210. Tsourdi E, Makras P, Rachner TD, Polyzos S, Rauner M, Mandanas S, Hofbauer LC, Anastasilakis AD. Denosumab effects on bone density and turnover in postmenopausal women with low bone mass with or without previous treatment. Bone. 2019 Mar 1;120:44–9.

211. Migliorini F, Colarossi G, Baroncini A, Eschweiler J, Tingart M, Maffulli N. Pharmacological management of postmenopausal osteoporosis: a level I evidence based expert opinion. Expert Rev. Clin. Pharmacol. 2020 Nov 12;

212. Quesnel AM, Seton M, Merchant SN, Halpin C, McKenna MJ. Third generation bisphosphonates for treatment of sensorineural hearing loss in otosclerosis. Otol. Neurotol. Off. Publ. Am. Otol. Soc. Am. Neurotol. Soc. Eur. Acad. Otol. Neurotol. 2012 Oct;33(8):1308–14.

213. Russell RGG, Watts NB, Ebetino FH, Rogers MJ. Mechanisms of action of bisphosphonates: similarities and differences and their potential influence on clinical efficacy. Osteoporos. Int. J. Establ. Result Coop. Eur. Found. Osteoporos. Natl. Osteoporos. Found. USA. 2008 Jun;19(6):733–59.

214. Hamrick M, Shi X, Zhang W, Pennington C, Thakore H, Haque M, Kang B, Isales CM, Fulzele S, Wenger K. Loss of Myostatin (GDF8) Function Increases Osteogenic Differentiation of Bone Marrow-Derived Mesenchymal Stem Cells but the Osteogenic Effect is Ablated with Unloading. Bone. 2007 Jun;40(6):1544–53.

215. Chen Y-S, Guo Q, Guo L-J, Liu T, Wu X-P, Lin Z-Y, He H-B, Jiang T-J. GDF8 inhibits bone formation and promotes bone resorption in mice. Clin. Exp. Pharmacol. Physiol. 2017;44(4):500–8.

216. Dankbar B, Fennen M, Brunert D, Hayer S, Frank S, Wehmeyer C, Beckmann D, Paruzel P, Bertrand J, Redlich K, Koers-Wunrau C, Stratis A, Korb-Pap A, Pap T. Myostatin is a direct regulator of osteoclast differentiation and its inhibition reduces inflammatory joint destruction in mice. Nat. Med. 2015 Sep;21(9):1085–90.

217. Park JH, Lee NK, Lee SY. Current Understanding of RANK Signaling in Osteoclast Differentiation and Maturation. Mol. Cells. 2017 Oct 31;40(10):706–13.

218. Maeda Y, Taipaleenmaki H, Zhang W, Jafferji M, Gordon JAR, Li Z, Croce CM, van Wijnen AJ, Stein JL, Stein GS, Lian JB. miR-218 directs a Wnt signaling circuit to promote differentiation of osteoblasts and osteomimicry of metastatic cancer cells. J. Biol. Chem. 2012 Dec 7;287(50):42084–92.

219. Veilleux L, Lemay M, Pouliot-Laforte A, Cheung M, Glorieux FH, Rauch F. Muscle Anatomy and Dynamic Muscle Function in Osteogenesis Imperfecta Type I | The Journal of Clinical Endocrinology & Metabolism | Oxford Academic. J. Clin. Endocrinol. Metab. 2014;99(2):E356–62.

220. Veilleux L-N, Darsaklis VB, Montpetit K, Glorieux FH, Rauch F. Muscle Function in Osteogenesis Imperfecta Type IV. Calcif. Tissue Int. 2017 Oct 1;101(4):362–70.

221. Oestreich, Kamp WM, McCray MG, Carleton SM, Karasseva N, Lenz KL, Jeong Y, Daghlas SA, Yao X, Wang Y, Pfeiffer FM, Ellersieck MR, Schulz LC, Phillips CL.

Decreasing maternal myostatin programs adult offspring bone strength in a mouse model of osteogenesis imperfecta. Proc. Natl. Acad. Sci. U. S. A. 2016 Nov 22;113(47):13522–7.

222. Kozloff KM. Osteogenesis Imperfecta: A Need to Understand Divergent Treatment Outcomes in a Disorder Rich in Heterogeneity. J. Bone Miner. Res. 2019;34(2):205–6.

223. Cianferotti L, Brandi ML. Muscle-bone interactions: basic and clinical aspects. Endocrine. 2014 Mar;45(2):165–77.

224. Omosule CL, Gremminger VL, Aguillard AM, Jeong Y, Harrelson EN, Miloscio L, Mastaitis J, Rafique A, Kleiner S, Pfeiffer FM, Zhang A, Schulz LC, Phillips CL. Impact of genetic and pharmacologic inhibition of myostatin in a murine model of osteogenesis imperfecta. J. Bone Miner. Res. [Internet]. 2020 [cited 2020 Dec 3];n/a(n/a). Available from: https://asbmr.onlinelibrary.wiley.com/doi/abs/10.1002/jbmr.4223

225. David L, Mallet C, Mazerbourg S, Feige J-J, Bailly S. Identification of BMP9 and BMP10 as functional activators of the orphan activin receptor-like kinase 1 (ALK1) in endothelial cells. Blood. 2007 Mar 1;109(5):1953–61.

226. Morello R. Osteogenesis imperfecta and therapeutics. Matrix Biol. 2018 Oct 1;71–72:294–312.

227. Folkestad L, Hald JD, Hansen S, Gram J, Langdahl B, Abrahamsen B, Brixen K. Bone geometry, density, and microarchitecture in the distal radius and tibia in adults

with osteogenesis imperfecta type I assessed by high-resolution pQCT. J. Bone Miner. Res. 2012 Jun;27(6):1405–12.

228. Patel RM, Nagamani SCS, Cuthbertson D, Campeau PM, Krischer JP, Shapiro JR, Steiner RD, Smith PA, Bober MB, Byers PH, Pepin M, Durigova M, Glorieux FH, Rauch F, Lee BH, Hart T, Sutton VR. A cross-sectional multicenter study of osteogenesis imperfecta in North America - results from the linked clinical research centers. Clin. Genet. 2015 Feb;87(2):133–40.

229. Gamsjaeger S, Buchinger B, Zwettler E, Recker R, Black D, Gasser JA, Eriksen EF, Klaushofer K, Paschalis EP. Bone material properties in actively bone-forming trabeculae in postmenopausal women with osteoporosis after three years of treatment with once-yearly Zoledronic acid. J. Bone Miner. Res. 2011 Jan;26(1):12–8.

230. Drake MT, Clarke BL, Khosla S. Bisphosphonates: Mechanism of Action and Role in Clinical Practice. Mayo Clin. Proc. Mayo Clin. 2008 Sep;83(9):1032–45.

231. Land C, Rauch F, Glorieux FH. Cyclical intravenous pamidronate treatment affects metaphyseal modeling in growing patients with osteogenesis imperfecta. J. Bone Miner. Res. 2006 Mar;21(3):374–9.

232. Hamrick MW. The skeletal muscle secretome: an emerging player in muscle–bone crosstalk. BoneKEy Rep. 2012 Apr 11;1:60.

233. Karsenty G, Olson EN. Bone and Muscle Endocrine Functions: Unexpected Paradigms of Inter-organ Communication. Cell. 2016 Mar 10;164(6):1248–56.

234. Alexandre C, Vico L. Pathophysiology of bone loss in disuse osteoporosis. Joint Bone Spine. 2011 Dec 1;78(6):572–6.

235. Arounleut P, Bialek P, Liang L-F, Upadhyay S, Fulzele S, Johnson M, Elsalanty M, Isales CM, Hamrick MW. A Myostatin Inhibitor (Propeptide-Fc) Increases Muscle Mass and Muscle Fiber Size in Aged Mice but Does not Increase Bone Density or Bone Strength. Exp. Gerontol. 2013 Sep;48(9):898–904.

236. Lee S-J. Regulation of muscle mass by myostatin. Annu. Rev. Cell Dev. Biol. 2004;20:61–86.

237. LeBrasseur NK, Schelhorn TM, Bernardo BL, Cosgrove PG, Loria PM, Brown TA. Myostatin Inhibition Enhances the Effects of Exercise on Performance and Metabolic Outcomes in Aged Mice. J. Gerontol. Ser. A. 2009 Sep 1;64A(9):940–8.

238. Bulfield G, Siller WG, Wight PA, Moore KJ. X chromosome-linked muscular dystrophy (mdx) in the mouse. Proc. Natl. Acad. Sci. U. S. A. 1984 Feb;81(4):1189–92.

239. Lodberg A, van der Eerden BCJ, Boers-Sijmons B, Thomsen JS, Brüel A, van Leeuwen JPTM, Eijken M. A follistatin-based molecule increases muscle and bone mass without affecting the red blood cell count in mice. FASEB J. 2019 Feb 13;33(5):6001–10.

240. Wallner C, Jaurich H, Wagner JM, Becerikli M, Harati K, Dadras M, Lehnhardt M, Behr B. Inhibition of GDF8 (Myostatin) accelerates bone regeneration in diabetes mellitus type 2. Sci. Rep. 2017 Aug 29;7:9878.

241. Bialek P, Parkington J, Li X, Gavin D, Wallace C, Zhang J, Root A, Yan G, Warner L, Seeherman HJ, Yaworsky PJ. A myostatin and activin decoy receptor enhances bone formation in mice. Bone. 2014 Mar 1;60:162–71.

242. de Caestecker M. The transforming growth factor-β superfamily of receptors. Cytokine Growth Factor Rev. 2004 Feb 1;15(1):1–11.

243. Jeong Y, Carleton SM, Gentry BA, Yao X, Ferreira JA, Salamango D, Weis MA, Oestreich AK, Williams A, McCray MG, Eyre D, Brown M, Wang Y, Phillips CL. Hindlimb Skeletal Muscle Function and Skeletal Quality and Strength in +/G610C Mice With and Without Weight-Bearing Exercise. J. Bone Miner. Res. 2015;30(10):1874–86.

244. Sinder BP, Eddy MM, Ominsky MS, Caird MS, Marini JC, Kozloff KM. Sclerostin Antibody Improves Skeletal Parameters in a Brtl/+ Mouse Model of Osteogenesis Imperfecta. J. Bone Miner. Res. 2013 Jan;28(1):73–80.

245. Cardinal M, Tys J, Roels T, Lafont S, Ominsky MS, Devogelaer J-P, Chappard D, Mabilleau G, Ammann P, Nyssen-Behets C, Manicourt DH. Sclerostin antibody reduces long bone fractures in the oim/oim model of osteogenesis imperfecta. Bone. 2019 Jul;124:137–47.

246. Jeong Y, Daghlas SA, Kahveci AS, Salamango D, Gentry BA, Brown M, Rector RS, Pearsall RS, Phillips CL. Soluble activin receptor type IIB decoy receptor differentially impacts murine osteogenesis imperfecta muscle function. Muscle Nerve. :n/a-n/a.

247. Kilkenny C, Browne WJ, Cuthill IC, Emerson M, Altman DG. Improving Bioscience Research Reporting: The ARRIVE Guidelines for Reporting Animal Research. PLoS Biol. 2010 Jun 29;8(6):e1000412.

248. Beamer WG, Shultz KL, Donahue LR, Churchill GA, Sen S, Wergedal JR, Baylink DJ, Rosen CJ. Quantitative Trait Loci for Femoral and Lumbar Vertebral Bone Mineral Density in C57BL/6J and C3H/HeJ Inbred Strains of Mice. J. Bone Miner. Res. 2001;16(7):1195–206.

249. Brown M, Ning J, Ferreira JA, Bogener JL, Lubahn DB. Estrogen receptor-alpha and -beta and aromatase knockout effects on lower limb muscle mass and contractile function in female mice. Am. J. Physiol. Endocrinol. Metab. 2009 Apr;296(4):E854-861.

250. Christiansen BA. Effect of micro-computed tomography voxel size and segmentation method on trabecular bone microstructure measures in mice. Bone Rep. 2016 May 27;5:136–40.

251. Bouxsein ML, Boyd SK, Christiansen BA, Guldberg RE, Jepsen KJ, Müller R. Guidelines for assessment of bone microstructure in rodents using micro–computed tomography. J. Bone Miner. Res. 2010;25(7):1468–86.

252. Niebur GL, Feldstein MJ, Yuen JC, Chen TJ, Keaveny TM. High-resolution finite element models with tissue strength asymmetry accurately predict failure of trabecular bone. J. Biomech. 2000 Dec 1;33(12):1575–83.

253. Zhang N, Magland JF, Rajapakse CS, Lam SB, Wehrli FW. Assessment of trabecular bone yield and post-yield behavior from high-resolution MRI-based nonlinear finite-element analysis at the distal radius of pre- and postmenopausal women susceptible to osteoporosis. Acad. Radiol. [Internet]. 2013 Dec [cited 2020 Jul 29];20(12). Available from: https://www.ncbi.nlm.nih.gov/pmc/articles/PMC3842221/

254. Latres E, Pangilinan J, Miloscio L, Bauerlein R, Na E, Potocky TB, Huang Y, Eckersdorff M, Rafique A, Mastaitis J, Lin C, Murphy AJ, Yancopoulos GD, Gromada J, Stitt T. Myostatin blockade with a fully human monoclonal antibody induces muscle hypertrophy and reverses muscle atrophy in young and aged mice. Skelet. Muscle. 2015;5:34.

255. Johnsson B, Löfås S, Lindquist G. Immobilization of proteins to a carboxymethyldextran-modified gold surface for biospecific interaction analysis in surface plasmon resonance sensors. Anal. Biochem. 1991 Nov 1;198(2):268–77.

256. Myszka DG. Improving biosensor analysis. J. Mol. Recognit. JMR. 1999 Oct;12(5):279–84.

257. Cheng Y, Rachagani S, Dekkers JCM, Mayes MS, Tait R, Reecy JM. Mapping genetic loci that interact with myostatin to affect growth traits. Heredity. 2011 Dec;107(6):565–73.

258. Jepsen KJ, Silva MJ, Vashishth D, Guo XE, van der Meulen MC. Establishing Biomechanical Mechanisms in Mouse Models: Practical Guidelines for

Systematically Evaluating Phenotypic Changes in the Diaphyses of Long Bones. J. Bone Miner. Res. 2015 Jun;30(6):951–66.

259. van ’t Hof RJ. Analysis of bone architecture in rodents using microcomputed tomography. Methods Mol. Biol. Clifton NJ. 2012;816:461–76.

260. Chiu C-S, Peekhaus N, Weber H, Adamski S, Murray EM, Zhang HZ, Zhao JZ, Ernst R, Lineberger J, Huang L, Hampton R, Arnold BA, Vitelli S, Hamuro L, Wang W-R, Wei N, Dillon GM, Miao J, Alves SE, Glantschnig H, Wang F, Wilkinson HA. Increased muscle force production and bone mineral density in ActRIIB-Fc-treated mature rodents. J. Gerontol. A. Biol. Sci. Med. Sci. 2013 Oct;68(10):1181–92.

261. McMahon CD, Popovic L, Jeanplong F, Oldham JM, Kirk SP, Osepchook CC, Wong KWY, Sharma M, Kambadur R, Bass JJ. Sexual dimorphism is associated with decreased expression of processed myostatin in males. Am. J. Physiol.-Endocrinol. Metab. 2003 Feb 1;284(2):E377–81.

262. Welle S, Tawil R, Thornton CA. Sex-Related Differences in Gene Expression in Human Skeletal Muscle. PLoS ONE. 2008 Jan 2;3(1):e1385.

263. Callewaert F, Venken K, Kopchick JJ, Torcasio A, Lenthe GH van, Boonen S, Vanderschueren D. Sexual dimorphism in cortical bone size and strength but not density is determined by independent and time-specific actions of sex steroids and IGF-1: Evidence from pubertal mouse models. J. Bone Miner. Res. 2010;25(3):617–26.

264. Iskenderian A, Liu N, Deng Q, Huang Y, Shen C, Palmieri K, Crooker R, Lundberg D, Kastrapeli N, Pescatore B, Romashko A, Dumas J, Comeau R, Norton A, Pan J, Rong H, Derakhchan K, Ehmann DE. Myostatin and activin blockade by engineered follistatin results in hypertrophy and improves dystrophic pathology in mdx mouse more than myostatin blockade alone. Skelet. Muscle. 2018 Oct 27;8(1):34.

265. Alves RDAM, Eijken M, Bezstarosti K, Demmers JAA, van Leeuwen JPTM. Activin A Suppresses Osteoblast Mineralization Capacity by Altering Extracellular Matrix (ECM) Composition and Impairing Matrix Vesicle (MV) Production. Mol. Cell. Proteomics MCP. 2013 Oct;12(10):2890–900.

266. Lee K, Park MS, Yoo WJ, Chung CY, Choi IH, Cho T-J. Proximal Migration of Femoral Telescopic Rod in Children With Osteogenesis Imperfecta: J. Pediatr. Orthop. 2015 Mar;35(2):178–84.

267. King JA, Marker PC, Seung KJ, Kingsley DM. BMP5 and the molecular, skeletal, and soft-tissue alterations in short ear mice. Dev. Biol. 1994 Nov;166(1):112–22.

268. Sugatani T, Agapova OA, Fang Y, Berman AG, Wallace JM, Malluche HH, Faugere M-C, Smith W, Sung V, Hruska KA. Ligand trap of the activin receptor type IIA inhibits osteoclast stimulation of bone remodeling in diabetic mice with chronic kidney disease. Kidney Int. 2017 Jan;91(1):86–95.

269. Sartori R, Gregorevic P, Sandri M. TGFβ and BMP signaling in skeletal muscle: potential significance for muscle-related disease. Trends Endocrinol. Metab. 2014 Sep 1;25(9):464–71.

270. Lee S-J, Lehar A, Meir JU, Koch C, Morgan A, Warren LE, Rydzik R, Youngstrom DW, Chandok H, George J, Gogain J, Michaud M, Stoklasek TA, Liu Y, Germain-Lee EL. Targeting myostatin/activin A protects against skeletal muscle and bone loss during spaceflight. Proc. Natl. Acad. Sci. U. S. A. 2020 Sep 22;117(38):23942–51.

271. Pouliot-Laforte A, Veilleux L-N, Rauch F, Lemay M. Physical activity in youth with osteogenesis imperfecta type I. J. Musculoskelet. Neuronal Interact. 2015 Jun;15(2):171–6.

272. Veilleux L-N, Trejo P, Rauch F. Muscle abnormalities in osteogenesis imperfecta. J. Musculoskelet. Neuronal Interact. 2017 Jun;17(2):1–7.

273. Brizola E, Staub ALP, Félix TM. Muscle strength, joint range of motion, and gait in children and adolescents with osteogenesis imperfecta. Pediatr. Phys. Ther. Off. Publ. Sect. Pediatr. Am. Phys. Ther. Assoc. 2014;26(2):245–52.

274. Veilleux L-N, Pouliot-Laforte A, Lemay M, Cheung MS, Glorieux FH, Rauch F. The functional muscle-bone unit in patients with osteogenesis imperfecta type I. Bone. 2015 Oct;79:52–7.

275. Rybalka E, Timpani CA, Debruin DA, Bagaric RM, Campelj DG, Hayes A. The Failed Clinical Story of Myostatin Inhibitors against Duchenne Muscular Dystrophy: Exploring the Biology behind the Battle. Cells. 2020 Dec 10;9(12).

276. Gentry BA, Ferreira JA, Phillips CL, Brown M. Hindlimb skeletal muscle function in myostatin-deficient mice. Muscle Nerve. 2011;43(1):49–57.

277. Amthor H, Macharia R, Navarrete R, Schuelke M, Brown SC, Otto A, Voit T, Muntoni F, Vrbóva G, Partridge T, Zammit P, Bunger L, Patel K. Lack of myostatin results in excessive muscle growth but impaired force generation. Proc. Natl. Acad. Sci. 2007 Feb 6;104(6):1835–40.

278. Rehfeldt C, Ott G, Gerrard DE, Varga L, Schlote W, Williams JL, Renne U, Bünger L. Effects of the compact mutant myostatin allele Mstn (Cmpt-dl1Abc) introgressed into a high growth mouse line on skeletal muscle cellularity. J. Muscle Res. Cell Motil. 2005;26(2–3):103–12.

279. Rahimov F, King OD, Warsing LC, Powell RE, Emerson CP, Kunkel LM, Wagner KR. Gene expression profiling of skeletal muscles treated with a soluble activin type IIB receptor. Physiol. Genomics. 2011 Apr 27;43(8):398–407.

280. Relizani K, Mouisel E, Giannesini B, Hourdé C, Patel K, Morales Gonzalez S, Jülich K, Vignaud A, Piétri-Rouxel F, Fortin D, Garcia L, Blot S, Ritvos O, Bendahan D, Ferry A, Ventura-Clapier R, Schuelke M, Amthor H. Blockade of ActRIIB Signaling Triggers Muscle Fatigability and Metabolic Myopathy. Mol. Ther. 2014 Aug;22(8):1423–33.

281. Wagner KR. The elusive promise of myostatin inhibition for muscular dystrophy. Curr. Opin. Neurol. 2020 Oct;33(5):621–8.

282. Morine KJ, Bish LT, Pendrak K, Sleeper MM, Barton ER, Sweeney HL. Systemic Myostatin Inhibition via Liver-Targeted Gene Transfer in Normal and Dystrophic

Mice. PLoS ONE [Internet]. 2010 Feb 11 [cited 2021 Feb 18];5(2). Available from: https://www.ncbi.nlm.nih.gov/pmc/articles/PMC2820101/

283. Cropp GJA, Myers DN. Physiological Evidence of Hypermetabolism in Osteogenesis Imperfecta. Pediatrics. 1972 Mar 1;49(3):375–91.

284. Porsborg P, Astrup G, Bendixen D, Lund AM, Ørding H. Osteogenesis imperfecta and malignant hyperthermia. Anaesthesia. 1996;51(9):863–5.

285. Koncarevic A, Cornwall-Brady M, Pullen A, Davies M, Sako D, Liu J, Kumar R, Tomkinson K, Baker T, Umiker B, Monnell T, Grinberg AV, Liharska K, Underwood KW, Ucran JA, Howard E, Barberio J, Spaits M, Pearsall S, Seehra J, Lachey J. A soluble activin receptor type IIb prevents the effects of androgen deprivation on body composition and bone health. Endocrinology. 2010 Sep;151(9):4289–300.

286. Palomo T, Glorieux FH, Schoenau E, Rauch F. Body Composition in Children and Adolescents with Osteogenesis Imperfecta. J. Pediatr. 2016 Feb;169:232–7.

287. Boraschi-Diaz I, Tauer JT, El-Rifai O, Guillemette D, Lefebvre G, Rauch F, Ferron M, Komarova SV. Metabolic phenotype in the mouse model of osteogenesis imperfecta. J. Endocrinol. 2017 Sep 1;234(3):279–89.

288. Souza TA, Chen X, Guo Y, Sava P, Zhang J, Hill JJ, Yaworsky PJ, Qiu Y. Proteomic identification and functional validation of activins and bone morphogenetic protein 11 as candidate novel muscle mass regulators. Mol. Endocrinol. Baltim. Md. 2008 Dec;22(12):2689–702.

289. Reid IR. Relationships between fat and bone. Osteoporos. Int. 2008 May 1;19(5):595–606.

290. Van Brussel M, Takken T, Uiterwaal CSPM, Pruijs HJ, Van der Net J, Helders PJM, Engelbert RHH. Physical Training in Children with Osteogenesis Imperfecta. J. Pediatr. 2008 Jan 1;152(1):111-116.e1.

291. Dutta S, Sengupta P. Men and mice: Relating their ages. Life Sci. 2016 May 1;152:244–8.

292. Deng B, Zhang F, Wen J, Ye S, Wang L, Yang Y, Gong P, Jiang S. The function of myostatin in the regulation of fat mass in mammals. Nutr. Metab. 2017 Mar 21;14(1):29.

293. Navein AE, Cooke EJ, Davies JR, Smith TG, Wells LHM, Ohazama A, Healy C, Sharpe PT, Evans SL, Evans BAJ, Votruba M, Wells T. Disrupted mitochondrial function in the Opa3L122P mouse model for Costeff Syndrome impairs skeletal integrity. Hum. Mol. Genet. 2016 Jun 15;25(12):2404–16.

294. Gao J, Feng Z, Wang X, Zeng M, Liu J, Han S, Xu J, Chen L, Cao K, Long J, Li Z, Shen W, Liu J. SIRT3/SOD2 maintains osteoblast differentiation and bone formation by regulating mitochondrial stress. Cell Death Differ. 2018 Feb;25(2):229–40.

295. Kang S, Fernandes-Alnemri T, Alnemri ES. A novel role for the mitochondrial HTRA2/OMI protease in aging. Autophagy. 2013 Mar;9(3):420–1.

296. Kassem M, Rungby J, Mosekilde L, Eriksen EF. Ultrastructure of human osteoblasts and associated matrix in culture. APMIS Acta Pathol. Microbiol. Immunol. Scand. 1992 Jun;100(6):490–7.

297. Brown D, Breton S. Mitochondria-rich, proton-secreting epithelial cells. J. Exp. Biol. 1996 Nov;199(Pt 11):2345–58.

298. Guntur AR, Gerencser AA, Le PT, DeMambro VE, Bornstein SA, Mookerjee SA, Maridas DE, Clemmons DE, Brand MD, Rosen CJ. Osteoblast-like MC3T3-E1 Cells Prefer Glycolysis for ATP Production but Adipocyte-like 3T3-L1 Cells Prefer Oxidative Phosphorylation. J. Bone Miner. Res. Off. J. Am. Soc. Bone Miner. Res. 2018;33(6):1052–65.

299. Rizzuto R. The collagen-mitochondria connection. Nat. Genet. 2003 Dec;35(4):300–1.

300. Malik AN, Czajka A. Is mitochondrial DNA content a potential biomarker of mitochondrial dysfunction? Mitochondrion. 2013 Sep 1;13(5):481–92.

301. Brand MD, Nicholls DG. Assessing mitochondrial dysfunction in cells. Biochem. J. 2011 Apr 15;435(Pt 2):297–312.

302. Detmer SA, Chan DC. Functions and dysfunctions of mitochondrial dynamics. Nat. Rev. Mol. Cell Biol. 2007 Nov;8(11):870–9.

303. Dröge W. Free radicals in the physiological control of cell function. Physiol. Rev. 2002 Jan;82(1):47–95.

304. Ray PD, Huang B-W, Tsuji Y. Reactive oxygen species (ROS) homeostasis and redox regulation in cellular signaling. Cell. Signal. 2012 May;24(5):981–90.

305. Arias-Loza P-A, Muehlfelder M, Pelzer T. Estrogen and estrogen receptors in cardiovascular oxidative stress. Pflüg. Arch. - Eur. J. Physiol. 2013 May 1;465(5):739–46.

306. Yang Y-H, Li B, Zheng X-F, Chen J-W, Chen K, Jiang S-D, Jiang L-S. Oxidative damage to osteoblasts can be alleviated by early autophagy through the endoplasmic reticulum stress pathway--implications for the treatment of osteoporosis. Free Radic. Biol. Med. 2014 Dec;77:10–20.

307. Filaire E, Toumi H. Reactive oxygen species and exercise on bone metabolism: friend or enemy? Jt. Bone Spine Rev. Rhum. 2012 Jul;79(4):341–6.

308. Nojiri H, Saita Y, Morikawa D, Kobayashi K, Tsuda C, Miyazaki T, Saito M, Marumo K, Yonezawa I, Kaneko K, Shirasawa T, Shimizu T. Cytoplasmic superoxide causes bone fragility owing to low-turnover osteoporosis and impaired collagen cross-linking. J. Bone Miner. Res. 2011 Nov 1;26(11):2682–94.

309. Bai X, Lu D, Liu A, Zhang Z, Li X, Zou Z, Zeng W, Cheng B, Luo S. Reactive Oxygen Species Stimulates Receptor Activator of NF-κB Ligand Expression in Osteoblast. J. Biol. Chem. 2005 Apr 29;280(17):17497–506.

310. Wauquier F, Leotoing L, Coxam V, Guicheux J, Wittrant Y. Oxidative stress in bone remodelling and disease. Trends Mol. Med. 2009 Oct 1;15(10):468–77.

311. Domazetovic V, Marcucci G, Iantomasi T, Brandi ML, Vincenzini MT. Oxidative stress in bone remodeling: role of antioxidants. Clin. Cases Miner. Bone Metab. 2017;14(2):209–16.

312. Matthews BG, Roeder E, Wang X, Aguila HL, Lee S-K, Grcevic D, Kalajzic I. Splenomegaly, myeloid lineage expansion and increased osteoclastogenesis in osteogenesis imperfecta murine. Bone. 2017 Oct;103:1–11.

313. Shaw PX, Werstuck G, Chen Y. Oxidative Stress and Aging Diseases [Internet]. Oxid. Med. Cell. Longev. 2014 [cited 2018 Sep 29]. Available from: https://www.hindawi.com/journals/omcl/2014/569146/

314. Callaway DA, Jiang JX. Reactive oxygen species and oxidative stress in osteoclastogenesis, skeletal aging and bone diseases. J. Bone Miner. Metab. 2015 Jul 1;33(4):359–70.

315. Larsen S, Nielsen J, Hansen CN, Nielsen LB, Wibrand F, Stride N, Schroder HD, Boushel R, Helge JW, Dela F, Hey-Mogensen M. Biomarkers of mitochondrial content in skeletal muscle of healthy young human subjects. J. Physiol. 2012 Jul 15;590(Pt 14):3349–60.

316. Liu B, Lu Y, Wang Y, Ge L, Zhai N, Han J. A protocol for isolation and identification and comparative characterization of primary osteoblasts from mouse and rat calvaria. Cell Tissue Bank. 2019;20(2):173–82.

317. Carpenter TO, Moltz KC, Ellis B, Andreoli M, McCarthy TL, Centrella M, Bryan D, Gundberg CM. Osteocalcin Production in Primary Osteoblast Cultures Derived from Normal and Hyp Mice. Endocrinology. 1998 Jan 1;139(1):35–43.

318. Miotto PM, Frendo-Cumbo S, Sacco SM, Wright DC, Ward WE, Holloway GP. Combined high-fat-resveratrol diet and RIP140 knockout mice reveal a novel relationship between elevated bone mitochondrial content and compromised bone microarchitecture, bone mineral mass, and bone strength in the tibia. Mol. Nutr. Food Res. 2016 Sep 1;60(9):1994–2007.

319. Niyibizi C, Smith P, Mi Z, Robbins P, Evans C. Potential of gene therapy for treating osteogenesis imperfecta. Clin. Orthop. 2000 Oct;(379 Suppl):S126-133.

320. McPherron AC, Lee S-J. Double muscling in cattle due to mutations in the myostatin gene. Proc. Natl. Acad. Sci. 1997 Nov 11;94(23):12457–61.

321. Ashournia H, Johansen FT, Folkestad L, Diederichsen ACP, Brixen K. Heart disease in patients with osteogenesis imperfecta — A systematic review. Int. J. Cardiol. 2015 Oct 1;196:149–57.

322. Weis SM, Emery JL, Becker KD, McBride DJ, Omens JH, McCulloch AD. Myocardial mechanics and collagen structure in the osteogenesis imperfecta murine (oim). Circ. Res. 2000 Oct 13;87(8):663–9.

323. Thiele F, Cohrs CM, Flor A, Lisse TS, Przemeck GKH, Horsch M, Schrewe A, Gailus-Durner V, Ivandic B, Katus HA, Wurst W, Reisenberg C, Chaney H, Fuchs H, Hans W, Beckers J, Marini JC, Hrabé de Angelis M. Cardiopulmonary

dysfunction in the Osteogenesis imperfecta mouse model Aga2 and human patients are caused by bone-independent mechanisms. Hum. Mol. Genet. 2012 Aug 15;21(16):3535–45.

324. Cohn RD, Liang H-Y, Shetty R, Abraham T, Wagner KR. Myostatin Does not Regulate Cardiac Hypertrophy or Fibrosis. Neuromuscul. Disord. NMD. 2007 Apr;17(4):290–6.

325. Matthews BG, Roeder E, Wang X, Aguila HL, Lee S-K, Grcevic D, Kalajzic I. Splenomegaly, myeloid lineage expansion and increased osteoclastogenesis in osteogenesis imperfecta murine. Bone. 2017 Oct;103:1–11.

326. Abdelaziz DM, Abdullah S, Magnussen C, Ribeiro-da-Silva A, Komarova SV, Rauch F, Stone LS. Behavioral signs of pain and functional impairment in a mouse model of osteogenesis imperfecta. Bone. 2015 Dec;81:400–6.

327. Rauch F, Bailey DA, Baxter-Jones A, Mirwald R, Faulkner R. The "muscle-bone unit" during the pubertal growth spurt. Bone. 2004 May;34(5):771–5.

328. Cundy T. Recent advances in osteogenesis imperfecta. Calcif. Tissue Int. 2012 Jun;90(6):439–49.

329. Greenhough J, Papadakis ES, Cutress RI, Townsend PA, Oreffo ROC, Tare RS. Regulation of osteoblast development by Bcl-2-associated athanogene-1 (BAG-1). Sci. Rep. 2016 Sep 16;6:srep33504.

VITA

Catherine (Cate) Laaripuoh Omosule (née Seidu) was born on January 10, 1993 in Tamale, Ghana, to Paul Seidu and Alice Abena Kugbie. Catherine attended Notre Dame Girls Senior High School in Sunyani, Ghana. At 17 years of age, she was awarded a scholarship through the U.S. Department of State Kennedy Lugar Youth Exchange and Service (YES) program to serve as a cultural ambassador to Ghana in St. Louis, Missouri, where she attended Normandy High School in St. Louis, Missouri for her senior year. At the end of her exchange year, Catherine was chosen as a recipient of the NSF-Mathematics in Life Sciences (MLS) Fellowship, and was awarded a full-ride scholarship to the University of Missouri, Columbia where she pursued a Bachelors in Biology. Under the mentorship of Dr. George P. Smith and Dr. Dix Pettey, curators of the MLS fellowship, Catherine participated in research in Dr. Zezong Gu's laboratory and discovered the joys of scientific research and the opportunity to influence lives through mentorship and scientific advancements. Upon graduating summa cum laude with her undergraduate degree, she enrolled in graduate school and pursued translational research under the mentorship of Dr. Charlotte Phillips. Catherine will begin a post-doctoral fellowship in Clinical Chemistry at the Washington University in St. Louis, with the hopes of eventually directing clinical chemistry laboratories in academia/industry.